CRANFIELD UNIVERSITY

DAXIN LI

MULTI-OBJECTIVE DESIGN OPTIMIZATION FOR HIGH-LIFT AIRCRAFT CONFIGURATIONS SUPPORTED BY SURROGATE MODELING

SCHOOL OF ENGINEERING

MSc By Research

MSc Thesis

Academic Year: 2012 - 2013

Supervisor: Dr. Asproulis Nikolaos

December 2013

CRANFIELD UNIVERSITY

SCHOOL OF ENGINEERING
MSc By Research

MSc Thesis

Academic Year 2012 - 2013

DAXIN LI

MULTI-OBJECTIVE DESIGN OPTIMIZATION FOR HIGH-LIFT AIRCRAFT CONFIGURATIONS SUPPORTED BY SURROGATE MODELING

Supervisor: Dr. Asproulis Nikolaos
December 2013

This thesis is submitted in partial fulfilment of the requirements for the degree of Master of Science
(NB. This section can be removed if the award of the degree is based solely on examination of the thesis)

ABSTRACT

Nowadays, the competition among airlines seriously depend upon the saving operating costs, with the premise that not to degrade its services quality. Especially in the face of increasingly scarce oil resources, reducing fleets operational fuel consumption, is an important means to improve profits.

Aircraft fuel economy is determined by operational management strategies and application technologies. The application of technologies mainly refers to airplane's engine performance, Weight efficiency and aerodynamic characteristics. A market competitive aircraft should thoroughly consider to all of these aspects.

Transport aircraft aerodynamic performance mainly is determined by wing's properties. Wings that are optimized for efficient flight in cruise conditions need to be fitted with powerful high-lift devices to meet lift requirements for safe takeoff and landing. These high-lift devices have a significant impact on the total airplane performance. The aerodynamic characteristics of the wing airfoil will have a direct impact on the aerodynamic characteristics of the wing, and the wing's effective cruise hand high-lift configuration design has a significant impact on the performance of transport aircraft. Therefore, optimizing the design is a necessary airfoil design process.

Nowadays engineering analysis relies heavily on computer-based solution algorithms to investigate the performance of an engineering system. Computational fluid dynamics (CFD) is one of the computer-based solution methods which are more widely employed in aerospace engineering. The computational power and time required to carry out the analysis increases as the fidelity of the analysis increases. Aerodynamic shape optimization has become a vital part of aircraft design in the recent years. Since the aerodynamic shape optimization (ASO) process with CFD solution algorithms requires a huge amount of computational power, there is always some reluctance among the aircraft researchers in employing the ASO approach at the initial stages of the aircraft design. In order to alleviate this problem, statistical approximation models are constructed for actual CFD algorithms. The fidelity of these approximation models are merely based on the fidelity of data used to construct these models. Hence it becomes indispensable to spend more computational power in order to convene more data which are further used for constructing the approximation models.

The goal of this thesis is to present a design approach for assumed wing airfoils; it includes the design process, multi-objective design optimization based on surrogate modelling. The optimization design stared from a transonic single-element single-objective optimization design, and then high-lift configurations were two low-speed conditions of multi-objective optimization design, on this basis, further completed a variable camber airfoil at low speed to high-lift configuration to improve aerodynamic performance. Through this study, prove a surrogate based model could be used in the wing airfoil optimization design.

Keywords: Airfoil Design, Supercritical Airfoil, Multi-element airfoil parameter, Variable Camber Airfoil, Droppable spoiler, Aerodynamic design.

ACKNOWLEDGEMENTS

There some days when I cannot find the light show the path of my research, I always knock the door F16, and the beam of the light from my supervisor, presents me a wide and deep research view. I thank him for his valuable guidance which helps me vanish the dark in front of the path to understand aerodynamic design and Optimization, and finish all of the tasks at the reasonable time.

It is a pleasure to acknowledge the kind and generous help I have received from so many people in the process of major research and writing this thesis, special thanks go to Prof. Tasos kokkalis，Prof. Rafal Zbikowski, Dr. Konozsy Laszlo, Dr. Antoniadis Antonios, Dr. Al Savvaris, Dr. Frank Michael and my COMAC colleagues. I'd especially like to thank English language teachers Joan and Chris, and Lady Caroline and Alison from the accommodation office, for their special care offered to me.

My great appreciation also to the *Journey to the West* TV series, which aroused the interest to fly from my childhood, thanks to Harbin Engineering University which trained my basic physics and engineering knowledge and Cranfield University. I will remember all my all breaths in here.

Thanks to someone who had given me examples how to study more efficiently.

Thanks to Mr. Martin Recksiek from Airbus Germany for his warm help.

My deepest thanks to my father, mother; and Geya & Mohuang and theirs parents for their love and care, especially to my grandfather and grandmother. Thanks to my grandfather's younger brother and his wife in Wuhan for their encouragement and support to me. And finally all the relatives and friends in ChaLing town, Hunan province of China.

TABLE OF CONTENTS

ABSTRACT ii
ACKNOWLEDGEMENTS iii
LIST OF FIGURES vi
LIST OF TABLES xii
LIST OF ABBREVIATIONS xiv
Chapter1. Introduction 1
1.1 Motivation 1
1.2 Historical review of Multi-Objective aerodynamic shape optimization 2
1.3 Aim and Objectives 3
1.4 Thesis Overview 3
Chapter2. Literature review of Airfoil Design 5
2.1 Introduction 5
2.2 Flight Economical 6
2.3 Aerodynamic Design of Transport Aircraft 8
2.4 Transonic flight 19
2.5 Supercritical Airfoil 20
2.6 Low-speed Flight 23
2.7 High-lift Configuration Airfoil 26
2.8 Optimization design strategy introduction 33
Chapter3. Mathematical Modelling 39
3.1 Design of Experiments 41
3.1.1 Overview of sampling methods 41
3.1.2 Sampling Techniques 43
3.1.3 Hammersley Sample 45
3.2 Airfoil Parameterization 46
3.2.1 Parameter of Single-element Airfoil 47
3.2.2 Parameterization of High-lift configuration Airfoil 55
3.2.3 Droop spoiler Parameter 57
3.3 Computational fluid dynamic 57
3.3.1 Aerodynamic characteristics evaluators review 58
3.3.2 Basic Principles of CFD 62
3.3.3 Panel method 63
3.3.4 Reynolds-averaged Navier–Stokes equations 64
3.4 Surrogate model construction 73
3.4.1 Overview of Surrogate Model Construction 74
3.4.2 Kriging Model 76
3.4.3 Model Comparison 79
3.5 Optimization Methods 80
3.5.1 Local/ Global Optimization 82
3.5.2 Single/Multi-objective optimization 82

3.5.3 Methods of Airfoil Optimization 85
Chapter4. Airfoil shape Optimization 91
4.1 Transonic single-element airfoil 92
4.1.1 Design space and Objective 93
4.1.2 Strategies 94
4.1.3 CFD simulation 95
4.1.4 Surrogate model construction 102
4.1.5 Result Comparison 104
4.2 HLC Airfoil Design Optimization 107
4.2.1 Design space and Objective 107
4.2.2 Strategy of Design Optimization 111
4.2.3 CFD simulation 112
4.2.4 HLC airfoil for Takeoff 115
4.2.5 Landing 121
4.3 Drop Spoiler Effect 124
Chapter5. Conclusions and Future Work 131
5.1 Conclusion 131
5.2 Future work 133
REFERENCES 134
APPENDICES 145

LIST OF FIGURES

Figure 2-1: Similarities between birds and aeroplanes [8-11] 5

Figure 2-2: Fuel efficiency gains since the early jet age [12] 7

Figure 2-3: Structure and aerodynamics efficiency is increasing [18] 7

Figure 2-4: Advanced technology contributions to improve B787 efficiency [20] 8

Figure 2-5: Flight object affect static air 9

Figure 2-6: Surface comparison between early and currently aircraft [31; 32] . 10

Figure 2-7: Drag Breakdown of Transport Aircraft in Cruise [15] 11

Figure 2-8: Wing root and outer sections (A380) and wing sections (A340) [34] 12

Figure 2-9: Wing span wise thickness and twist distribution (A380) [34] 12

Figure 2-10: Effects of sweep on wing transonic drag coefficient 13

Figure 2-11: Internal components of a wing [36] 14

Figure 2-12: Airbus A380 wing high-lift devices layout 15

Figure 2-13: Aerodynamic efficiency improves from variable camber airfoil [39] 15

Figure 2-14: Airfoil definition parameters 16

Figure 2-15: Experiment lift curve, drag polar and pitching curve for airfoil [41] 17

Figure 2-16: Progression of shock waves with increasing Mach number [42] .. 17

Figure 2-17: Sketch of the variation of profile drag coefficient with free-stream Mach number, illustrating the critical and drag-divergence Mach numbers and showing the large drag rise near Mach 1 [43] 17

Figure 2-18: A broadbrush categorization of drag [22] 18

Figure 2-19: Variable camber airfoil [44] 18

Figure 2-20: Variable camber airfoil [39] 20

Figure 2-21: Progression of supercritical airfoil shape [45] 21

Figure 2-22: Two uses of supercritical wing [46] 22

Figure 2-23: flow fields around supercritical and conventional airfoils [45] 22

Figure 2-24: Example of airfoil drag rise date [48; 49] 22

Figure 2-25: Three main parameters determine the transport aircraft performance 23

Figure 2-26: Takeoff and Landing procedure for civil transport airplanes [53].. 25

Figure 2-27: The effect to lift coefficient from slat and flap [34] 26

Figure 2-30: High-lift configuration [54] Figure 2-31: Basic effect of high-lift . 28

Figure 2-28: slat effect and Circulation effect [48] 30

Figure 2-29: Interaction effects in multi-element high-lift devices [48; 49] 30

Figure 2-32: Definition of gap (Gs/Gf) and overlap (Os/Of) Fowler motion [50] 31

Figure 2-33: Constant **CLmax** loci for slot gap and overlap values 31

Figure 2-34: Flow field around the wing section of a 3-element wing [4] 32

Figure 2-35: Evolution of high lift systems [58] 33

Figure 2-36: Scheme of High-Lift Design Process for transport aircraft [2] 35

Figure 2-37: Sequence of the CFD-based high-lift design process [3] 36

Figure 2-38: Pitch moment balance [59]..... 37

Figure 2-39: Horizontal tail trim affect to wing lift and drag..... 37

Figure 2-40: HLC airfoil optimization design process 38

Figure 3-1: CFD-based optimization process [60] 39

Figure 3-2: General CFD-surrogate-based Optimization process [60] 40

Figure 3-3: Classical and modern DOE approaches [Source: A. J. Booker (1998)]..... 43

Figure 3-4: Classical DOE for a 3-factor, 3-level Problem..... 44

Figure 3-5: 50 and 100 Sample Points (12 Dimensions)..... 46

Figure 3-6: Dotes, Curves and surface..... 47

Figure 3-7: Generic aircraft shape production using PDE's..... 48

Figure 3-8: Hicks-Henne Bump Functions apply on a basis airfoil [72] 50

Figure 3-9: A set of 16 Hicks-Henne Bump Functions with parameter (t_2 =10) [71] 51

Figure 3-10: Joukowski transformation..... 52

Figure 3-11: Parametric Section control parameters 52

Figure 3-12: PARSEC validation 54

Figure 3-13: HLC airfoil Parameter..... 56

Figure 3-14: CFD takes more job than Wind tunnel test [79] 58
Figure 3-15： Approaches as aerodynamic evaluator 59
Figure 3-16: Wind tunnel capability and model mounted in test section [82; 83] 60
Figure 3-17: Morden Wind tunnel short and long term repeatability accuracy [84] 60
Figure 3-18: F-8A flight test with supercritical Airfoil wing [85] 61
Figure 3-19: Representation of a smooth airfoil with straight line segments [24] 64
Figure 3-20: A finite-Difference model 66
Figure 3-21: A finite control volume model 67
Figure 3-22: Turbulence on up wing surface [95], turbulent viscosity around a transonic flow airfoil. 69
Figure 3-23: A schematic overview of turbulence modelling [96] 70
Figure 3-24: Turbulence used in predictions of maximum lift for HLC airfoil [100] 70
Figure 3-25: Typical velocity profile for a turbulent boundary layer [103] 72
Figure 3-26: Schematic representation of a Multi-layered ANN 76
Figure 3-27: Example of local/global optimum 82
Figure 3-28: Single/Multi-objective model 83
Figure 3-29: Example of a Pareto frontier [110] 84
Figure 3-30: A classification of optimization schemes 86
Figure 3-31: The structure of the SA algorithm [114] 87
Figure 4-1: Tail trim efficiency 91
Figure 4-2: Airfoil optimization process 92
Figure 4-3: Developed code to general airfoils 95
Figure 4-4: Airfoil No. 50, 150, 250, 350 95
Figure 4-5: Simulation process for samples 96
Figure 4-6: RAE 2282 Airfoil profile 97
Figure 4-7: Far field and blocks divided strategy for RAE 2282 airfoil 97
Figure 4-8: mesh generation (51200 Grids) 98

Figure 4-9: Case a pressure coefficient and Mach number counter [121] 98

Figure 4-10: CP comparison between WT test and study results (Case a).Mach number counter with $Y+=10$ 98

Figure 4-11: CP distribution comparison [122] 99

Figure 4-12: ICEM CFD blockage partition and Fluent convergence historical 100

Figure 4-13: shape of No.12 sample airfoils 100

Figure 4-14: Trim effects on CL/CD of sample points 101

Figure 4-15: (CL/CD)i, i=1 to 9 Vs. average (CL/CD) 101

Figure 4-16: Objective Difference between samples and surrogate model 102

Figure 4-17: Transonic airfoil optimization 103

Figure 4-18: Transonic airfoil optimization process of Case 2 104

Figure 4-19: Comparison between Airfoil A and No.12, and Airfoil B and No.352 104

Figure 4-20: Optimum design result compare to sample in case a..... 105

Figure 4-21: Optimum design result compare to sample in case b..... 106

Figure 4-22: Comparison Airfoil B and B+ 108

Figure 4-23: CL~α comparison between Airfoil A+ and B+ at Ma=0.2..... 109

Figure 4-24: Airfoil partition 110

Figure 4-25: Geometry dimensions to PARSEC contours 110

Figure 4-26: sample geometries (No. 50, 150, 250 and 350). 111

Figure 4-27: Two optimization processes of the HLC airfoil design 111

Figure 4-28: MDA 30P/30N HLC airfoil and simulation domain [124; 125] 112

Figure 4-29: Meshes generation..... 113

Figure 4-30: Comparison between Experiment and Computational (16°) 113

Figure 4-31: Pressure (Left), Mach number and streamlines (Right) (16°)..... 114

Figure 4-32: Comparison between CFD simulation and Experiment data [114; 115] 114

Figure 4-33: Convergence historical (No.161 sampling airfoil) 115

Figure 4-34: Result of 400 sampling HLC airfoil CL/CD for Takeoff 116

Figure 4-35: CL distribution 117

Figure 4-36: K' distribution 117
Figure 4-37: Objective Difference between samples and surrogate model 118
Figure 4-38: Optimization (Takeoff) 118
Figure 4-39: The Pareto-optimization model of the $1/CL \sim CD/CL$ 119
Figure 4-40: Comparison of the takeoff HLC airfoils 119
Figure 4-41: Comparison flow with Ma contours 120
Figure 4-42: Comparison flow with Pressure contours 120
Figure 4-43: CP comparison 120
Figure 4-44: Airfoil No. 50, 150 121
Figure 4-45: Objective Difference between samples and surrogate model at sample points (Landing) 122
Figure 4-46: Objective Difference between 122
Figure 4-47: landing HLC airfoil optimization comparison 123
Figure 4-48: Ma contour and streamline comparison 123
Figure 4-49: Pressure comparison 123
Figure 4-50: CP comparison 123
Figure 4-51: Drop Spoiler 124
Figure 4-52: Ma contours comparison 125
Figure 4-53: Pressure contours comparison 126
Figure 4-54: CP distribution comparison 127
Figure 4-55: Mach Contour comparison 128
Figure 4-56: pressure contours comparison 129
Figure 4-57: CP comparison 130
Figure 5-1: Parameter 1 ~ Parameter 2 of 400 samples 145
Figure 5-2: Parameter 1 ~ Parameter 3 of 400 samples 145
Figure 5-3: Parameter 1 ~ Parameter 4 of 400 samples 146
Figure 5-4: Parameter 1 ~ Parameter 5 of 400 samples 146
Figure 5-5: Parameter 1 ~ Parameter 6 of 400 samples 147
Figure 5-6: Parameter 1 ~ Parameter 7 of 400 samples 147
Figure 5-7: Parameter 1 ~ Parameter 8 of 400 samples 148

Figure 5-8: Parameter 1 ~ Parameter 9 of 400 samples 148
Figure 5-9: Parameter 1 ~ Parameter 10 of 400 samples 149
Figure 5-10: Parameter 1 ~ Parameter 11 of 400 samples 149
Figure 5-11: Parameter 1 ~ Parameter 12 of 400 samples 150
Figure 5-12: Parameter 1 ~ Parameter 2 of 200 samples 150
Figure 5-13: Parameter 1 ~ Parameter 3 of 200 samples 151
Figure 5-14: Parameter 1 ~ Parameter 4 of 200 samples 151
Figure 5-15: Parameter 1 ~ Parameter 5 of 200 samples 152
Figure 5-16: Parameter 1 ~ Parameter 6 of 200 samples 152

LIST OF TABLES

Table 2-1: Sweep effect to aerodynamic design 13

Table 2-2: Different High-lift device effect on aerodynamic characteristics 27

Table 2-3: Optimization condition and objectives 36

Table 3-1: PARSEC parameters for NACA 2411 airfoil 54

Table 3-2: One point of view regarding computational aerodynamics capability [80] 58

Table 3-3: Aerodynamic evaluation methods utilization properties comparison 61

Table 3-4: Qualitative overview of aerodynamic design methods for high-lift systems. 62

Table 4-1: CFD Simulation Cases specification 93

Table 4-2: PARSEC parameter ranges for transonic airfoil optimization [119] . 94

Table 4-3: Two simulation cases 97

Table 4-4: Y+ effect on accuracy 99

Table 4-5: $Pham$ comparison between optimum and sample airfoils 104

Table 4-6: Comparison between best in sample and optimum 107

Table 4-7: PARSEC parameter ranges for HLC airfoil optimization 110

Table 4-8: Parameters for Counters with PARSEC method 110

Table 4-9: parameters for meshes generation and CFD simulation [126] 113

Table 4-10: Parameters comparison between optimum and sample airfoils .. 119

Table 4-11: Improve of CL/CD and CL after optimization 120

Table 4-12: landing configuration design space 121

Table 4-13: landing configuration bounds 122

Table 4-14: Improve of CL after optimization 124

Table 4-15: Spoilers setting 124

Table 4-16: Drop spoiler affect to CL/CD and CL 127

Table 4-17: Drop spoiler affect to CL/CD and CL 130

Table 5-1: 400 airfoil Transonic simulation result (9 cases) 153

Table 5-2: Transonic airfoil optimization sample points of Case 1 162

Table 5-3: Transonic airfoil optimization sample points of Case 2 163

Table 5-4： Takeoff Samples 163
Table 5-5: Takeoff optimization process 166
Table 5-6: Landing samples 167
Table 5-7: Landing optimization process 168

LIST OF ABBREVIATIONS

ASO	Aircraft shape optimization
CD	Drag coefficient
CFD	computational fluid dynamics
CL	lift coefficient
CP	Pressure coefficient
CU	Cranfield University
DOE	Design of experiments
ESDU	Engineering Sciences Data Unit
HLC	High-lift configuration
HPC	High performance computing
IRP	Individual research program
Ma	Mach number
MODO	Multi-objective design optimization
MOP	Multi-Objective optimization
OEM	Operational empty weight
PARSEC	Parametric section
RANS	Reynolds-averaged Navier-Stokes equations
SODO	Single objective design optimization
WTT	Wind tunnel testing
SST	shear stress transport turbulence model

Chapter1. Introduction

1.1 Motivation

Computational simulation is the trend in current industrial design and research Field, especially support by increasingly sophisticated hardware and comprehensive algorithm. It saves huge design and research budget, shortens product development cycle, which previously based on physical experiments and objects.

Computational based simulation fluid dynamic is a simulation method, which uses numerical methods and algorithms to solve and analyse problems that involve fluid flows. It is mainly dedicated to the areas of aerospace widely. Currently, aircraft design engineers mainly use it as the evaluator of the aerodynamic characteristics, comparing with other methods to design and optimize aircraft aerodynamic shape, it can help the engineers get the design objectives with lower cost and more convenience and adequate accuracy.

CFD is a very powerful tool in aircraft aerodynamic design. However, sometimes it is computational costly. In order to execute a high-fidelity simulation with CFD, it requires employing Reynolds-averaged Navier–Stokes equations (RANS) and turbulence modeling. Meanwhile a fine mesh is necessary, which could be tens of millions of elements, sometimes a simulation takes days, weeks and even months [1]. Furthermore sometimes the optimization design will base on hundreds, thousands or more high-fidelity evaluations, it is computational resource and time costly, so it is necessary to seek a way to assist the CFD to do the aircraft aerodynamic characteristics evaluation work.

In order to resolve the aircraft design and optimization phase computational costly problem, some researchers have utilized the surrogate models as another variables evaluator to give its objectives. The surrogate modelling is referred to a technique that makes use of the sampled data to build the surrogate models, which sufficient to predict the output of an expensive computer code at untried points in the design space.

Aircraft wing High-lift configuration (HLC) design is an important and challenging design part of the whole aircraft aerodynamic configuration design, even deal with a 2-D HLCs design task which is an essential step for the 3-D HLC design [2; 3]. As the shapes, relative-positions and relative-orientations of the multi-elements yield several design parameters that constitute a hypercube design space, the n-dimension variables optimization design needs huge computational resource. Furthermore, even in low speed flying phase, the flow around the HLCs is complex [4], so it is necessary to employ the RANS numerical method and a fine boundary mesh to do the CFD calculation, both of them means computationally costly to some extent. In order to minimize the computational costs referring to HCLs optimization design, this thesis will study a way to achieve it.

1.2 Historical review of Multi-Objective aerodynamic shape optimization

Aerodynamics is the science that deals with the interactions of fluid flows and objects. This interaction is governed by conservation laws which are mathematically expressed by means of the Navier-Stokes equations, which comprise a set of partial differential equations. Nowadays, the use of Computational Fluid Dynamics (CFD), technology to simulate the flow of complete aircraft configurations, has made it possible to obtain very impressive results with the help of high performance computers and fast numerical algorithms.

There exist some cases that successfully employed DOE in the airfoil or blades optimization design. Lian and Liou [5] in order to perform the NASA rotor67 transonic compressor blade multi-objective optimization design, to achieve the maximum stage pressure ratio and minimize the compressor weight. They used genetic algorithm to find the global optima of high-dimension design problems, while using the gradient-base method to accelerates the optimization convergence rate. After the optimization design, they obtained a stage pressure ratio increase 1.8% and decrease the weight by 5.4% compared to the baseline design.

Song and Keane [6] performed the shape optimization of a civil aircraft engine nacelle. The primary goal of the study was to identify the trade-off between aerodynamic performance and noise effects associated with various nacelle geometric features. Two objective functions were defined in the study: scarf angle and total pressure recovery. The authors argued that they obtained a design similar to the previous one, but requiring a lower computational cost because of the use of a reduced number of variables in the Kriging model.

Arabnia and Ghaly [7] presented the aerodynamic shape optimization of turbine stages in three-dimensional fluid flow, so as to minimize the adverse effects of three-dimensional flow features on the turbine performance. The authors adopted an artificial neural network based model. The design optimization result indicated that they were able to obtain design solutions which were better than the reference turbine design.

1.3 Aim and Objectives

The primary aim of this study is to develop and perform a multi-objective design optimization for high-lift configuration aircraft while taking the advantage of a surrogate model, which could reduce the huge computational involved. In order to achieve this purpose, the following objectives will be studied.

Objectives:

a) Literature Review for aerodynamic shape optimization design through surrogate modelling;
b) Develop a methodology to describe HLC airfoil;
c) Perform CFD based optimization for single airfoil;
d) Perform CFD based optimization for HLC airfoil.

1.4 Thesis Overview

Chapter 2: General reviews of factors affect flight economical, transonic airfoil and high-lift configuration airfoil aerodynamic design characteristic;

Chapter 3: deals with mathematical technical, such as computational fluid dynamic, Airfoil parameterize, Design of experiments, optimization methods and surrogate model construction;

Chapter 4: demonstrate a transonic airfoil optimization design based on surrogate model;

Chapter 5: demonstrate two High-lift configuration airfoils optimization design based on surrogate model, and a droop spoiler assist to improve high-lift airfoil performance;

Chapter 6: made a conclusion, unfolded an initial future work.

Chapter2. Literature review of Airfoil Design

2.1 Introduction

Referring to flight mechanic, aircraft act more or less like bird or some flyable insects basically. While they are flying, their wings generate lift to act against gravity, which is the same way airplane to stay airborn, as illustrate in Figure 2-1.

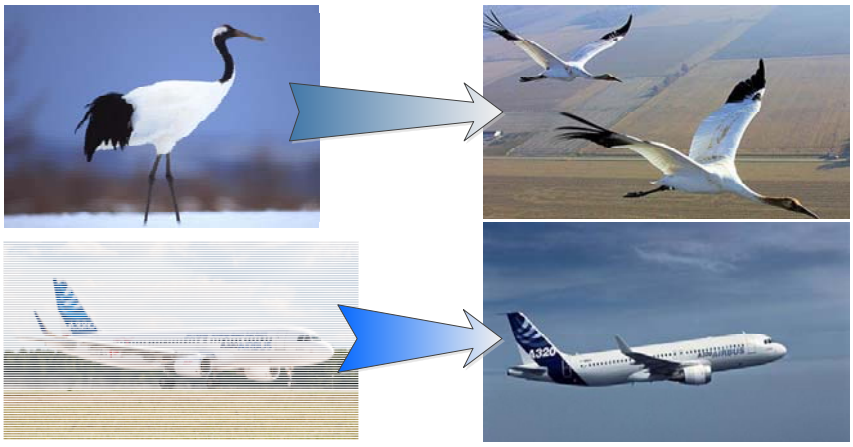

Figure 2-1: Similarities between birds and aeroplanes [8-11]

However, there exists significant difference between airplanes and birds. Birds can leave the ground and enjoy flight without having to grow huge and relative heavy parts attach on its body or under its wings to propel it. But airplanes require the help of some expensive, heavy; unwelcome both from airlines or its customers and environment unfriendly equipment---- engines. The cost expensive does not only refer to the cost to purchase it, but also includes the resource consumption, environment pollution, maintenance and even the huge part of the wing lift.

Even the aircraft engine, lets more accuracy refer to the jet engine are respected as the shining modern industry star, the main strength symbol and an important temperament aspect of airplane. It almost uses all the cutting-edge technology in it involves fields as aerodynamic, material and production crafts. Years by years to improve it's efficient by about 1% per year averagely [12]. While it still cannot fulfil the demand from the customers, which leaves another challenge to the airplane industrial companies.

2.2 Flight Economical

Transport Aircraft provide a fast, reliable mode of transport with no comparable alternative for long distance travel. Its overall mission is to carry safely the highest commercial value payload, with the minimum environmental impact and cost. Air travel continues to experience an averagely 4–5% [13] growth each year, although the energy intensity continues to decline. Aviation fuel consumption and emissions of many pollutants have risen. This trend gives the pressure to airlines and airline industries.

During the early development of aircraft, the attention was paid to aerodynamic efficiency is not too much. Structural design did not yet allow for cantilever wings, resulting in numerous struts and wires to support the aerodynamic forces. The huge amounts of parasite drag caused by these struts and wires prohibited true optimization of the external shape. This started to change during WWI, when speed and range became important for military aircraft. Since the drag of an aircraft scales with the square of its speed, drag reduction suddenly appeared high on the agenda [14]. Reducing drag also contributes to stretch specific range (SR) improves performance of aircraft, which is illustrated by Equation 2-1 [15].

$$SR = \underbrace{1/TSFC}_{engine} \cdot \underbrace{V \cdot L/D}_{aerodynamics} \cdot \underbrace{1/W}_{structure} \quad \textbf{(2-1)}$$

where $TSFC$ is the thrust specific fuel consumption, V is the speed, L is the lift, D is the drag, and W is the weight.

Energy intensity which expresses the energy consumption per available seat-mile of the transport system mainly depends on following aircraft parameters [16]:

- Engine efficiency, in terms of thrust specific fuel consumption, a method for Turbofan engine decrease TSFC is increasing bypass ratio.
- Aerodynamic efficiency, specifically the lift-to-drag ratio during cruise; that could benefit both from reduces friction drag and lift-dependent drag. Such as delay the laminar/turbulence transition and elliptic lift dis-

tribution, wingtip devices and flexible wing, this used to adapt different flight condition.

- Weigh efficiency, in terms of the share of payload in maximum take-off weight (MTOW) or the ratio between operating empty weight (OEW) and MTOW. It depends on structure efficiency, material Specific strength, system equipment integrated features, etc. ;

Throughout the years, technology improvements have been made to aircraft and engines to make them more fuel efficient. Historic trends in improving efficiency levels show that aircraft entering today's fleet are around 80% more fuel efficient than they were in the 1960's with the benefit both from the engines and aircrafts, which demonstrates in figure 2-2. The newest civil transport aircraft already reach the goal less than 3 litres per passengers/ 100km [17], this also benefit from the structure and aerodynamics efficiency improve (figure 2-3).

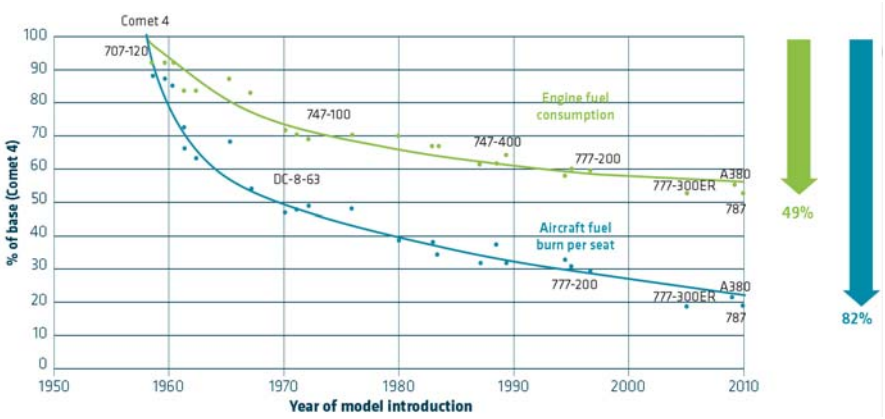

Figure 2-2: Fuel efficiency gains since the early jet age [12]

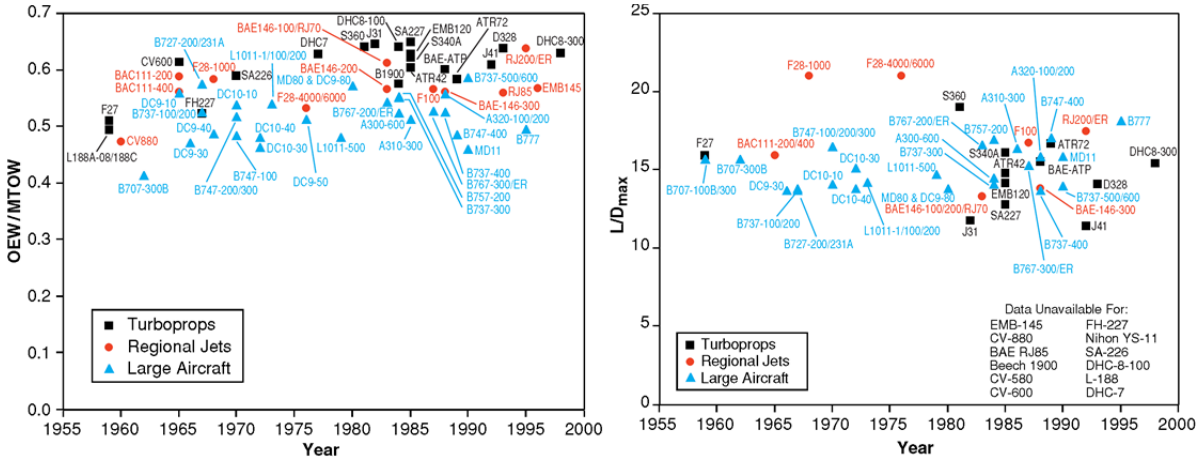

Figure 2-3: Structure and aerodynamics efficiency is increasing [18].

It should be mentioned that the operational impacts such as load factors, efficient routing, holding, weather impacts and delays also have an effect on energy intensity of the fleets [12].

2.3 Aerodynamic Design of Transport Aircraft

Transport aircraft design is a multi-disciplinary [19], multi-interaction and multi-iteration design process and activity. Hence, to design a challenging new aircraft, aircraft design engineer should have thoughtful consideration at its every aspect. How the newest civil aircraft Boeing 787 gets the benefit from different disciplinary is shown in figure 2-4. It shows that aerodynamics offer a big contribution to its whole performance improvement.

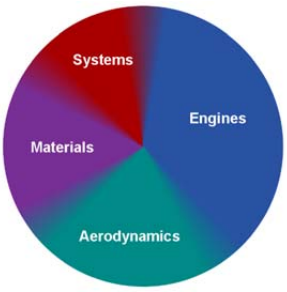

Figure 2-4: Advanced technology contributions to improve B787 efficiency [20]

The statistics showed between 1960 and 2000, aerodynamic improvements contributed 27% to overall improvement, and 87% component contribution to the energy intensity improve excluding the contribution from engine improvement [16].

To improve the aerodynamic efficiency, more clearly to say to reduce drag while generating the same amount lift, focus could be paid to the following kinds of work [21; 22]:

- Lower drag fuselage: direct reduction of turbulent skin friction drag, better fuselage section area distribution to reduce pressure drag.
- Lower interface drag: optimization the couple between wing, fuselage, power platform and tail.
- Higher efficient wing: utilize sophisticated winglet; efficient high-lift devices; high aspect ratio elastic wing; and variable airfoil camber continuous trailing edge flap.

2.3.1.1 Principle of Drag

If an object has motion relative to a fluid, the fluid always produces some force try to stop or decrease the speed of the object, it is called drag. Meanwhile the object will push the air downward and forward as illustrated in figure 2-5, the disturbed air mass will have a vertical and horizontal displacement ΔY and ΔX relative to the ground, that respectively corresponding to lift and drag, For a Boeing 747-400 Cruising at 39000 feet, the mass around the wing is about 42 tones per second [23].

According to the theory aerodynamic, drag exists since the fluid has the natural property of viscosity, which is the reason panel method does not arise any drag when it deal with inviscid flow field around airfoils [24]. Hence, In order to overcome the drag and to maintain the flight speed, the flying object should do some effort to overcome it. Birds need to flap their wings, to induce some mass of air downward and backward. That is the reason migratory birds double their body mass by means of fat storage before flights over large inhospitable areas [25]. It was reported that the famous reconnaissance aircraft U-2 can glide about 265 nautical miles with the penalty of losing 70000 FT [26] altitude at the condition of losing propels. Boeing 747 consumes roughly 3 percent of its own weight each hour [27].

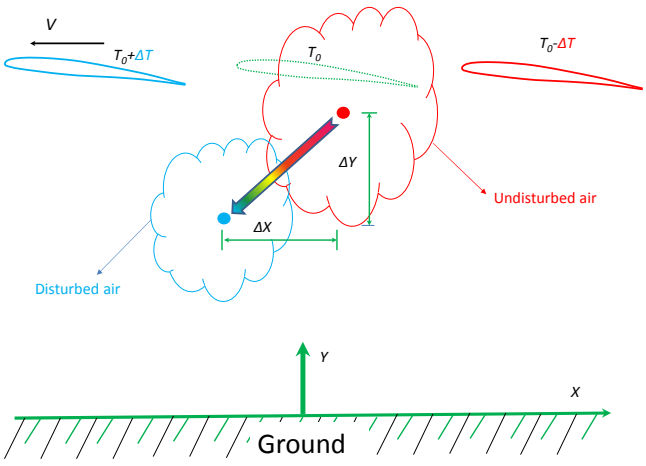

Figure 2-5: Flight object affect static air

Drag is not just the challenge for flight, but also is the enemy [28] of the flight economy. As to the Concorde, the payloads have the relationship with drag as:

a one count drag increase (Δ CD = 0.0001) requires 2 out of the 90 ~ 100 passenger capacity, be taken off from the North Atlantic flight [29]. For a typical long range transonic aircraft as A340-300, 3% total drag reduce can bring the airlines about US$ 1 million more profit from each aircraft per year [30].

Drag is the integral of flow direction momentum change of extreme number air molecules due to them striking on the aircraft shell. In order to describe the ways drag is made, we artificially name the drag as [28]:

- Friction Drag: The drag on a body resulting from viscous shearing stresses over its contact surface ;
- Form Drag: The drag on a body resulting from the integrated effect of the static pressure acting normal to its surface resolved in the drag direction.

There exits some ways to reduce the friction drag, the simplest one also is a intuition method, increase the quality of airplane surface smoothness, maximum the laminar flow area, this work heavy rely on manufacturing technology; figure 2-6 demonstrates a histrionically airplane surface changed from "*fried egg*" to "*boiled egg*". The second method is give a proper thickness distribution, keep the leading edge suck peak lower certain value, maintain the negative pressure gradient along the boundary flow at a certain level, delay the transit at the upper surface of the wing. Some research had been done base on bionics from the shark skin function, to reduce the aircraft's total drag by about 4%, but particulate matter in the air will contaminate the surface [30].

Figure 2-6: Surface comparison between early and currently aircraft [31; 32]

For an airplane, the total drag come from the cumulative component drag of nacelle, wing, fuselage, tail, landing gear and other structures. When put them as components of a whole aircraft, the total drag could be changed due to the factors as interference, trim, compressibility, lift, volume, cooling, exposed surface area, etc. Since these factors affect the total amount and distribution both of frication and form drag. The relationship between them could refer to [28]. Typical civil transport aircraft cruises drag breakdown and possible reduction potential shows in figure 2-7.

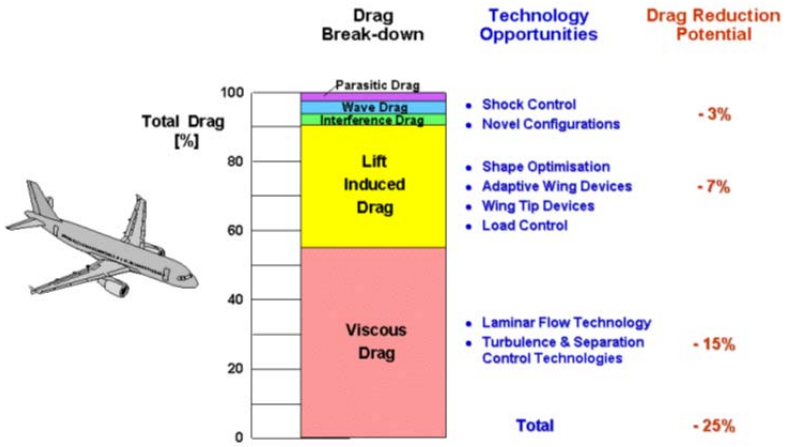

Figure 2-7: Drag Breakdown of Transport Aircraft in Cruise [15]

2.3.1.2 Principle of Transport aircraft wing design

The fundamental of aircraft aerodynamic design is the ability to estimate the lift and drag capability of the aircraft in various configurations and phases. All components will need to be considered in the total estimation process but the wing is the most significant component.

The functions of all of the airplane main components are significant differently. Fuselage shape and size is mainly determined by the requirements from the payload. Nacelle shape is associated with engine geometry and flow requirements into and away from the core engine. Tail sizing is mostly a function of stability and control requirements. On the other hand the wing size and shape has considerable impact on the lift and drag of the aircraft. Careful selection of the wing geometrical features will be a central issue in the design of the aircraft to meet lift requirements and to reduce overall drag.

The wing is the surfaces that support the aircraft by means of dynamic reaction on the air. Any aircraft may have several wings as fixed with respect to the fuselage or have any of several motions as helicopters or ornithopters [33]. it produce almost all the lift to balance the airplane weight, which takes the role as landing gears when the airplane stay on ground in term of fly mechanics.

Transport aircraft, normally have a fix wing relative to the fuselage, it use the terms wing area, span, aspect ratio, taper ratio, airfoil profile(Figure 2-8), thickness distribution(Figure 2-9 left), twist distribution (Figure 2-9 right), sweep angle(Figure 2-10), incidence angle (Figure 2-8 left top), dihedral angle (Figure 2-8 right) to describe the wing size ,layout and installation relationship relate to fuselage.

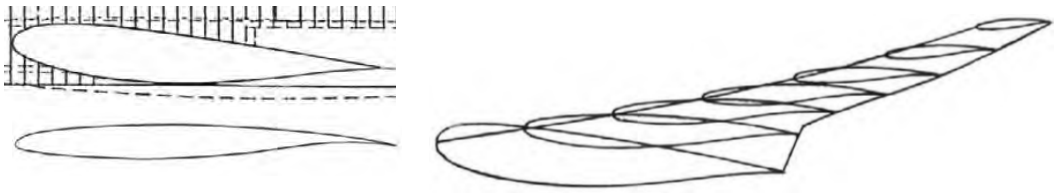

Figure 2-8: Wing root and outer sections (A380) and wing sections (A340) [34]

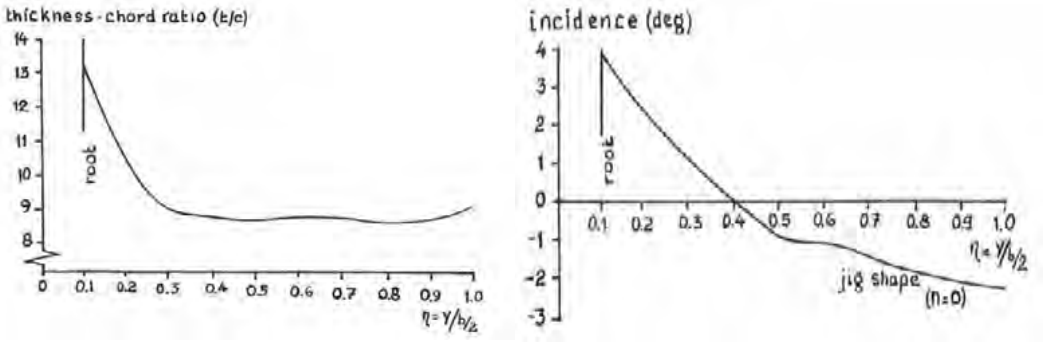

Figure 2-9: Wing span wise thickness and twist distribution (A380) [34]

In order to reduce transonic drag, almost the entire transonic airplane wing has the feature of sweep; figure 2-10 left curves demonstrates the CD vs. Ma at different sweep angles; it demonstrates a bigger sweep angle can delay the CD increase sharply at bigger Mach number. According to the sweep theory the effective Ma, CL and airfoil thickness have the relationship shows in table 2-1 [34].

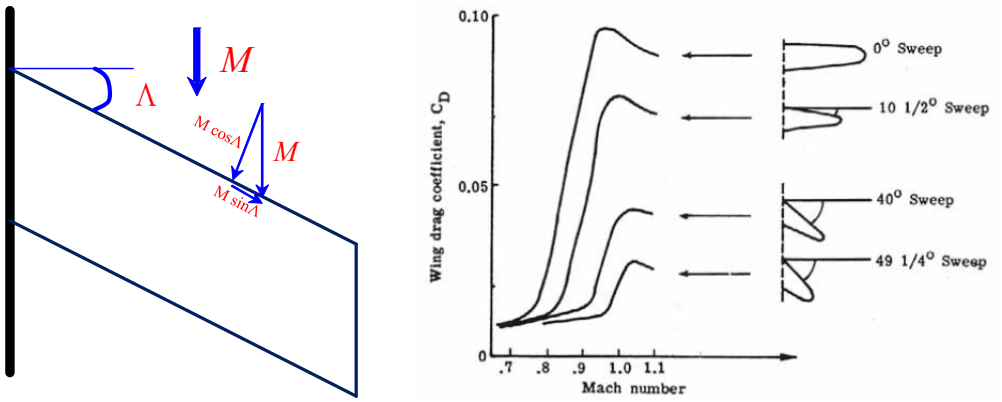

Figure 2-10: Effects of sweep on wing transonic drag coefficient

Table 2-1: Sweep effect to aerodynamic design

3D Quantity	Value for equivalent 2D Airfoil
M	**M cos Λ**
CL	**CL sec ^{2} Λ**
(t/c)	**(t/c) sec Λ**

Wing design involves multidisciplinary and is an extreme challenge task in the whole aerodynamic design subject of the aircraft, its main design parameters can be identified under four aspects [35]:

- Performance requirements

"The performance requirements will have to be considered in the conceptual phase. The size of the wing necessary to meet the mandatory (airworthiness) requirements and the design (specification) requirements will need to be evaluated. Certain climb rates and operating speeds will be laid down in the airworthiness requirements. The design requirements will specify the field length and cruise speeds."

- Flying qualities

"Ensuring that the aircraft flight handling qualities are acceptable will affect the choice of wing geometry (e.g. wing platform will dictate the stall and post-stall behaviour of the aircraft at low speed). The design requirements will specify the field length and cruise speeds. At high speed, aeroelasticity and aerodynamic buffet will be criteria to be considered. Vehicle ride will be affected by the gust responsiveness of the wing but this may be alleviated by automatic flight control systems coupled to wing surface controls. For control and stability, Dutch roll and lateral response will be important parameters. Again these may be beneficially influenced by the aircraft automatic flight control systems. The influence of wing platform on flying quality is difficult to predict and often results in 'fixes' to correct inherent deficiencies. "

♦ Structural framework

"The main criteria for structural considerations are safety and minimum weight. The wing structural framework must support all the non-wing components (e.g. engine, undercarriage), house all the flying controls and the high-lift devices (e.g. ailerons, flaps, airbrakes, etc.). Within all these requirements, the wing must be easy to manufacture and simple to maintain throughout its full service life. "

♦ Internal volume

"The internal volume of the wing should be sufficient to hold the required fuel and the landing gear (if retracted into the wing profile) and the high-lift devices and other control surfaces and its actuators."

A typical wing section is shown in figure 2-11, the shell of the airfoil is used to general the aerodynamic, and the spars and the stiffeners are used to transfer the forces and moments of the wing, while the space between the spars normally used to contain the fuel.

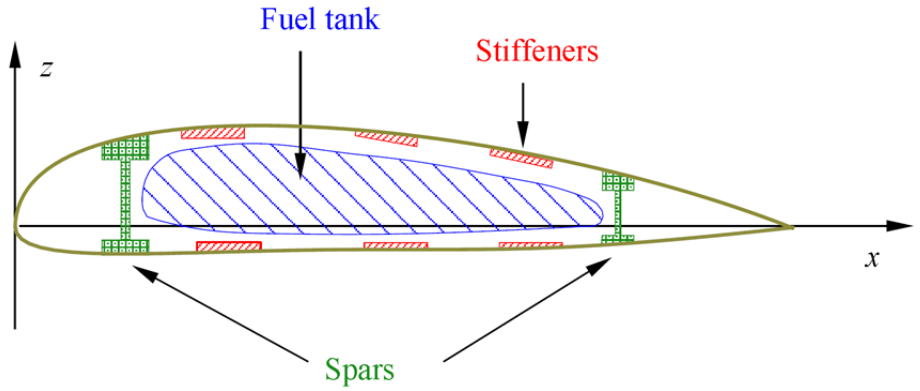

Figure 2-11: Internal components of a wing [36]

The wing not just has the properties as terms used to describe its fix geometry in pre-sections, passengers next to the cabin window may found that the wing have some change when they close to the airport, the main change is from the use of high-lift devices to form a high-lift configuration. A jumbo aircraft's [37] high-lift device layout is shown in Figure 2-11.High-lift device will have a more deeply discuss in following contents.

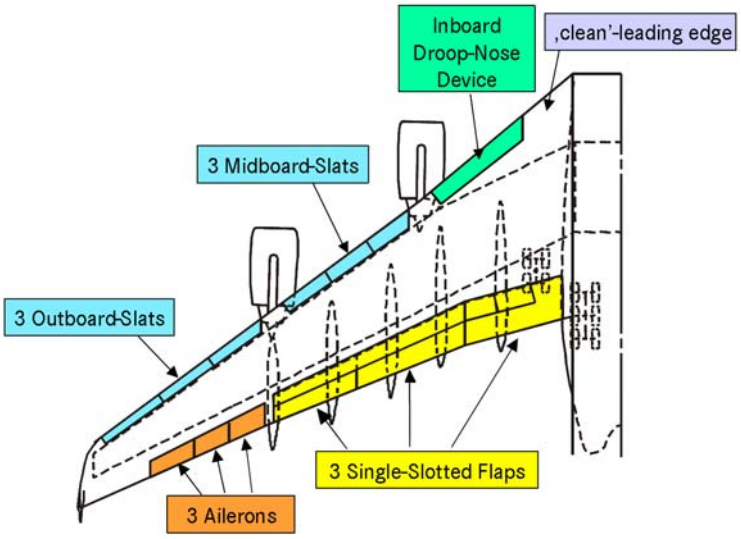

Figure 2-12: Airbus A380 wing high-lift devices layout

The mainly use for increase CL when the aircraft experience the flight phase such as takeoff, approach and landing, for the lower flight speed cannot have dynamic pressure as in the phase of cruise. Today, engineers used the droop-spoiler which trailing edge downward deflection to achieve airfoil variable camber function [38], so the whole fly process, the wing can offer a better fly-adaption, it can further improve the aircraft aerodynamic performance (Figure 2-12), this issue will be discussed in the following sections.

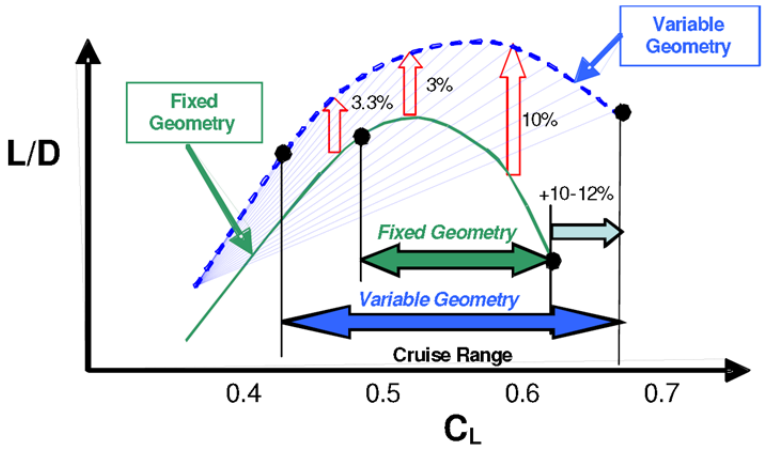

Figure 2-13: Aerodynamic efficiency improves from variable camber airfoil [39]

2.3.1.3 Principle of airfoil design

Airfoil is 2-d profile from wing or propeller; it is the important design point of the airplane in many respects. The airfoil affects the cruise speed, takeoff and landing distances, stall speed, handing qualities (special near the stall), and overall aerodynamic efficiency during all phase of flight [40].

The detailed specification of airfoil profile shape requires the definition of wing chord length, camber shape, maximum thickness and the leading edge, LE, radius as shows in Figure 2-14. To generalise the geometry, the lengths are Non-dimensionalized by dividing each parameter by the chord length to create a ratio (e.g. thickness/ chord ratio). Airfoil section data available at the conceptual design stage will be related to two-dimensional flows over a constant section shape. This data will need to be modified to take account of three-dimensional flow conditions and to integrate the changing section shapes along the wing span. The sectional shape will vary along the wing span to provide smooth chordwise flow conditions over the different parts of the wing and to guard against outboard (tip) stalling of the wing (figure 2-8).

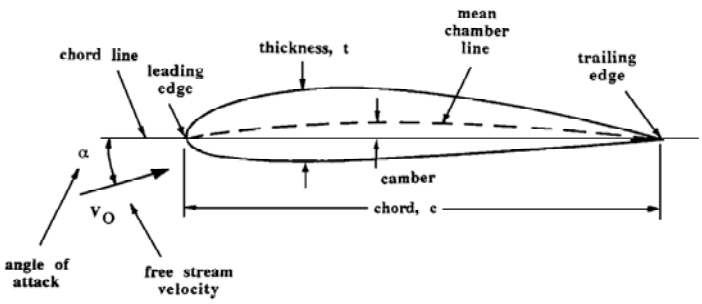

Figure 2-14: Airfoil definition parameters

Wing's aerodynamic characteristics will be strongly affected by wing sections, due to the section shape will determine the maximum practicable lift coefficient CL, stall characteristics, lift curve shape (CL versus wing incidence angle), profile drag, critical Mach number and shape and extent of compressibility drag rise. An example of the airfoil aerodynamic characteristics is given in figure 2-15. All these criteria are important as they dictate overall aircraft operational and design parameters. The pressure distribution integration around the airfoil will pro-

duce another important aerodynamic character Moment, it not only relate to handling characteristics, but also have a certain degree of influence to the aircraft performance, owing to the undemand pitching moment requires some aerodynamic control surface to trim it, which will reduce lift and increase drag to the whole aircraft.6

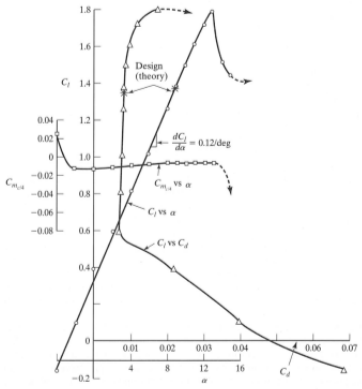

Figure 2-15: Experiment lift curve, drag polar and pitching curve for airfoil [41]

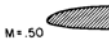

Figure 2-16: Progression of shock waves with increasing Mach number [42]

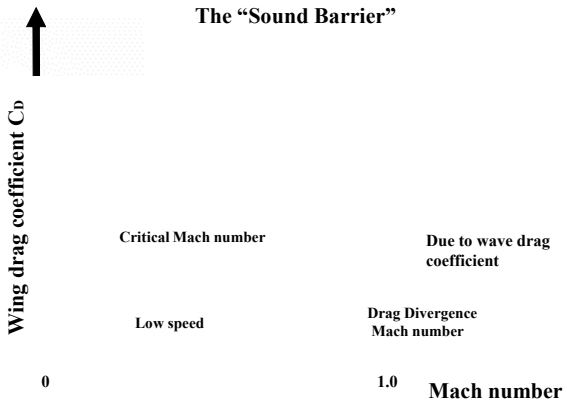

Figure 2-17: Sketch of the variation of profile drag coefficient with free-stream

Mach number, illustrating the critical and drag-divergence Mach numbers and showing the large drag rise near Mach 1 [43]

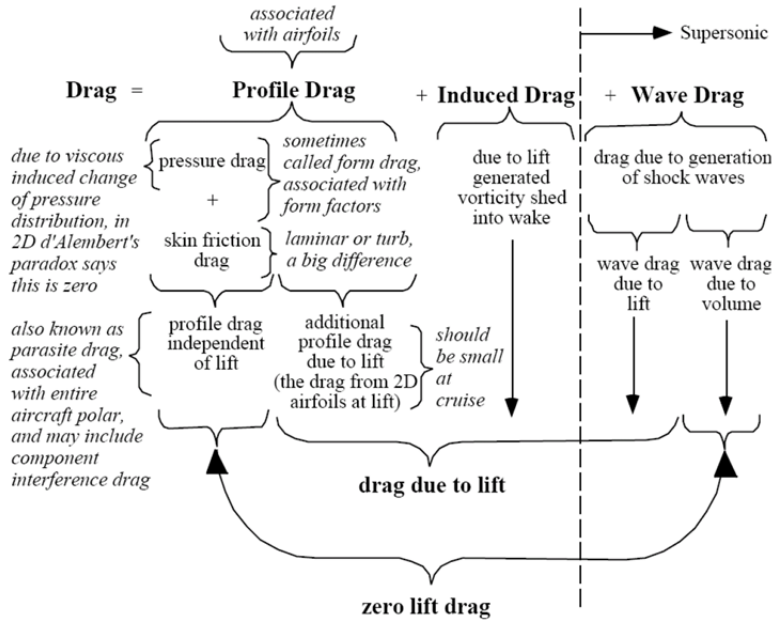

Figure 2-18: A broadbrush categorization of drag [22]

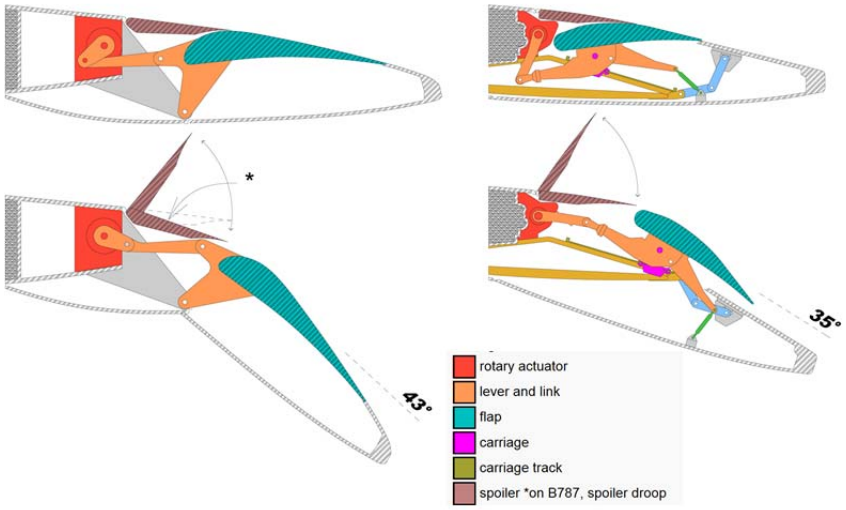

Figure 2-19: Variable camber airfoil [44]

To design efficiency wing for aircraft, or could use the term of high lift-drag ratio. It takes the most design circle and human resource in airplane industrial Company for a new serial aircraft.

Selecting an Airfoil is a part of the overall wing design. Selection of an airfoil for a wing begins with the clear statement of the flight requirements. For instance, a subsonic flight design requirements are very much different from a supersonic

flight design objectives. On the other hand, flight in the transonic region requires a special airfoil that meets Mach divergence requirements. The designer must also consider other requirements such as airworthiness, structural, manufacturability, and cost requirements.

2.4 Transonic flight

Transonic flow occurs when there is mixed sub- and supersonic local flow in the same flow field (typically with free stream Mach numbers from M = 0.6 or 0.7 to 1.2). Usually the supersonic region of the flow is terminated by a shock wave, allowing the flow to slow down to subsonic speeds. Therefore, shock waves, buffet, airflow separation, etc., take place above critical Mach number (figure 2-17).

For civil aircraft, transonic flight mainly occurs during cruise phase, current civil jet aircrafts normally have a cruise speed within Mach number from 0.78 to 0.89, within attitude from ISA 11000 to 13000 meters (mainly within stratospheric). Cruise phase is the main flying phase from the views of flight duration, speed and fuel consumption, the main airfoil performance requirement should follow the wing design requirement, and especially pay attention to:

- leave certain margin to drag diversity Mach number;
- Better low speed behaviour, which refers to Maximum lift and stall behaviour, it is good for HLC performance;
- A good thickness distribution to design high-lift devices, especially to flower flap.

Nowdays, there developed some airfoil such as supercritical airfoil and variable camber airfoil. The later uses a mechanical device to control the leading edge and trailing edge has some rotation moment, it deforms the whole airfoil profile, in order to suit different flight condition. When it use in transport aircraft, it mainly used to increase CL/CD in cruise flight phase.

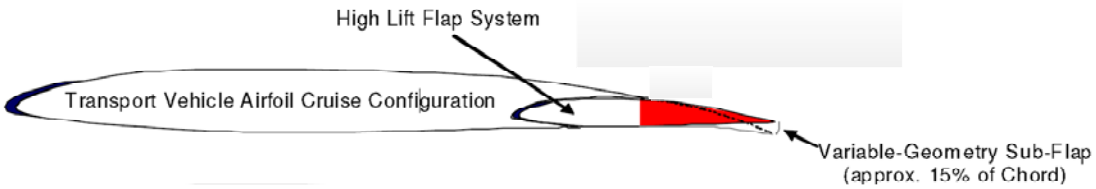

Figure 2-20: Variable camber airfoil [39]

2.5 Supercritical Airfoil

Supercritical Airfoil first proposed by Richard T. Whitcomb of Langley research central on the basis of intuitive reasoning and substantiating experimentation in the early 1960's. The Airfoil was made up by two parts as sketched in top of figure 1, the upper front portion and the lower trailing portion, between them there is a slot. When supersonic flow over a major portion of the upper surface and subsonic drag rise well beyond the critical Mach number. The Airfoil had a slot between the upper and lower surfaces near the three-quarter chord to energize the boundary layer and delay separation on both surfaces. A 2-D wind tunnel testing had shown that the this slotted kind airfoil have 0.14 bigger drag-rise Mach number than NACA 64A-series airfoil, at the condition of general same lift coefficient and same airfoil thickness [45].

Because of this kind slotted airfoil can have be used efficiently above critical Mach number with an extensive region of supersonic flow on the upper surface, it was named as “supercritical airfoil” . It was recognized that the presence of a slot increased skin friction drag and structural complications. Furthermore, both two-dimensional and three dimensional investigations of the slotted airfoil indicated that the shape of the lower surface just ahead of the slot itself was extremely critical and required very close dimensional tolerances. Because of these disadvantages, an unslotted or integral supercritical airfoil was developed in 1966, which was sketched in figure 1 middle.

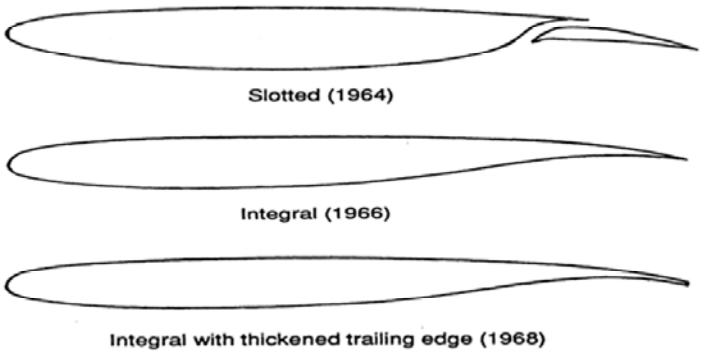

Figure 2-21: Progression of supercritical airfoil shape [45]

Compare to conventional airfoil, the supercritical airfoil have the properties:

- Well-Round leading edge (it offer the good base for leading edge high-lift device design);
- Relatively flat upper surface (The airfoil has a flattened upper surface which delays the formation and strength of the shocks to a point closer to the trailing edge, Additionally, the shock- induced separation is greatly, decreased. The critical Mach number is delayed even up to 0.99. This delay represents a major increase in commercial airplane performance);
- Incurved camber at the trailing edge (The curvature of a wing gives the wing its lift. Because of the flattened upper surface of the supercritical airfoil, lift is reduced. However, to counteract this, the new supercritical wing has increased camber at the trailing edge. The incurved camber narrowed the flap contour design space)

There are two main advantages of the supercritical airfoil as shows in figure 2-14. First, by using the same thickness-chord ratio, the supercritical airfoil permits high subsonic cruise near Mach 1 before the transonic drag rise. Alternatively, at lower drag divergence Mach numbers, the supercritical airfoil permits a thicker wing section to be used without a drag penalty. This airfoil reduces structural weight and permits higher lift at lower speeds for its round leading edge and bigger thickness.

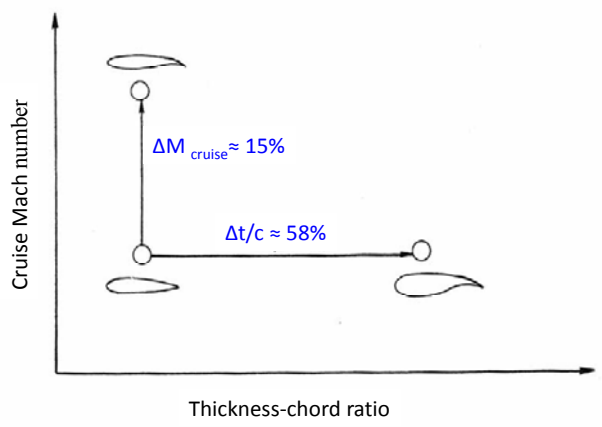

Figure 2-22: Two uses of supercritical wing [46]

Supercritical wings are routinely used even for subsonic aircraft; some documents had reported the jumbo civil aircraft airbus A380 uses the airfoil similar to SC (02)-0610 at wing root section [47].

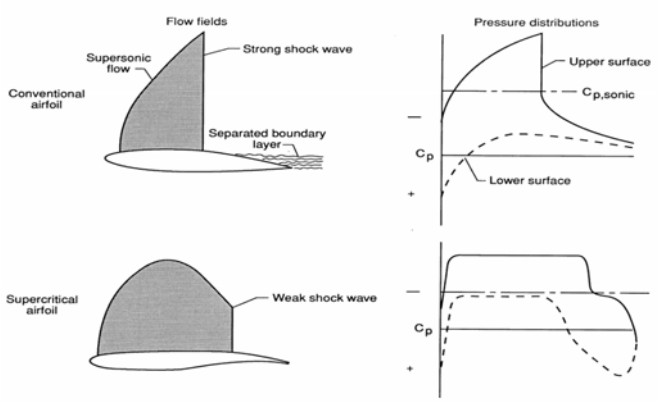

Figure 2-23: flow fields around supercritical and conventional airfoils [45]

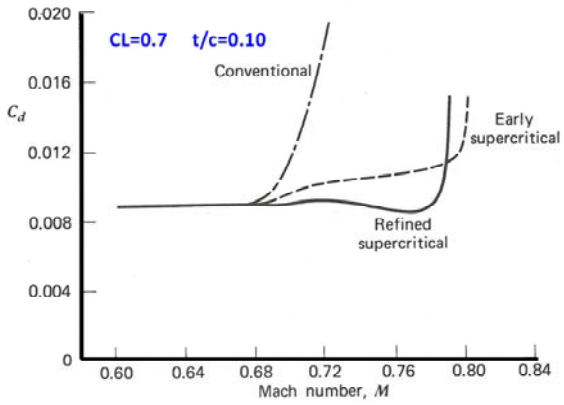

Figure 2-24: Example of airfoil drag rise date [48; 49]

2.6 Low-speed Flight

Before an aircraft layout can be stated, the three most dominant parameters should be specified; they are aircraft weight, engine thrust and wing size. Design philosophies between these three parameters could be mentioned as [40]:

1) *A heavy aircraft need a more powerful engine which may bring a heavier engine and more fuel consumption, it will cause a heavier aircraft. Meanwhile, at a given flight speed, the heavy aircraft needs bigger wing size to produce more lift to balance its gravity, while the bigger wing size could add another weight to the aircraft.*
2) *A more powerful engine may bring aircraft good accelerate performance, especially during the phase of takeoff, while in the phase of the cruise, as the engine' thrust/weight ratio goes to decrease. Another aspect is the powerful engine need a stronger structure to support it, which means a heavier structure weigh.*
3) *A bigger wing size could offer a good takeoff/ landing performance, while in cruise phase, it may not so efficient, its bigger size could bring additional weight and friction drag to the aircraft, and both of them are unwelcome in terms of the economical.*

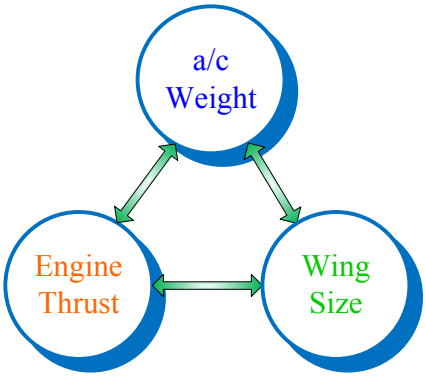

Figure 2-25: Three main parameters determine the transport aircraft performance

The early slow commercial airplanes did not require high-lift systems because their wing loadings were low and their speed ratios between cruise and low speed (takeoff and landing) were about 2:1. But Simple trailing-edge flaps can improve pilot vision over the nose by reducing attitude during low-speed flight [50].

High-lift configuration for transport airplane normally used at the flying phase of takeoff, approach and landing, for these flying phases the dynamic pressure is lower, it is hard for the wing to general enough lift with the cruise configuration airfoil, hence, it is necessary to development some

$$L = Q \cdot A \cdot C_L \qquad \textbf{(2-2)}$$

Where: L is lift force; $Q = \frac{1}{2}\rho v^2$ is the dynamic pressure, ρ is air density; v is true airspeed; A is wing planform area, and C_L is the lift coefficient at the desired AOA, Mach number,and Reynolds number.

As commercial-airplane cruise speeds increased with the development of more powerful engines, wing loadings increased and a real need for high-lift devices emerged to keep takeoff and landing speeds within reasonable limits. The high-lift devices of that era were generally trailing-edge flaps. When jet engines matured sufficiently in military service and were introduced commercially, airplane speed capability had to be increased to best take advantage of jet engine characteristics. This speed increase was accomplished by introducing the wing sweep and by further increasing wing loading. Whereas increased wing loading called for higher lift coefficients at low speeds, wing sweep actually decreased wing lift at low speeds. Takeoff and landing speeds increased on early jet airplanes, and, as a consequence, runways worldwide had to be lengthened. There are economical limits to the length of runways; there are safety limits to takeoff and landing speeds; and there are speed limits for tires. So, in order to hold takeoff and landing speeds within reasonable limits, more powerful high-lift devices were required.

The High-lift device is necessary, since wings sized for efficient cruise are too small to take-off and land in reasonable distances. As a simple calculation had demonstrated by C.P. van Dam, if use a lager single-element wing which could have the same landing performance as the airplane equipped with High-lift devices, it will bring the cruise efficiency $M_\infty L/D$ 18.3% down [51].

Early HLCs designs focused mainly on maximum lift requirements to satisfy the high cruise wing loading needs of jet transport aircraft while retaining acceptable take-off and landing distances. Recently, the attention has turned to reducing the complexity and weight of the HLC device while keeping an acceptable lift level [50; 51] (figure 2-14). According to Rudolph [50], the high-lift system accounts 6%~11% of the production cost of typical jet transport. Another report presented by Meredith [52] who illustrated the HLC importance at the aspect of aircraft performance, as a generic large twin engine transport:

1) *An increase in maximum lift coefficient (CL) of 1.0% could bring 22 passengers or 4400 lb more payloads for a fixed approach speed on landing.*
2) *An improvement in lift-to-drag ratio of 1.0% during take-off translates into an increase in payload of 14 passengers or 2800 lb for a given range.*
3) *An increase ΔCL = 0.10 of the lift curve in the linear range results in a 1。Reduction in altitude for a given glideslope angle. This allows a reduction in required landing gear height of 14 in. for a given tail strike attitude angle and a decrease in OEW of 1400 lb.*

Takeoff and landing performance for subsonic civil transport airplanes are governed by the requirements as FAR part 25 [20], which illustrate in the figure A, in order to meet the low speed performance demands, it is necessary to obtain enough lift to balance the weight of the airplane according to the equation 2-2

As the total lift generated by the aircraft is constrained by the factor as air density, speed, effective area, and lift coefficient. Air density is a hard changeable nature variable, it is decided by the airport location and temperature. Speed is a factor that relative many other aspects, both with aircraft itself, airports facilities, airworthiness items, so that cannot change arbitrarily. However, some time we can take advantage of some favourable resources, for example, the aircraft always take-off or landing at the direction of agrees with the direction of the aircraft carrier navigation. The effective area is a possible way that can increase the lift, however, if alter the effective area too much, it could give the penalty to cruise phase since it not necessary to take the waste weight. The final option to keep the total lift that can balance the aircraft weight is to enhance the lift coefficient of the whole aircraft.

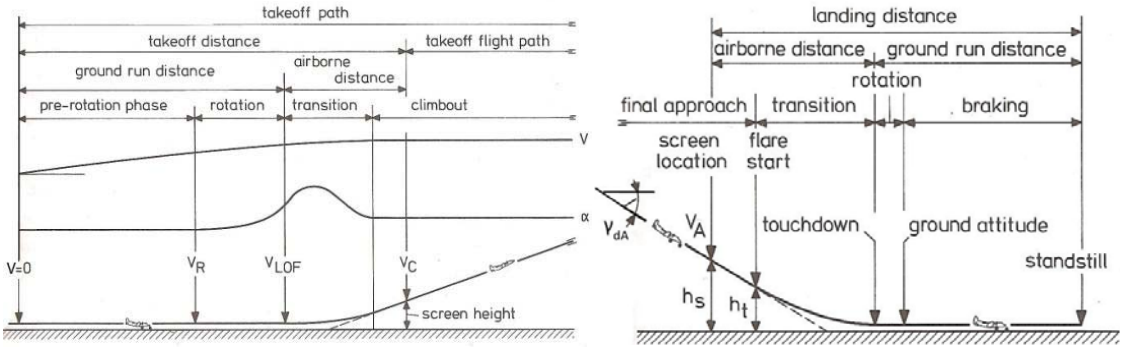

Figure 2-26: Takeoff and Landing procedure for civil transport airplanes [53]

Maximum lift coefficients for airplanes without any high-lift devices typically do not exceed 1.2 [51].

2.7 High-lift Configuration Airfoil

High-lift configuration normally constitute by leading edge device, main wing box and trailing edge device. The first and the third part calls High-lift devices, for their initial purpose used by engineering are to improve lift. Leading edge device mainly increase the maximum lift on the wing by preventing wing leading edge stall increasing the maximum angle of attack, but it reduce the whole configuration lift when the AOA below medium. Currently, almost all the new civil airplane uses a full span of leading edge devices. Main wing box is the biggest part in the High-lift configuration; it does not just take the role as moments and forces taker, but also the main lift generator. Trailing edge devices decrees the zero lift AOA, for it increase the whole high-lift configuration airfoil camber , thus increase the lift for a given angle of attack as shows in Figure 2-27.

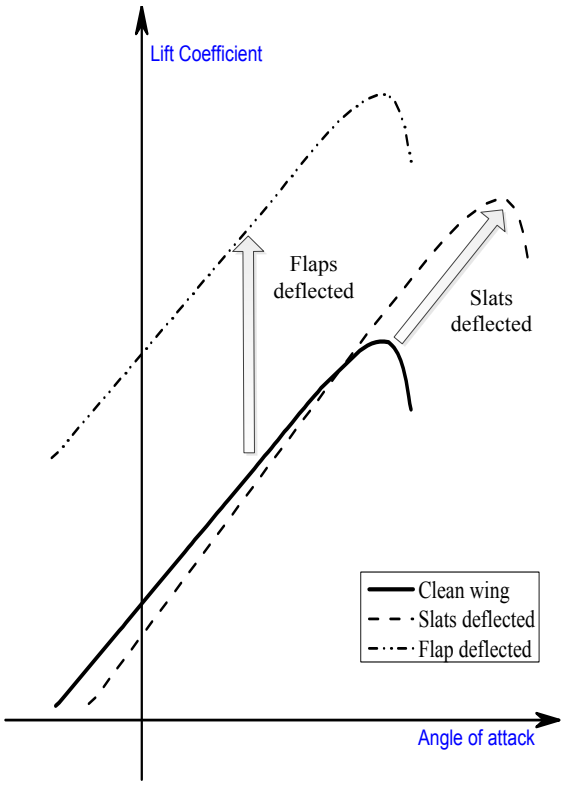

Figure 2-27: The effect to lift coefficient from slat and flap [34]

Table 2-2: Different High-lift device effect on aerodynamic characteristics

Type	Subtype	Schematic	maximum deflection angle δ_{max}	Reynolds number of test	Coefficient change at δ_{max}		
					ΔC_L	$\Delta C_{D(C_L=0)}$	ΔC_m
Nose Flap	*Hinged LE*		30°	$6 \cdot 10^6$	0.55 - 0.75	0.00	-0.09
Krüger Flap	*Simple Krüger*		40°-45° (straight wings) 60° (swept wings)	$8.2 \cdot 10^5$	0.50	0.00	-0.10
Slat	*Three-position slat*		26°-30° (straight wings) 45°-60° (swept wings)	$6 \cdot 10^6$	0.93	0.00	+0.11
Non-slotted Flap	*Split flap*		60°	$6 \cdot 10^6$	0.8	0.23	-0.275
	Plain flap		60°	$6 \cdot 10^6$	0.90	0.12	-0.275
Slotted Flap	*Simple slotted flap*		40°	$3.5 \cdot 10^6$	1.18	0.13	-0.33
	Single slotted Fowler flap		30°	$3.5 \cdot 10^6$	1.67	0.10	-0.42
	double-slotted flap		30°/55°	$6 \cdot 10^6$	1.4	0.23	-0.41
	Triple-slotted flap		30°/44°/55°	$6 \cdot 10^6$	1.6	0.23	-0.44

According to the thin airfoil aerodynamic theory, the lift was generated by the three factors, the airfoil camber, thickness and effect angle of attack for a given airfoil before the upper surface separation onset. The camber and the thickness will affect C_{L0}, while the AOA will continue change C_L value at a given flow condition, the lift coefficient normally increase due to a bigger angle of attack, but after a certain angle, the lift will not increase any more at the given fly condition. At a certain angle of attack, continue increase the airfoil angle of attack, the lift decline quantity due to the upper surface separation and cosine function act on lower surface lift contribution will be equal to the increase quantity from the area as the upper leading edge suck peak. At that point, the wing is going to stall. Stall is a natural behaviour in the subject of aerodynamic. Hence, in order to have a bigger lift coefficient, it should have a bigger stall angle, which means it is necessary to suppress the separation.

$$C_L = C_{L0} + 2\pi\alpha \qquad \textbf{(2-3)}$$

Where: C_L is the section lift coefficient, C_{L0} is the section lift coefficient when the incidence angle is zero, α is the incidence angle in radians, measured relative to the chord line.

According to the boundary layer theory proved by Prandtl, when a Streamline object moves in a fluid, on the contact surface between object and fluid, there exists a thin to thick boundary layer from the front edge to the backward, at some distance, the airstream near the surface will reverse direction, form a separation between the main flow and the object's surface, according to Bernoulli's principle,….., so in order to conquer the viscosity effect that cause the separation, there exist just two ways to: increase the Pressure at the beginning of the upper surface, and the second is weaken or eliminate the viscosity boundary layer. That is the role that the High-lift devices play.

Compared to a single airfoil, the High-lift airfoil should have at least one more portion. Generally, it has three or more portions to make the combination to be a high-lift airfoil. The addition portions may have different functions in the role to assist the whole airfoil to generate more lift, but all of them can be divided into two kinds of the high-lift devices, leading edge device and trailing edge device, according to the position relative to the main portion figure 2-30 and 2-31.

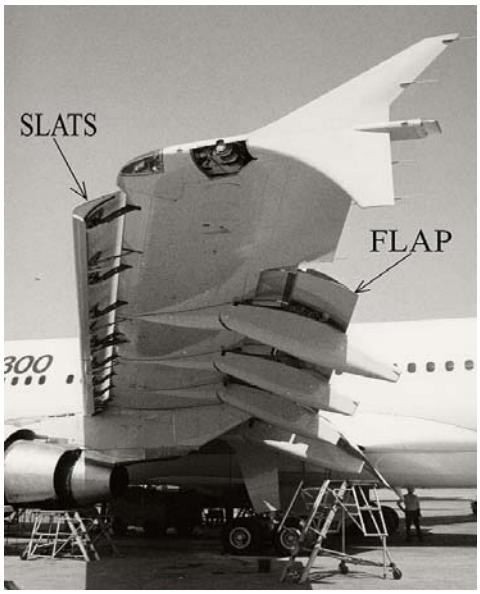

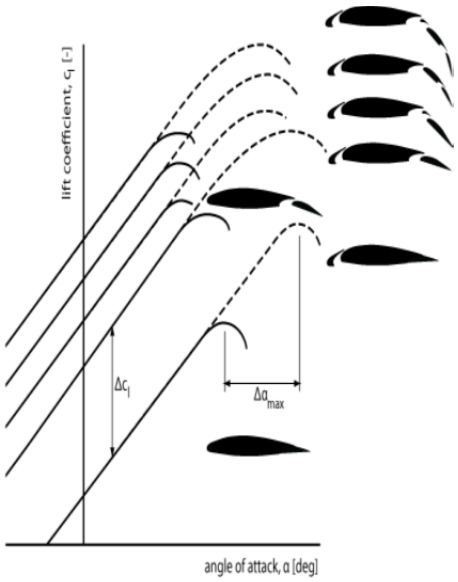

Figure 2-28: High-lift configuration [54]

Figure 2-29: Basic effect of high-lift devices on lift curve [34].

From the intuition view to understand the high-lift configuration, the HLC develop from a single airfoil, it increase the airfoil size, increase the camber and use the slots to eliminate the boundary layer, that could maximum the all parts lift contribution to the total lift force.

There exist many ways to recognize the high-lift elements interaction, According to A.M.O smith's theory [55] , the multi-elements have the following 5 effects.

- Slat effect: The velocities at the leading edge of the downstream element (main airfoil) are reduced due to the circulation of the upstream element (slat) thus reducing the pressure peaks of the downstream element (figure 2-28 left).
- Circulation effect (or vortex induce effect): velocities on an upstream element are increased and inclined to the mean line due to the circulation of a downstream element. Figure 2-28 right shows that a deflected flap can be represented by a point vortex, increasing velocities and thereby pressure differences on the upstream element. The larger pressure differences lead to higher lift generation. In terms of circulation of the upstream element, one can say that the increased flow inclined to the mean line implies circulation has to be increased to keep satisfying the Kutta condition, which makes sure the flow is smoothly leaving the top and bottom surfaces of the airfoil at the trailing edge.
- Dumping effect: The discharge velocity at the trailing edge of the slat is increased due to the circulation of the main airfoil thus alleviating separation problems or increasing lift (figure 2-29 left).
- Off the surface pressure recovery: The deceleration of the slat wake occurs in an efficient manner, out of contact with a wall (figure 2-29 right).
- Fresh boundary layer effect: Each new element starts out with a fresh boundary layer at its leading edge. Thin boundary layers can withstand stronger adverse gradients than thick ones (figure 2-29 right).

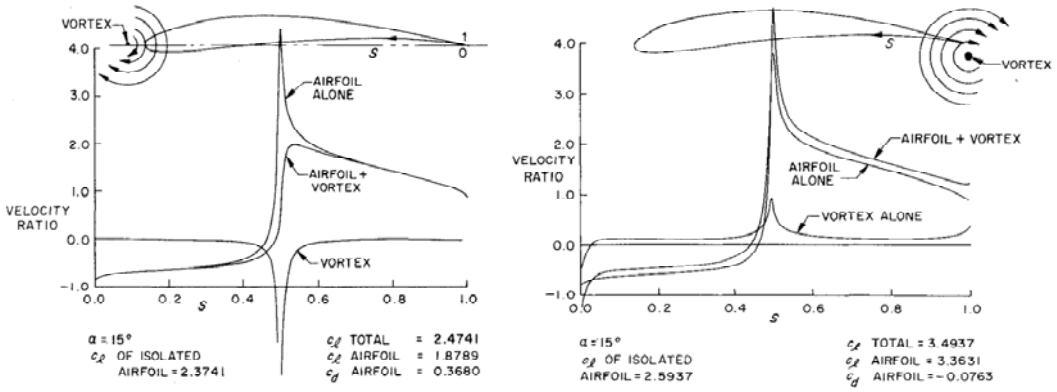

Figure 2-30: slat effect and Circulation effect [48]

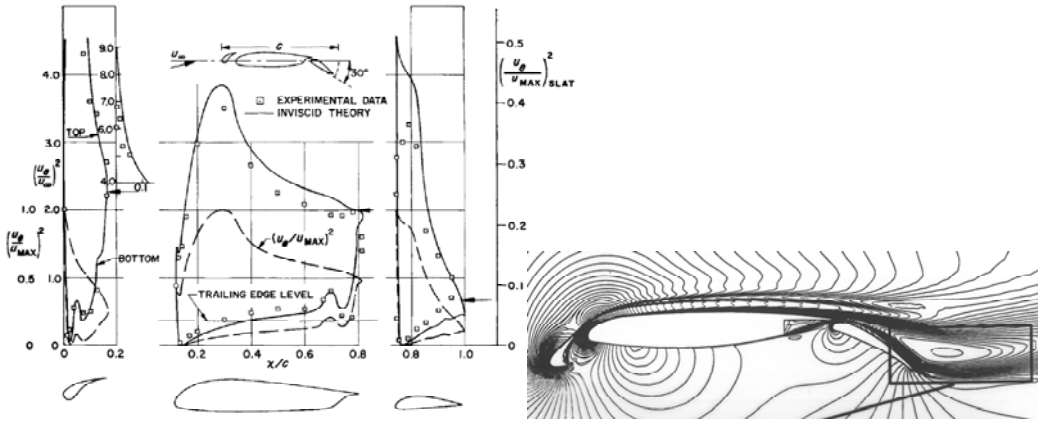

Figure 2-31: Interaction effects in multi-element high-lift devices [48; 49]

In another point of view from Obert, E. [34]:

- An increase in camber

It is well known that cambered airfoil sections have a higher maximum lift coefficient than symmetrical sections. But airfoil camber also produces (at excessive camber excessive) drag. This is why, already in an early stage of aviation history, variable camber was employed in the form of split or plain flaps.

- An increase in effective chord.

Deflection of a high-lift device can increase the effective chord length if there is a chord extension. A fixed-hinge flap with the hinge close to the chord line for example does not change the chord length, but a Fowler flap moves aft and does increase the effective chord. The same holds for a slat that usually moves

down and forwards thereby increasing the effective chord length. Chord extension increases.

- The mutual interaction effect.

The lift on an airfoil section can be analysed by replacing the actual section by a series of vortices on the section camber line. This series of vortices may vary between a continuous vortex sheet which allows the analysis of the chordwise lift distribution and a single vortex at the quarter chord position producing the total lift when the angle-of-attack is increased relative to the angle-of-attack for zero-lift, the zero-lift line. By means of Joukowski conformal transformations exact solutions without linearization can be obtained for the lift on a flat plate or a circle segment at any angle-of-attack.

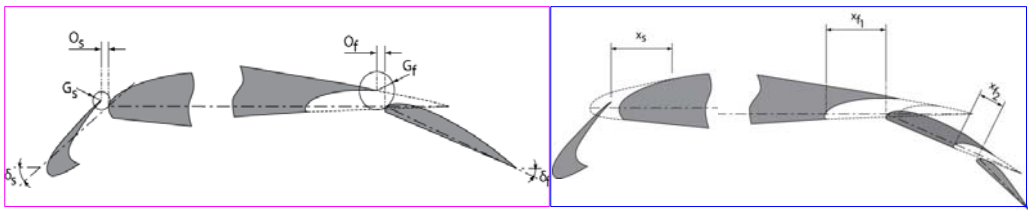

Figure 2-32: Definition of gap (Gs/Gf) and overlap (Os/Of) Fowler motion [50]

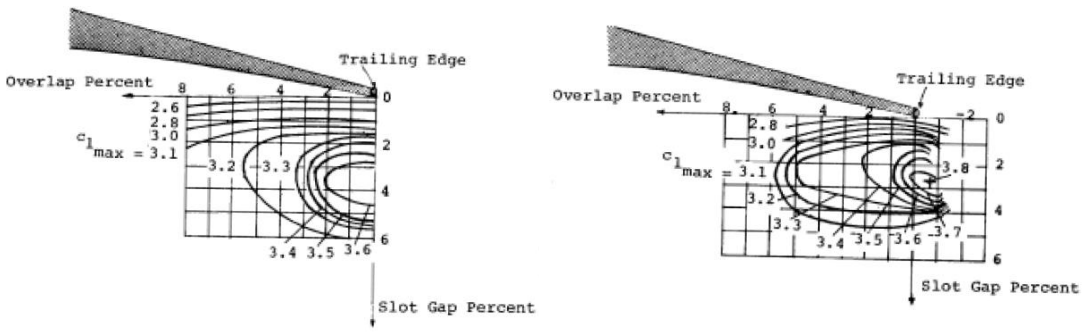

Figure 2-33: Constant C_{Lmax} loci for slot gap and overlap values

(Left 35° flap deflection, right 40° flap deflection, with single slotted flap and no LE device at Re = 2.2 to 2.9 million.)

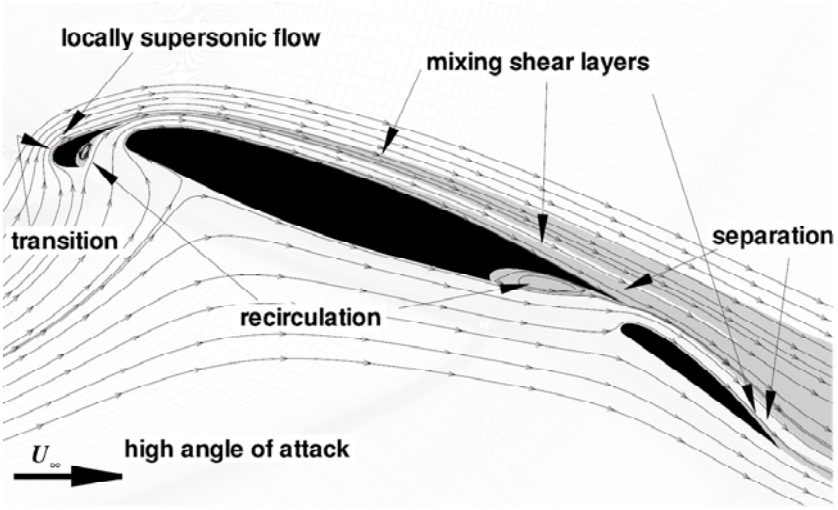

Figure 2-34: Flow field around the wing section of a 3-element wing [4]

2.8 Optimization design strategy introduction

This research use ANSYS Fluent 14.0 as the high fidelity aerodynamic characteristics evaluator, it will take the work as samples objectives evaluator and check the new potential points which suggested by optimizer based one surrogate model. And use Genetic Algorithm (GA) optimizer [56] to search the optimum from the surrogate model which construct by Kriging [57].

The airfoil is design for a civil transport wing, the optimization process started from cruise single-element airfoil, since the supercritical airfoil have the advanced for transport aircraft save fuel in cruise flight, so the transonic airfoil will do the research with supercritical airfoils. After get the optimum transonic airfoil at the mainly consideration transonic flight efficiency CL/CD, then base the optimum transonic airfoil to design the HLC airfoil, since the trend of currently civil aircraft is using simple HLC as shown in figure 2-35. As for this design step, it is necessary take the consideration CL/CD at the premise that the $\mathrm{CL} \geq 2.4$, as for this step it is necessary to define the contours of the main wing leading edge and flap leading edge.

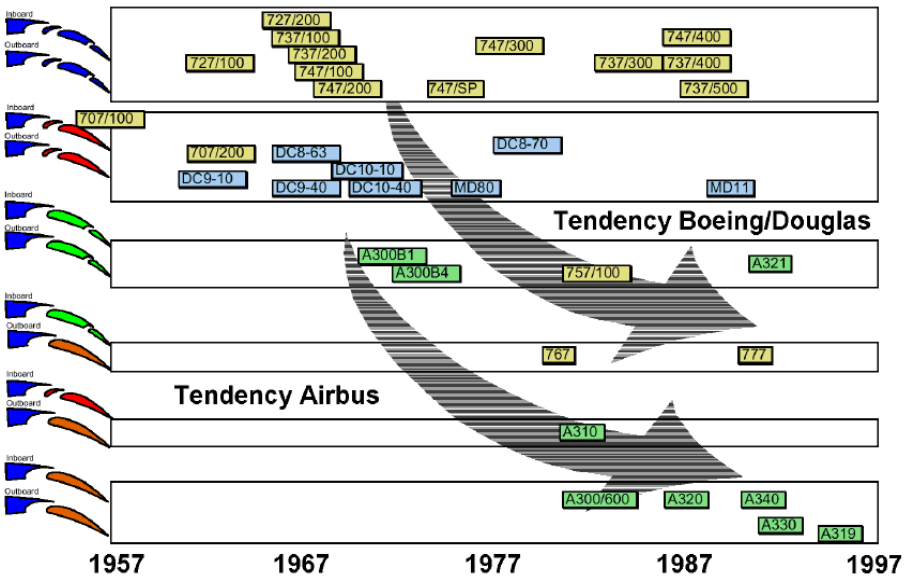

Figure 2-35: Evolution of high lift systems [58]

To provide transonic flight drag reduction, almost all wings have some sweep character, in order to reduce effect flow speed around the specific airfoil, to re-

duce to the wave drag. It brings the benefit that can delay the critical Mach number. In engineering there exist two ways to get the airfoil, the first one is parallel to the free airflow, the second one is perpendicular to an equal relate chord length for example as a quarter of the airfoil chord. The selection between them is up to their design philosophy. Physically their different airfoils can get a wing but the different Geometry relationship between two airfoils described by equation 2-1 and 2-2. From the equation 2-2, it is easy to find the thickness of the airfoil which cut by the perpendicular chord plane is thicker than the airfoil which cut by the parallel free stream, but as the flow around the limit span wing, it has the flow of 3-D, that means the airflow around the perpendicular airfoil is smaller, some literature give the equation as 2-3.

Since there used two methods to study the 2-D airfoil flow, for transonic airfoil, it use the airfoil that perpendicular wing 0.25 chord, and the HLC airfoil use the airfoil parallel free stream. The parameters about the geometry and effect Mach number follow the equations as:

In this research, the Multi-objective design of the HLC it assume a transport aircraft with a wing with 25 degree back sweep angle, and a typical wing section at transonic flight condition after taking consideration of sweep is the range from Mach 0.720 to 0.740, correspond to flight flow Mach 0.794 to 0.817 [34]. And the angle of attack is from 2 to 3 degree. It is assumed all the Reynolds numbers are unified as has the value as 20,000,000. After get the optimum single airfoil, and then design the high-lift configuration airfoil to maximum the CL/CD at the condition of $CL \geqslant 2.4$. Then from the single airfoil, setting the position of the slat upper and lower trailing edge position, and optimization the counter of the interface between the slat and main wing, for the HLC will use three elements equipment, the slat, main wing and flap.

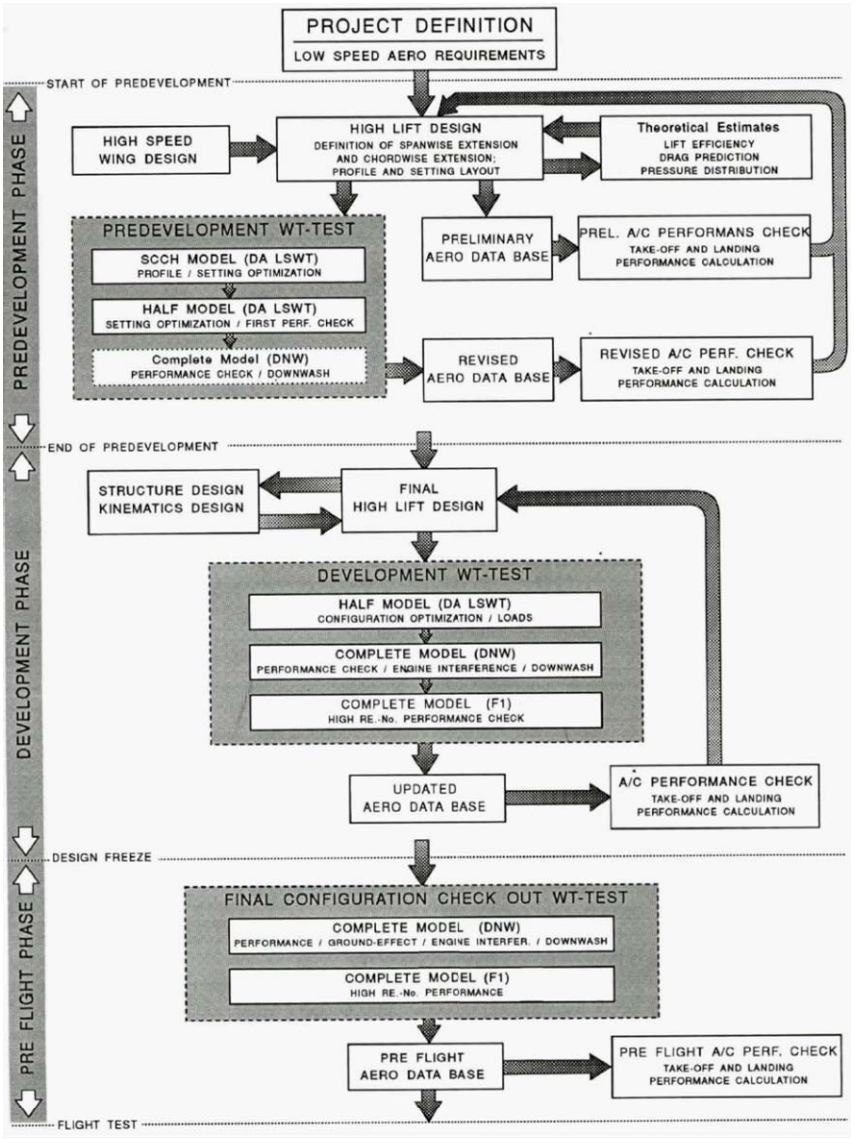

Figure 2-36: Scheme of High-Lift Design Process for transport aircraft [2]

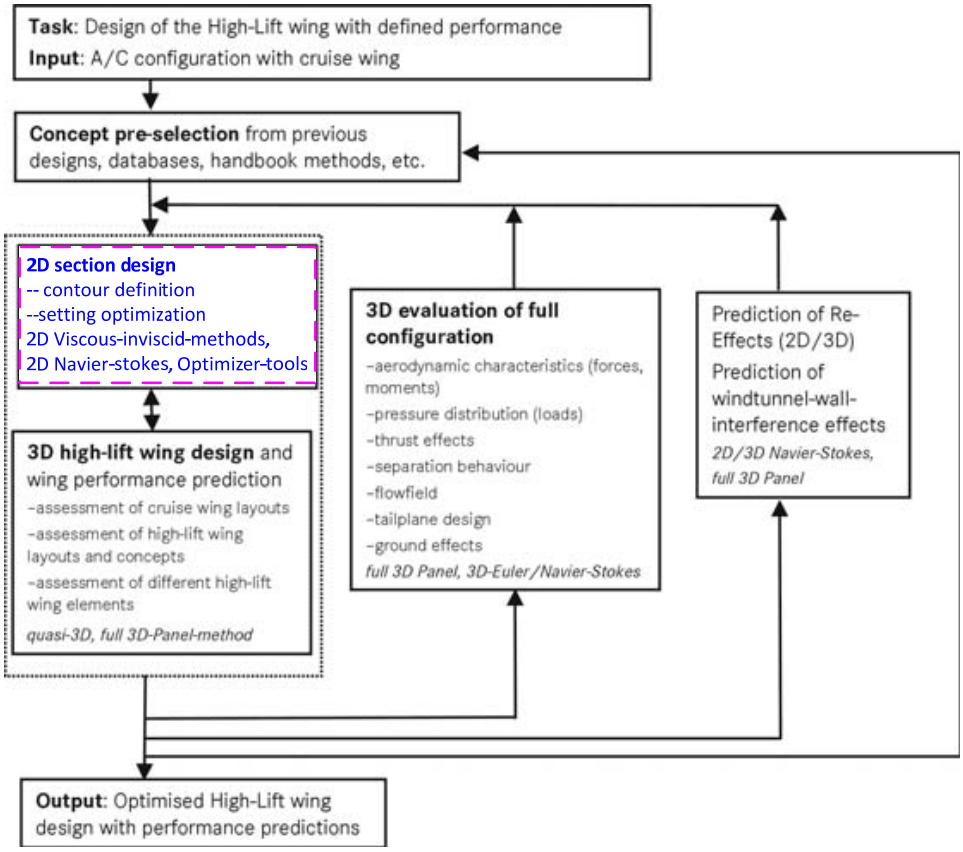

Figure 2-37: Sequence of the CFD-based high-lift design process [3]

High-lift configurations have a major influence on the sizing, economics, and safety of most transport airplane configurations. The combination of complexity in flow physics, geometry, and system support and actuation has historically led to a lengthy and experiment intensive development process [51].

Table 2-3: Optimization condition and objectives

Case	Transonic (9 conditions)			Takeoff	landing
Mach number	0.72	0.73	0.74	0.2	0.2
AOA (°)	**2, 2.5, 3**	**2, 2.5, 3**	**2, 2.5, 3**	8	10
Reynolds Number	20,000,000				
Object is Maximum	Average CL/CD			CL/CD @CL≥2.4	CL

This research will use an optimization design strategy as the flowing steps:

1 Optimization design single airfoil for transonic flow;

2 Optimization design HLC airfoil for takeoff;

4 Optimization design HLC airfoil for landing with the geometry from step 2.

3 Study drop spoiler effect on takeoff configuration airfoil;

for both the supercritical airfoil and HLC airfoil with Flower motion will produce relative bigger negative moment, which ask the horizontal tail produce certain negative lift to balance it to take a stable flight.

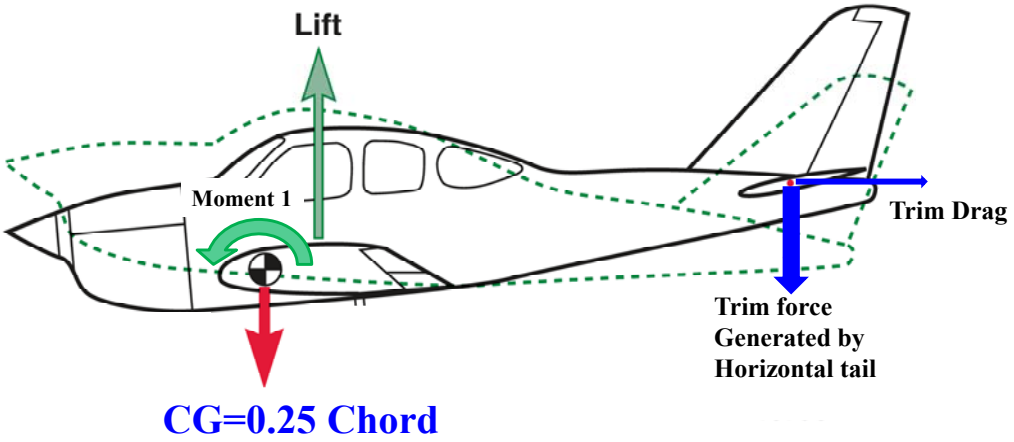

Figure 2-38: Pitch moment balance [59]

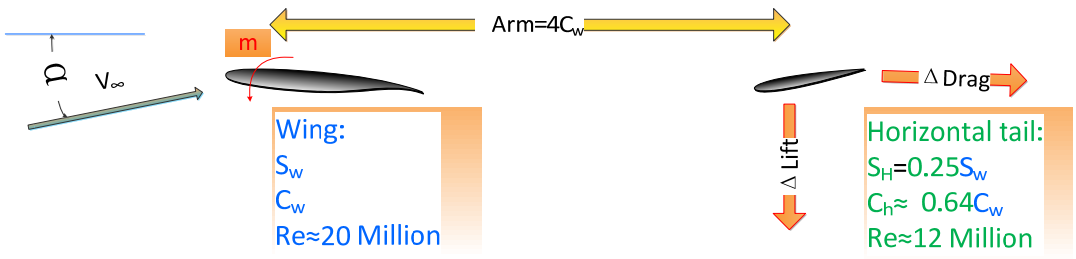

Figure 2-39: Horizontal tail trim affect to wing lift and drag

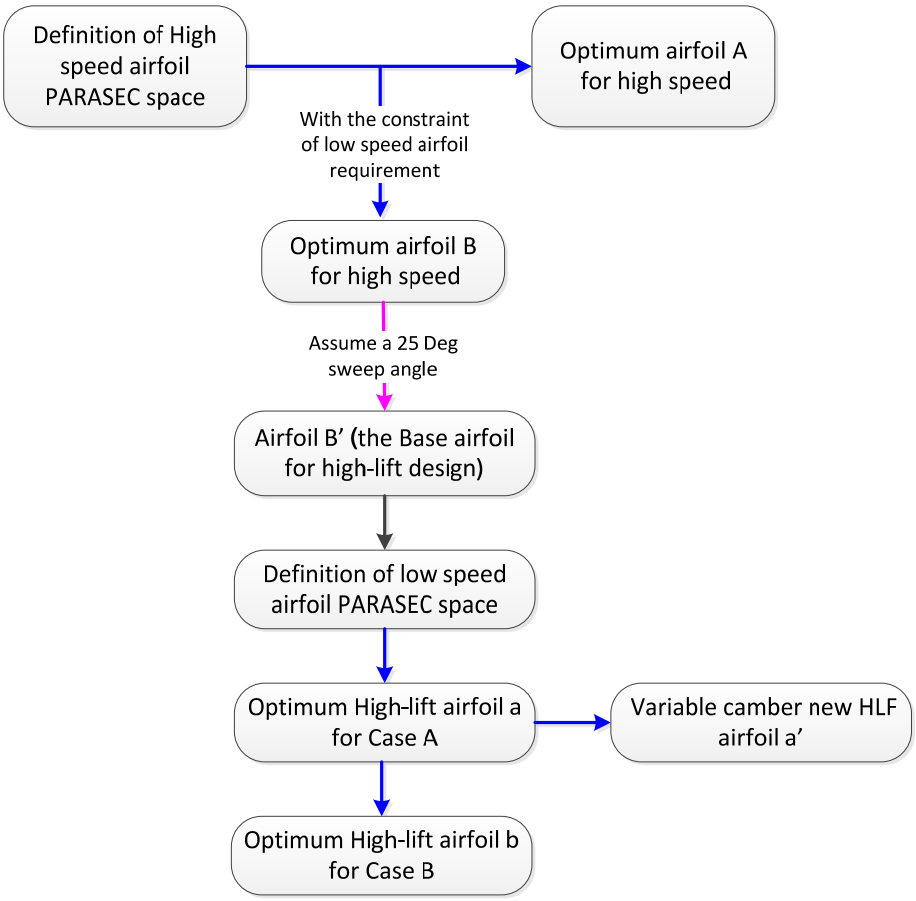

Figure 2-40: HLC airfoil optimization design process

Chapter3. Mathematical Modelling

In aerodynamic design and optimization (ADO) problems, a new design's aerodynamic characteristic is estimated using numerical models based on CFD techniques. These high-fidelity models proved to be a reliable, efficient, flexible, and relatively cheap means of analysis and design especially compared with physical experiments. The main drawback of using CFD is that they are computationally expensive, highly memory demanding, and time consuming.

These drawbacks become more severe in facing the optimization tasks since it involves more computations. The conventional gradient-based search techniques require hundreds or thousands of CFD simulations. Consequently, the optimization cost of complex designs becomes rather expensive. Moreover, since the sequence of gradient-based search (figure 3-1) techniques is deal the design once a time, parallel computation that can minimizes the simulation cost cannot be utilized. And the numerical errors may lead the search algorithm to false optima. Another feature related to these codes is that a majority of them are originally designed as stand-alone modules and complications arise when trying to interfere their performance, sometimes the source codes are not accessible at all [60]. Consequently, an increasing effort has been devoted to search for cheap alternatives of the high fidelity analysis codes in analysis, design, and optimization.

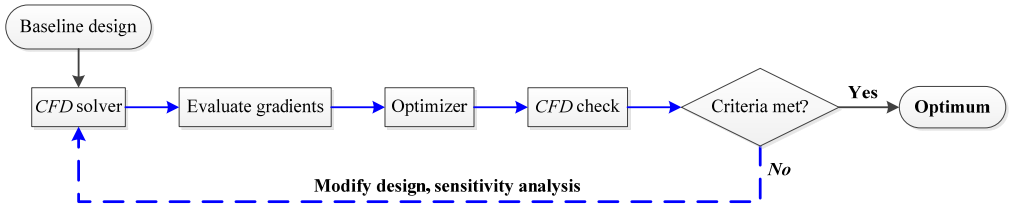

Figure 3-1: CFD-based optimization process [60]

One of these alternatives is the use of surrogate models (or approximation models or Meta models). Surrogate models is a model that can evaluate the new design objective(s) base on exists training samples, it is a statistics or approximation mathematics methods. Before a technical explain of surrogate models, words from Bandler [61] :

"...the surrogate model is constructed using an available, low-fidelity (and physically meaningful) model of the object response (the model being a function of the design variables), rather than pure interpolation/ approximation. This is in keeping with the engineering tradition of developing for design purposes meaningful (not necessarily complex, often very simple) models of components of the physical world..."

An intuitive example is people needs prepare in advance warm clothes when the winter coming in the northern hemisphere, this mind buried in people minds are according to the years by years life experiences, it is a surrogate model to forecast a general weather trends, while sometimes abnormal weather in winter create conditions let people can expose more their skin, so this kind estimate according to statistics is a low-fidelity evaluation method. Nowadays, the advanced meteorological science and technology, it can use the collected information from meteorological satellite, ground weather station, statistics data and simulations to forecast the weather in high-fidelity. Compare these two approaches that can give the variables objective(s), the surrogate model can give a faster, lower cost, lower fidelity result compare to the high-fidelity approach. A new ADO methodology can be built by the combination of these two approaches, call it CFD-surrogate-based optimization, it use the surrogate model to predict the design objective(s), and use a optimizer to search the optimum from the surrogate modelling, and finally use the high-fidelity approach to check the objective(s) (figure 3-2). This ADO method can do the optimization more effective, especially with the tasks as multi-dimension design space and multi-local optimum.

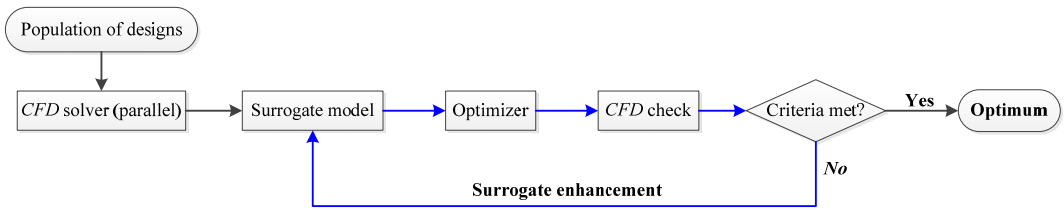

Figure 3-2: General CFD-surrogate-based Optimization process [60]

Before implementing the ADO optimization research, some mathematical modelling subjects that will be involved should be reviewed and studied.

In this chapter, following subjects mathematical modelling will be discussed:

a) Design of Experiments
b) Airfoil Parameterization
c) Computational fluid dynamic
d) Surrogate model constructor
e) Optimization methods

3.1 Design of Experiments

Nowadays, even the computational ability has considerable development, while in face of the some CFD simulations, such as whole aircraft N-S equation simulation, it still consume large computational resources and time for one simulation; and when deal multi-dimension optimization problem; it needs huge number samples, which use to form an effect surrogate model, all of them rise a question to us, how to use the experimental recourse efficiency, collected data are further analysed for understanding the underlying concept. While in this research task, the process of constructing an approximation model involves: do sample in the multi-dimension space, construct the surrogate model based on the sample points.

Design of experiments (DOE) as a subject belongs to methodology, discipline. It came out from the resolving the question how we can use limited resources to explore the optimum or a specified interesting design space, get response between design variables and objectives

3.1.1 Overview of sampling methods

There exits two DOE strategies widely employed by the scientific community, called:

a) Classical DOE techniques;
b) Modern DOE techniques.

Both classical and modern design of experiments (DOE) techniques has the common goal of extracting as much information as possible from a limited set of

laboratory or computer experiments. The classical DOE techniques, which are mainly used for physical experiments, assume that the measured response (y_m) will have a random error term (ε) and will be different from the true value of the response (y_t). It can be mathematically described by the relation given in Equation 3-1 [62]. In order to minimize the random error influence to wind tunnel testing result, Alan Pope [63] suggested that the basic run of a low speed wind tunnel should be repeated occasionally prevent variety of factors that affect the results deviate from the true value.

$$y_m(x) = y_t(x) + \varepsilon \tag{3-1}$$

The fundamental difference between classical and modern DOE stems from the assumption that random error exists in a physical experiment, but does not exist in a computer experiment. The modern DOE strategies are more widely applied to deterministic computer-based simulations for its properties of no random errors and repeatable.

Before getting into the discussion, some of the standard terms which are more often used in DOE discussions are presented in order have a more precise understanding about different DOE strategies. In order to construct the surrogate model, it is necessary to get the initial objective data that would be used to construct the surrogate model, so how to choose the sampling points in the multi-dimension design space is a question need an answer. Here the five terms used frequently:

Design of Experiments: The approaches to conduct and organize experiments that can be performed at high efficiently and quality;

Sample: A design point which will fall within the design space and is defined by the design variables;

Design Space: It is the region defined by the lower and upper bounds that constrain the sample point values and design variables. The space could be a one-dimension or hypercube;

Response: a dependent quantity that derived from a mathematically describe to the samples;

Response Surface: Any function that represents the trends of a response over the range of the design variables.

3.1.2 Sampling Techniques

Since the assumed that random error exits in physical experiment, so in order to reduce the random value, normally a test point will test more than once, and it more like it will place more sample points near the boundaries of the design space [64]. On the other hand, the modern DOE strategies are more widely applied to deterministic computer-based simulations. Since there are no random errors exists in the deterministic computer simulations. In addition, the modern DOE approach follows the replicated sampling. Hence the same objective(s) value can be obtained for the same inputs. They also assume that the trend of the true response is unknown. Due to this reason, there is no need to place more sample points near the boundaries of the design space. Hence more sample points are placed at the interior space of the design space. It shows that the modern DOE strategies are more efficient in space filling (figure 3-1).

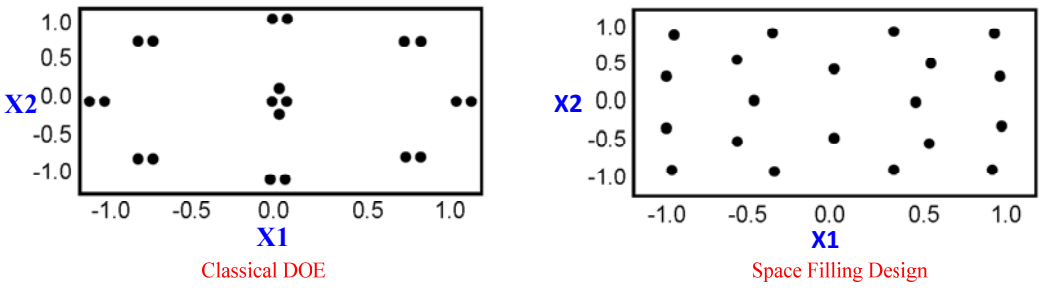

Figure 3-3: Classical and modern DOE approaches [Source: A. J. Booker (1998)]

The classical DOE were primarily designed for physical experiments where random errors are expected. However, they are used in numerical experiments as well. The basic idea is to select points from the design space extremes. The classical DOE is relatively simple and easily implemented. Some of them as Box-Behnken design [65], full factorial design (FFD), central composite design (CCD), D-optimal design (figure 3-4), partial factorial design (PFD), and face

centred cubic (FCC) design are examples of the classical technique [60]. And in case the dimensions “n” of the problem increase, the sample number will scales as n^2 for many of the classical DOE techniques such as central composite design (CCD)

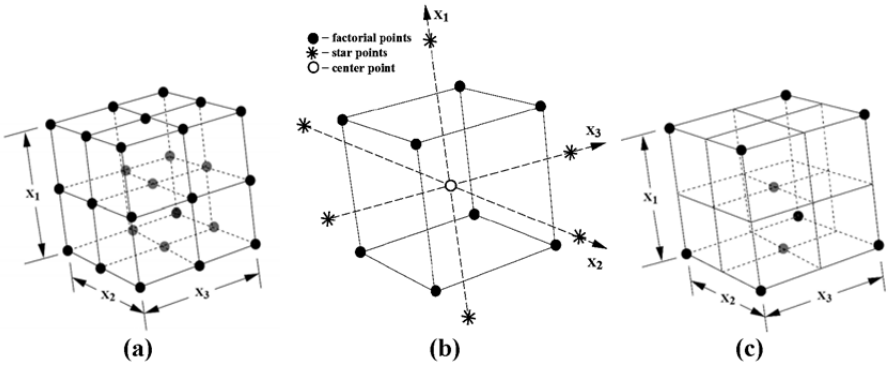

Figure 3-4: Classical DOE for a 3-factor, 3-level Problem

(a) FFD, 27 points, (b) CCD, 15 points, and (c) D-optimal, 10 points

In the modern DOE technique, sample points tend to cover uniformly the whole design space rather than focusing on the extremes only. Such DOE is more suited for numerical experiments where deterministic errors are more likely to occur. Space filling designs are relatively more sophisticated in implementation. Latin hypercube sampling (design), Orthogonal arrays (OA), and minimum discrepancy sequences adopt the space-filling technique.

- Latin Hypercube Sampling

The basic idea of the Latin Hypercube Sampling (LHS) is to divide each factor k into p levels of equal probability. Consequently, when a one-dimensional projection of the hypercube is takes, there will be a single sample point at each level. A Latin hypercube is a matrix of p rows and k columns. This design has the advantage of offering flexible sample sizes and well-distributed sampling. On the other hand, space-filling is not always guaranteed. Some modifications, e.g. optimal LHD, were introduced to ensure evenly distributed points.

- Orthogonal arrays

Orthogonal array (OA) is a matrix of p rows and k columns with every element being an integer between 0 and q −1. An orthogonal array has a strength t reflecting the number of combinations of l levels appearing in any of the r columns of the array. Orthogonal array

can be viewed as an LHD with uniform spacing between points when projected to any factor.

♦ Minimum Discrepancy Sequences

The discrepancy of a design matrix is a measure of non-uniformity of samples distribution. A minimum discrepancy sequence aims to construct a deterministic sequence of samples to finally produce a uniform space-filling distribution. They are suitable for models that are built incrementally. Typical examples of the methods are Hammersley, Sobol, Halton, and Faure sampling sequences.

3.1.3 Hammersley Sample

Here choose Hammersley Sequence sampling as for the future research sampling method, for it is a low-discrepancy sampling approach which generates 'N' sample points in a k-dimensional hypercube.

The algorithm that generates a set of N-Hammersley points makes use of the radix-R notation of an integer. That is, a specific integer, p, in radix-R notation can be represented as:

$$P = P_m P_{m-1} \cdots P_2 P_1 P_0 \tag{3-2}$$

$$P = P_0 + P_1 R + P_2 R^2 + \cdots + P_m R^m \tag{3-3}$$

Where m equal to the integer part of $[(\ln P)/(\ln R)]$.

The inverse radix number function constructs a unique number on the range $[0,1]$ by reversing the order of the digits of P around the decimal point. The inverse radix number function is:

$$\emptyset_R(P) =. P_0 P_1 P_2 \cdots P_m \tag{3-4}$$

$$\emptyset_R(P) = P_0 R^{-1} + P_1 R^{-2} + \cdots P_m R^{-m-1} \tag{3-5}$$

Finally, the Hammersley sequence of n-dimensional points is generated as:

$$x_n(P) = \left(\frac{P}{N}, \emptyset_{R_1}(P), \emptyset_{R_2}(P), \cdots \emptyset_{R_{n-1}}(P)\right) \tag{3-6}$$

Where $P = 0,1,2,\ldots,\mathrm{N}-1$; and the values for $R_1, R_2, \cdots R_{n-1}$ are the first *n-1* prime numbers (2, 3, 5, 7, 11…). This approach generates a set of N points in the *n*-dimensional design space $[0,1]^n$. A validation of Hammersley Sequence sampling technique is shown in figure 3-5. In this research a Visual Basic sub program used to do the N points sampling in a multi-dimension design space.

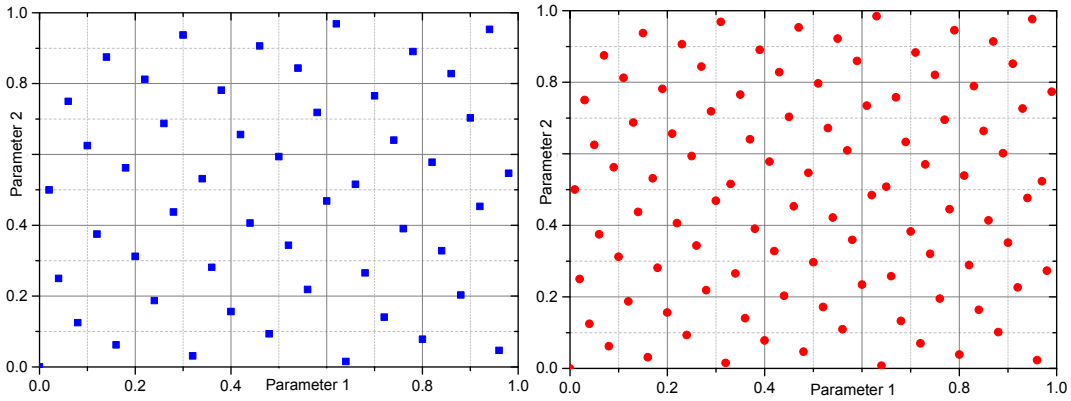

Figure 3-5: 50 and 100 Sample Points (12 Dimensions)

3.2 Airfoil Parameterization

Any real object that can be imaged could be described by three basic elements, the dot (or point), Curve (take the line as special curve), surface (take the Planar as special surface). The connection between dots could be the curves, Surface can be generated by the different section curves and the sweep conduct curves. The 3-D objects can utilize the seal surfaces to isolate the space from other (figure 3-6). These geometry representation methods are routinely used in computer aided design (CAD), computer-aided engineering (CAE) and Computational fluid dynamic (CFD) software.

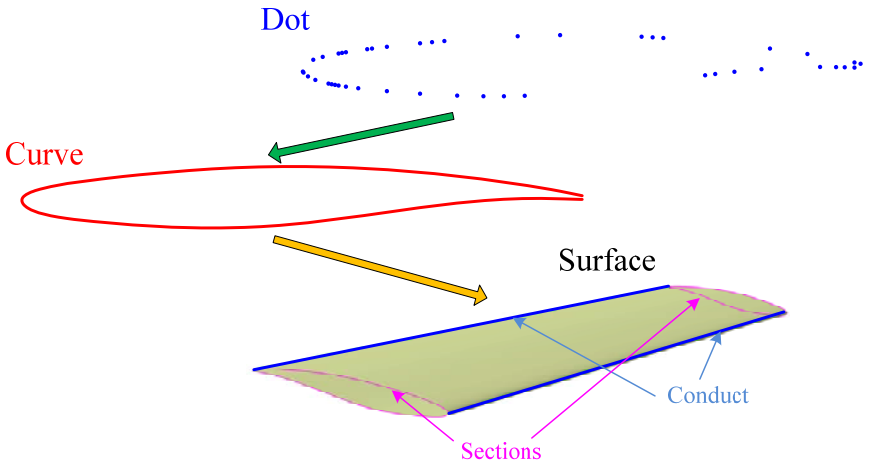

Figure 3-6: Dotes, Curves and surface

Airfoil is a section shape of wing and refers 2-D geometry, Hence in this work, it needs a 2-D modelling methods. Finding an optimum representation scheme for aerodynamic shape optimization problems is an important step for a successful aerodynamic optimization task. Several options can be used for airfoil shape parameterization: discrete point, partial differential equation, Hicks-Henne bump functions, Bezier parameterization, and polynomial and Parameter section.

3.2.1 Parameter of Single-element Airfoil

Single-element airfoil is the design base of the HLC airfoil, it is a main design objective in this thesis, some of the single-element airfoil discuss in the following section.

3.2.1.1 Discrete Points Method

This method is the most simple and intuition way (Figure 3-6), software such as ICEMCFD and CATIA use it and together with spline function or lines to represent the geometry. This method can present any geometry with an accuracy which could meet engineering criteria. This method places points on the boundary of the geometry, seems like the State boundary markers to state that the inner side area belong to the geometry that it stand for.

However, for the discrete points just contain the information of themselves Coordinate data, it has not enough power to control its neighboring area this ap-

proach is quite easy for the implementation, but difficult to maintain geometrical smoothness, if used to express curves, especially when dealing with high curvature variance, it needs lots of points to state it. Its high accuracy at specific points while lower power to control shape generation, limit this methods application in multi-design objectives area.

3.2.1.2 Partial Differential Equations method

Geometric modeling using Partial Differential Equations (PDEs) method has been widely studied in computer graphics since Bloor et al.'s PDE method was first introduced in blend surface generation two decades ago [66]. The PDEs has been gradually recognized due to its smooth instinct, as well as the ability to generate a variety of geometric shapes by intuitively manipulating a relatively small set of PDE boundary curves, that makes numerous film industries and the games industry to use it as facial geometry parameterization [67]. PDEs is more suitable for complex geometries like complete aircraft which can be easily defined by a compact set of parameters. But the process of dividing the geometry and grouping the differential equations make this approach to be computationally very expensive [68].

Athanasopoulos et al. [69] created a parametric design method based on PDE's. In their method, each surface is generated by a number of curves that represent the character lines of a given part of the aircraft shape. Other surfaces then blend to create the full shape of the airplane as shows in figure 3-7. The shapes are defined through boundary conditions and a small set of design parameters.

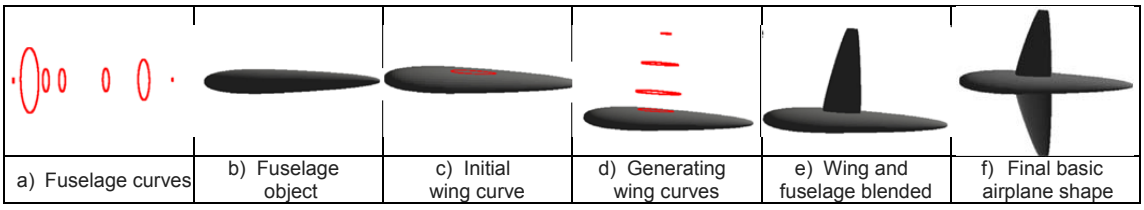

Figure 3-7: Generic aircraft shape production using PDE's

3.2.1.3 Polynomial Approach

In the Polynomial approach, the number of design parameters will

3.2.1.4 NACA Digital Airfoil

Airfoil geometry can be characterized by the coordinates of the upper and lower surface. It is often summarized by a few parameters such as: maximum thickness, maximum camber, position of maximum thickness, position of maximum camber, and nose radius. One can generate a reasonable Airfoil section given these parameters. This was developed by the National Advisory Committee for Aeronautics (NACA). The shape of the NACA airfoils is described using a series of digits following the word "NACA". The parameters in the numerical code can be entered into equations to precisely generate the cross-section of the airfoil and calculate its properties. Equation 3-12 can be used for a symmetrical 4-digit NACA airfoil.

$$\pm y_t = \frac{t}{0.20}\left(0.29690\sqrt{x} - 0.12600x - 0.35160x^2 + 0.28430x^3 - 0.10150x^4\right) \quad \textbf{(3-7)}$$

where t is the maximum airfoil thickness, presented as a fraction of chord, x is the chord direction position and y is the airfoil thickness direction position [33]. $t = 0.12$ is the value of NACA 0012 airfoil; NACA airfoil families had developed several digit airfoil families [33]. Different family could be used by different purpose [70].

3.2.1.5 Bezier Parameterization

A Bezier curve is a parametric curve frequently used in computer graphics and related fields, it is widely used in computer graphics to model smooth curve. A Bezier curve of order n is described as:

$$\mathrm{z}(t) = \sum_{t=0}^{n} B_i^n(t) \cdot P_i \quad \textbf{(3-8)}$$

Where B_i^n is the Bernstein polynomial, P_i represents the set of n+1 control points, and t is curvilinear coordinate. The Bernstein polynomials are described by:

$$\mathrm{B}_i^n(t) = \binom{n}{i} t^i (1-t)^{n-i}, \qquad i = 0,1,\ldots\ldots,n \quad t \in [0,1] \quad \textbf{(3-9)}$$

Bezier curve is accurate when representing simple curves, as the curve complexity increases, the degree of polynomials increased, which results in a large

error. In order to represent a complex curve, it is more efficient to separate the curve into segments and use a set of lower-order Bezier curves instead.

The B-spline is the generalization of the Bezier curve, it is defined as:

$$\mathrm{z}(t) = \sum_{i=0}^{m} p_i \cdot N_{i,p}(t) \qquad \textbf{(3-10)}$$

Where P the order of the Polynomial is, P_i is asset of control points, N_i, p is B-spline airfoil generated with 13 control points.

3.2.1.6 Hicks - Henne Bump Functions

The Hicks-Henne Bump Functions method is a good choice for local shape optimization; it is convenience to model moderate or small Perturbations of initial airfoil geometry. This method define that the new airfoil is the combination of a basis shape and a bump (figure 3-8) which is the sum of suitably defined and weighted sine functions, it can be stated as [71]:

$$\mathrm{y} = y_{basis} + \sum_{j=1}^{M} a_j f_j(x) \qquad \textbf{(3-11)}$$

$$f_j(x) = \left\{ sin\left[\pi x^{\log(0.5)/\log(t_1)}\right] \right\}^{t_2} \quad 0 \le \mathrm{x} \le 1 \qquad \textbf{(3-12)}$$

Where: α maximum bump magnitude; t_1 locates the maximum point of the bump; t_2 controls the width of the bump.

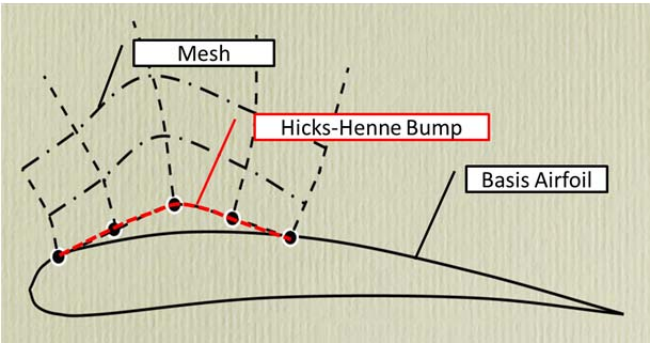

Figure 3-8: Hicks-Henne Bump Functions apply on a basis airfoil [72]

This flexibility allows one to place the bump at strategic points where a redesign is preferred while leaving other parts of the airfoil intact. Figure 3-9 shows a set of 16 Hicks-Henne bump function with parameter t_2 = 10.

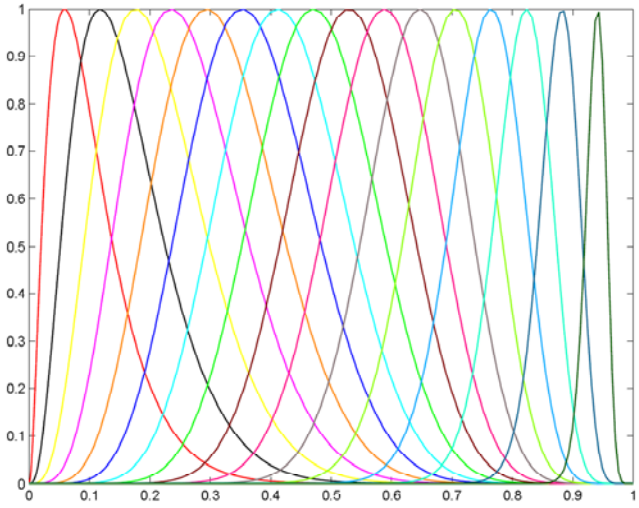

Figure 3-9: A set of 16 Hicks-Henne Bump Functions with parameter (t_2 =10) [71]

Hicks-Henne bump function is a smooth, so it would not influence the Smoothness characteristics of the initial airfoil. Only a few Hicks-Henne sine bump functions are required to provide an acceptable span of the design space thus requiring fewer design variables.

3.2.1.7 Joukowski Transformation

This approach has another name as conformal transformation. It uses mathematical method to map a region of one plane on another plane in such a way that the detail shape of infinitesimal elements of area is not changed. This method is used to solve for the two-dimensional potential flow around a class of airfoils known as Joukowski airfoils. It could use either complex variables [33] or real variables [73]. Figure 3-10 expresses two Joukowski Transforms; the first one is the cylinder in Z plane transfer to a non-cambered airfoil in w plane, while the second one is use cylinder in Z plane transforms a cambered airfoil in w plane [74]. For this method is just used for incompressible flow, also this method need several Preconditions, so it cannot be used in this research.

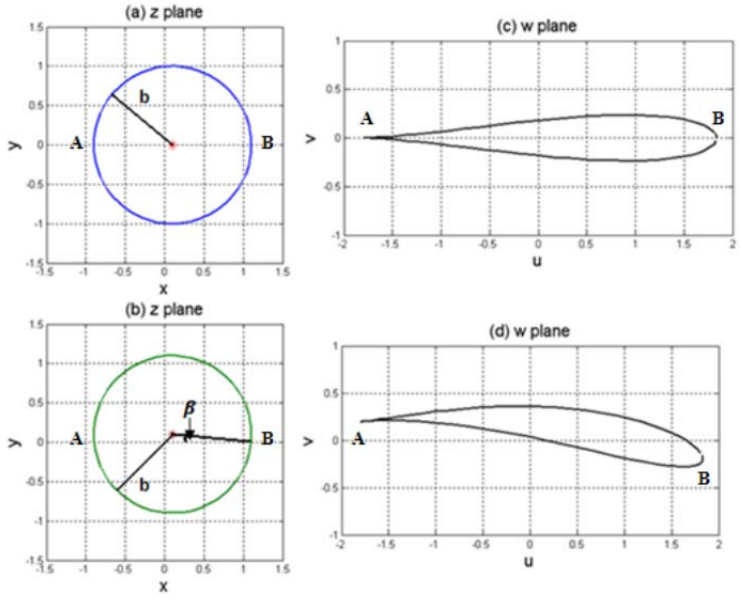

Figure 3-10: Joukowski transformation

3.2.1.8 Parametric Section

Parametric Section (PARSEC) parameterization method, which is employed in this research, proposed by Sobieczky [75], it used 11 parameters which directly manipulate the shape of the airfoil. They are the leading edge radius (), upper crest position (). Upper crest curvature (),lower crest position (xlow, ylow), lower crest curvature ([d2y dx2]low), trailing edge location (xte, yte) and trailing edge angles (te,up, te,low). They are shown in Figure 3.

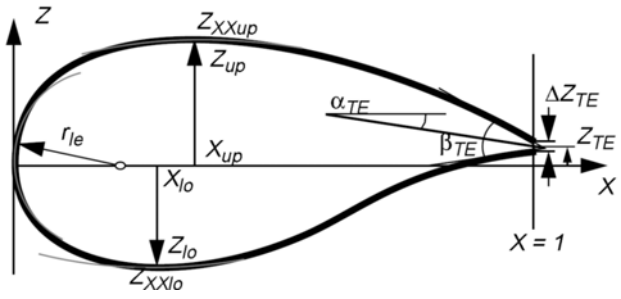

Figure 3-11: Parametric Section control parameters

Two polynomials are used to define the upper and lower surface of the airfoil:

$$y_{up} = \sum_{n=1}^{6} a_n x^{n-\frac{1}{2}} \qquad \textbf{(3-13)}$$

$$y_{lo} = \sum_{n=1}^{6} b_n x^{n-\frac{1}{2}} \tag{3-14}$$

Where y_{up} is the coordinate of the upper surface and y_{lo} is the coordinate of the lower surface and x is the chordwise location. The coefficients a_n and b_n can be found by imposing the following conditions.

$$y(x_{te}) = y_{te} \tag{3-15}$$

$$\mathrm{Tan}(\theta_{te,up}) = \left[\frac{dy}{dx}\right]_{x=x_{te}} = \sum_{n=1}^{6}\left(n-\frac{1}{2}\right) a_n x_{te}^{n-\frac{3}{2}} \tag{3-16}$$

$$y(x_{up}) = \sum_{n=1}^{6} a_n x_{te}^{n-\frac{3}{2}} = y_{up} \tag{3-17}$$

$$\left[\frac{dy}{dx}\right]_{x=x_{up}} = \sum_{n=1}^{6}\left(n-\frac{1}{2}\right) a_n x_{up}^{n-\frac{3}{2}} = 0 \tag{3-18}$$

$$\left[\frac{d^2y}{dx^2}\right]_{x=x_{up}} = \sum_{n=1}^{6}\left(n-\frac{3}{2}\right)\left(n-\frac{1}{2}\right) a_n x_{up}^{n-\frac{5}{2}} = Z_{xx,up} \tag{3-19}$$

$$\left[\frac{\frac{d^2y}{dx^2}}{\left[1+\frac{dy^2}{dx}\right]^{\frac{3}{2}}}\right]_{x=x_{le}} = \frac{2}{a_1^2} = R_{le,up} \tag{3-20}$$

The same equations apply for the lower surface. The coefficients a_n and b_n can therefore be found by solving the following system of equations:

$$\begin{bmatrix} 1 & 0 & 0 & 0 & 0 & 0 \\ x_{te}^{\frac{1}{2}} & x_{te}^{\frac{3}{2}} & x_{te}^{\frac{5}{2}} & x_{te}^{\frac{7}{2}} & x_{te}^{\frac{9}{2}} & x_{te}^{\frac{11}{2}} \\ x_{up}^{\frac{1}{2}} & x_{up}^{\frac{3}{2}} & x_{up}^{\frac{5}{2}} & x_{up}^{\frac{7}{2}} & x_{up}^{\frac{9}{2}} & x_{up}^{\frac{11}{2}} \\ \frac{1}{2}x_{te}^{-\frac{1}{2}} & \frac{3}{2}x_{te}^{\frac{1}{2}} & \frac{5}{2}x_{te}^{\frac{3}{2}} & \frac{7}{2}x_{te}^{\frac{5}{2}} & \frac{9}{2}x_{te}^{\frac{7}{2}} & \frac{11}{2}x_{te}^{\frac{9}{2}} \\ \frac{1}{2}x_{up}^{-\frac{1}{2}} & \frac{3}{2}x_{up}^{\frac{1}{2}} & \frac{5}{2}x_{up}^{\frac{3}{2}} & \frac{7}{2}x_{up}^{\frac{5}{2}} & \frac{9}{2}x_{up}^{\frac{7}{2}} & \frac{11}{2}x_{up}^{\frac{9}{2}} \\ -\frac{1}{4}x_{up}^{-\frac{3}{2}} & \frac{3}{4}x_{up}^{-\frac{1}{2}} & \frac{15}{4}x_{up}^{\frac{1}{2}} & \frac{35}{4}x_{up}^{\frac{3}{2}} & \frac{53}{4}x_{up}^{\frac{5}{2}} & \frac{99}{4}x_{up}^{\frac{7}{2}} \end{bmatrix} \begin{bmatrix} a_1 \\ a_2 \\ a_3 \\ a_4 \\ a_5 \\ a_6 \end{bmatrix} = \begin{bmatrix} \sqrt{\frac{2}{R_{le}}} \\ y_{te,up} \\ y_{up} \\ \tan(\theta_{te,up}) \\ 0 \\ \left[\frac{d^2y}{dx^2}\right]_{x=x_{up}} \end{bmatrix} \tag{3-21}$$

$$\begin{bmatrix} 1 & 0 & 0 & 0 & 0 & 0 \\ x_{te}^{\frac{1}{2}} & x_{te}^{\frac{3}{2}} & x_{te}^{\frac{5}{2}} & x_{te}^{\frac{7}{2}} & x_{te}^{\frac{9}{2}} & x_{te}^{\frac{11}{2}} \\ x_{lo}^{\frac{1}{2}} & x_{lo}^{\frac{3}{2}} & x_{lo}^{\frac{5}{2}} & x_{lo}^{\frac{7}{2}} & x_{lo}^{\frac{9}{2}} & x_{lo}^{\frac{11}{2}} \\ \frac{1}{2}x_{te}^{-\frac{1}{2}} & \frac{3}{2}x_{te}^{\frac{1}{2}} & \frac{5}{2}x_{te}^{\frac{3}{2}} & \frac{7}{2}x_{te}^{\frac{5}{2}} & \frac{9}{2}x_{te}^{\frac{7}{2}} & \frac{11}{2}x_{te}^{\frac{9}{2}} \\ \frac{1}{2}x_{lo}^{-\frac{1}{2}} & \frac{3}{2}x_{lo}^{\frac{1}{2}} & \frac{5}{2}x_{lo}^{\frac{3}{2}} & \frac{7}{2}x_{lo}^{\frac{5}{2}} & \frac{9}{2}x_{lo}^{\frac{7}{2}} & \frac{11}{2}x_{lo}^{\frac{9}{2}} \\ -\frac{1}{4}x_{lo}^{-\frac{3}{2}} & \frac{3}{4}x_{lo}^{-\frac{1}{2}} & \frac{15}{4}x_{lo}^{\frac{1}{2}} & \frac{35}{4}x_{lo}^{\frac{3}{2}} & \frac{53}{4}x_{lo}^{\frac{5}{2}} & \frac{99}{4}x_{lo}^{\frac{7}{2}} \end{bmatrix} \begin{bmatrix} b_1 \\ b_2 \\ b_3 \\ b_4 \\ b_5 \\ b_6 \end{bmatrix} = \begin{bmatrix} -\sqrt{\frac{2}{R_{le}}} \\ y_{te,lo} \\ y_{lo} \\ \tan(\theta_{te,lo}) \\ 0 \\ \left[\frac{d^2y}{dx^2}\right]_{x=x_{lo}} \end{bmatrix} \quad \textbf{(3-22)}$$

In this research a visual basic Program was designed to deal with the PARSEC, it use Gauss elimination to get the coefficients of the polynomial. And in order to have a more flexible leading edge, the upper and lower leading edge radius values are independent, while it will not affect the smooth leading edge. In order to validation the methods. A NACA 2411 airfoil was used. And two morph have taken, one is 0.025 chord offset, the second is with an up surface have an curved inwards trailing edge.

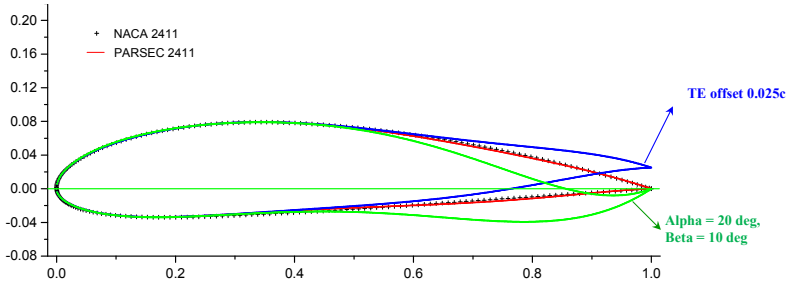

Figure 3-12: PARSEC validation

Table 3-1: PARSEC parameters for NACA 2411 airfoil

Parameters	r_{leUp}	x_{up}	y_{up}	Z_{xxup}	r_{lelo}	x_{lo}	y_{lo}	Z_{xxlo}	β_{TE} deg	α_{TE} deg	Z_{TE}	ΔZ_{TE}
value	0.0170	0.3445	0.07912	-0.6448	0.008	0.16912	-0.03379	0.6948	14.902	-5.88	0	0

3.2.1.1 Parameterization methods comparison

There have been several attempts at comparison of parameterization methods [36; 76] , a more recently study [77] about the methods of parameter single airfoil methods, the author used following five indexes to assess their ability of parameter, and the comparison result shows that the PARSEC is a

a) **Parsimony**

Parsimony defines the preference for the parameterization method which can induce significant changes in the main geometric features of the airfoil by using the smallest number of parameters.

b) Completeness

Completeness assesses whether the parameterization can describe any airfoil, up to a specific degree of accuracy.

c) Orthogonality

Orthogonality guarantees that each airfoil shape corresponds to a unique set of input parameters.

d) Flawlessness

Flawlessness guarantees that the parameterization technique will not generate an "ill-behaved" shape.

e) Intuitiveness

Intuitiveness considers whether the method relates to the physical design meaning of the parameters, which in turn simplifies the choice of input bounds or design judgement.

3.2.2 Parameterization of High-lift configuration Airfoil

Compare to parameter single airfoil, parameter HLC airfoil need parameters to constrain the High-lift devices' displace and orientation, moreover, since the new leading edge contours of the main wing and the flap exposes, it needs additional parameters to sketch it (figure 3-13).

A generally process to produce a HLC airfoil, it begins with a given single-element airfoil (or calls cruise airfoil) which uses at the transonic flight phase. The interface bounds definition at the training edges, which as illustrates in the top chart of Figure 3-13. Four special points should be defined before the layout of all of the contours; they are point A, B, C and D respectively. Normally this kind data should be given with the consent from aerodynamics, structure and system design departments [2; 78]. From the slat and main wing upper trailing edge transition to the after element is 0.02 chord length. The flap cabin was design according to some experience data, in this thesis its main data similar to the 30N/30P HLC airfoil.

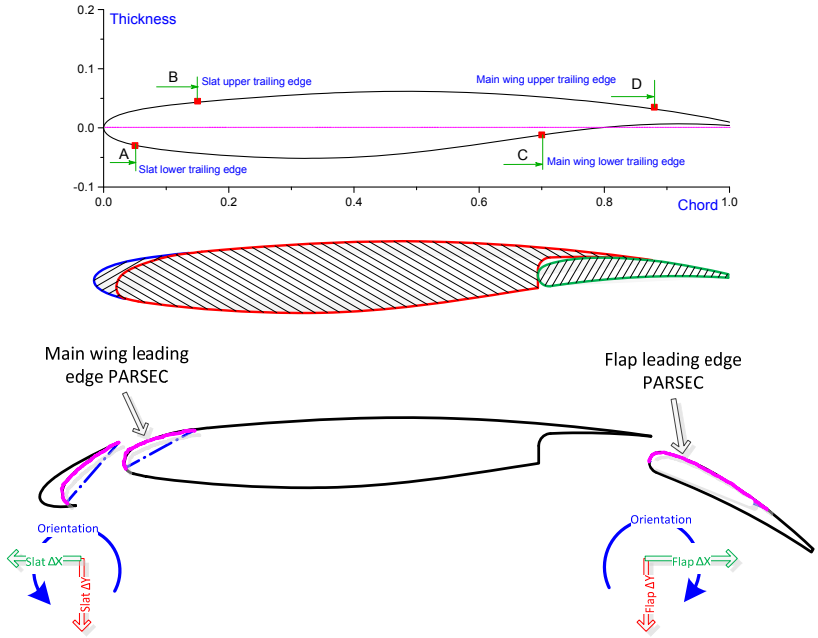

Figure 3-13: HLC airfoil Parameter

After define the contact area, then it should define the detailed profile of the expose area, here use the PARSEC method to parameter it, since the expose areas have the properties likes a upper curve of the airfoil, even the chord length relative small. After all the HLC airfoil components' profile had been defined, all of the components have clearly definition. As to the aerodynamic study, normally a simplify at the shape of the slat cabin and flap cabin, this could be benefit for the aerodynamic research, especially reduce wind tunnel model production and CFD meshing difficulty [75]. Then the high-lift devices position and orientation setting should be given, which illustrate in. this research use the rotation which form a suitable orientation, and then implement a X direction and Y direction translation, which mainly form the overlap and gap.

$$\begin{bmatrix} cos\theta & -sin\theta \\ sin\theta & cos\theta \end{bmatrix} \begin{bmatrix} X_0 \\ Y_0 \end{bmatrix} + \begin{bmatrix} \Delta X \\ \Delta Y \end{bmatrix} = \begin{bmatrix} X_1 \\ Y_1 \end{bmatrix} \quad \textbf{(3-23)}$$

Where θ is the rotation angle, X_0 and Y_0 represent the original coordinate relative the rotation point, ΔX and ΔY are the Vertical and horizontal translation, the and X_1 and Y_1 the demanded coordinate relative the rotation Point.

In this work, it uses a Visual Basic Program to carry out the HLC airfoil parameter.

3.2.3 Droop spoiler Parameter

A droop spoiler can offer the wing have a more arbitrary ability to control the flow around the wing. it brought out from the ideal that when use the flap change the whole airfoil camber properties for long endurance aircraft missions, in order to optimize performance for high dynamic pressure flight phase, it will shape a gap between the main wing upper surface and the flap, so a droppable spoiler can remedy this kind problem, reshape the whole upper main wing surface to be a smooth curve. Meanwhile the droppable spoiler can improve its low-speed flying qualities. This kind auxiliary device not only has the function as a normal spoiler by rise its trailing edge, but also can be dropped its trailing edge by using a “software coupling”. For it can let the main wing have more perfect camber distribution and gap between the main wing and flap, this kind computer-controlled spoiler automatically moves into the most efficient position [58] can give the whole wing have higher efficiency.

In order to parameter the spoiler, a 2-D rotation method use, which has describes in equation 3-23, while the ΔX and ΔY are zero.

3.3 Computational fluid dynamic

Computational fluid dynamics (CFD) CFD has been successfully applied in many areas of fluid mechanics. These include aerodynamics of cars and aircraft, hydrodynamics of ships, flow through pumps and turbines, combustion and heat transfer, chemical engineering, etc. Nowdays, in the transport airplane aerodynamic design activities, CFD takes the biggest part of the work of aerodynamic design (figure 3-15). Since its capability, speed and accuracy had improved in a certain degree (table 3-2).

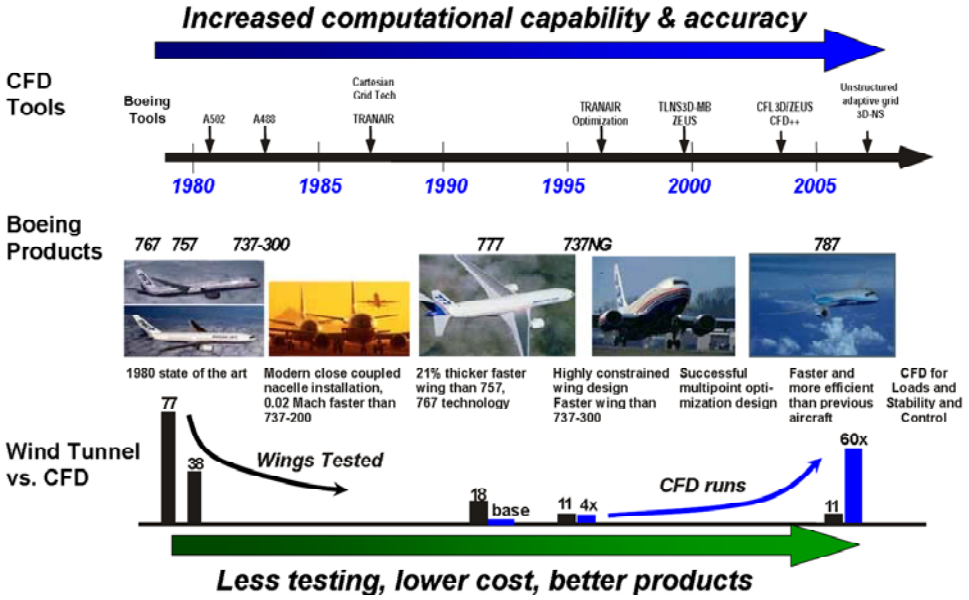

Figure 3-14: CFD takes more job than Wind tunnel test [79]

Table 3-2: One point of view regarding computational aerodynamics capability [80]

	Attached Flow	Separated Flow	Vortex Flow	Mixed Vortex Attached	Mixed Vortex Separated	Dynamic	Complex Geometry Coupling
Axisymmetric and 2-D	good	fair	poor	poor	poor	fair	N/A**
Research Wing/Body	good	fair	fair	fair	poor	fair	poor
Transport Aircraft	good	fair	fair	fair	poor	fair	fair
Fighter Aircraft	fair	poor	fair	fair	poor	poor	poor
Special Purpose Aircraft	fair	poor	poor	poor	poor	poor	poor

** Not applicable.

3.3.1 Aerodynamic characteristics evaluators review

Air is a hard to be observed material; but it is the most basic precondition permit the aeronautical vehicle above the ground. In order to have a flight, it is necessary to have an appropriate interaction between the vehicle and the air, for it needs the pressure difference between the upper and lower surfaces to balance the weight, basically. The interaction study between the airfoil and the wind in the wind tunnel by Wright Brothers ensure their success [40]. Following the flight activity boosts, the technical means to measure or calculate the interactive

between air and flight vehicle obtain innovation and development. Nowdays, there mainly exists three means that can be used by engineers to evaluate airplane aerodynamic characteristics. They are called Simi-empirical, computational and experiment respective (Fig.3-4), all of them use the aerodynamic theory, physical and mathematical.

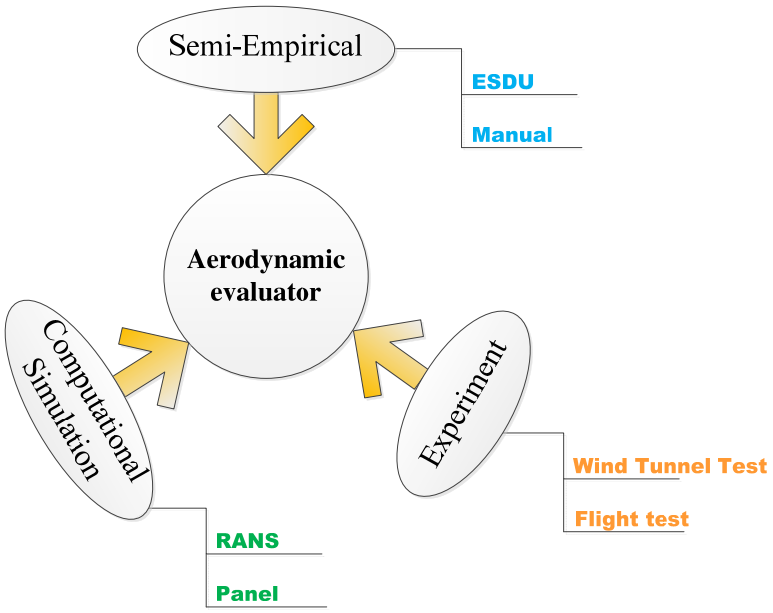

Figure 3-15： Approaches as aerodynamic evaluator

The semi-empirical approach utilize previous designs, databases and handbook, or some statistics results together with method summarised form to commercial document as ESDU [81]. It is very efficient to use this kind document to evaluate aircraft aerodynamic characteristics, but it is a general method, so it is hard to guarantee the accuracy for a special task. The semi-empirical approach is mainly used in the conception or pre-selection design phase.

Experiment method mainly refers to two subjects, Wind tunnel test (WTT) and flight test (FT). A wind tunnel is a tool used in aerodynamic research to study the effects of air moving past solid objects. Its related technologies and methods have been developed maturely. Today, reduced by the number of tens times model in a section area size as 2×2 m^2 (figure 3-17 right), it can do the test meet condition as full scale aircraft encounter compression and viscosity, or in term of Mach number and Reynolds number (figure 3-17 left). A good design

and adjust wind tunnel test could reach a good accuracy (figure 3-18). The disadvantage of the wind tunnel test is lower productivity while budget costly even for a single test entry, and need a proper corrections work to link the WTT data to full scale aircraft; normally, the correction should contain both WT facilities interface and scale effect [63] . All of them limit its application in current aircraft design. So currently the wind tunnel testing normally takes the role as calibration of the computational simulation and the final design.

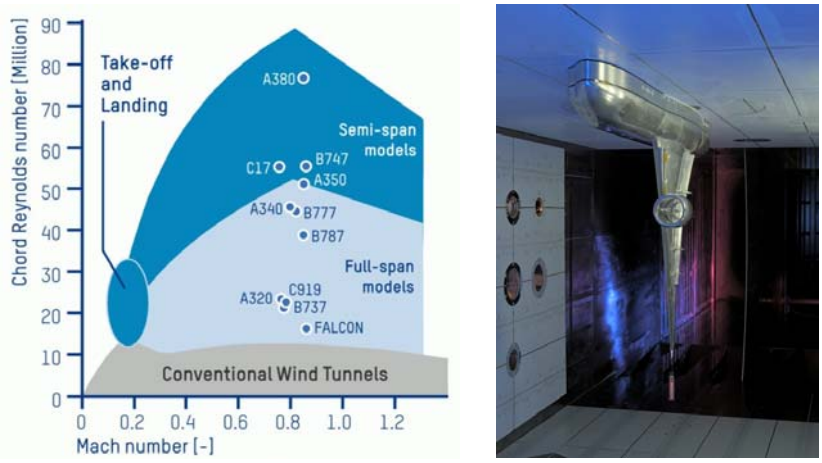

Figure 3-16: Wind tunnel capability and model mounted in test section [82; 83]

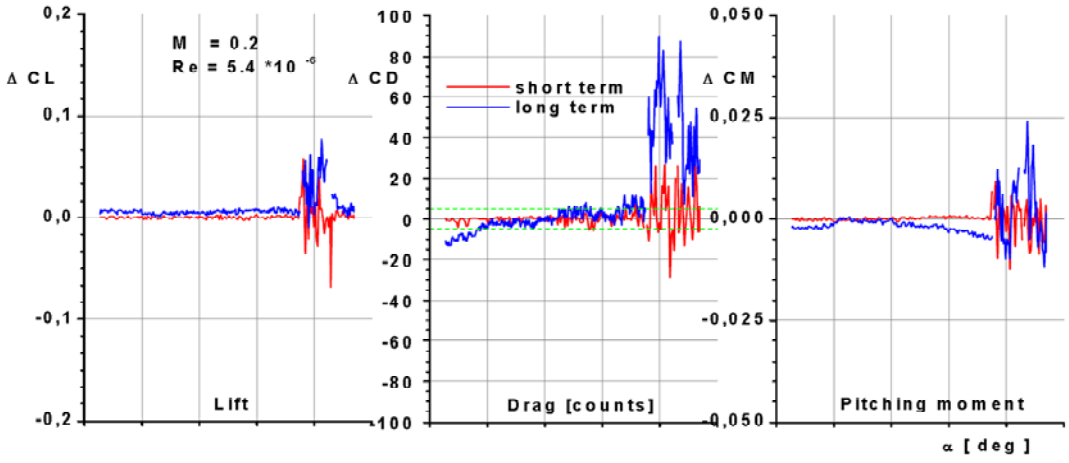

Figure 3-17: Morden Wind tunnel short and long term repeatability accuracy [84]

Flight test is another important method. As it normally does not require scaling, so its results more directly represent the real design compare to WTT. Figure 3-18 demonstrates the supercritical Airfoil flight test with a changed wing F-8A aircraft [85]. Flight test heavily dependent on budget and weather condition [86],

since the turbulence and gusts exists in atmosphere, hence normally one test object need repeat several times. Another difference compare to wind tunnel test for its lack of some devices as the balance, some data as lift and drag characteristics data seriously rely on long flight time, and there are also exist some errors which occur in the sensors use to measure the flight parameters and engine thrust output. From above states, it is clear that flight test is a lower productivity and high cost experiment. For a new aircraft the flight test normally takes number years after the first aircraft roll out.

Figure 3-18: F-8A flight test with supercritical Airfoil wing [85]

Table 3-3: Aerodynamic evaluation methods utilization properties comparison

Methods	Accuracy	Productive	Budget consumption	Design Phase①	Applications scope②	Independent③
Simi-empirical	poor	very high	very lower	C	++++	good
Wind tunnel test	very good	low	high	P+D	++++	poor
Flight test	good	very low	very high	D	++	very poor
CFD	up to the task	up to the task	medium	C+P+D	+++++	medium

① C: Conceptual design; P: preliminary design; D: detailed design.

② +: narrow; +++++: wide.

③ This item mainly refers the degree of difficulty to obtain the avialable resource, it includes software license, hardware, experiment facilities and weather, etc. resources.

Since both the hardware and numerical methods which used in CFD are developing, we can believe it that a more powerful and reliable.

3.3.2 Basic Principles of CFD

There exits two kinds of the CFD simulation method according to the different aerodynamic theory used, they called Panel and RANS respectively. Panel is developed according to the potential flow; a series of singularities as sources, sinks, vortex points and doublets are used to model the panels and wakes. While RANS is developed according to the governing fluid-flow conservation equations relate to three physicals, they are mass, momentum and energy. Compare to panel method which just discrete the boundaries, RANS needs discrete whole simulation flow zones.

Both Panel and RANS can simulate the 2D and 3D airflow, while RANS used more widely for it can simulate the compressible and separation conditions, which seems is the exclusion area for Panel method. However, panel codes are still used for preliminary aerodynamic analysis as the time required for an analysis run is significantly less due to a decreased number of elements

This kind of simulation only needs to discrete the boundary and N-s equations, both of them include some different versions according to the simulation detailed degree. Panel approach is the earliest method [87],

Some comparison of the CFD approaches had been done by Moerland [88],

Table 3-4: Qualitative overview of aerodynamic design methods for high-lift systems.

Method	Coding easiness	Program size	Computational speed	accuracy	design phase
Inviscid panel	easy	compact	fast	very poor	C
Panel+IBL①	poor	extensive	average	very good	C+P⑧
Euler	poor	extensive	slow	poor	N/A
RANS②	very poor	very extensive	very slow	excellent	D⑧

① IBL: Integral Boundary Layer method, used to incorporate viscous boundary layer effects.

② C: Conceptual design, P: preliminary design, D: detailed design.

As both the flow of single element in transonic or HLC in low Mach number are coupled with compressible and separation, hence, it is necessary to use RANS to get a high-fidelity predictions of the configurations aerodynamic characteristics.

However, due to the trim drag from the horizontal tail will use the Panel+IBL method, for an assumption that the flow around the trim device is lower sonic and not separation has happened, so the trim drag increase will directly relate to induced drag.

3.3.3 Panel method

Hess and Smith, while working at Douglas Aircraft Company in the early 1960's, started work on what is now commonly referred to as the Aerodynamic Panel Method [24]. Panel method widely used for solving incompressible potential flows. However, it can also be used for describing compressible flows with the cost of accuracy of the solution. Panel methods continue to be widely used for initial design studies due to their ease of use and rapid solution times.

In this method, the surface of the airfoil is discretised into a large number of straight line segments, called panels as depicted in Figure 3-20. The flow field is computed subject to the following two assumptions: (a) Vortex strength is equal and constant in all the panels and (b) Source strength is constant and can have different values at each panel. In addition to these two assumptions, the effects of compressibility and viscosity of air are excluded. But it is important for the viscosity to satisfy the flow condition that the flow leaving the airfoil trailing edge should be smooth. The total potential function(Φ), which is computed as a sum of the potentials of vortex($\emptyset_v$), source($\emptyset_s$) and free stream($\emptyset_\infty$), is given by Equations ? and ?. These equations are solved by breaking the integral for each panel as given by Equation 4.1.3. Once this equation is solved, then the pressure coefficient ($\mathrm{C}_p(\mathrm{x},\mathrm{y})$) at the mid-point of each panel can be calculated from the relation 4.1.4.

The method:

a) Set a series connected line segments to present the geometry;
b) Placing distributions of sources and vortices on each line.

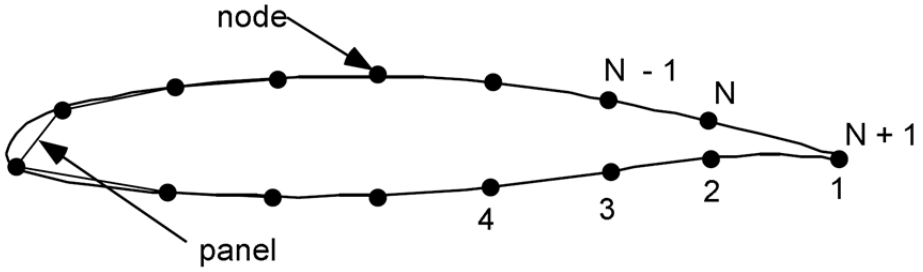

Figure 3-19: Representation of a smooth airfoil with straight line segments [24]

$$\emptyset = \emptyset_\infty + \emptyset_s + \emptyset_v \quad \textbf{(3-24)}$$

$$\emptyset = \emptyset_\infty + \int_s \left(\left(\frac{q(s)}{2\pi}\right)\ln r - \left(\frac{r(s)}{2\pi}\right)\theta\right) ds \quad \textbf{(3-25)}$$

$$\emptyset = V_\infty(x\cos(\alpha) + y\sin(\alpha)) + \sum_{j=1}^{N}\int_j \left(\left(\frac{q(s)}{2\pi}\right)\ln r - \left(\frac{r(s)}{2\pi}\right)\theta\right) ds \quad \textbf{(3-26)}$$

$$C_p(x,y) = 1 - \left(\frac{V_t^2}{V_\infty^2}\right) \quad \textbf{(3-27)}$$

where $\ln \mathrm{r}$ is the source singularity, $\theta = \arctan\left(\frac{\mathrm{y}}{\mathrm{x}}\right)$, $\mathrm{q(s)}$ is the source strength, $\mathrm{r(s)}$ is the vortex strength, α is the angle of attack, V_t and V_∞ are the panel tangential velocity (computed at the midpoint of each panel) and free stream velocity respectively.

This thesis will use Panel method to predict the induce drag of the assumed horizontal tail, when it trim the moment of the wing airfoil to the point of 0.25 wing chord. Drag. XFLR5 [89; 90] is an open source software based on Xfoil.

3.3.4 Reynolds-averaged Navier–Stokes equations

Osborne Reynolds proposed an averaging concept for the Navier–Stokes equations that significantly reduces the complexity of simulating turbulent flows. The resulting Reynolds-averaged Navier–Stokes (RANS) equations are formulated in terms of the (time-) averaged flow field (velocity field, pressure, density and

temperature). Turbulence fluctuations are eliminated by this process, and the equations become amenable to computational fluid dynamics (CFD) on today's desktop computers [91].

Since the flow in the real world is have some turbulence, cause the viscosity exists; and in the high speed flow, the compress also affect

Compare to Panel methods, there exist a more complex and accuracy method, it call

3.3.4.1 Navier-Stokes equations

The N-S equation [92] is governed by air state equations and three conservation laws, as following individual research project (IRP) will deal with 2-D flow, so here only take the 2-D N-S equation as example, the way to deal with 3-D is the same. 2-D conserver equation can be written [92]:

$$\frac{\partial U}{\partial t}+\frac{\partial F}{\partial x}+\frac{\partial G}{\partial y}=J \qquad \textbf{(3-28)}$$

U is the scalar variable, F and G are the fluxes in the x and y directions respectively. J is the source term. Their relations with state variables are given below [92].

$$U=\begin{pmatrix}\rho\\ \rho u\\ \rho v\\ \rho E\end{pmatrix} \qquad F=\begin{pmatrix}\rho u\\ \rho u^2+P-\tau_{xx}\\ \rho uv-\tau_{xy}\\ \rho uE+Pu-k\frac{\partial T}{\partial x}-u\tau_{xx}-v\tau_{xy}\end{pmatrix}$$

$$G=\begin{pmatrix}\rho v\\ \rho uv-\tau_{yx}\\ \rho v^2+p-\tau_{yy}\\ \rho vE+Pv-k\frac{\partial T}{\partial y}-u\tau_{yx}-v\tau_{yy}\end{pmatrix} \qquad U=\begin{pmatrix}0\\ \rho f_x\\ \rho f_y\\ \rho\left(uf_x+vf_y\right)+\rho\dot{q}\end{pmatrix}$$

Here ρ is the density, u and v are the x and y directional velocities respectively, $\mathrm{E}=[\mathrm{e}+\mathrm{V}^2/2]$ is the total energy, τ_{xx} and τ_{yy} are the normal stresses, τ_{xy} is the shear Stress, k is the thermal conductivity of the fluid element, T is the temperature and f_x and f_y are the components of body forces of the fluid element per unit mass.

3.3.4.2 The Main Discretisation Methods

It has developed three discrete methods in N-S based CFD simulation:

♦ Finite-Difference Method

Finite-difference methods are based on the direct approximation of a differential form of the governing equations. It discretises the governing differential equations;

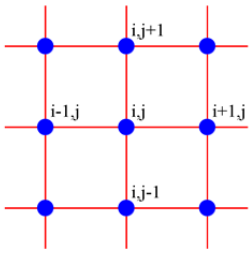

Figure 3-20: A finite-Difference model

$$0 = \frac{\partial u}{\partial x} + \frac{\partial v}{\partial y} \approx \frac{u_{i+1,j} - u_{i-1,j}}{2\Delta x} + \frac{v_{i,j+1} - v_{i,j-1}}{2\Delta y} \quad \textbf{(3-29)}$$

♦ Finite-Element Method

Express the solution as a weighted sum of shape functions $S_\alpha(x)$; e.g. for velocity:

$$\mathbf{u}(\boldsymbol{x}) = \sum \boldsymbol{u_\alpha S_\alpha}(\boldsymbol{x}) \quad \textbf{(3-30)}$$

Substitute into some form of the governing equations and solve for the coefficients weights $\boldsymbol{u_\alpha}$. The finite-element method is popular in solid mechanics, because it has considerable geometric flexibility.

♦ Finite-volume method (FVM)

Finite-volume method (FVM) or names box method is mainly employed for numerical solution of problems in fluid mechanics; it is a numerical method (Discretisation Methods) for the approximate solution of partial differential equations (PDEs). It was introduced in 1970s by McDonald, MacCormack and Paullay [93]. FVM mainly use property of its balance principles, which is the basis for the mathematical modelling of continue mechanical problems. Compare to another

two spatial discrete methods finite difference method (FDM) and the finite element method (FEM), it has the advantaged as:

1) it rigorously enforces conservation;
2) it is flexible in terms of both geometry and the variety of fluid phenomena;
3) It is directly relatable to physical quantities (mass flux, etc.).

Discretize the governing integral or control-volume equations, e.g.

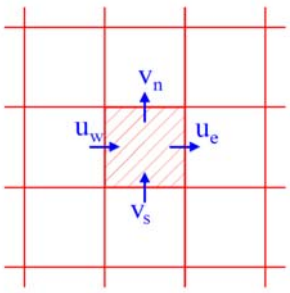

Figure 3-21: A finite control volume model

$$\frac{\partial}{\partial t}\iint Q\,dA + \int F ds = 0 \tag{3-31}$$

Where Q is the vector of conserved variables, F is the vector of fluxes, A is the volume of the control volume element at 2D condition, and s is the boundary of the 2D control volume element.

In general, the FVM involves the following steps:

1) Decomposition of the problem domain into control volumes;
2) Formulation of integral balance equations for each control volume;
3) Approximation of integrals by numerical integration;
4) Approximation of function values and derivatives by interpolation with nodal values;
5) Assembling and solution of discrete algebraic system.

Currently, the most well established CFD codes such as CFX/ANSYS and Fluent are using FVM approach.

3.3.4.3 Turbulence modelling

Turbulence is the most challenging area in fluid dynamics and the most limiting factor in accurate computer simulation of engineering flows. It constitutes a classical multi-scale problem, which is far beyond human intuitive understanding and beyond resolution capabilities of even the most powerful modern parallel computers [91]. Most flows exist in nature world or engineering applications are turbulent. Earth's atmosphere boundary layer, flow around wing (Figure 3-6), below ocean's surface water currents, etc. turbulence is a natural form of flow; it has the features [94]:

- Irregularity, or randomness, this makes a deterministic approach to turbulence problems impossible;
- Diffusivity, which causes rapid mixing and increased rates of momentum, heat, and mass transfer;
- Large Reynolds numbers, Turbulent flows always occur at high Reynolds numbers;
- Three-dimensional vorticity fluctuations, Turbulence is rotational and three dimensional;
- Dissipation, Turbulent flows are always dissipative. Viscous shear stresses perform deformation work which increases the internal energy of the fluid at the expense of kinetic energy of the turbulence.
- Continuum, Turbulence is a continuum phenomenon, governed by the equations of fluid mechanics.
- Turbulent flows are flows; Turbulence is not a feature of fluid but of fluid flows.

Turbulence is a natural phenomenon; it cannot be suppressed or eliminated. While the most of time of the aerodynamics only interest at the average quality, as lift and drag. For the vary part of the forces compare to average is secondary or vary fast that do not affect the overall flight. From a more pragmatic standpoint, however, one could argue that a complete understanding of turbulence is not required (and there is actually no indication that humans can comprehend complex nonlinear problems), but a sufficiently accurate solution of the underlying equations (better, a general method for achieving those) would suffice. Such numerical methods exist and allow a direct numerical simulation (DNS) of Navier–Stokes equations for all turbulence scales in space and time. However, due to the inherent scaling laws of turbulence, DNS can be applied only to very low Reynolds (Re) numbers and very simple and limited geometries. The numerical effort for DNS scales with Re^3, and with technical Re numbers in the range of 10^4 to 10^9, practically no numerical solution for flows of interest to engineers can be obtained. Turbulence

modelling is the attempt to develop approximate formulations that, despite our incomplete understanding and limited computational resources, allow engineers to obtain approximate solutions for their pressing technological applications. When dealing with turbulence models, keep in mind that they often need to bridge a gap of many orders of magnitude in computing power relative to DNS.

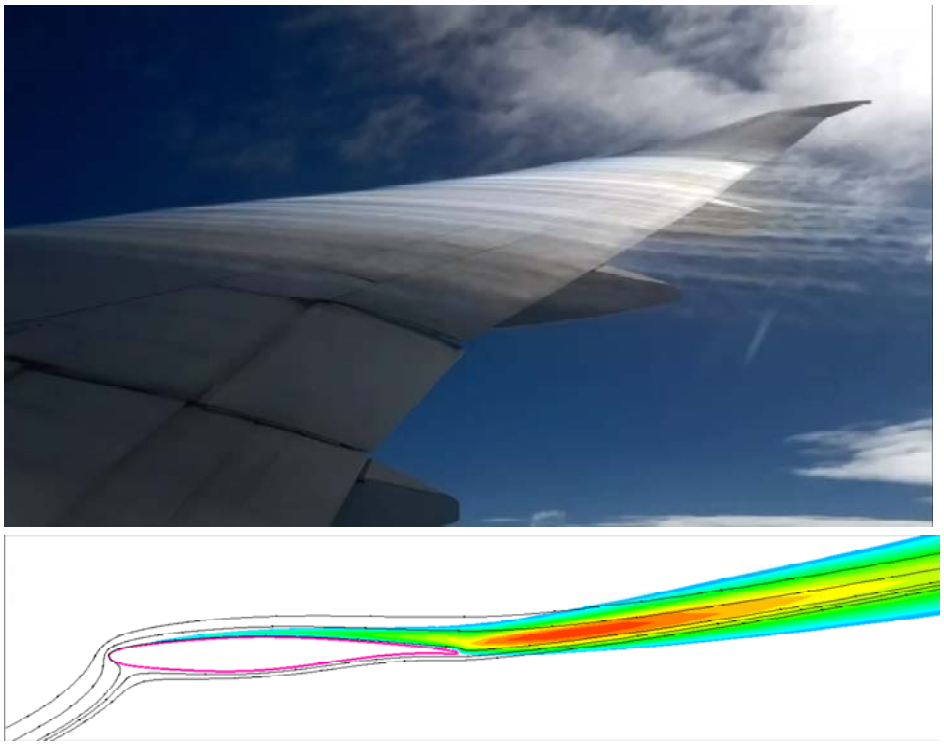

Figure 3-22: Turbulence on up wing surface [95], turbulent viscosity around a transonic flow airfoil.

The main field of application of Navier-Stokes method in aerodynamics will be for complex turbulent flows that cannot be treated by inviscid or viscous-inviscid interaction schemes.

Solving CFD problem usually consists of four main components: geometry and grid generation, setting-up a physical model, solving it and post-processing the computed data. The way geometry and grid are generated, the set problem is computed and the way acquired data is presented is very well known. Precise theory is available. Unfortunately, that is not true for setting-up a physical model for turbulence flows.

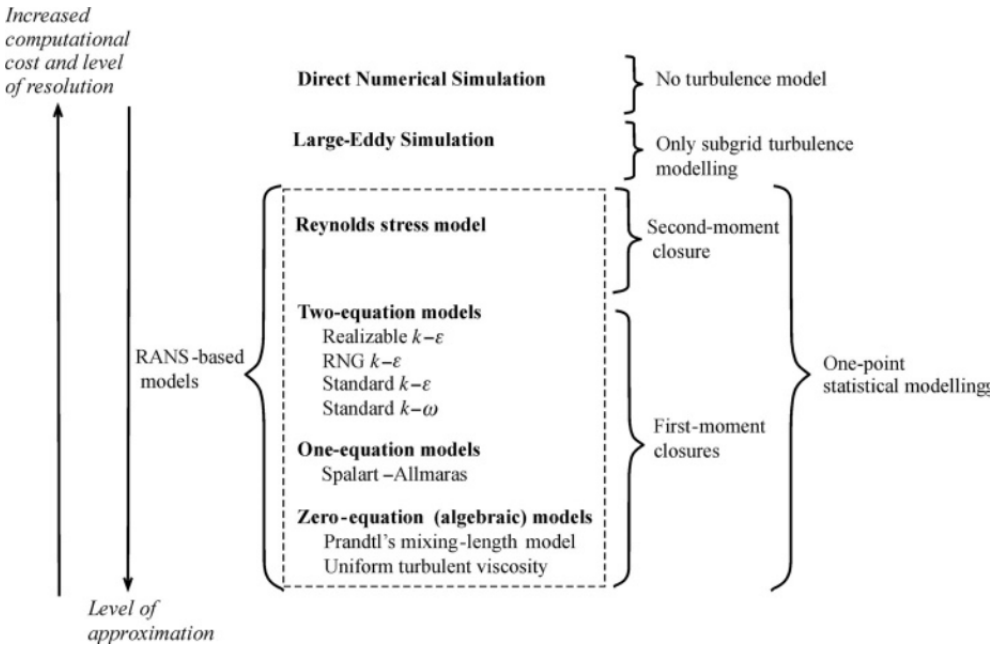

Figure 3-23: A schematic overview of turbulence modelling [96].

As this research will deal with transonic flow and low speed high angle simulation, the HLC airfoil low speed at high AOA, it will together with transonic, separation, according to figure 3-26 choose S-A model , and transonic choose T-W SST [97-99] .

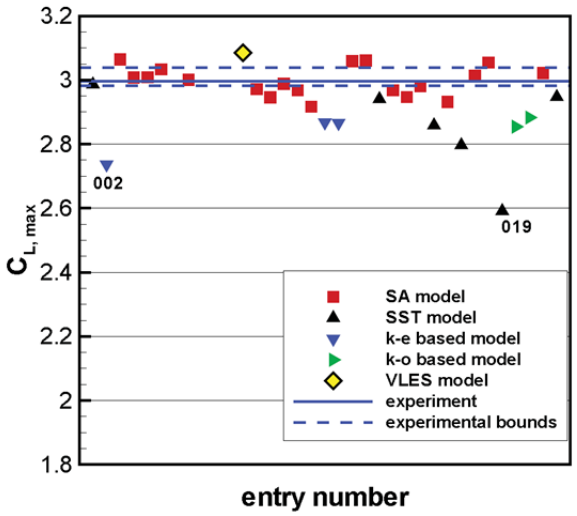

Figure 3-24: Turbulence used in predictions of maximum lift for HLC airfoil [100]

♦ Spalart-Allmaras turbulence model

In order to modelling the turbulence of the flow around HLC, the Spalart-Allmaras turbulence model [101] will be utilized, it is a one-equation model, and could provide very good computation result even with coarse mesh.

$$\frac{\partial}{\partial t}(\rho\tilde{v}) + \frac{\partial}{\partial x_i}(\rho\tilde{v}u_i) = G_v + \frac{1}{\sigma_{\tilde{v}}}\left(\frac{\partial}{\partial x_j}(\mu + \rho\tilde{v})\frac{\partial\tilde{v}}{\partial x_j} + C_{b2}\rho\left(\frac{\partial\tilde{v}}{\partial x_j}\right)^2\right) - Y_v + S_{\tilde{v}} \qquad \textbf{(3-32)}$$

Where $\sigma_{\tilde{v}}$ and C_{b2} are constants, G_V is the turbulent viscosity production, Y_v is the turbulent viscosity destruction, μ is the dynamic viscosity, v is the kinematic viscosity and $S_{\tilde{v}}$ is a source term which is ignored in estimating Reynolds stress since the model doesn't calculate the turbulent kinetic energy.

In this work S-A model was using to model the turbulence in the simulation of HLC airfoil.

- K-W SST turbulence model

The starting point for the development of the SST [98] model was the need for the accurate prediction of aeronautics flows with strong adverse pressure gradients and separation. $SST\ k-\omega$ turbulence model is a variant of the standard $k-\omega$ model. Combines the original Wilcox's $k-\omega$ model for use near walls and standard $k-\varepsilon$ model away from walls. It is the best of the two-equation worlds [102].

The $SST\ k-\omega$ turbulence model [98] is a two-equation eddy-viscosity model which has become very popular. The use of a $k-\omega$ formulation in the inner parts of the boundary layer makes the model directly usable all the way down to the wall through the viscous sub-layer; hence the $SST\ k-\omega$ model can be used as a Low-Re turbulence model without any extra damping functions. The SST formulation also switches to k-ε behaviour in the free-stream and thereby avoids the common $k-\omega$ problem that the model is too sensitive to the inlet free-stream turbulence properties. Authors who use the $SST\ k-\omega$ model often merit it for its good behaviour in adverse pressure gradients and separating flow. The $SST\ k-\omega$ model does produce a bit too large turbulence levels in regions with large normal strain, like stagnation regions and regions with strong acceleration. This tendency is much less pronounced than with a normal k-ε model though.

As in this research work, the $SST\ k-\omega$ model will be employed in the transonic simulation. Equations [97; 98]

$$\frac{\partial(\rho k)}{\partial t}+\frac{\partial(\rho U_i K)}{\partial x_i}=\tilde{P}_K-\beta^*\rho k\omega+\frac{\partial}{\partial x_i}\left[(\mu+\sigma_k\mu_t)\frac{\partial k}{\partial x_i}\right] \quad \textbf{(3-33)}$$

$$\frac{\partial(\rho\omega)}{\partial t}+\frac{\partial(\rho U_i\omega)}{\partial x_i}=\alpha\rho S^2-\beta\rho\omega^2+\frac{\partial}{\partial x_i}\left[(\mu+\sigma_\omega\mu_t)\frac{\partial\omega}{\partial x_i}\right]+2(1-F_1)\rho\sigma_{\omega2}\frac{1}{\omega}\frac{\partial K}{\partial x_i}\frac{\partial\omega}{\partial x_i} \quad \textbf{(3-34)}$$

Where the blending function F_1 is defined by:

$$F_1=tanh\left\{\left\{min\left[max\left(\frac{\sqrt{k}}{\beta^*\omega y},\frac{500v}{y^2\omega}\right),\frac{4\rho\sigma_{\omega2}k}{CD_{k\omega}y^2}\right]\right\}^4\right\} \quad \textbf{(3-35)}$$

With $CD_{k\omega}=max\left(2\rho\sigma_{\omega2}\frac{1}{\omega}\frac{\partial k}{\partial x_i}\frac{\partial\omega}{\partial x_i},10^{-10}\right)$ and y is the distance to the nearest wall. F_1 is equal to zero away from the surface ($k-\varepsilon$ model), and switches over to one inside the boundary layer ($k-\omega$ model), $\mu_t$is the turbulent eddy viscosity. All constants are computed by a blend from the corresponding constants of $k-\varepsilon$ and $k-\omega$ model via $=\alpha_1F+\alpha_2(1-F)$ $\beta^*=0.09$. S is the strain rate. $\sigma_k=0.85$, $\sigma_\omega=0.5$, $\sigma_{\omega2}=0.856$.

3.3.4.4 Near wall treatment

The success of RANS models is mostly manifested by the accuracy achieved in computation of wall-bounded flows. The wall is the main source of turbulence in external flows. This is the reason why a lot of effort has to be put to model accurate enough the flow in the zone closed to the walls.

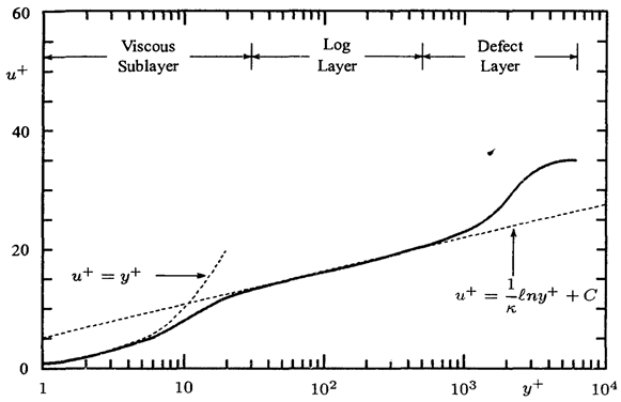

Figure 3-25: Typical velocity profile for a turbulent boundary layer [103]

In this work following equations used to calculate the near wall grid dimensions [104].

$$\mathrm{Re} = \frac{\rho \cdot U \cdot C}{\mu} \tag{3-36}$$

$$C_f = [2\log_{10}(Re) - 0.65]^{-2.3} \quad for\ Re < 10^9 \tag{3-37}$$

$$\tau_\omega = C_f \cdot \frac{1}{2}\rho U^2 \tag{3-38}$$

$$u_* = \sqrt{\frac{\tau_\omega}{\rho}} \tag{3-39}$$

$$y = \frac{y^+ \mu}{\rho u_*} \tag{3-40}$$

Where Re is the Reynolds number; ρ , μ and U is the free-stream density, velocity and dynamic viscosity respectively; C is the chord of the airfoil; C_f is the skin-friction coefficient, τ_ω is the wall shear stress, u_* is the friction velocity, y^+ is the dimensionless wall distance and y is the required wall distance. In this thesis a proper y^+ will be gotten by validation.

3.4 Surrogate model construction

Surrogate models are especially useful for multi-dimensional CFD projects, which might require on the order of millions of multi-hour simulation cases to fully explore the design space. A surrogate model provides a faster way to confirm your results, identify trends, establish correlations, and locate areas of interest from an initially limited number of cases.

The process of constructing an approximation model involves:

a) Getting initial computational results (sample or training);
b) Constructing a surrogate Model based on the learning from the samples.

By use the high-fidelity method, it uses equation to express the design variables and the output result.

$$\mathrm{y} = \mathrm{f}(x) \tag{3-41}$$

where $x = \{x_1, x_2, \cdots x_n\} \in R^n$ is the vector of n design parameters, and y is the scale output (or calls response). While a surrogate model is expressed as:

$$\mathrm{y} = \hat{\mathrm{f}}(x, \alpha) \approx \mathrm{f}(x) \tag{3-42}$$

where α is the vector of undetermined parameters that must be evaluated prior to applying the surrogate model.

3.4.1 Overview of Surrogate Model Construction

The basically function of surrogate model is for predicting the trend of the relationship between objectives and variables, based on the sample populations. Following listed model could be used in constructing surrogate models.

1) Response Surface Model
2) Radial Basis Function Model
3) Artificial Neural Network Model
4) Kriging Model

The accuracy of the surrogate model relies on the number and on the distribution of samples provided in the search space, as well as on the selection of the appropriate model to represent the objective functions and constraints.

- **Response Surface Model**

Response surface model (RSM) also called polynomial regression; it uses samples' response to estimate the unknown parameters α.

$$\mathrm{y} = \mathrm{y} + \varepsilon \tag{3-43}$$

$$\hat{y} = \beta_0 + \sum_{i=1}^{K} \beta_i x_i + \sum_{i=1}^{k} \sum_{j \geq i}^{k} \beta_{ij} x_i x_j \tag{3-44}$$

$$\beta = [A^T \quad A]^{-1} A^T y \tag{3-45}$$

$$A(n \times m) = \begin{bmatrix} 1 & x_{11} & \cdots & x_{11}x_{12} & \cdots & x_{1k}^2 \\ 1 & x_{21} & \cdots & \cdots & \cdots & x_{1k}^2 \\ \cdot & \cdot & \cdots & \cdots & \cdots & \cdot \\ \cdot & \cdot & \cdots & \cdots & \cdots & \cdot \\ 1 & x_{n1} & \cdots & x_{n1}x_{n2} & \cdots & x_{nk}^2 \end{bmatrix} \tag{3-46}$$

- **Radial Basis Function Model**

Radial Basis Function (RBF) Model is a nonparametric regression modelling technique. It is designed to suit outputs with deterministic errors. The method uses linear combinations of radially symmetric functions based on the Euclidean distance from a given "centre" as the basis functions to approximate response functions.

$$\hat{f}(x, m, \mathbf{w}) = \sum_{i=0}^{m} (w_i x_i) \tag{3-47}$$

$$f = \Phi \mathbf{W} \tag{3-48}$$

$$\Phi = \begin{Bmatrix} 1 & \mathrm{x}_1 & \mathrm{x}_1^2 & \cdots & \mathrm{x}_1^{\mathrm{m}} \\ 1 & \mathrm{x}_2 & \mathrm{x}_2^2 & \cdots & \mathrm{x}_2^{\mathrm{m}} \\ \vdots & \vdots & \vdots & \ddots & \vdots \\ 1 & \mathrm{x}_{\mathrm{n}} & \mathrm{x}_{\mathrm{N}}^2 & \cdots & \mathrm{x}_{\mathrm{N}}^{\mathrm{m}} \end{Bmatrix} \tag{3-49}$$

$$\hat{f}(\boldsymbol{x}) = \sum_{i=0}^{N_{RBF}} (w_i h_i(\boldsymbol{x})) \tag{3-50}$$

$$h_i(\boldsymbol{x}) = \exp\left(\frac{-(X-c)^2}{\delta^2}\right) \tag{3-51}$$

$$\Phi = \begin{Bmatrix} \boldsymbol{h_1}(\boldsymbol{x}^{(1)}) & \boldsymbol{h_2}(\boldsymbol{x}^{(1)}) & \cdots & \boldsymbol{h_{N_{RBF}}}(\boldsymbol{x}^{(1)}) \\ \boldsymbol{h_1}(\boldsymbol{x}^{(2)}) & \boldsymbol{h_2}(\boldsymbol{x}^{(2)}) & \cdots & \boldsymbol{h_{N_{RBF}}}(\boldsymbol{x}^{(2)}) \\ \vdots & \vdots & \ddots & \vdots \\ \boldsymbol{h_1}(\boldsymbol{x}^{(N)}) & \boldsymbol{h_2}(\boldsymbol{x}^{(N)}) & \cdots & \boldsymbol{h_{N_{RBF}}}(\boldsymbol{x}^{(N)}) \end{Bmatrix} \tag{3-52}$$

$$\hat{f}(\boldsymbol{x}) = \mathbf{h}^T \hat{\mathbf{w}} \tag{3-53}$$

- **Artificial neural network Model**

Artificial neutral network (ANN), are also known as neural networks, are information processing system with their design inspired by the studies of the ability of the human brain to learn from observations and to generalize by abstraction. The main advantage of neural networks is their ability to represent complex input/output relationships. They are well suited for use in data classification, function approximation, and signal processing, among others [105].

The process of the ANN works states in Figure 3-28,

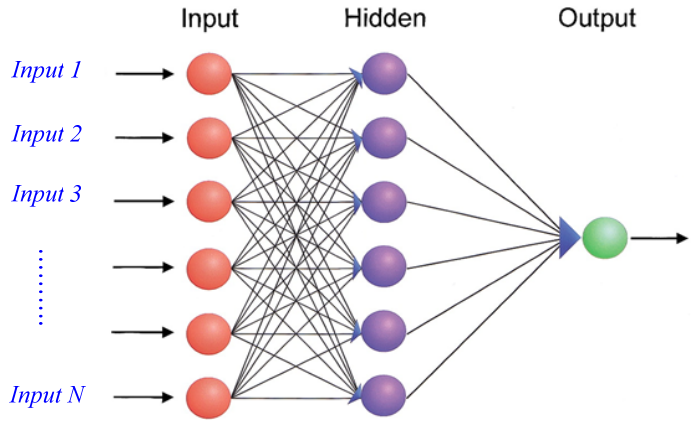

Figure 3-26: Schematic representation of a Multi-layered ANN

$$\hat{y} = \sum_{i=1}^{K} \alpha_i \emptyset(a_i) \quad \textbf{(3-54)}$$

$$a_i = \sum_{j=1}^{K} \gamma_{ij} x_j + \beta_j \quad \textbf{(3-55)}$$

$$\emptyset(a) = (1 + e^{-a})^{-1} \quad \textbf{(3-56)}$$

- **Kriging Model**

Kriging is one of the interpolation techniques more widely used in spatial and geostatistics. Though it is mainly used in these two fields its application is now widely extended to biostatistics, agriculture, and human geography and computer experiments. It was initially proposed by Danie G. Krige. He is a South African geologist who pioneered the field of geostatistics. This method was further developed by Georges Matheron, a French geologist. Kriging is a geostatistics and linear interpolation method which can predict the response value at an unexplored sample point placed within a defined design space based on the observed data available at some other sample points within the same design space. A much detail discuss about Kriging model in the following section.

3.4.2 Kriging Model

Kriging also knows as design and analysis of computer experiments DACE; it is a nonparametric interpolation model base on Gaussian stochastic process models. Compare to RSM, Kriging was initially design for computational-based

experiments characterized by deterministic errors [106]. Kriging uses a global model that interpolates all design points plus “localized” functions representing the deviations from the global model at all points. The response is expressed in terms of the design parameters as:

$$\hat{y}(\mathbf{X}) = f(\mathbf{X}) + Z(\mathbf{X}) \tag{3-57}$$

where $f(\mathbf{X})$ is the low-order polynomial that interpolates the design points. Typically a constant value was found sufficient for modelling complex input-output dataset from the training relations [107]. Hence, the output can be viewed as a random field with mean ,

$$\hat{y}(\mathbf{X}) = \boldsymbol{\beta} + Z(\mathbf{X}) \tag{3-58}$$

$Z(\mathbf{X})$ is a Gaussian stochastic function that represents the realization of random process with zero mean, variance σ^2, and covariance given by

$$Cov(Z) = \sigma^2 \mathbf{R}(\mathbf{X}^{\boldsymbol{i}}, \mathbf{X}^{\boldsymbol{j}}) \tag{3-59}$$

where $\mathbf{R}(\mathbf{X}^{\boldsymbol{i}}, \mathbf{X}^{\boldsymbol{j}})$ is the correlation matrix which is an $n \times n$ symmetric matrix with ones in the diagonal and n is the number of training set. Other terms in the matrix are given by the spatial correlation function

$$R_{ij} = \prod_{l=1}^{k} scf_k\left(x_k^i - x_k^j\right) \tag{3-60}$$

where i and j denote two training points, l refers to a design parameter, and k is the number of design parameters. The spatial correlation function can be viewed as functions of the "weighted" distance between samples. It can have many forms; typically a linear, a cubic, or an exponential (Gaussian) function,

$$scf(d) = \begin{cases} 1 - \dfrac{1}{\theta}|d|, & |d| < 0 \\ 0 & |d| \geq 0 \end{cases} \tag{3-61}$$

$$scf(d) = \begin{cases} 1 - 6\left(\frac{d}{\theta}\right)^2 + 6\left(\frac{|d|}{\theta}\right)^3, & |d| < \frac{\theta}{2} \\ 2(1 - \frac{1}{\theta}|d|)^3, & \frac{\theta}{2} \leq |d| < 0 \\ 0, & |d| \geq 0 \end{cases} \quad \textbf{(3-62)}$$

$$scf(d) = \exp(-\theta \times d^p) \quad \textbf{(3-63)}$$

The mean parameter $\boldsymbol{\beta}$ is evaluated by minimizing the sum of squares of error of the estimated error using the equation

$$\boldsymbol{\beta} = [\mathbf{A}^T\mathbf{R}^{-1}\mathbf{A}]^{-1}\mathbf{A}^T\mathbf{R}^{-1}\boldsymbol{y} \quad \textbf{(3-64)}$$

where $\mathbf{A}$ is an $n \times m$ matrix of training set points depending on the choice of the function $f(\mathbf{X})$; in the constant case, A is a $n \times 1$ vector of all ones. The parameters θ (and p) that ensure the "best fit" of the model to the training data are evaluated by maximizing the likelihood estimation *MLE* (or minimizing its negative). *MLE* can have a variety of forms:

$$-\frac{1}{2}\left[n\ln(2\pi) + n\ln\sigma^2 + \ln|\mathbf{R}| + \frac{1}{2\sigma^2}(\mathbf{y} - \mathbf{A}\boldsymbol{\beta})^T\mathbf{R}^{-1}(\mathbf{y} - \mathbf{A}\boldsymbol{\beta})\right] \quad \textbf{(3-65)}$$

$$\frac{1}{(2\pi\sigma^2)^{n/2}\sqrt{|\mathbf{R}|}}\exp\left(\frac{-(\mathbf{y} - \mathbf{A}\boldsymbol{\beta})^T\mathbf{R}^{-1}(\mathbf{y} - \mathbf{A}\boldsymbol{\beta})}{2\sigma^2}\right) \quad \textbf{(3-66)}$$

$$-\frac{1}{2}[n\ln(2\pi) + n\ln\sigma^2 + \ln|\mathbf{R}| + n] \quad \textbf{(3-67)}$$

$$-\frac{1}{2}[n\ln\sigma^2 + \ln|\mathbf{R}|] \quad \textbf{(3-68)}$$

$$-\frac{n}{2}[\ln\sigma^2 + \ln|\mathbf{R}|] \quad \textbf{(3-69)}$$

where the maximum likelihood estimation of σ^2 is expressed as:

$$\sigma^2 = \frac{1}{n}(\mathbf{y} - \mathbf{A}\boldsymbol{\beta})^T\mathbf{R}^{-1}(\mathbf{y} - \mathbf{A}\boldsymbol{\beta}) \quad \textbf{(3-70)}$$

Generally, evaluating the *MLE* is a nonlinear unconstrained optimization subproblem where σ^2 and $\mathbf{R}$ are functions of the unknown parameters. The response at a new point $\overline{\mathbf{X}}$ in the design space $\hat{y}(\overline{\mathbf{X}})$ is directly evaluated by applying the equation:

$$\hat{y}(\overline{\mathbf{X}}) = \boldsymbol{\beta} + \mathbf{r}^T(\overline{\mathbf{X}})\mathbf{R}^{-1}(\mathbf{y} - \mathbf{A}\boldsymbol{\beta}) \quad \textbf{(3-71)}$$

where $\mathbf{r}(\overline{\mathbf{X}})$ is the correlation vector between x and all points in the training set.

3.4.3 Model Comparison

Different surrogate model has its own characteristics when deal with special task, some of the researches had done the comparisons as [60].

Response surface model

AD: Well established model, easy to implement, require fewer calls of the high fidelity model. Better performance with low order nonlinear functions. Best suited for small scale applications with less than 10 design parameters. Due to the "smoothing" capabilities of polynomials, optimization converges relatively faster with noisy functions.

Dis-AD: a drawback is expected with highly non-linear and irregular performance problems. - Higher order polynomials can be adopted. However, a large number of training points is needed. Using higher-order polynomials invokes instabilities and yield false optima.

Radial Basis Functions

AD: yields good results for a wide range of sampling size and design. Produces good approximations to response functions with various patterns of both random and deterministic errors. For high-order nonlinear and small scale problems, RBF models are relatively more accurate and robust.

Dis-AD: the evaluation of the model parameters involves computational complications especially with large number of design parameters; such computations can be highly expensive regarding computation and memory.

Artificial Neural Networks

AD: yield better approximations compared to the classical response surface methods in cases if the nature of the problem is unknown, involves large number of design parameters, or not completely bounded design spaces

Dis-AD: a relatively large number of parameters are involved; the evaluation of these parameters requires high computation and memory requirements. Many sophisticated procedures for estimating the number of neurons, initialization, training, and regularization.

Kriging

AD: well suited for numerical experiments with deterministic errors. Extremely flexible by virtue of a wide range of correlation functions. Even when a constant term is used for the global part of the model, the performance is comparable to a quadratic regression model. has a higher performance when applied to low-order nonlinear and large scale problems over a wide range of samples size and design.

Dis-AD: model construction can be time consuming for large scale problems. It involves matrices operations, optimization sub-problems. Such costs may overweight the benefits. If the training points are relatively "close" to each other, the correlation matrix can become singular. Additional points are needed to assess the accuracy of the model.

3.5 Optimization Methods

Optimization could be happens in daily life.

“A student may visit one restaurant more frequently than others on campus, after she or he had tried the food in several restaurants of the school.”

Optimizations do not just happen in human activity, some are unconscious natural behaviour such as when we play ball games, and we always need to change our eyeball dioptre to obtain a clearer view, in order to locate the ball position. The process of changing eyeball dioptre is an optimization process. The human being was derived from apes also is the process of optimization, the driver for this optimization is natural selection rules.

Any Optimization activity should have the common properties:

- Exists different possible choices or tendencies of development;
- Reasons to make the choice;
- Have constrains.

Take a thousand-kilometers travel as the example, the traveler can utilize the car, bus, train or airplane to be the transport method, different people may take different travel options. The holiday couples may enjoy the sights along the way while at easy, some may favor the driving feeling on the highway, someone may

take a business travel. So time efficiency may be important to him. And the possible constrains for the travel could be the travel budget, time allowance, personal favors and physical condition, etc.

Optimization has not always happened unconsciously, people have learned and studied to use different optimization methods to conduct their design and research to get the optimum design.

As for airplane wing optimal design, it is a multi-objective involving structure efficient, aerodynamic efficient and production economy.

In mathematics, computer and management science, optimization is a method that selects a best element from some set of available alternatives with regard to some constrains, it can be described in the formulation as:

Without loss of generality, minimization is assumed in the following definitions, since any maximization problem can be transformed into a minimization one. A multi-objective optimization problem (MOP) can be mathematically defined as [108]:

$$\min \ \vec{f}(\vec{x}) \coloneqq [f_1(\vec{x}), f_2(\vec{x}), \dots \dots f_k(\vec{x})] \qquad \textbf{(3-72)}$$

Subject to:

$$g_i(\vec{x}) \leq 0 \quad i = 1,2, \dots, m$$

$$h_i(\vec{x}) = 0 \quad i = 1,2, \dots, p$$

Where $\vec{x} = [X_1, X_2, \dots, X_n]^T$ is the vector of decision variables; $\vec{f}$ Are the objective functions; g_i and h_i are the constraint functions.

As it says, that a multi-objective optimization is based on N-dimension variables $\vec{x} = [X_1, X_2, \dots, X_n]^T$, the link between the variables and design objectives is the functions as f_i , and the decision variables have the constrain as g_i And h_i. In order to take whole optimization process, it need following list steps [108]:

1) Model to use
2) Global/local surrogate model
3) Sample size and distribution for initial surrogate training

4) Infilling criterion

Optimizer could base pre-iteration data to train new variables and its objectives.

3.5.1 Local/ Global Optimization

It has developed many optimization methods could be used in ASO. According to the research manner and capability, they can be categorised into two kinds: local optimization and global optimization.

A local optimum of an optimization problem is a solution that is optimal (either maximal or minimal) within a neighbouring set of candidate solutions. This is in contrast to a global optimum, which is the optimal solution among all possible solutions, not just those in a particular neighbourhood of values, the different function owing to the different search mechanism.

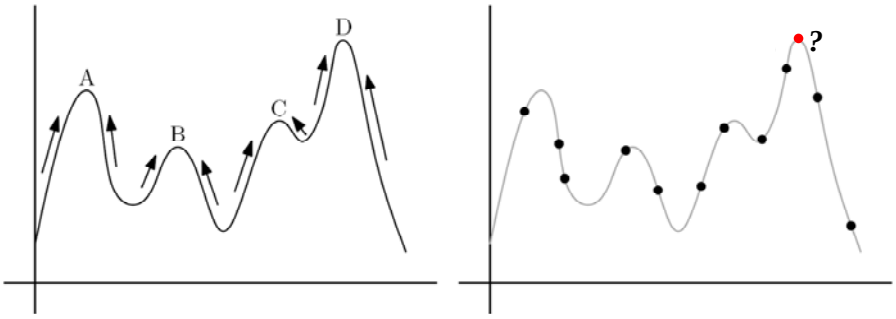

Figure 3-27: Example of local/global optimum

3.5.2 Single/Multi-objective optimization

As implied by its name, single-objective optimization is the optimization activity that only care its main design objective, like a traveller needing to go to airport catch his airplane, but the time is too tight, in this case, he will consider times of all of the possible public traffic as an alternate choose, but does not care the difference in fares.

$$f_{i=1,2,\ldots K} \begin{cases} k = 1 \rightarrow Single - objective \\ k \geq 2 \rightarrow Multi - objective \end{cases}$$ Objective function(s),

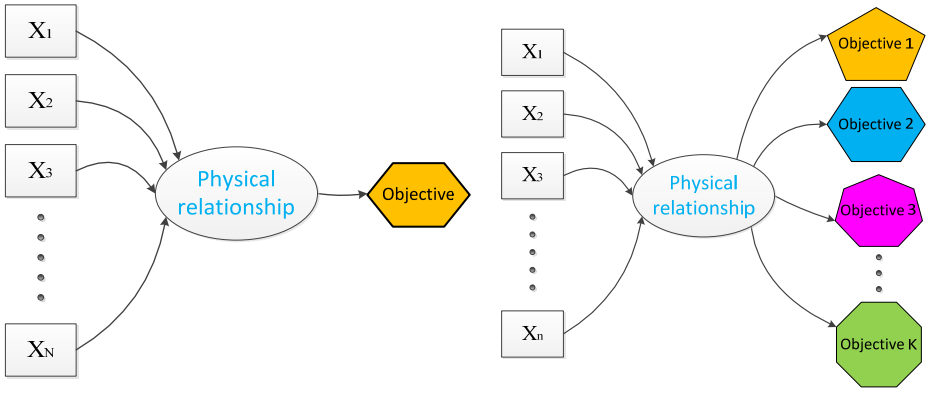

Figure 3-28: Single/Multi-objective model

In airplane aerodynamic design process, there exists some design tasks that only need consider one objective, as for the cruise phase, cruise efficiency index MC_L/C_D. While in landing phase, the most important aerodynamic characteristic is the maximum CL can be used. These two objectives will be discussed in the following chapters.

Different from single-objective optimization, Multi-Objective has more than one design objective should be taken consideration that derived from the variables and theirs physical relationship. Some examples may be easily to found, for a given amount of budget to buy a tablet PC, the input may be not only the Money, but also the time as the newest tablet PC will be release in a Regular or specified day, so it need the consumer to wait for a certain of time. Also there exist several brands could be alternate, as Apple, Nokia, Samsung or Lenovo, and theirs different versions, as IPad Air, IPad 4, etc. , different choice options could give the buyer the objective as performance, available external resources and saving, etc. . These different objectives are some-times comparable, while some of them hard to compare, so that needs take consideration how to coordinate it according to the wishes of the buyer's subjective.

Multi-objective optimization also frequently rise the interest to aircraft design engineers when deal with aircraft wing design, for example a complex high-lift devices may bring a good aerodynamic performance at low speed, while it may bring a heavier useless weight to high speed flight, in this case aerodynamic performance and weight are the two objectives. In such case an optimal deci-

sions need to be taken in the presence of the trade-off between this two conflicting objectives. This kind question was described by Italy economical Pareto [109]. The Pareto optimum (or efficiency) points that all individuals hard reach their optimum point simultaneously with the allocated resources. In the Pareto Optimum theory it has the term as Pareto frontier; it is states as a setting point that cannot be improve itself while not reduce others value. The C point in Figure 3-3 is not the Pareto frontier points; because point B and A are better that it both refers the objective f1 and f2. Normally a multi-objective design would be a choice from the Pareto frontier.

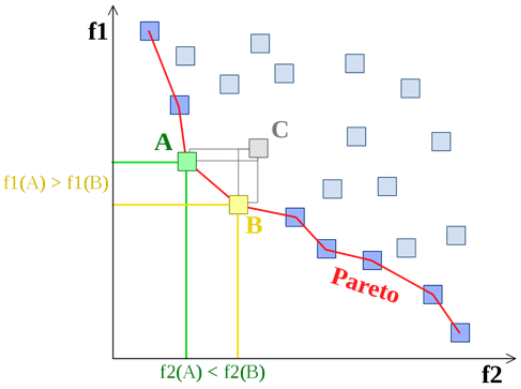

Figure 3-29: Example of a Pareto frontier [109]

There exist several trade-off strategies can be utilized in the Multi-objective optimization application:

- Convert into single- objective method

Convert multi-objective into single-objective optimization task, it is a relatively simple and popular method [110]. A simple covert method is weighting method;

- Main objective priority method

Some objectives among the objectives may have the priority than others, so the optimization will begin with some of the objectives, after search the new design space meet the criteria of the priority objective.

- Sequentially iterations method

It begin with part objective(s) optimization, after meeting the criteria(s), then fix the optimization space, then going to do the optimization at the consideration of other objective(s), after this optimization

- Step method

  The basic idea of step method is: firstly a solution of the original ideal multi-objective problems need to find (f1 *, f2 *, ..., fp *). In fact, these solutions fi * (i = 1,2, ..., p) cannot be achieved simultaneously, it can be used as an ideal set of optimum values. The ideal solution as a standard, efficient solution can be estimated, and then through dialogue, constantly revised target and targets to reduce the requirements as new constraints added to the original constraint conditions recalculated until strategy makers get a satisfactory solution.

3.5.3 Methods of Airfoil Optimization

Nowadays, there are wide varieties of optimization schemes that are being used in attending engineering optimization activities. The optimization schemes can be categorized into two types: gradient-based (or derivative) optimization schemes and evolutionary (or non-derivative) optimization schemes.

Local approach: such as gradient-base, stepping search and steepest decent scheme.

Global approach: such as Simulate Annealing, Particle swarm, Tabu search and Genetic algorithm.

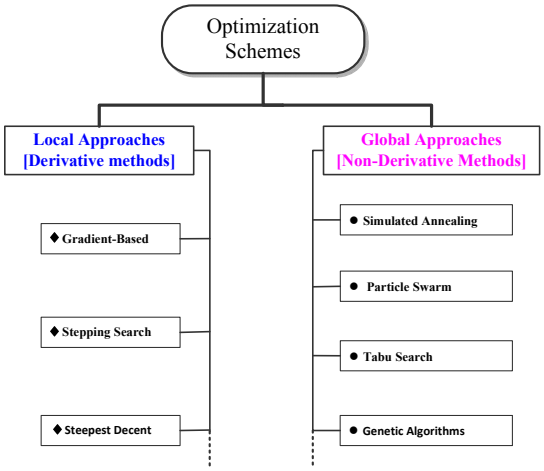

Figure 3-30: A classification of optimization schemes

♦ Gradient-Base

The gradient based schemes use iterative approach to perform the optimisation for finding the minimum (maximum search can convert to minimum search) of the function.

♦ Stepping search

The stepping search method is one of the gradient-based optimization schemes. In which, the best solution of the objective function is calculated by evaluating the derivatives of the governing equations.

♦ Steepest decent

It also knows finite-difference approaches. In the above stepping search approach, if the actual calculation of the objective functions is done using the, then it will be known as steepest descent.

● Simulated Annealing

Simulated Annealing (SA) is probabilistic heuristic for solving the global optimization problem, it is a random-search technique which exploits an analogy between the way in which a metal cools and freezes into a minimum energy crystalline structure (the annealing process) [111]. Simulated annealing was developed in 1983 to deal with highly nonlinear problem, the key feature of simulated annealing is that it provides a means to escape local optima by allowing hill-climbing moves [112]; a more easily understood metaphor [113] as:

"*SA approaches the global maximization problem similarly to using a bouncing ball that can bounce over mountains from valley to valley. It begins at a high "temperature" which enables the ball to make very high bounces, which enables it to bounce over any mountain to access any valley, given enough bounces. As the temperature declines the ball cannot bounce so high, and it can also settle to become trapped in relatively small ranges of valleys.*"

The Structure of the SA algorithm states in Figure 3-31. Simulated annealing can deal with highly nonlinear models, chaotic and noisy data and many constraints.

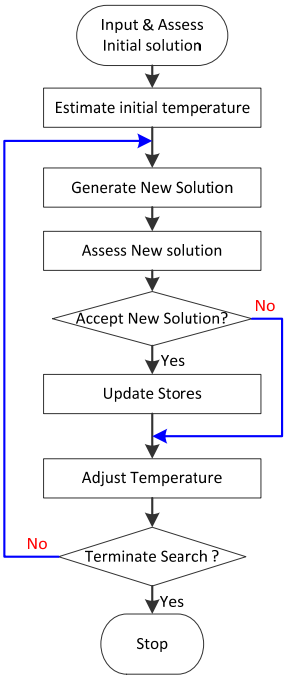

Figure 3-31: The structure of the SA algorithm [113]

- **Particle Swarm**

Particle swarm optimization (PSO) is a population-based search algorithm inspired by the behaviour of biological communities that exhibit both individual and social behaviour; examples of these communities are flocks of birds, schools of fishes and swarms of bees. Members of such societies share common goals (e.g., finding food) that are realized by exploring its environment while interacting among them. Each particle's movement is influenced by its local best known position but, is also guided toward the best known positions in the search-space, which are updated as better positions are found by other particles. This is expected to move the swarm toward the best solutions [114]. The initial ideas on particle swarms of Kennedy and Eberhart were essentially aimed at producing computational intelligence by exploiting simple analogues of social interaction, rather than purely individual cognitive abilities [115]. In computer science, particle swarm optimization is a com-

putational method that optimizes a problem by iteratively trying to improve a candidate solution with regard to a given measure of quality.

- **Tabu Search**

Tabu Search (TS) is a metaheuristic that guides a local heuristic search procedure to explore the solution space beyond local optimality. It has achieved widespread successes in solving practical optimization problems. Applications are rapidly growing in areas such as resource management, process design, logistics, technology planning, and general combinatorial optimization. Hybrids with other procedures, both heuristic and algorithmic, have also produced productive results [116].

TS use a local or neighbourhood search procedure to iteratively move from one potential solution x to an improved solution x' in the neighbourhood of x, until some stopping criterion has been satisfied. One of the main components of TS is its use of adaptive memory, which creates a more flexible search behaviour. Memory-based strategies are therefore the highlight of TS approaches, founded on a quest for “integrating principles,” by which alternative forms of memory are appropriately combined with effective strategies for exploiting them [117].

- **Genetic Algorithms**

But easily the most amazing nature is a very important optimization methods have been overlooked is that our evolution, relying on evolution, biological can live several kilometres deep in the Earth's deep oceans, but also be able to soar above the Qomolangma Mountain of migratory birds; there able to hold more than 70 degrees below zero multiply endless glacier penguins, also manoeuvre in submarine caldera worms. All of the amazing and naturally phenomena are governing by a rule calls evolutionary. In the area of

GAs is a type of Evolutionary Algorithms (EAs), which illustrates the human being developed from Ancient biologicals.

The concept of genetic algorithms (GA) was developed by Holland and his colleagues in the 1960s and 1970s [18]. GA is inspired by the evolutionist theory explaining the origin of species. In nature, weak and unfit species within their environment are faced with extinction by natural selection. The strong ones have greater opportunity to pass their genes to future generations via reproduction. In the long run, species carrying the correct combination in their genes become dominant in their population. Sometimes, during the slow process of evolution, random changes may occur in genes. If these

changes provide additional advantages in the challenge for survival, new species evolve from the old ones. Unsuccessful changes are eliminated by natural selection.

In GA terminology, a solution vector $x \in X$ is called an individual or a chromosome. Chromosomes are made of discrete units called genes. Each gene controls one or more features of the chromosome. In the original implementation of GA by Holland, genes are assumed to be binary numbers. In later implementations, more varied gene types have been introduced. Normally, a chromosome corresponds to a unique solution x in the solution space. This requires a mapping mechanism between the solution space and the chromosomes. This mapping is called an encoding. In fact, GA works on the encoding of a problem, not on the problem itself.

GA operates with a collection of chromosomes, called a population. The population is normally randomly initialized. As the search evolves, the population includes fitter and fitter solutions, and eventually it converges, meaning that it is dominated by a single solution. Holland also presented a proof of convergence (the schema theorem) to the global optimum where chromosomes are binary vectors.

GA use two operators to generate new solutions from existing ones: crossover and mutation. The crossover operator is the most important operator of GA. In crossover, generally two chromosomes, called parents, are combined together to form new chromosomes, called offspring. The parents are selected among existing chromosomes in the population with preference towards fitness so that offspring is expected to inherit good genes which make the parents fitter. By iteratively applying the crossover operator, genes of good chromosomes are expected to appear more frequently in the population, eventually leading to convergence to an overall good solution.

The mutation operator introduces random changes into characteristics of chromosomes. Mutation is generally applied at the gene level. In typical GA implementations, the mutation rate (probability of changing the properties of a gene) is very small, typically less than 1%. Therefore, the new chromosome produced by mutation will not be very different from the original one. Mutation plays a critical role in GA. As discussed earlier, crossover leads the population to converge by making the chromosomes in the popula-

tion alike. Mutation reintroduces genetic diversity back into the population and assists the search escape from local optima.

Reproduction involves selection of chromosomes for the next generation. In the most general case, the fitness of an individual determines the probability of its survival for the next generation. There are different selection procedures in GA depending on how the fitness values are used. Proportional selection, ranking, and tournament selection are the most popular selection procedures. The procedure of a generic GA is given as follows:

Step 1: Set t =1. Randomly generate N solutions to form the first population, P1. Evaluate the fitness of solutions in P1.

Step 2: Crossover: Generate an offspring population Qt as follows.

- *Choose two solutions x and y from Pt based on the fitness values.*
- *Using a crossover operator, generate offspring and add them to Qt.*

Step 3: Mutation: Mutate each solution $x \in Qt$ with a predefined mutation rate.

Step 4: Fitness Assignment: Evaluate and assign a fitness value to each solution $x \in Qt$ based its objective function value and infeasibility.

Step 5: Selection: Select N solutions from Qt based on their fitness and assigned them Pt+1.

Step 6: If the stopping criterion is satisfied, terminate the search and return the current population, else, set t=t+1 go to Step 2.

For airfoil shape optimization, two choices of optimizer can be made: either using a global optimization method, which can be a GA or a simulated annealing (SA), or gradient-based method.

The gradient-based method can only be used if the fitness function (the function we need to optimize) is differentiable. The entire article agreed that the GA is more robust (it can find global maximum while the gradient-based optimizer can be trapped into local maximum) but less accurate and more expensive in CPU time. So, some article proposes hybrid optimizer, using GA to find where the global maximum is and the gradient-based optimizer to define this maximum precisely.

Chapter4. Airfoil shape Optimization

This chapter deals with the airfoil design optimization within the subject of aerodynamic; it involves both transonic single-element airfoil and low-speed High-lift configuration multi-element airfoil design optimization. Because this research paid the attention of the trim effect to the whole airfoil performance, so it induced a trim model, the airfoil is assumed is NACA 0010, which is an asymmetry airfoil [33], its transonic performance and low-speed aerodynamic characteristics performance is shown in Figure 4-1, from the two curves get the induce drag factor is 0.0035 and 0.0038 respectively. These data was gotten by using XFLR5 panel-based CFD software. It is trim efficiency is based on the equation 4-1 to 4-3. In order to balance the moment on the wing airfoil, so the horizontal tail needs general a lift ΔC_L to balance combination with its location 4 chords after the wing quarter point, refer to the wing airfoil moment reference point, which is 0.25 Chord from the leading edge. And the owing to the ΔC_L produce raises a drag increase to the horizontal tail according to equation 4-2, even the horizontal tail defection will bring a small amount of the Moment, and the induce drag will produce an additional balance effect to the whole aircraft, but these secondary balance effect not take consideration within this research.

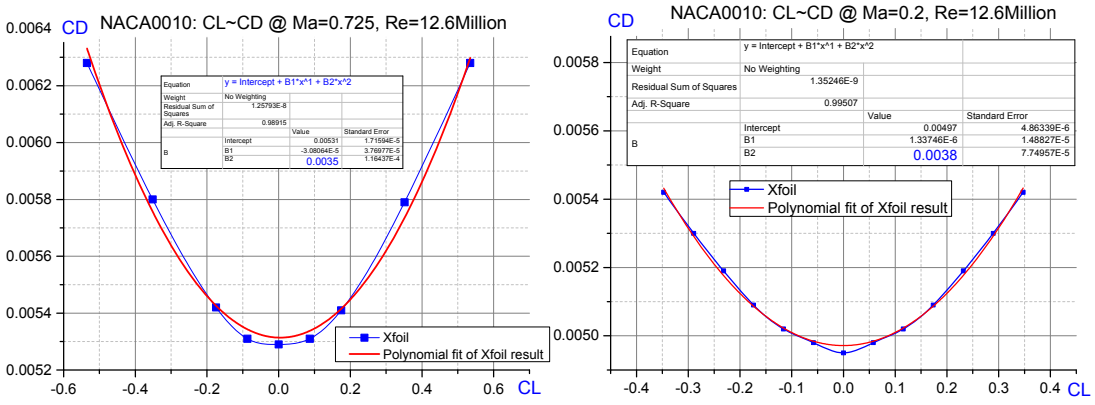

Figure 4-1: Tail trim efficiency

$$\Delta C_L = \frac{m}{Arm} / \cos(\alpha) \qquad \textbf{(4-1)}$$

$$C_D = C_{D0} + \Delta C_L^2 \times \varepsilon \qquad \textbf{(4-2)}$$

$$\Delta C_D = \Delta C_L^2 \times \varepsilon \quad \textbf{(4-3)}$$

where ε is the induce drag factor, at the linearly area use a parabolic equation, so the C_L and C_D after trim can be gotten by equation 4-4 and 4-5.

$$C_L = C_{L1} - \Delta C_L \quad \textbf{(4-4)}$$

$$C_D = C_{D1} + \Delta C_D \quad \textbf{(4-5)}$$

where C_{L1} and C_{D1} is the data from the simulations without trim, and C_L and C_D is the data which be used in the following optimization activities.

In this chapter, the practical steps and strategies used to optimize the shape of airfoil are given in Figure 4-2.

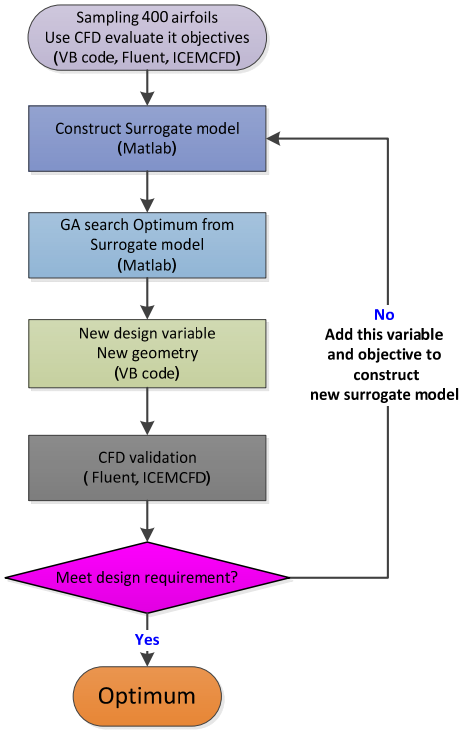

Figure 4-2: Airfoil optimization process

4.1 Transonic single-element airfoil

Transonic airfoil aerodynamic properties affect the transport aircraft performance as cruise speed and voyage directly. In this flight phase the wave drag appearances, so an airfoil with lower drag while enough lift airfoil can be take

advanced by the design. And as a relative “Fat” airfoil which will have a more round leading edge and bigger thickness can have better lower speed aerodynamic performance, and also can offer a high efficiency wing structure design space and volume for contain fuel or some systems. All of them could take the advance of the supercritical airfoil. So in order to PARSEC the transonic airfoil, a supercritical airfoil properties was given, which mainly refer to a downward deflection trailing edge, and flat upper surface and round leading edge.

4.1.1 Design space and Objective

As a long voyage flight, the whole transonic flight phase will have a different Re, Ma and AOA. Normally the Reynolds number bigger than 10 Million affect the aerodynamic characteristics very limited, so in this research, the Reynolds number is fixed to 20 Million, it also is applicable to low-speed flight. Any flight to Ma and AOA they can be changed continuously, this research will take consideration of 9 flight cases, the will be the combination between the Mach number and AOA, which gives in Table 4-1. It should be noticed the Mach number was reduced because a 25deg sweep angle was employed; the relationship between the effective Mach number and flight speed is given in table 4-1. This entire design objective is the aerodynamic efficiency $K = \frac{1}{9}\sum_{i=1}^{9}(CL/CD)_i$. Since each sample airfoil needs execute 9 different simulations as described in Table 4-1. That means there totally $400 \times 9 = 3600$ simulations should be taken, and all of the CL/CD will do average after trimmed at the position of 0.25 chords.

Table 4-1: CFD Simulation Cases specification

Case	Re(million)	Ma	Ma(free flow)	α (°)
1	20	0.72	0.794	2
2	20	0.73	0.805	2
3	20	0.74	0.816	2
4	20	0.72	0.794	2.5
5	20	0.73	0.805	2.5
6	20	0.74	0.816	2.5
7	20	0.72	0.794	3
8	20	0.73	0.805	3
9	20	0.74	0.816	3

4.1.2 Strategies

In this optimization phase, there will take two optimizations, the first one is within the bounds states in Table 4-2 case a, while the second optimization will use the limitation of some Parameters Bounds in order to guarantee the optimization toward a "Fat" shape, which will good for following HLC airfoil design. The design bounds are shown in table 4-2 case b.

Table 4-2: PARSEC parameter ranges for transonic airfoil optimization [118]

		Case a				Case b			
Variable	Par.	Lower bound		Upper bound		Lower bound		Upper bound	
r_{LeUp}	1	0.0063	0	0.0151	1	**0.0133**	**0. 8**	0.0151	1
x_{up}	2	0.3170	0	0.5250	1	0.3170	0	0.5250	1
y_{up}	3	0.0497	0	0.0683	1	**0. 0664**	**0. 9**	0.0683	1
Z_{xxup}	4	-0.5135	0	-0.2393	1	-0.5135	0	-0.2393	1
r_{Lelo}	5	0.0063	0	0.0151	1	**0. 0133**	**0. 8**	0.0151	1
x_{lo}	6	0.2835	0	0.3418	1	0.2835	0	0.3418	1
y_{lo}	7	-0.0603	0	-0.0478	1	-0.0603	0	**-0.0553**	**0. 4**
Z_{xxlo}	8	0.2535	0	0.8405	1	0.2535	0	0.8405	1
β_{TE}	9	0.0655	0	0.2618	1	0.0655	0	0.2618	1
α_{TE}	10	-0.2405	0	-0.0026	1	-0.2405	0	-0.0026	1
Z_{TE}	11	-0.0050	0	0.0200	1	-0.0050	0	0.0200	1
ΔZ_{TE}	12	0.0020	0	0.0150	1	0.0020	0	0.0150	1

Both the two cases optimization are based on the same 400 airfoils' sample [119], The Parameters use the Hammersley method to the sample, the 400×12 samples is given in appendix Figure 1 to Figure 11, so the parameters use in the PARSEC is

$$P_{Par_i} = \left(Upper_{Bound_i} - Lower_{Bound_i}\right) \times P_{ham_i} + Lower_{Bound_i} \quad \textbf{(4-6)}$$

Where P_{Par} is the parameters used in PARSEC, i is the parameter sequence of the 12 parameters, P_{ham} is the parameters from the Hammersley sample. In order to monitor the quality of the airfoil shape, the VB program was developed to genera the vector graphics of the generated airfoils. The VB program (figure 4-2) concludes the sub program of Hammersley, PARSEC and Vector graphics generation functions. Four airfoils showed in figure 4-3.

Figure 4-3: Developed code to general airfoils

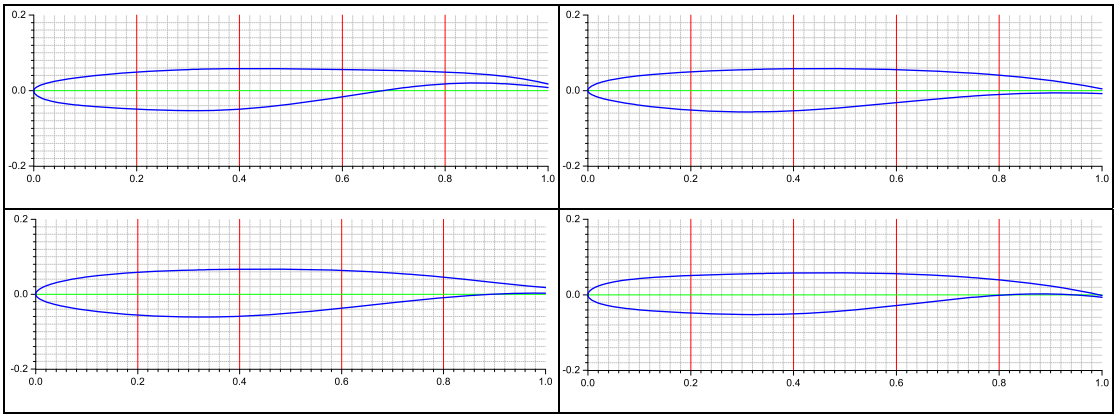

Figure 4-4: Airfoil No. 50, 150, 250, 350

4.1.3 CFD simulation

After get all the airfoils, the next step is to assess its aerodynamic characteristics. It uses the high-fidelity tools to evaluate its aerodynamic. This single airfoil transonic flow simulation used ANSYS software package ICEM CFD and Fluent, and used Visual Basic (VB) code to general the airfoils, and general the Scrip

files both use at ICEM CFD and Fluent by the VB code, after the script file was generated, the time to mesh all the 400 airfoil was about 1 hour with an intel-i7 CPU. After the mesh generation is finished, the following work is to general case files to use in following CFD simulation, this work was done by Desktop PC, required another 1 hour. When all of the case files were generated, then submit all of the case file to HPC, which can do the CFD simulation with Intel 32 cores, all of the 3600 simulations could be finished one by one within about 30 days, each simulation using 15000 iterations, the whole process about set the database to construct the surrogate model is depict in figure 4-4. Before the batch simulation stared, transonic airfoil CFD simulation convergence properties had been studied.

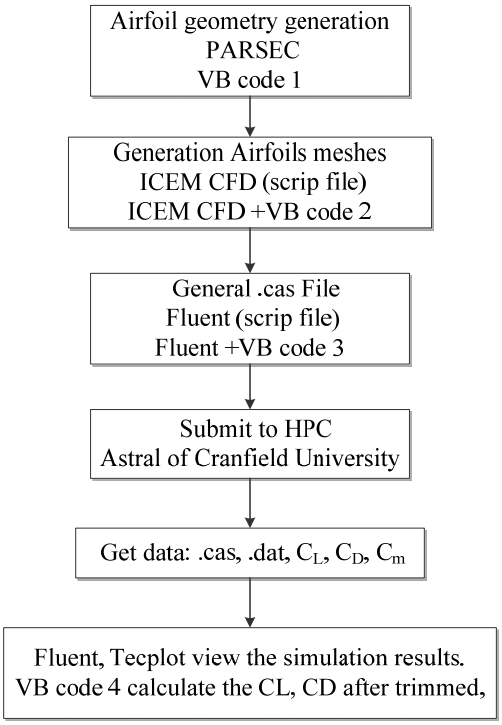

Figure 4-5: Simulation process for samples

4.1.3.1 Validation

In order to set a proper way to simulation transonic flow around a single 2-D airfoil, following work had been done.

Choose a reference airfoil, which could easily access its experimental data and airfoil geometry, in order have more convincing to following simulations in sam-

pling and optimization word in following, a supercritical airfoil will be welcome, such as RAE 2282 airfoil, it has the thickness 12.14% at 37.8% chord, a zero-thickness trailing edge and a downward trailing edge; meanwhile it has lots experiment and CFD results available resource from papers and website.

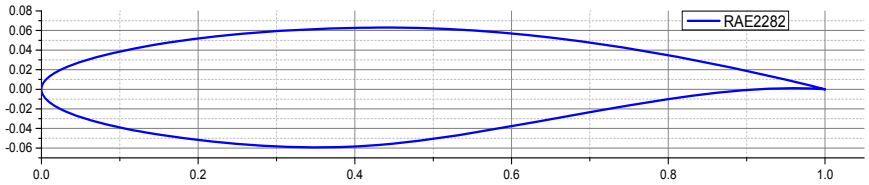

Figure 4-6: RAE 2282 Airfoil profile

The validation following two cases (Case1, source [120]; Case2, source [121]), all of them are transonic airflow (table 4-3).

Table 4-3: Two simulation cases

	Case 1	Case 2
α	2.72 °	2.8°
Mach	0.75	0.74
Re	6.2 Million	2.7 Million

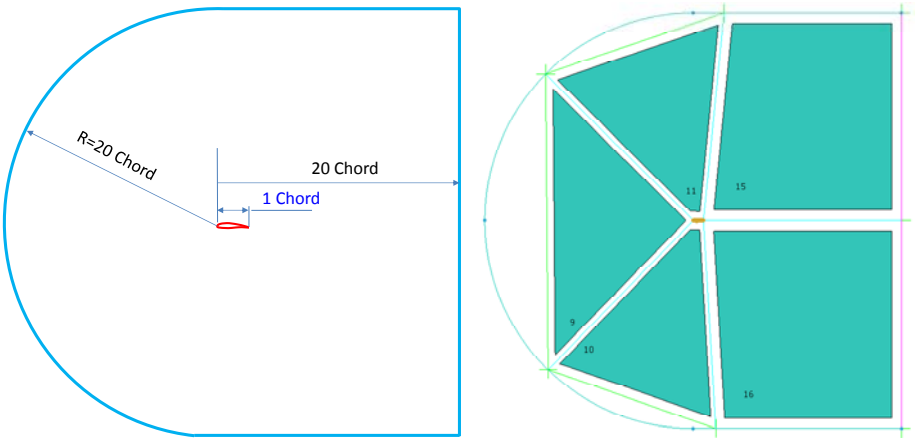

Figure 4-7: Far field and blocks divided strategy for RAE 2282 airfoil

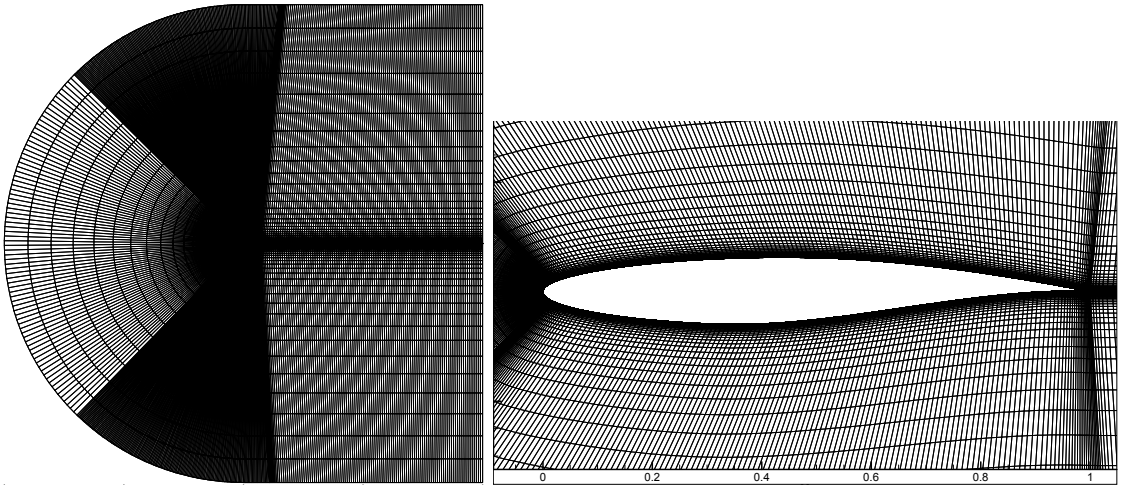

Figure 4-8: mesh generation (51200 Grids)

- Case 1:

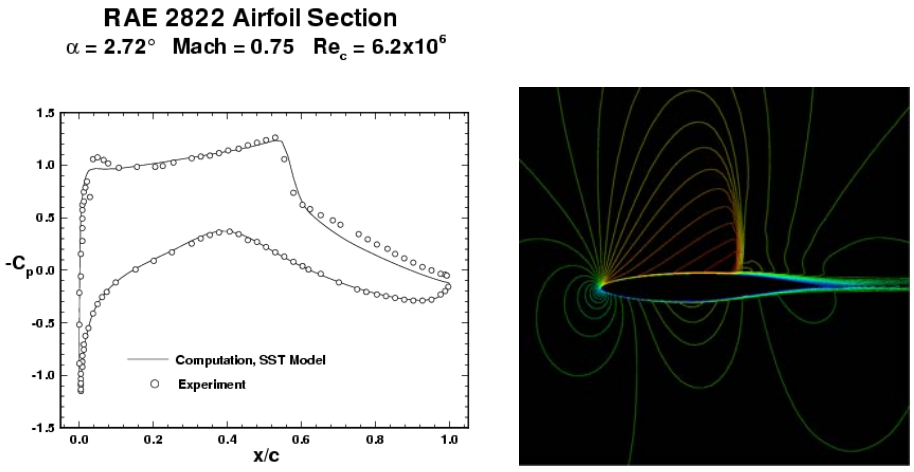

Figure 4-9: Case a pressure coefficient and Mach number counter [120]

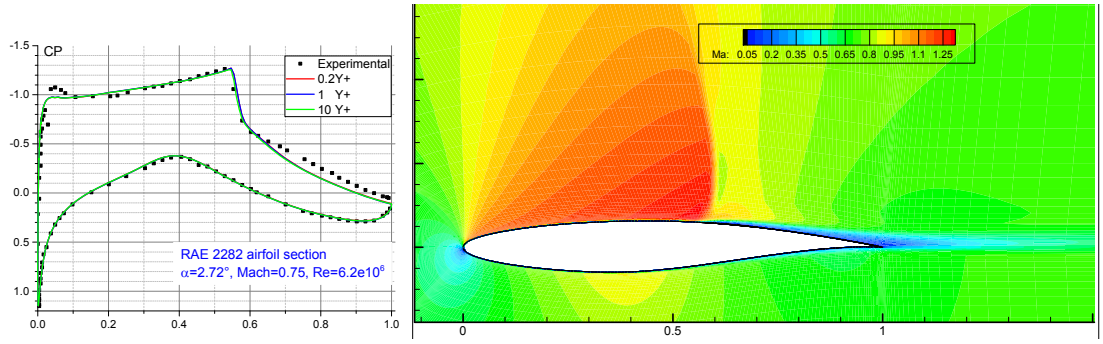

Figure 4-10: CP comparison between WT test and study results (Case a).Mach number counter with $Y^+ = 10$

◆ Case 2:

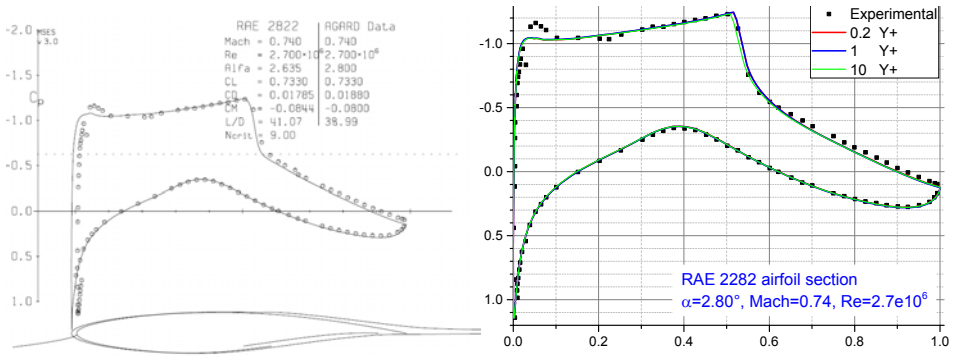

Figure 4-11: CP distribution comparison [121]

Table 4-4: Y+ effect on accuracy

Y+	CL	CD
0.2	0.713	0.0203
1	0.719	0.0202
10	0.721	0.0207

From these two cases study, sing airfoil in transonic air flow with AOA less than 3 ° , use the K-W SST turbulence model can get a proper result, and the first layer Y+ height from 1 to 10 do not have significant influence to the simulation result, while the Y+ equal 10 has a faster convergence speed, As to efficiently to use computational resource, this research choose a first layer thickness equal 10 Y+.

4.1.3.2 Simulation Results

Because these 400 airfoils geometry character have a difference with reference airfoil RAE 2282, owing to they have a none-zero trailing edge thickness, so the simulation field block strategy have to need redesign as Figure 4-12 left, and a typical Fluent simulation convergence is shown in Figure 4-12 right. It demonstrates that the simulation is effective.

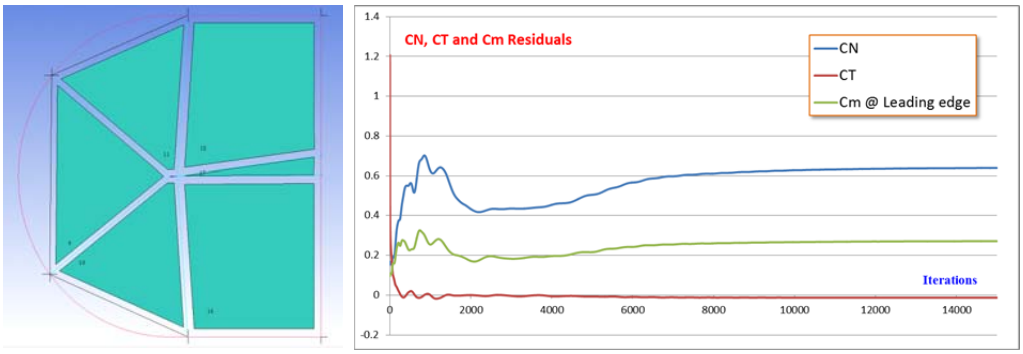

Figure 4-12: ICEM CFD blockage partition and Fluent convergence historical

The CL/CD of the 3600 simulations' result is given in the appendix table 5-1. In order to give a more convenient way to show the result relate with the 400 airfoils, reorder the airfoil number according to the average CL/CD. The bigger in the front of the new sequence; in the new order, the first airfoil is the number 12 airfoil figure 4-12 in the sample sequence, for it has the maximum $\mathrm{CL}/\mathrm{CD} = 65.31$ in all of the 400 samples, and the last one is No.392 airfoil in the samples, for it has the minimum $\mathrm{CL}/\mathrm{CD} = 18.81$. In order to express the trim affect to the CL/CD, figure 4-13 dedicate to demonstrate the trim bring the whole airfoil performance. And the phenomena can be found is that generally a bigger CL/CD has a relative bigger trim effect, this owing to the after-loading of the supercritical airfoil. Since it's in curve camber at the trailing edge, that produces a big amount lift contribution that can increase the CL/CD. However, it produces a relatively bigger moment that could cause the airfoil have a nose-down trend, so the corresponding relationship between them is bigger CL while big cm, this phenomenon is an another important consideration point especially for supercritical airfoil [45; 122].

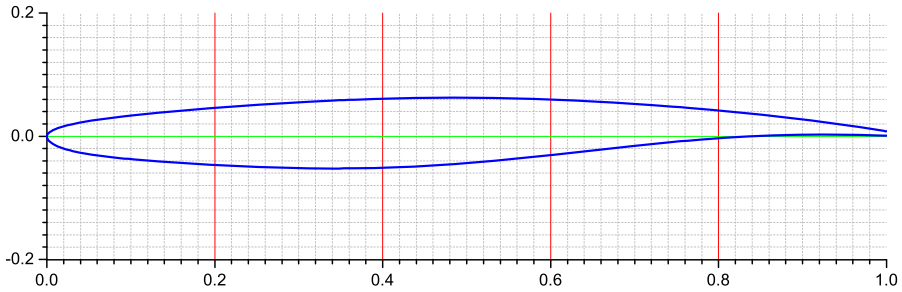

Figure 4-13: shape of No.12 sample airfoils

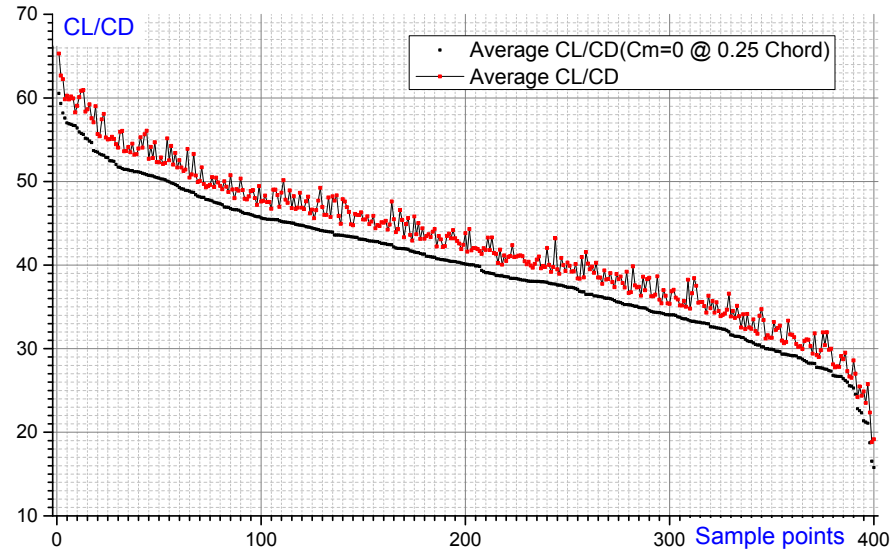

Figure 4-14: Trim effects on CL/CD of sample points

In order to study the Ma and AOA effect to CL/CD, Figure 4-15 uses 9 lines to fitting the CL/CD distribution of the 400 airfoils of the 9 cases result. from the lines, it shows that both the Ma and AOA have a significant impact to the airfoils aerodynamic Characteristics, lower AOA and Ma can have the trend of bigger CL/CD. Conversely, high AOA combined with high Ma can bring down the CL/CD a lot (Case 9)

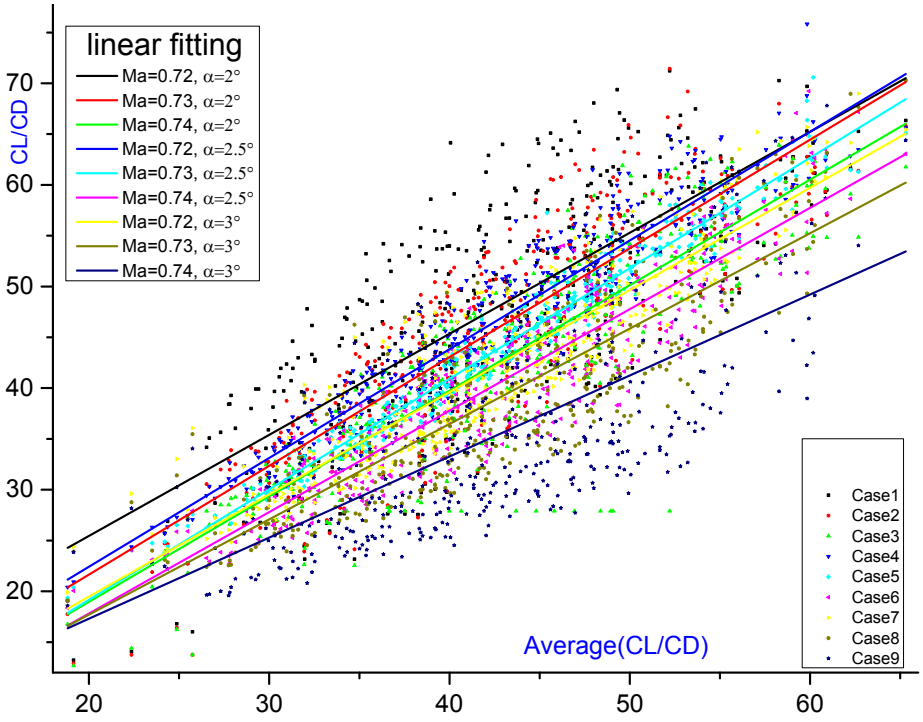

Figure 4-15: (CL/CD)i, i=1 to 9 Vs. average (CL/CD)

4.1.4 Surrogate model construction

In order to construct the Kriging surrogate model, a MATLAB toolkit had been utilized, it use Kriging model to construct the surrogate model; and the GA search engine of the MATLAB 2012 do the global research. After the surrogate model constructed, a comparison (equation 4-7) between the sample point and surrogate at the training point is showed in figure 4-16. And it shows the errors are in reasonable range.

$$error = abs(\widehat{f}_i - f_i) \quad i = 1,2,3 \ldots..400 \tag{4-7}$$

where $\widehat{f}_i$ is the response objectives from surrogate model with the samples variables, while f_i is the objectives from high-fidelity approach.

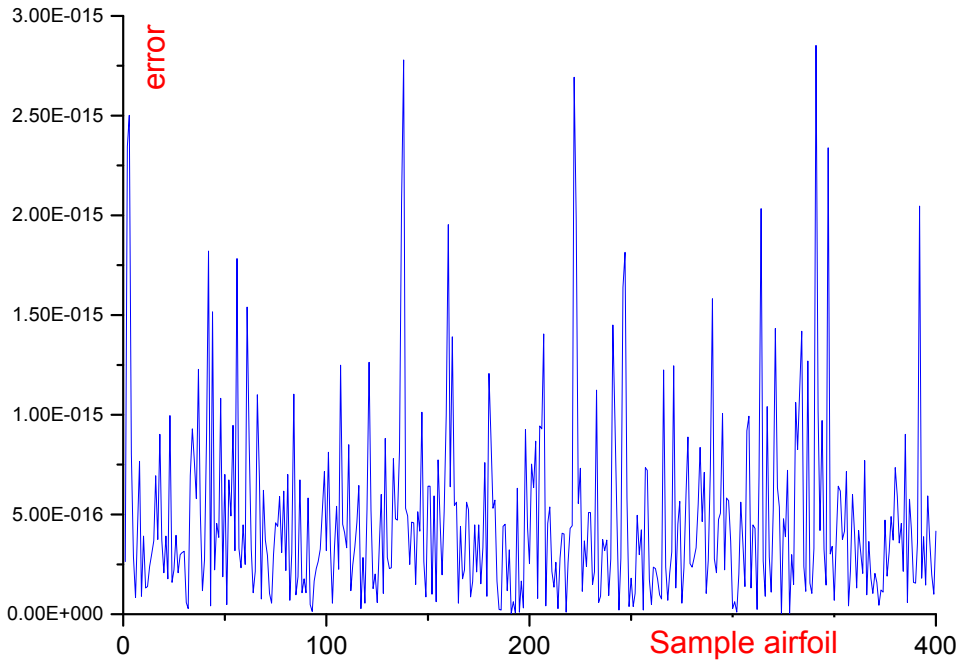

Figure 4-16: Objective Difference between samples and surrogate model

The following two optimization are based on the same surrogate model, while the, while use different search space.

- Case a:

Optimization range in the Matlab GA search for this case is from $[0,0,0,0,0,0,0,0,0,0,0,0]$ to$[1,1,1,1,1,1,1,1,1,1,1,1]$.This case optimization had pro-

cessed 12 optimization points, and the points' variables are given in appendix table 5-2, and the points objectives both from surrogate model and CFD simulation is given in figure 4-18 (left), the error from the surrogate model at each optimization point is showed in Figure 4-18 (right), from the error chart, it shows it is a convergence optimization. From figure 4-18 left, the best one is the No. 6 of the optimization point, here name it airfoil A.

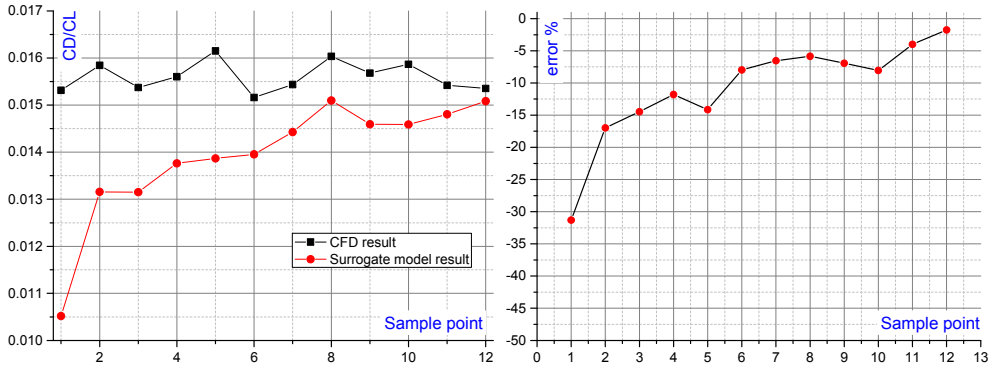

Figure 4-17: Transonic airfoil optimization

◆ Case b:

In order to have a good low-speed performance, which mainly refer to C_{Lmax} and stall α. it is necessary to give constrains to the leading edge radius and thickness dimension, hence, in this optimization process, the space of the 4 from the 12 variables had been shrink to a small range, it is from [0.8,0,0.8,0,0.8,0,0,0,0,0,0,0] to [1,1,1,1,1,1,0.4,1,1,1,1,1] in this case. And the points objectives both from surrogate model and CFD simulation is given in figure 4-19 (left), the error from the surrogate model at each optimization point is showed in Figure 4-19 (right), from the error chart, it shows it is a convergence optimization. From figure 4-19 left, the best one is the No. 2 of the optimization point, here name it airfoil B.

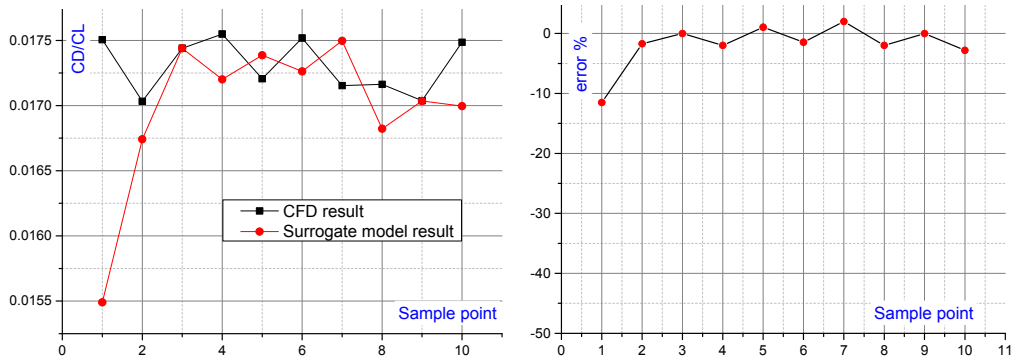

Figure 4-18: Transonic airfoil optimization process of Case 2

4.1.5 Result Comparison

From the above two cases optimization, there two new airfoils reached, they together with the two comparable sample airfoils' Hammersley parameters is given in table 4-5, their airfoil profiles are given in Figure 4-19. The design objective was given in table 4-6.

Table 4-5: P_{ham} comparison between optimum and sample airfoils

	Airfoil	Par.1	Par.2	Par.3	Par.4	Par.5	Par.6	Par.7	Par.8	Par.9	Par.10	Par.11	Par.12
Case a	A	0.230	0.619	0.558	0.269	0.566	0.867	0.936	0.644	0.517	0.444	0.554	0.265
	No.12	0.028	0.813	0.556	0.280	0.429	1.000	0.846	0.647	0.579	0.478	0.379	0.355
Case b	B	0.813	0.795	0.992	0.190	0.825	0.711	0.28	0.775	0.618	0.337	0.506	0.326
	No.352	0.878	0.979	1.000	0.235	0.93	0.877	0.007	0.658	0.468	0.198	0.118	0.267

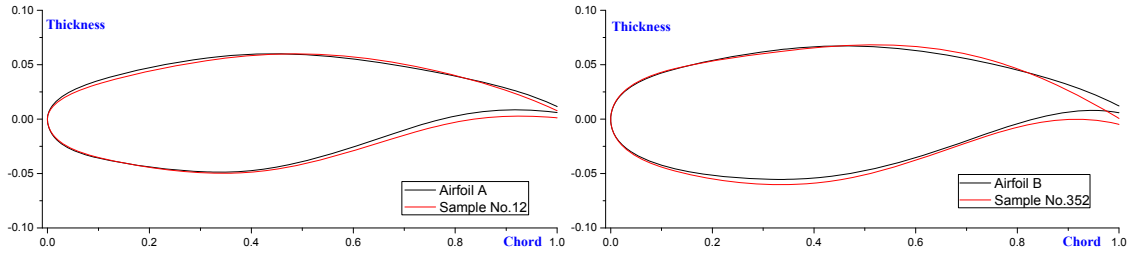

Figure 4-19: Comparison between Airfoil A and No.12, and Airfoil B and No.352

Result analyses mainly focus to two groups, the first group two airfoils aerodynamic characteristic is from case 1, the second group two airfoil aerodynamic characteristic is case 2. The comparison will focus on Mach number and static pressure coefficient, between airfoils in the same cases.

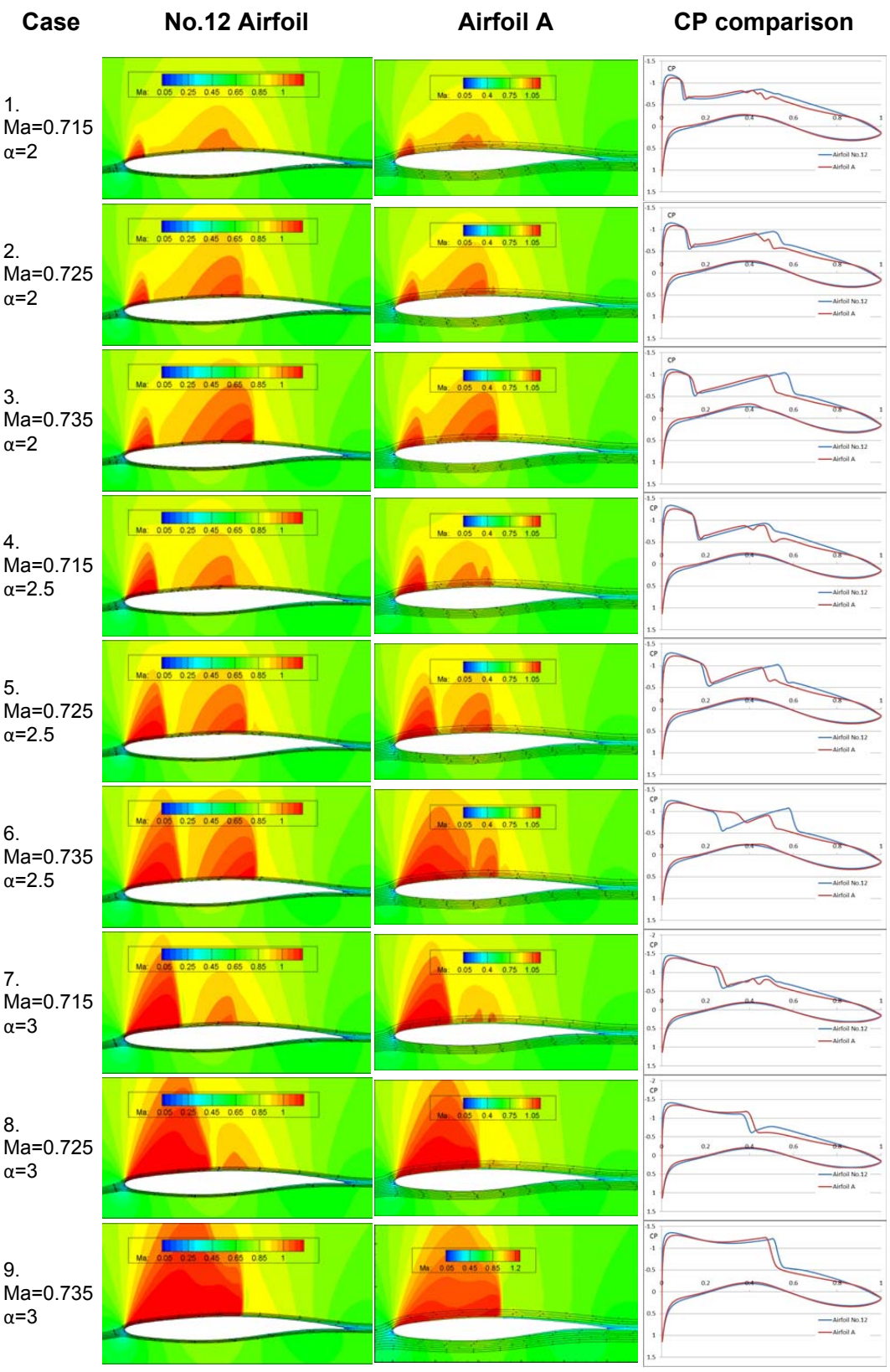

Figure 4-20: Optimum design result compare to sample in case a

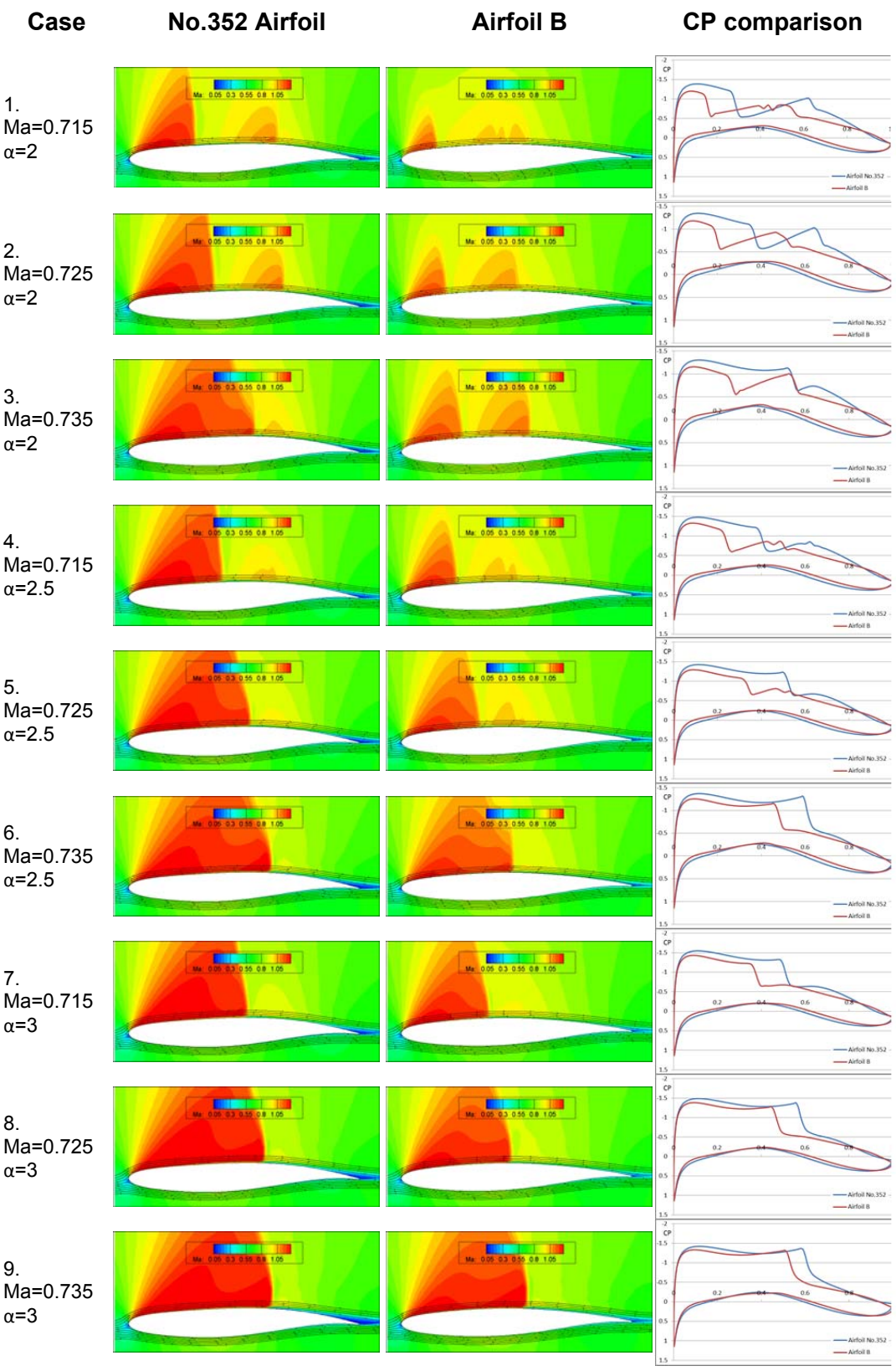

Figure 4-21: Optimum design result compare to sample in case b

Table 4-6: Comparison between best in sample and optimum

Case	Airfoil	CL/CD	Δ(CL/CD)
a	No.12	65.31	/
	A	65.96	0.997%
b	No.352	49.6	/
	B	58.71	18.38%

4.2 HLC Airfoil Design Optimization

In this airfoil design optimization phase, it will do two configurations high-lift, takeoff and landing, after them a droppable spoiler effect will be studied. In order to parameter the HLC airfoil, a multi-element parameter methods used, within the takeoff configuration, the parameter method will model both the exposed contours and the high-lift devices' position and orientation. While in the landing HLC airfoil optimization phase, it will inherit all the parts contours from the takeoff, while redesign the position and orientation, in order to produce more lift. As for the study about the droppable spoiler, it will use both the optimum HLC airfoils from takeoff and landing, and do comparison between spoiler deflected and the neutral position.

The objective(s) for takeoff configuration is optimization CL/CD with the prerequisites$\mathrm{CL} \geq 2.4$; while for landing configuration is the maximum CL.

4.2.1 Design space and Objective

In pre-section of this chapter, it gets two optimum airfoils from case a and case b. In order to choose an airfoil from them at the consideration of low speed aerodynamic characteristic, a Ma 0.2 $C_L \sim \alpha$ polar had get by CFD simulation. Before the CFD simulation starts, the airfoils deformation had been done according to equation in table 2-1. As to airfoil B, the difference between them is showed in Figure 4-24. From this figure, it shows that the original and derived airfoils have the similar geometry but the thickness distribution is different.

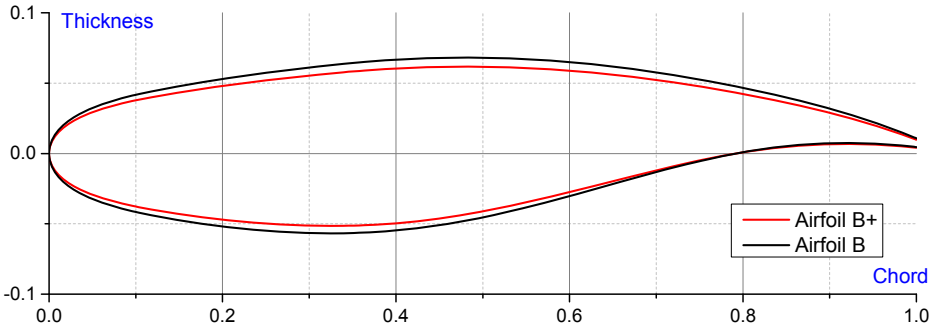

Figure 4-22: Comparison Airfoil B and B+

Comparison between airfoil A+ and airfoil B+ at low speed 0.2 Mach is shown in Figure 4-23. The HLC airfoil design concerns point as stall AOA, maximum lift, and its stall process. A bigger stall AOA and maximum lift, and a gentle stall process will do favor to the HLC airfoil aerodynamic characteristics. From Figure 4-23 it shows Airfoil B+ better than airfoil A+ with relative three indexes. Hence, in this chapter, the HLC airfoil will be design base on airfoil B+.

To design a HLC airfoil, there exist two design tasks. The first one is the contours about main wing leading edge and flap upper leading edge contour. The second one is the relative positions between main wing and slat, main wing and flap.

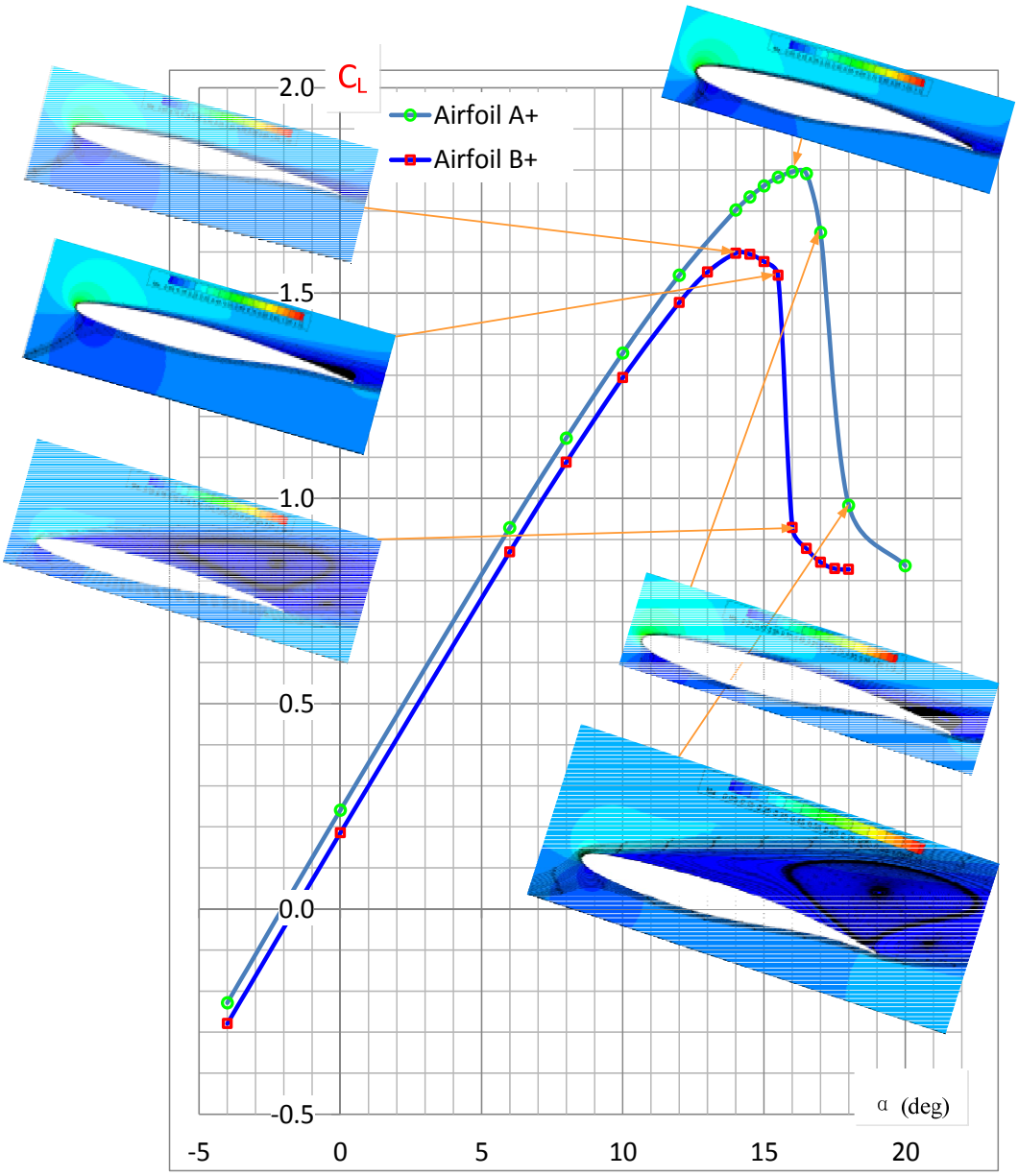

Figure 4-23: CL~α comparison between Airfoil A+ and B+ at Ma=0.2

This research uses 12 variables (table 4-7) to PARSEC HLC airfoil, together with 6 constant parameters to describe the counters of wing leading edge under slat and flap leading edge under main wing. The 6 constant parameters for the two counters showed in Table 4-8. And the four trailing edge position is given in figure 4-24; all of the transition length from tailing edge to downstream element is 0.02 chords. As in order to the meshing issue, a tiny geometry change had been given (Figure 4-25). As it have same design variables numbers as in transonic, so it uses the same 400 sample P_{ham} dataset which gives in appendix figure 1 to figure 11.

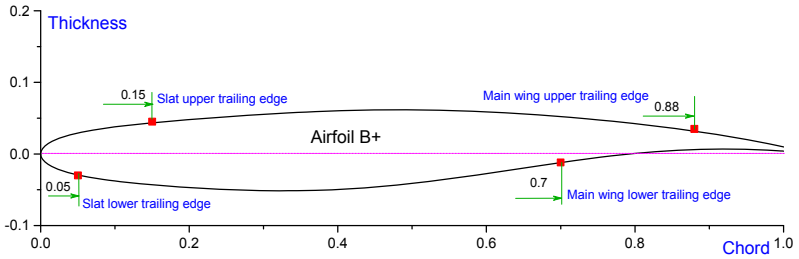

Figure 4-24: Airfoil partition

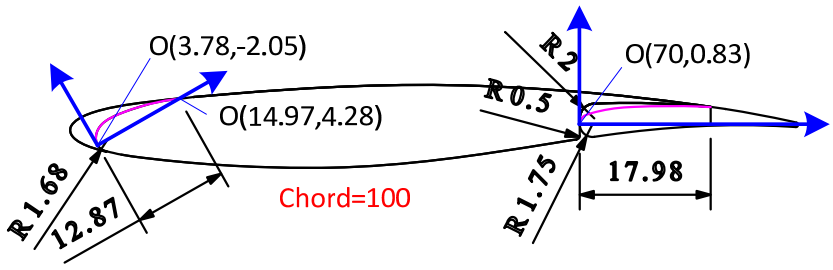

Figure 4-25: Geometry dimensions to PARSEC contours

Table 4-7: PARSEC parameter ranges for HLC airfoil optimization

	Case Takeoff				
Variables	Par.	**Lower bound**		**Upper bound**	
X_{slat}	1	-0.08	0	-0.04	1
Y_{slat}	2	-0.04	0	-0.01	1
α_{slat}	3	10 deg	0	20 deg	1
r_{Leslat}	4	0.1	0	0.15	1
Z_{xxslat}	5	-2	0	-2.5	1
α_{Teslat}	6	0.314	0	0.419	1
X_{flap}	7	0.2	0	0.35	1
Y_{flap}	8	-0.01	0	-0.08	1
α_{flap}	9	20 deg	0	30 deg	1
r_{Leflap}	10	0.06	0	0.1	1
Z_{xxflap}	11	-0.001	0	-0.0015	1
α_{Teflap}	12	0	0	0.105	1

Table 4-8: Parameters for Counters with PARSEC method

Parameter	Main wing leading edge	Flap leading edge
x_{up}	0.26	0.555
y_{up}	0.18	0.15
$Z_{TE} + \Delta Z_{TE}/2$	0	0.129

400 HLC airfoils were generated from another developed parameter VB program, four of them is showed in figure 4-26.

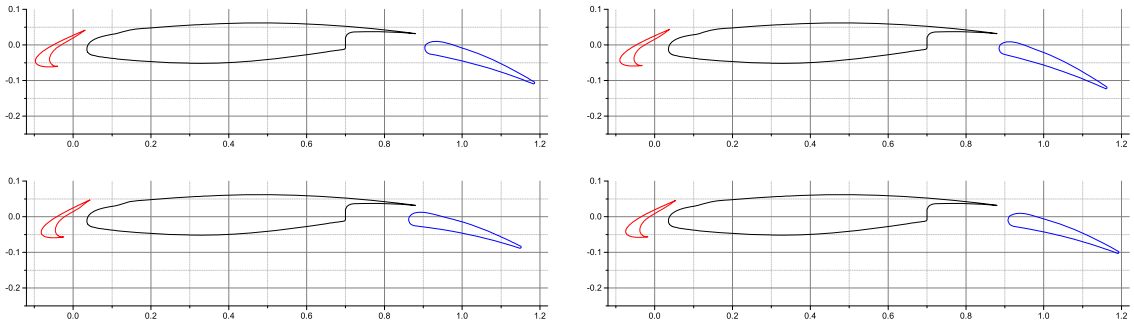

Figure 4-26: sample geometries (No. 50, 150, 250 and 350).

4.2.2 Strategy of Design Optimization

As the HLC airfoil compare to the single airfoil, it requires more design parameters to define High-lift devices position and orientation. So the optimization can do the shape, position and orientation at same time. another way is fix the position and orientation at an empirical value, and then optimization the shape of the geometries, after get the geometries of the HLC airfoil, then do the position and Orientation optimization, after get the new position and Orientation, then redo the shape optimization. With a new shape, can do the position and orientation optimization forward, till the result meet the design criterion.

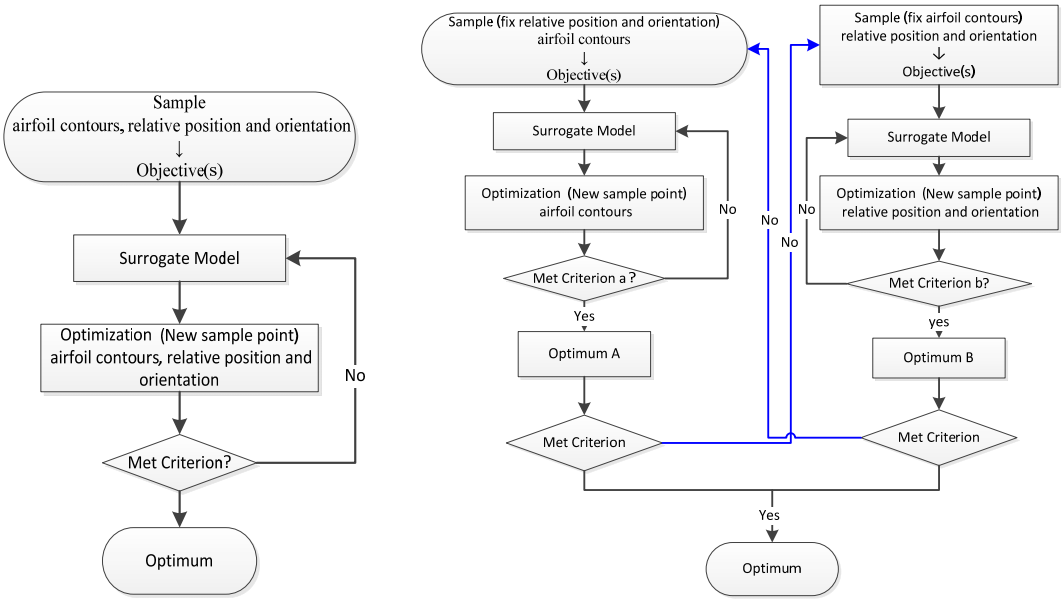

Figure 4-27: Two optimization processes of the HLC airfoil design

Both the two optimization processes competently the HLC airfoil optimize, while cause the first one it need do the research at the full dimensions at once, so in order construct an effective surrogate model, it needs more samples. While the second method, owing to it separate the contour describe parameters with position and orientation parameters, so it consume less samples to construct the surrogate model at a sub optimization activity. It more accuracy to capture the optimum design while at lower computational cost. However, because it has two more criterions, so it need more time with the human intervene. As in this research work, it uses the first method to do the optimization.

4.2.3 CFD simulation

In order to use a proper way to get the HLC airfoils aerodynamics characteristics, a proper CFD simulation validation had been done. After the validation meet the requirement, the method used at the following samples' objective evaluation and optimization CFD check. And because the ICEM CFD is not efficient when deal the HLC airfoil meshing, after the validation, the meshing tool was replaced by Pointwise V17, while the meshing strategy is the same as the used in the validation.

4.2.3.1 Validation

It uses the MDA 30P/30N HLC airfoil and its experiment data as the reference data, the geometry of the HLC airfoil is showed in figure 4-28 (left), and the simulation domain setting in figure 4-28 (right), and the meshing parameters setting is showed table 4-9 ,and the mesh generated in figure 4-30.

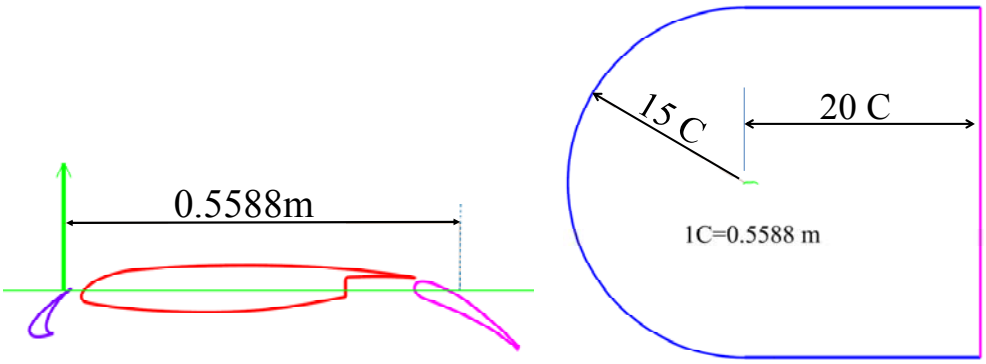

Figure 4-28: MDA 30P/30N HLC airfoil and simulation domain [123; 124]

Table 4-9: parameters for meshes generation and CFD simulation [125]

ICEM CFD	Value	Fluent	Value
Y+	*10*	Ma	*0.2*
Boundary layers, height increase ratio	*20 layers. main wing 1.2, others 1.15*	Re	*$9x10^6$*
Total meshes	*82545*	α	*16°*
Mesh type	*Hybrid*	Turbulence model	*Spalart-Allmaras*

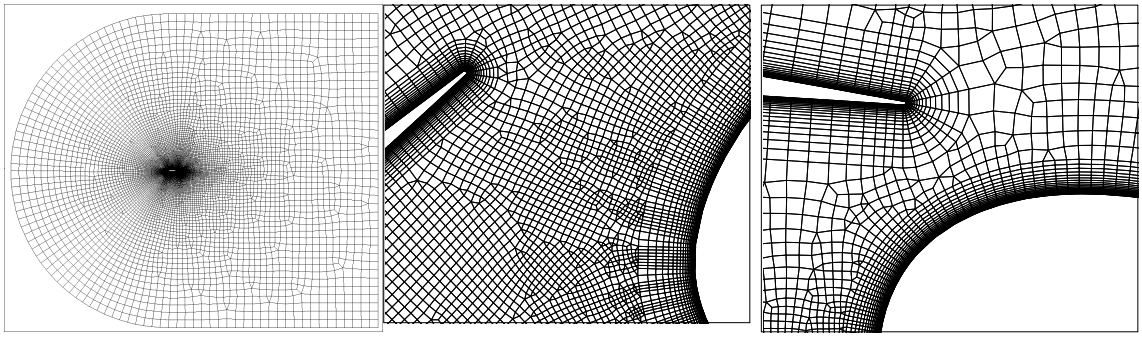

Figure 4-29: Meshes generation

The Fluent simulations condition setting is given in table 4-9, compare the data of the experiment as CP distribution (figure 4-30). Figure 4-31 shows the Ma contours and pressure contours at an angle, figure 4-31 shows component parts and total lift compare to experiment data.

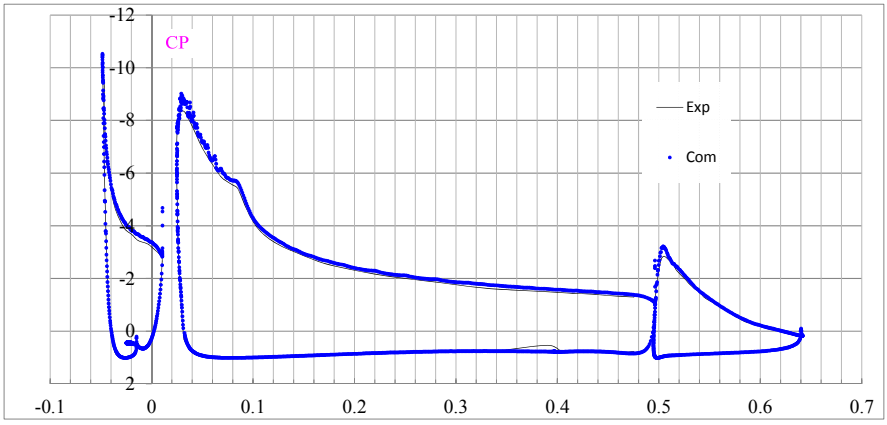

Figure 4-30: Comparison between Experiment and Computational (16°)

From the CP comparison and the CL comparison, it demonstrates the CFD simulation method used adequately take the role as the HLC airfoil aerodynamic evaluator.

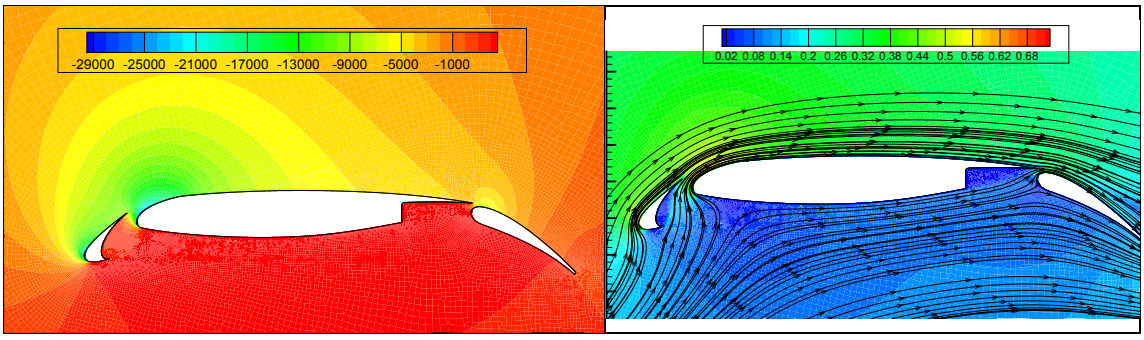

Figure 4-31: Pressure (Left), Mach number and streamlines (Right) (16°)

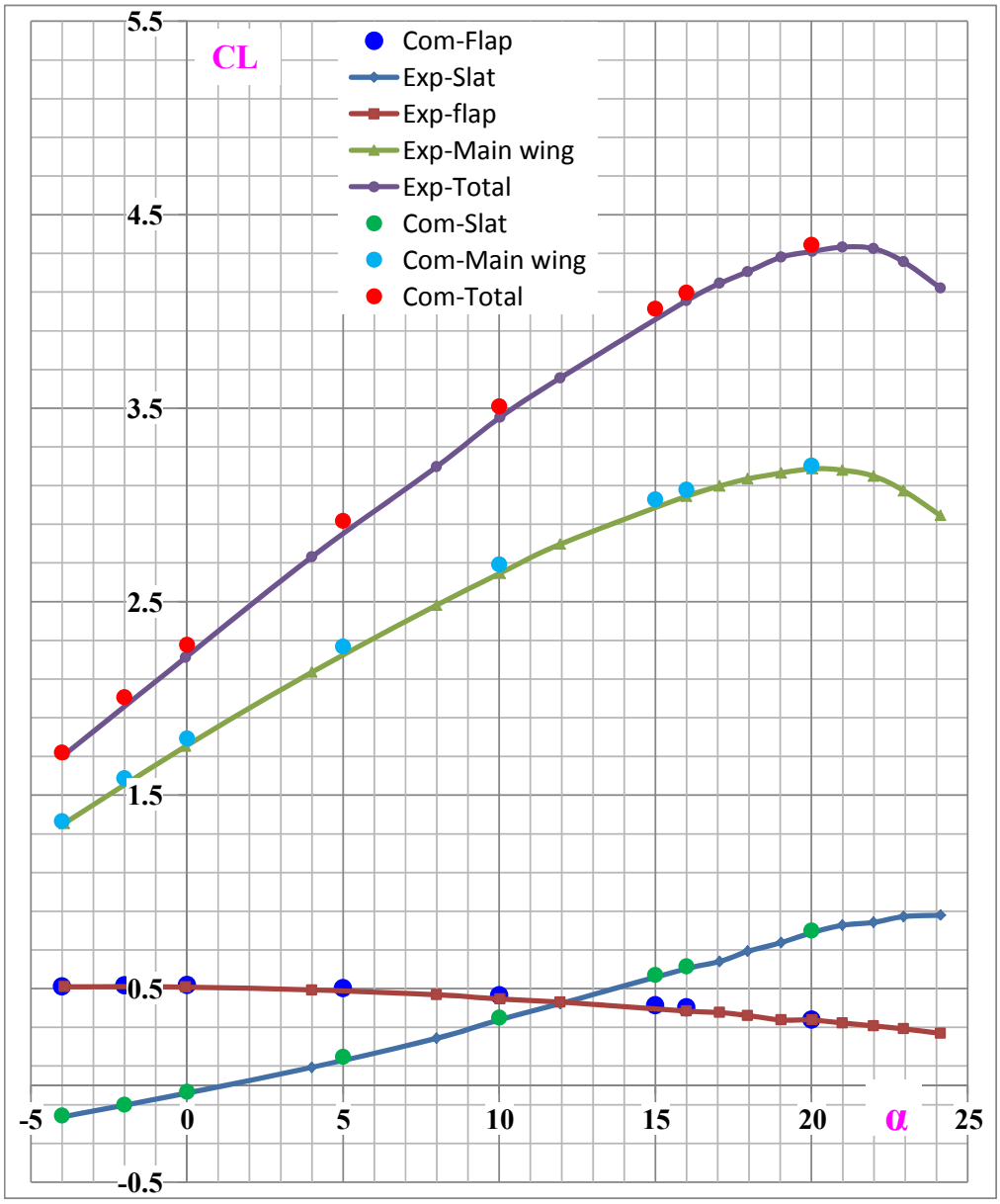

Figure 4-32: Comparison between CFD simulation and Experiment data [114; 115]

4.2.4 HLC airfoil for Takeoff

Normally the takeoff phase of a transport aircraft will pay attention to two factors, they are the CL/CD and CL, it directly relative the aircraft's safety and performance. Hence, in this configuration optimization phase two objectives defined, they are CL/CD and CL.

4.2.4.1 Simulation Results

A convergence history is shown in Figure 4-33, it demonstrates the simulation can provide a so accuracy result.

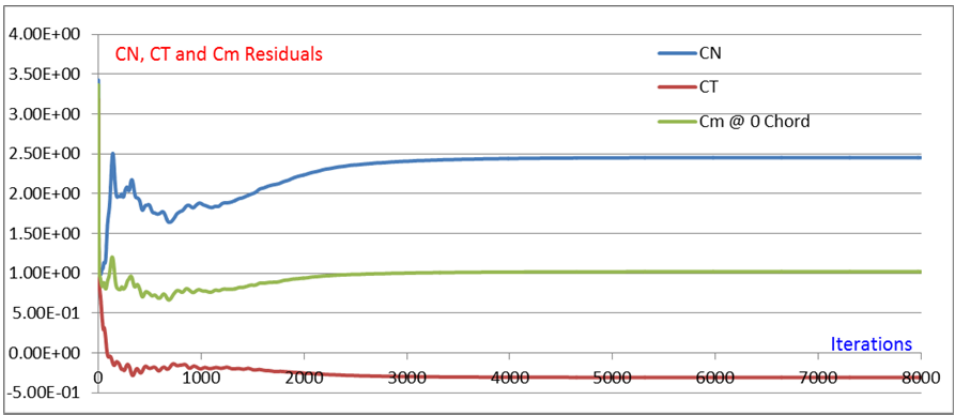

Figure 4-33: Convergence historical (No.161 sampling airfoil)

After the CFD simulation, the objectives can be gotten by the same way which offered in Figure 4-5. As this optimization not only cares the maximumCL/CD, the airfoil should meet the Preconditions is $\mathrm{CL} \geq 2.4$, in order to deal with these two objectives, following new objective given:

$$K' = \left(\frac{C_L}{C_D}\right) \times \left(\frac{C_L}{2.4}\right) \tag{4-8}$$

where $\left(\frac{C_L}{2.4}\right)$ is the motivating factors, new objective K' could get by the simulation result which given in appendix table 5-4.

4.2.4.2 Surrogate model construction

Before the further optimization, a trim effect study has been taken; reorder the samples according to the CL/CD value, the bigger in the front of the new sequence. The trim effect is showed in figure 4-34, it shows that after the trim, the

CL/CD have bring down a lot especially at the relative bigger CL/CD area. and the CL distribution is showed in figure 4-35, and the objective K' distribution in figure 4-36.

It used a same way to construct the surrogate model, the input variables are the 12 parameters with 400 samples and its corresponded objective K'. After the model been had constructed, a validation had been taken (figure 4-37, equation 4-7), it shows the surrogate model have a good consistency with the training points.

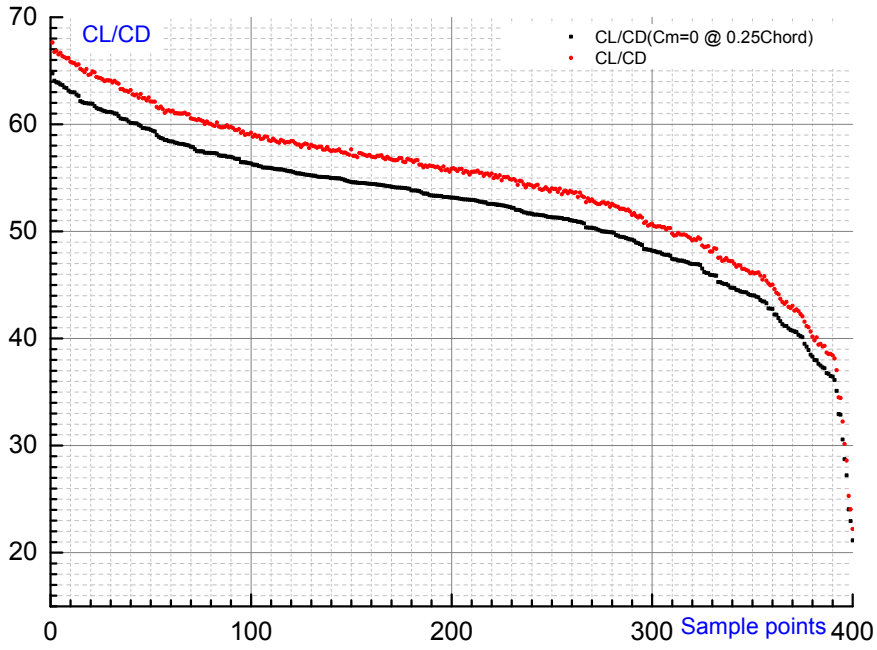

Figure 4-34: Result of 400 sampling HLC airfoil CL/CD for Takeoff

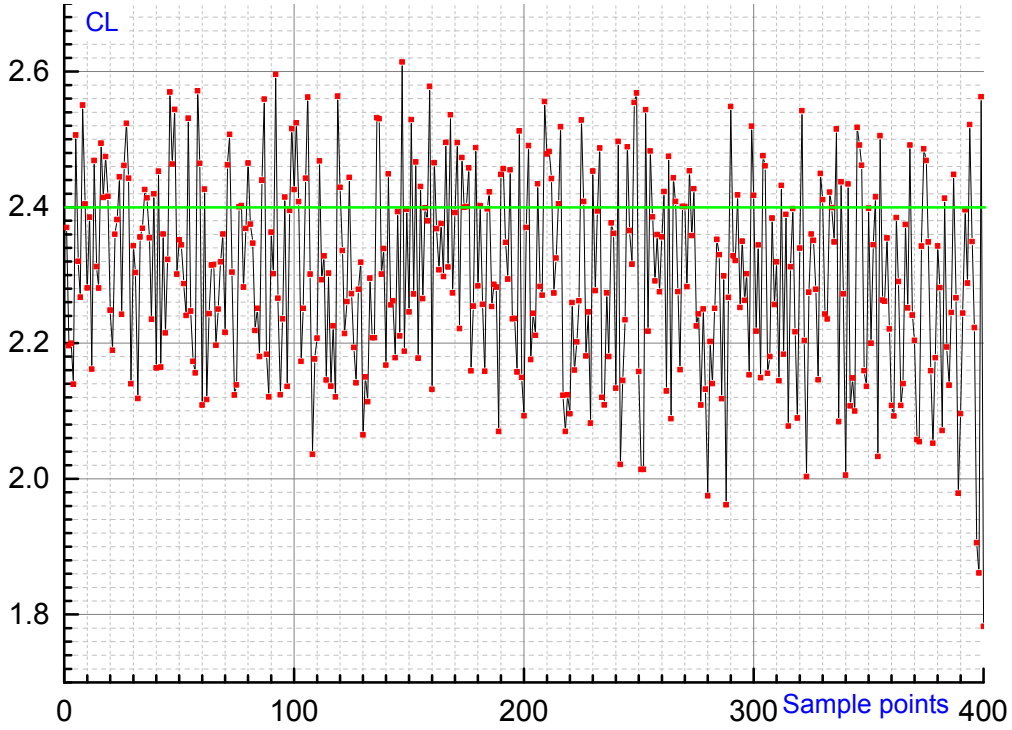

Figure 4-35: CL distribution

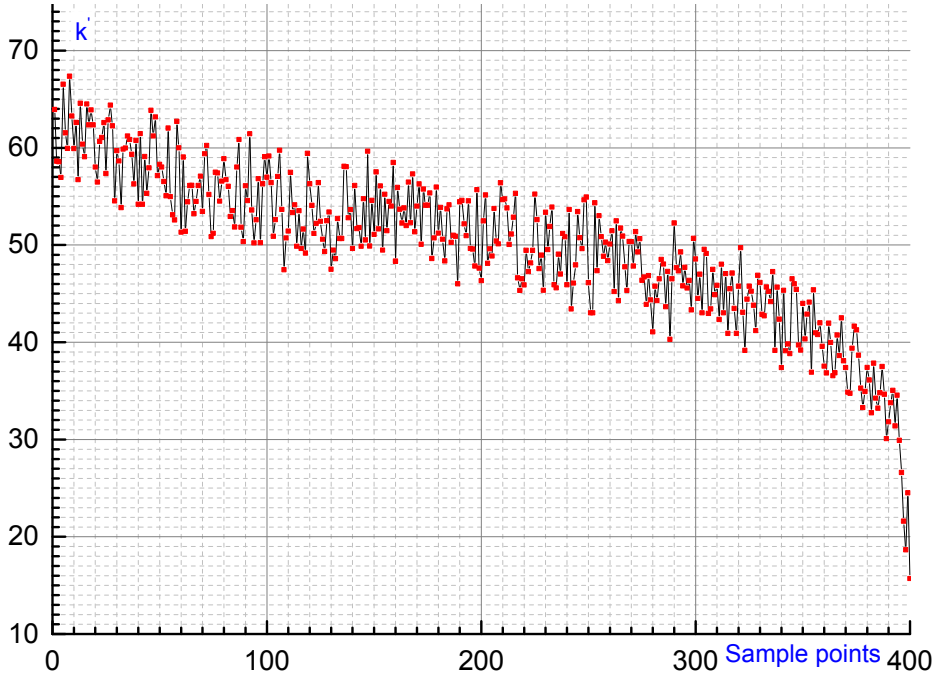

Figure 4-36: K' distribution

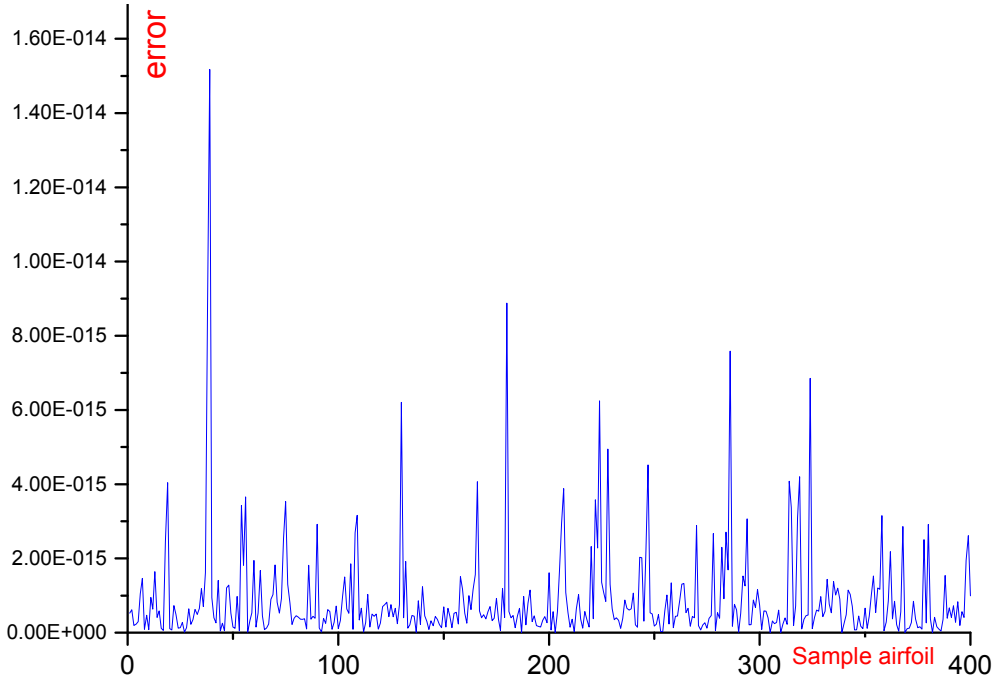

Figure 4-37: Objective Difference between samples and surrogate model

The optimization processed 16 points, and the points objectives both from surrogate model and CFD simulation is given in figure 4-38 (left), the error from the surrogate model at each optimization point is showed in Figure 4-38 (right). From figure 4-38 left, the best one is the 16th point. Here name it airfoil C. for it is a two objectives design optimization problem, the can shape a Pareto-optimization model as in figure 4-39. From this figure, it shows the optimization is taken in a proper way. The optimum airfoil parameters in both of the samples and the optimization points are given in table 4-10. And the two airfoil shape comparison is given in figure 4-39.

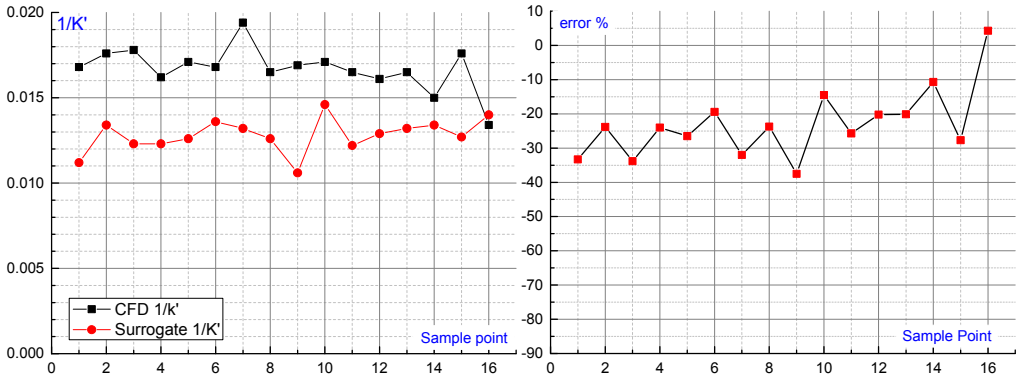

Figure 4-38: Optimization (Takeoff)

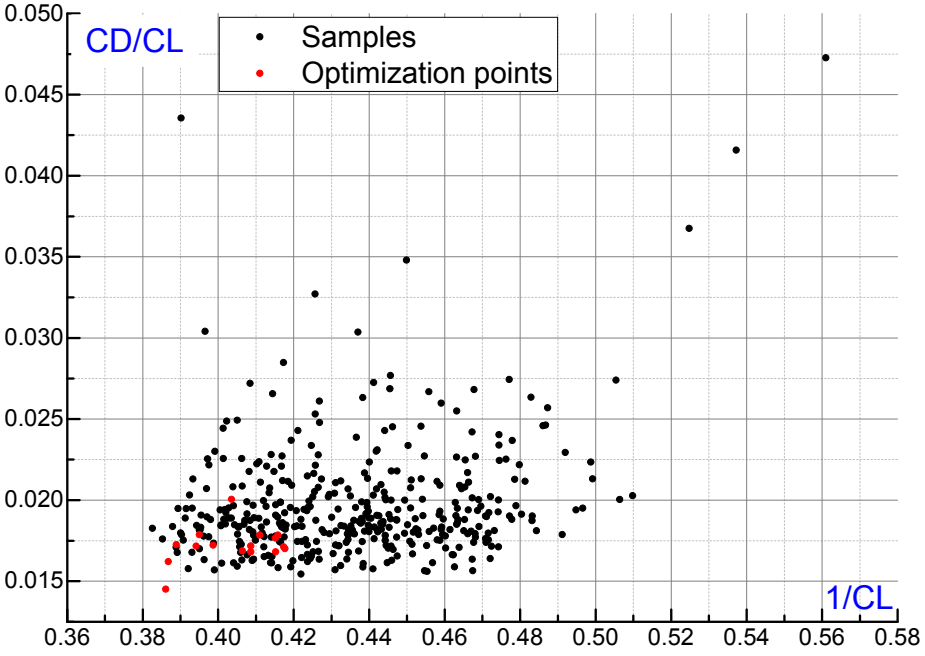

Figure 4-39: The Pareto-optimization model of the $1/CL \sim CD/CL$

Table 4-10: Parameters comparison between optimum and sample airfoils

	No.	Par.1	Par.2	Par.3	Par.4	Par.5	Par.6	Par.7	Par.8	Par.9	Par.10	Par.11	Par.12
Takeoff	Airfoil C	0.389	0.412	0.214	0.199	0.298	0.126	0.292	0.654	0.919	0.755	0.247	0.890
	No.209	0.520	0.043	0.000	0.666	0.513	0.860	0.018	0.277	0.920	0.968	0.181	0.649

The two airfoils aerodynamic characteristics comparison is given in figure 41, 42 and 43. From them we can notice that the main difference between them is the airflow around the main wing leading edge, airfoil C has a more smooth and nature curve than the airfoil No.209.

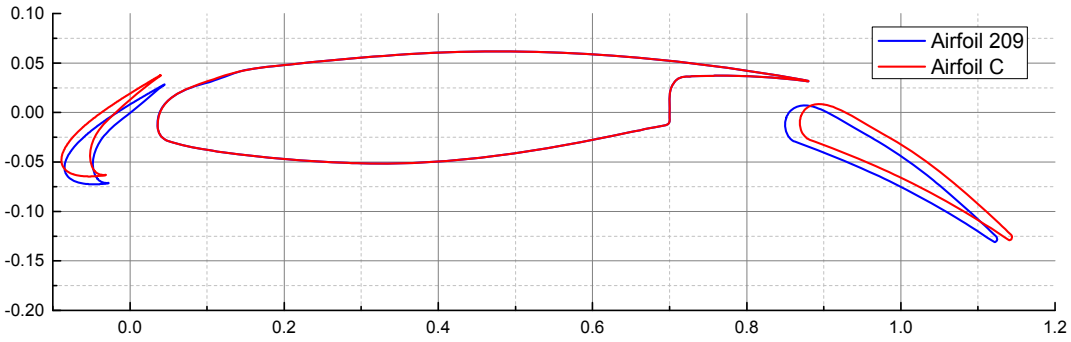

Figure 4-40: Comparison of the takeoff HLC airfoils

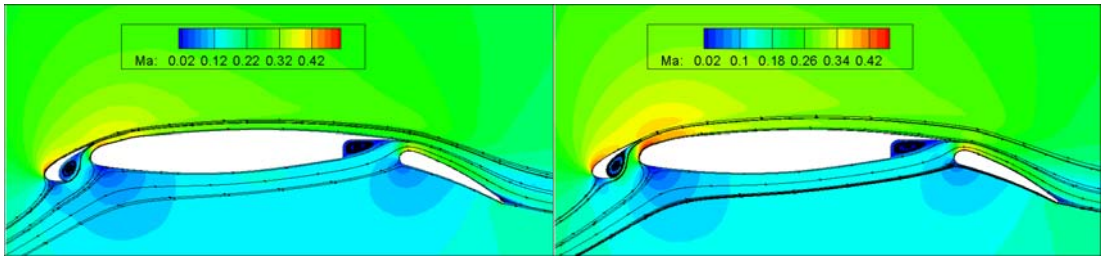

Figure 4-41: Comparison flow with Ma contours

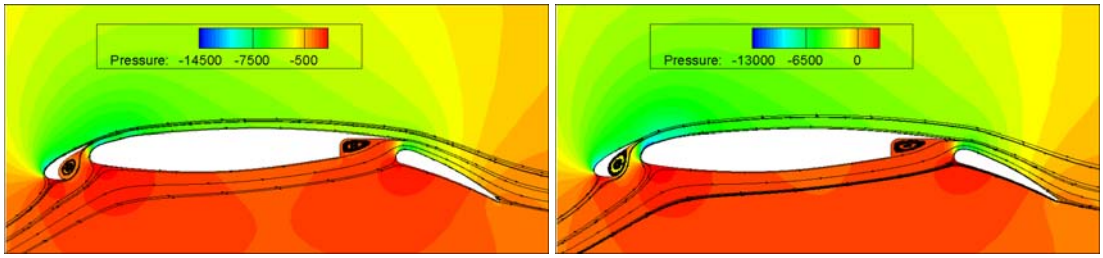

Figure 4-42: Comparison flow with Pressure contours

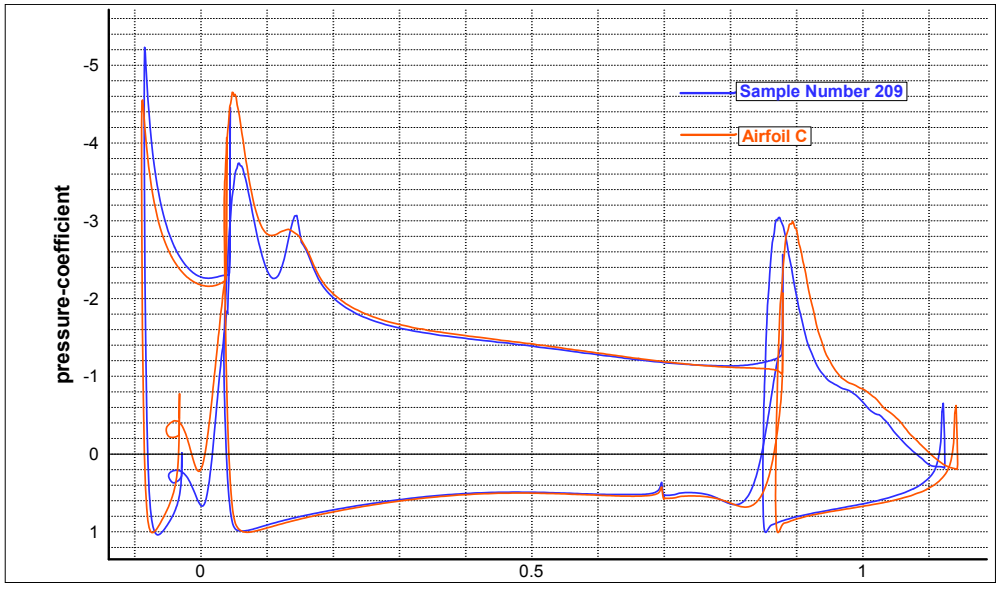

Figure 4-43: CP comparison

The benefit from this optimization is given in table 4-11.

Table 4-11: Improve of CL/CD and CL after optimization

Airfoil	CL/CD	CL
Sample 209	63.38	2.55
C	68.94	2.59
Δ	8.77%	1.57%

4.2.5 Landing

It uses the same method to get the Landing configuration. All the components' geometry of the HLC airfoil inherit the contour parameters from takeoff airfoil C, while readjust the position and orientation range table 4-12. While the position and the orientation of the high-lift devices design space is given in table 4-12. Since in this optimization task there have 6 variables, so it use 200 samples, the new Hammersley sample are given in appendix figure 12 to 16. All of the sample, parameter and the vector graphics generation used a VB program. Two of the sampling HLC airfoils are showed in figure 4-44.

Table 4-12: landing configuration design space

	Case Landing				
Variables	Par.	**Lower bound**		**Upper bound**	
X_{slat}	1	-0.1	0	-0.06	1
Y_{slat}	2	-0.065	0	-0.05	1
α_{slat}	3	25 deg	0	30 deg	1
r_{Leslat}	4	0.110			
Z_{xxslat}	5	-2.140			
α_{Teslat}	6	20.506 deg			
X_{flap}	7	0.15	0	0.22	1
Y_{flap}	8	-0.015	0	-0.008	1
α_{flap}	9	25 deg	0	35 deg	1
r_{Leflap}	10	0.090			
Z_{xxflap}	11	-0.001			
α_{Teflap}	12	5.340 deg			

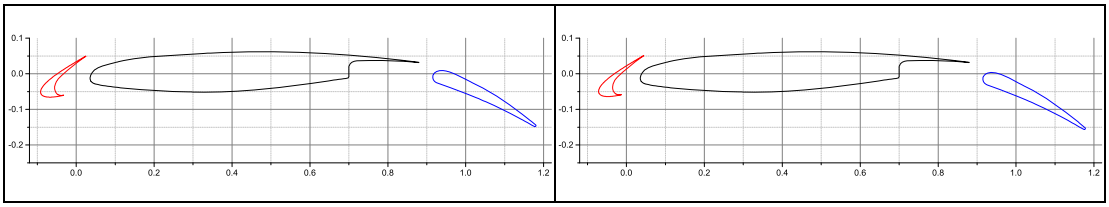

Figure 4-44: Airfoil No. 50, 150.

The biggest CL is the airfoil No.177, the CL value after trim is 3.04.

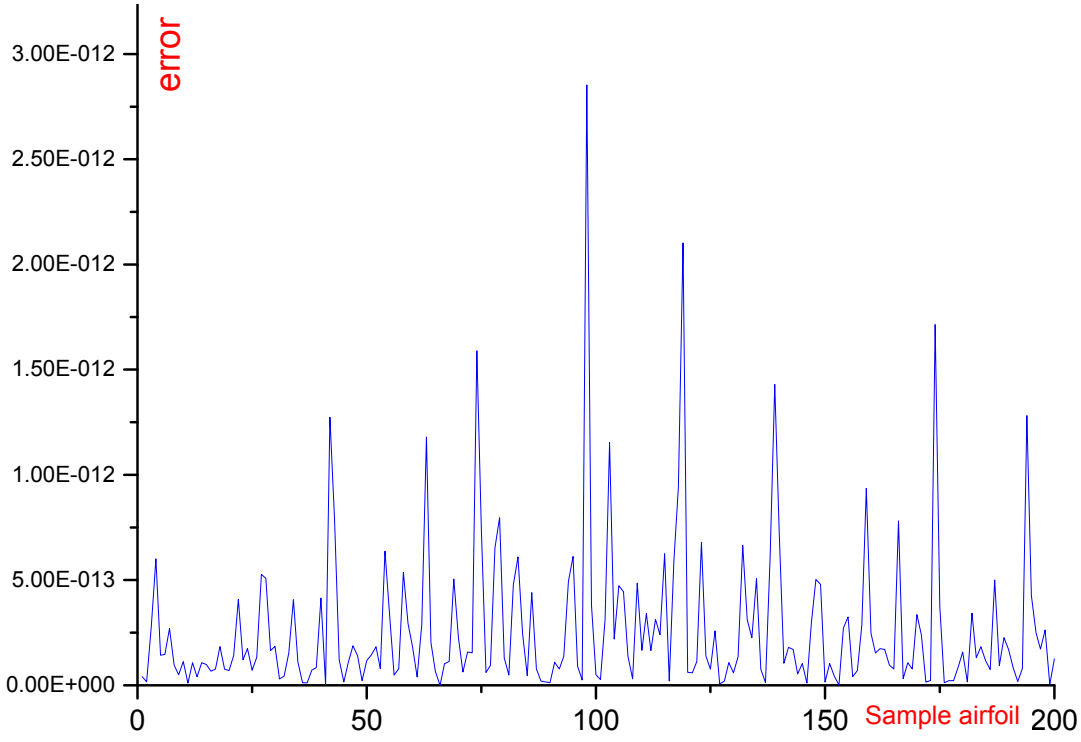

Figure 4-45: Objective Difference between samples and surrogate model at sample points (Landing)

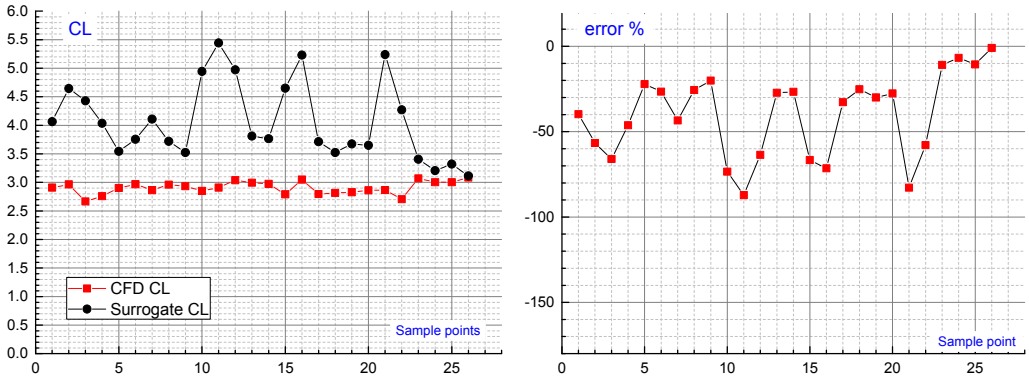

Figure 4-46: Objective Difference between

The best one is the No. 16, name it Airfoil D.

Table 4-13: landing configuration bounds

	No.	Par.1	Par.2	Par.3	Par.7	Par.8	Par.9
Landing	Airfoil D	0.789	0.001	0.300	0.317	0.999	0.999
	No.177	0.880	0.051	0.444	0.218	0.980	0.926

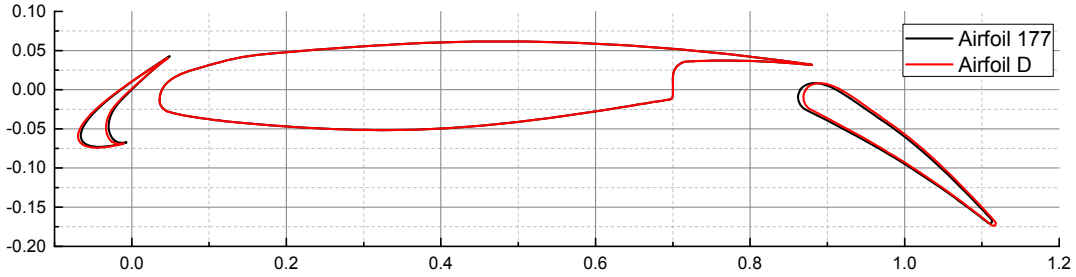

Figure 4-47: landing HLC airfoil optimization comparison

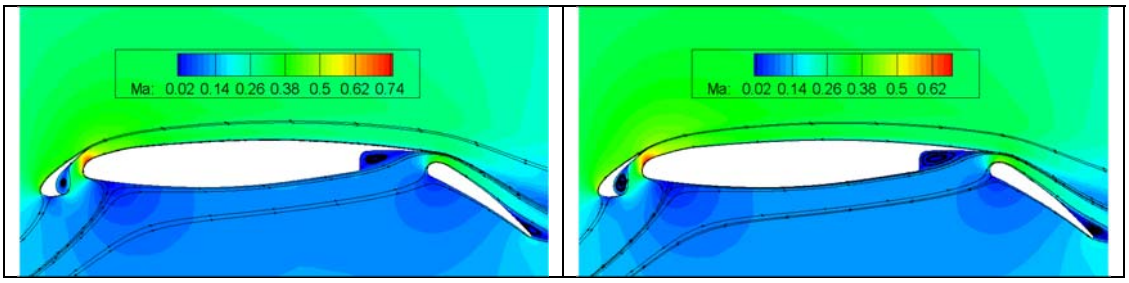

Figure 4-48: Ma contour and streamline comparison

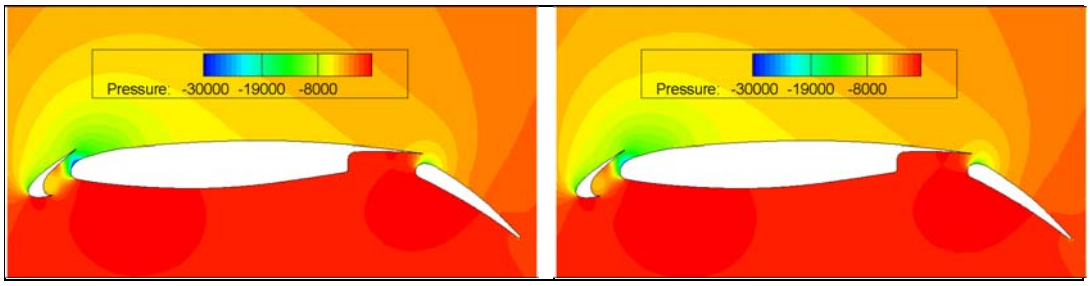

Figure 4-49: Pressure comparison

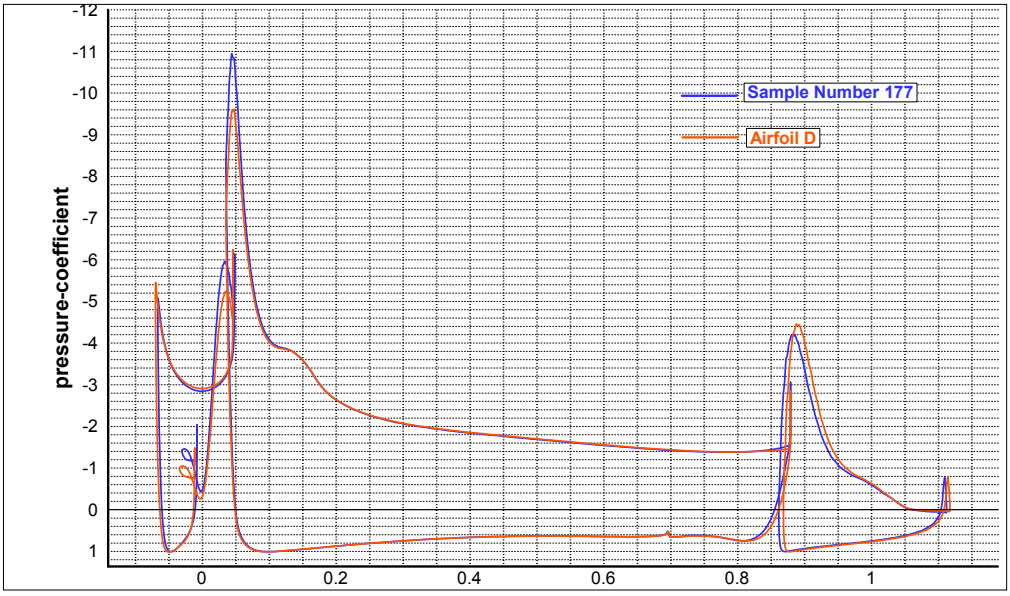

Figure 4-50: CP comparison

Table 4-14: Improve of CL after optimization

Airfoil	CL
Sample 177	3.040
Airfoil D	3.086
Δ	1.57%

4.3 Drop Spoiler Effect

In order to study the drop spoiler function to HLC airfoils' aerodynamics characteristics', a drop spoiler model was employed to study its function, the spoiler hinge point was locates at 0.8 chord, and the effective spoiler size is 0.08 chord, the study use a symmetric deflection, the maximum deflection at both side is 4 deg, the step for the deflection is 2 deg. The deflection motion is described by equation 3-23. In this kind deflection the main wing can vary its camber, meanwhile control the gap between the flap and main wing.

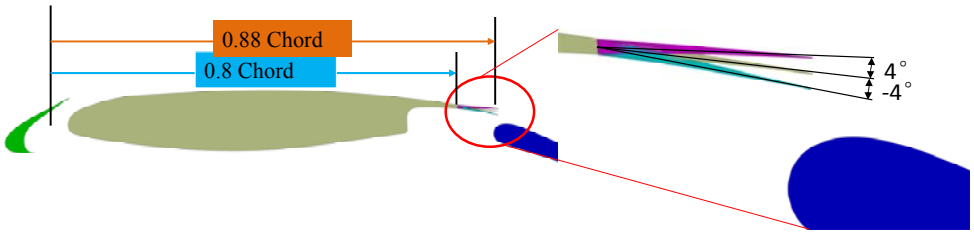

Figure 4-51: Drop Spoiler

Table 4-15: Spoilers setting

Baseline	Airfoil C	Airfoil D
δ_s	+4°	+4°
δ_s	+2°	+2°
δ_s	0°	0°
δ_s	-2°	-2°
δ_s	-4°	-4°

The CFD simulation result is showed in figure 4-52, 53 and 54.

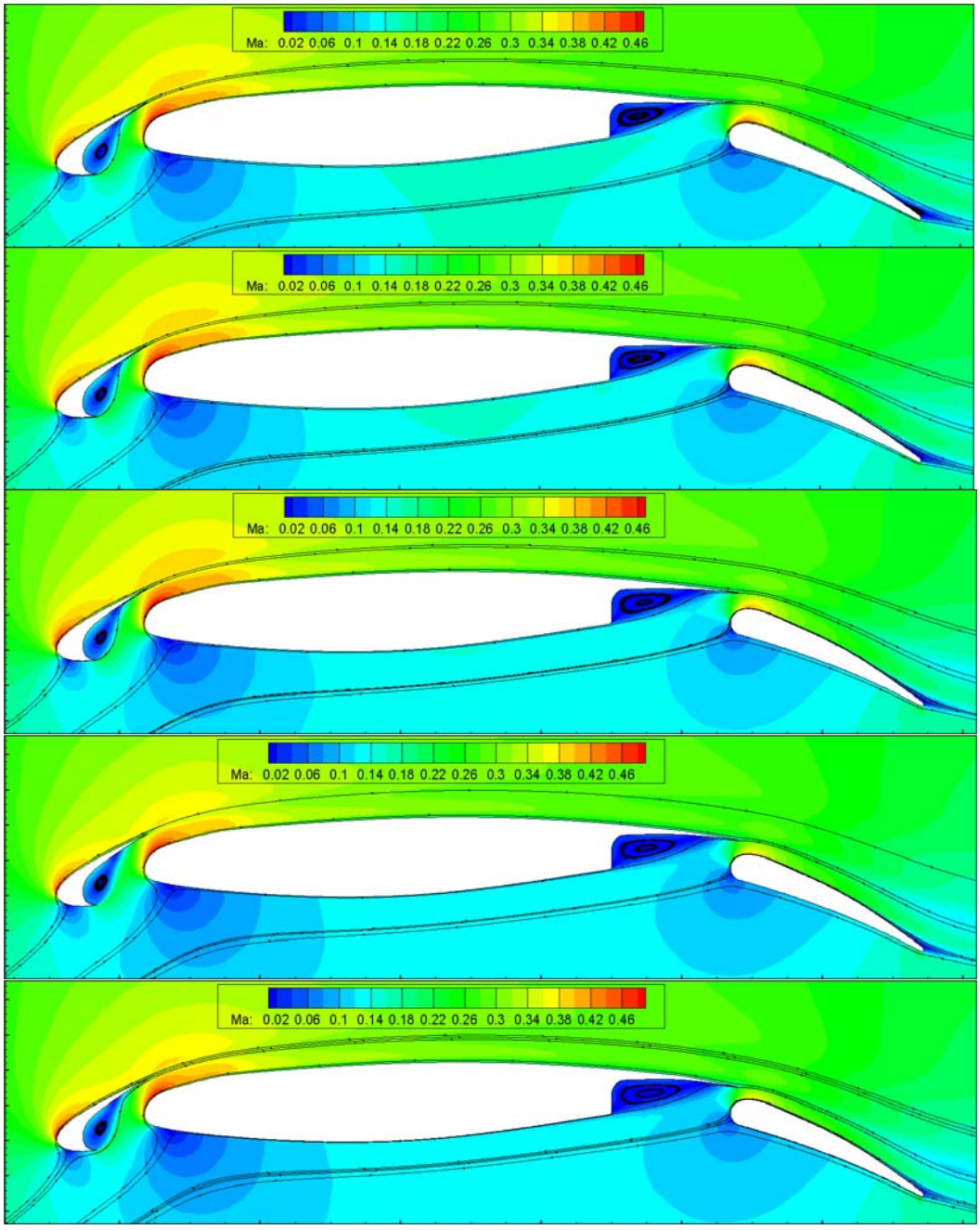

Figure 4-52: Ma contours comparison

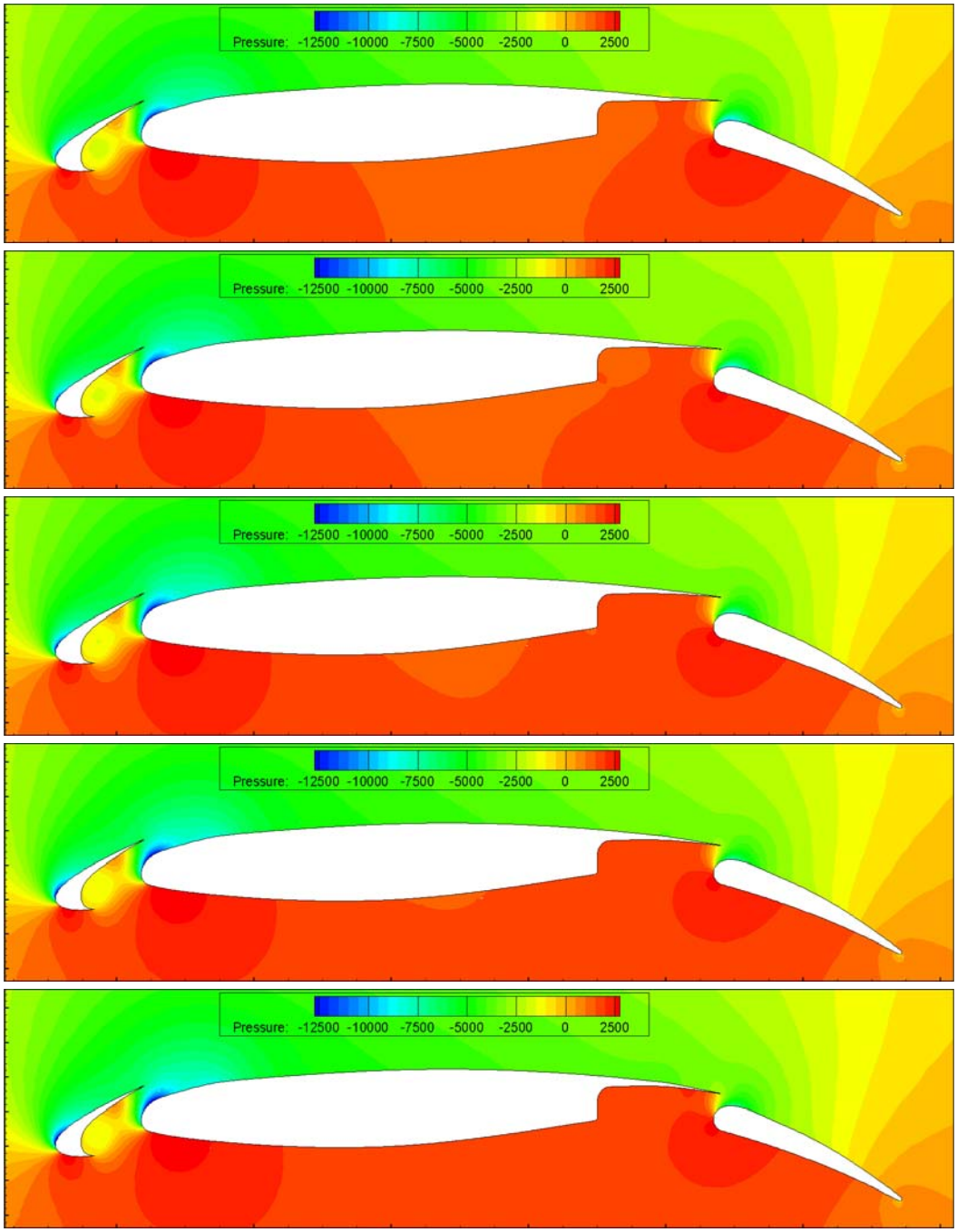

Figure 4-53: Pressure contours comparison

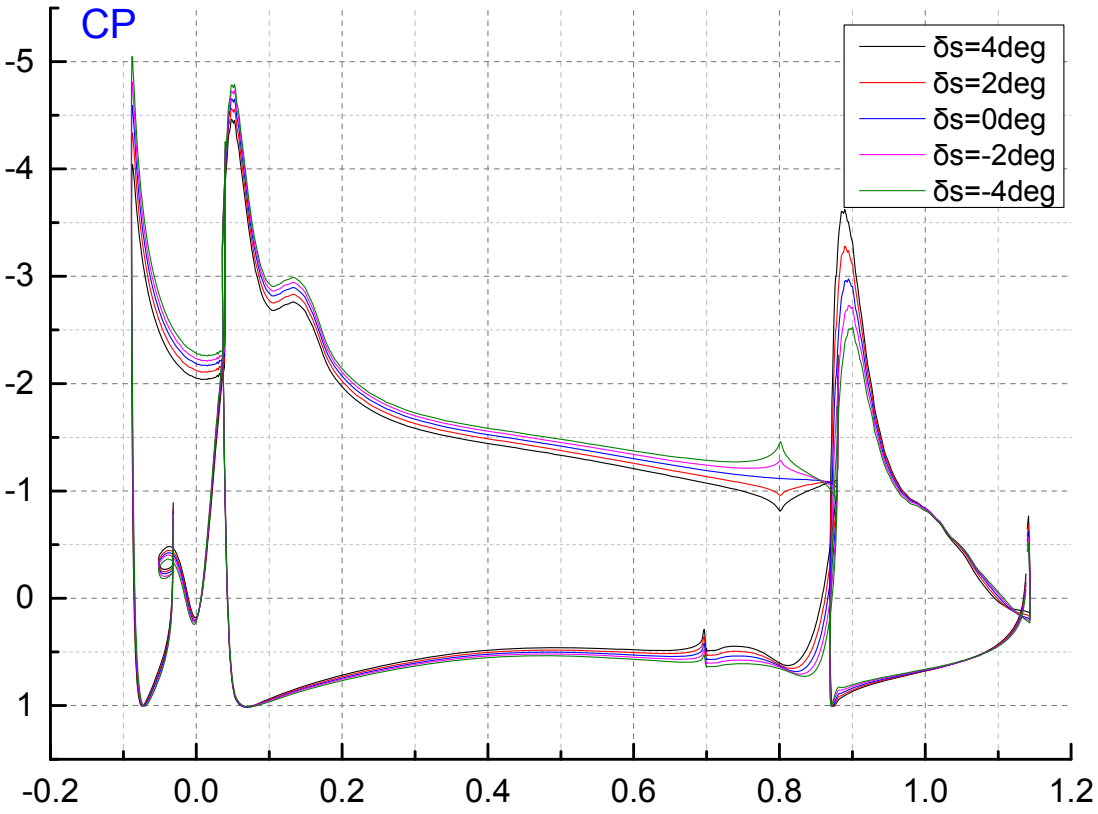

Figure 4-54: CP distribution comparison

Table 4-16: Drop spoiler affect to CL/CD and CL

δ_s	CL/CD	CL	Δ(CL/CD)	ΔCL
4 deg	65.85	2.460	-4.48%	-5.00%
2 deg	68.79	2.530	-0.22%	-2.33%
0 deg	68.94	2.590	/	
-2 deg	69.01	2.638	0.11%	1.85%
-4 deg	73.29	2.682	6.31%	3.57%

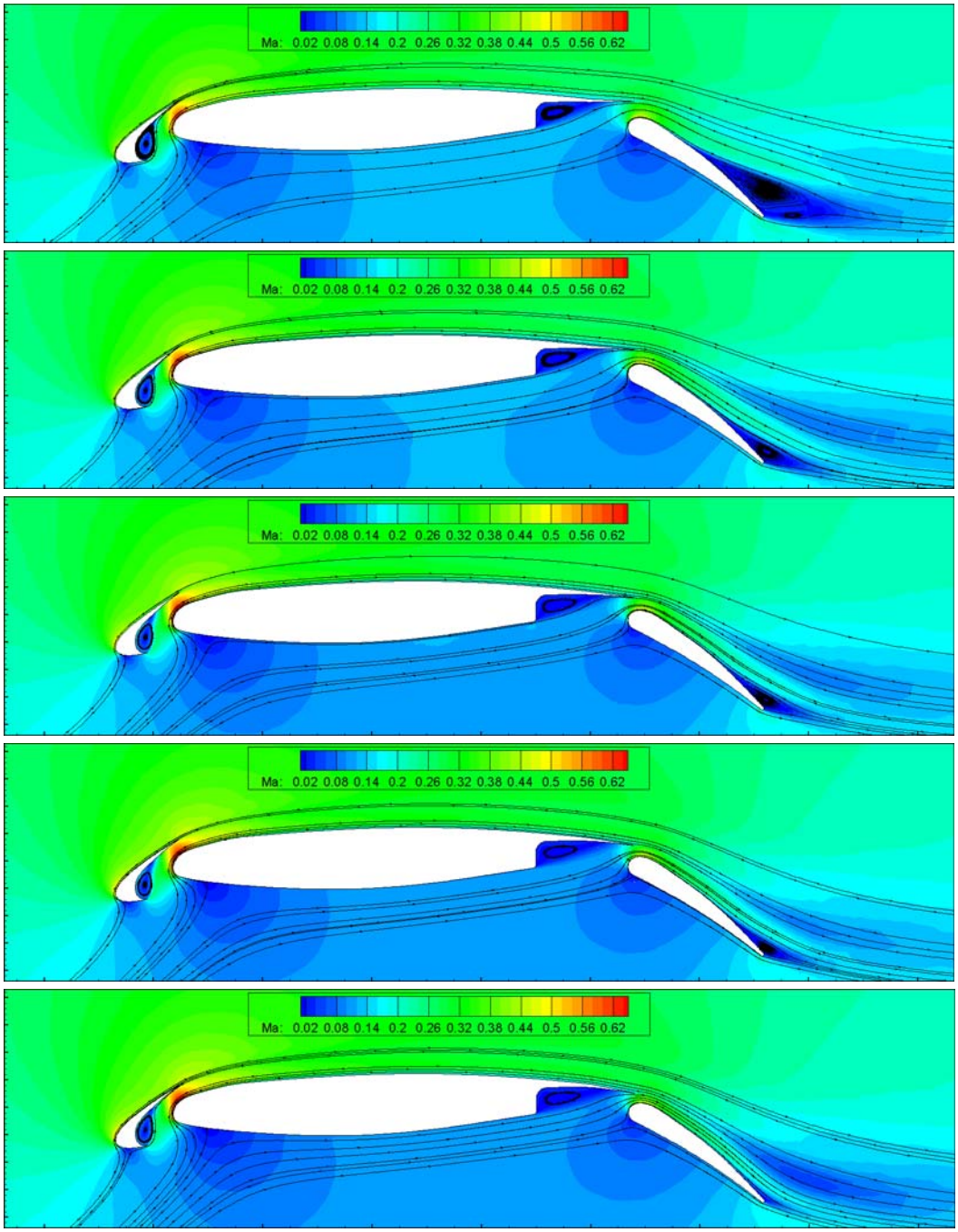

Figure 4-55: Mach Contour comparison

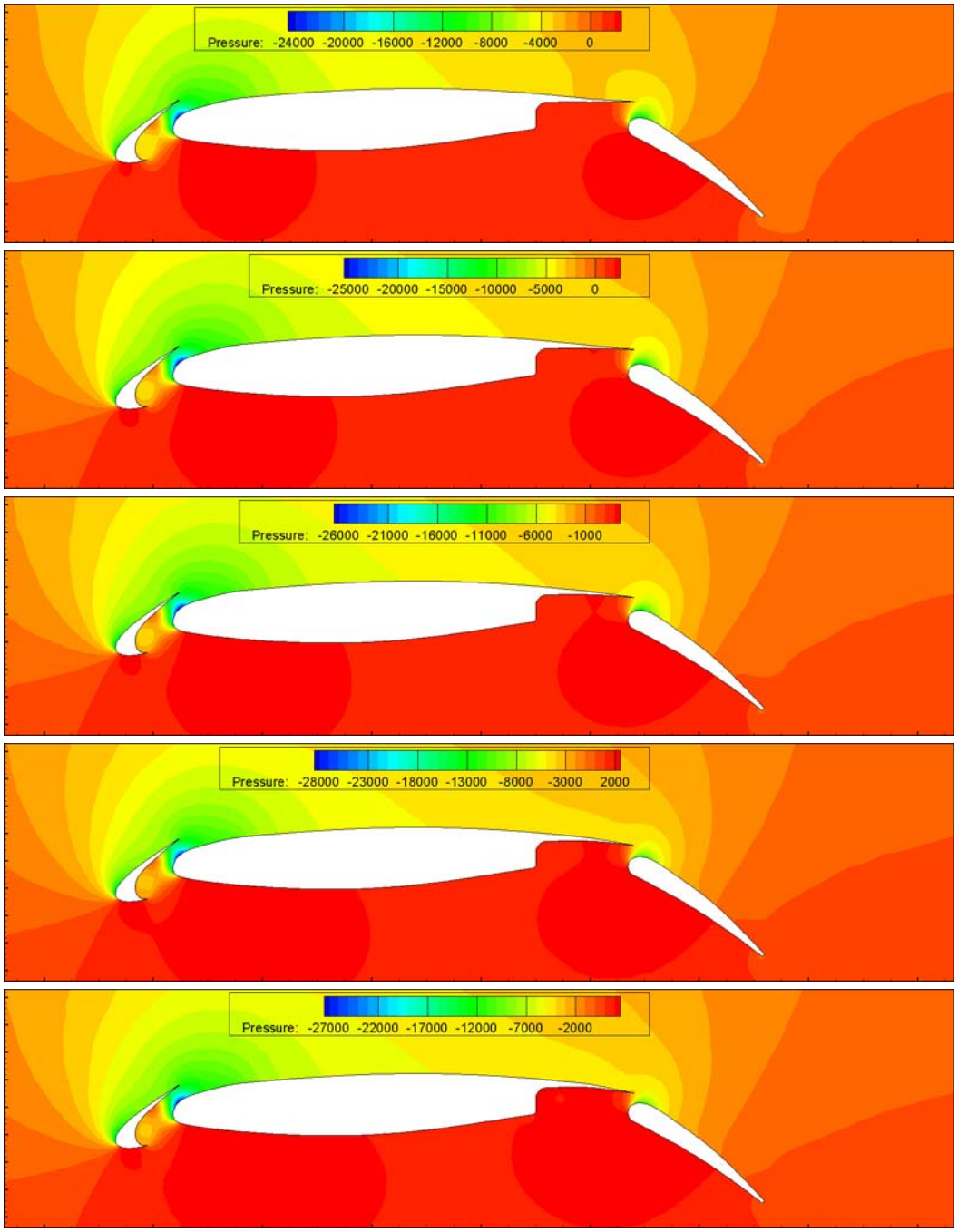

Figure 4-56: pressure contours comparison

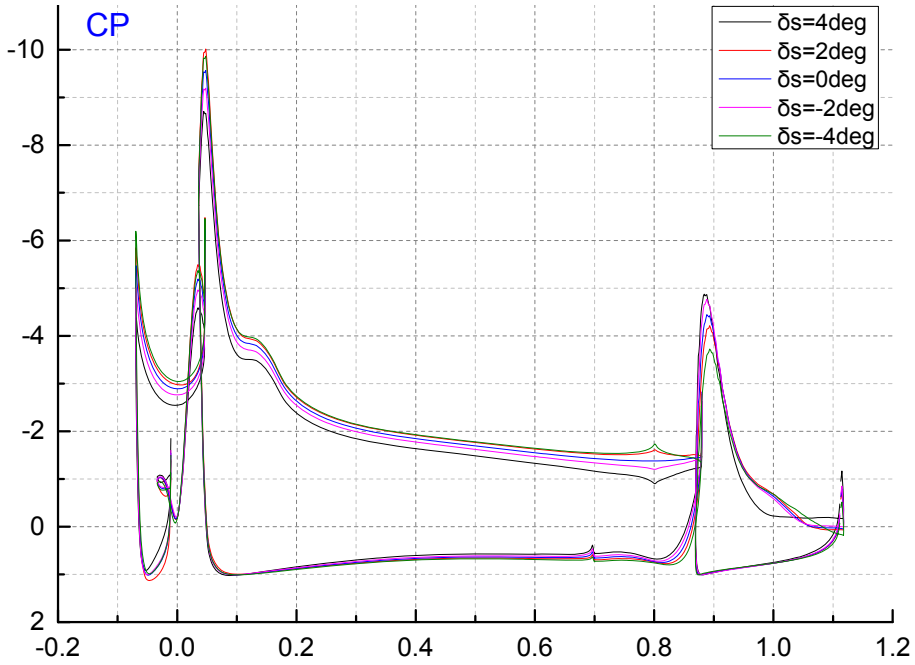

Figure 4-57: CP comparison

Table 4-17: Drop spoiler affect to CL/CD and CL

δ_s	CL	ΔCL
4 deg	2.758	-10.62%
2 deg	2.977	-3.52%
0 deg	3.086	/
-2 deg	3.187	3.27%
-4 deg	3.209	3.97%

Chapter5. Conclusions and Future Work

5.1 Conclusion

The main goal of this thesis was to develop a design approach based on CFD-surrogate-optimization for the wing airfoil. The highly complex design of single/multi-element airfoils involves different areas of subjects, such as structural, aerodynamic and systems design. These subjects hard to be studied entire within this MSc program; hence in this thesis just involves an aerodynamic design subject, while other subjects are barely taken into account. In order to fulfil the overall thesis goal, an entire wing airfoil aerodynamic design process which means from transonic single-element airfoil to low speed HLC multi-element airfoil optimization design, they are transonic single-element airfoil optimization design, HLC airfoil for takeoff and landing, a further droppable spoiler effect to HLC was studied in this thesis. In these optimization design activities, different design objectives had been defined according to the different flight phase's requirements.

In order to achieve better understanding of the disciplines involved, a literature research was conducted on the wing airfoil design process, it mainly refer to a general describe of the flight mechanic and flight economic, a more detail discuss about wing and wing airfoil design was conducted in the flowing sections of that chapter, and because the after-load issue both refers supercritical and HLC airfoil, it will bring relative big negative pitch moment to the whole aircraft, so in order conduct more practice airfoil optimization design, a assumed trim model have been introduced and used in the following chapters. Because this research is a CFD-surrogate-based optimization, an entire chapter illustrates the mathematics modelling methods that could be used in the following research. They are approaches that involve the design of experiments, airfoil parameter methods, computational fluid dynamic, and surrogate construct and optimization method. In this chapter a multi-element airfoil mathematic modelling was developed, it could be used as a general approach to model the HLC airfoil, as it intuitive and simply properties. In order to do the optimization of the transonic and HLC airfoil optimization design, two separate chapters had given in

the following context, the first one is the transonic airfoil optimization, the second one is the HLC airfoil optimization, after this optimization design, a further study about the droppable spoiler contribute to the control surround airfoil flow was studied in the chapter. The following conclusions are made from these successful optimization design activities.

- Wing airfoil design is a critical design task in whole aircraft aerodynamic design, it involves multi-principles. So in order offer a better performance to the whole aircraft, the detail study about the wing design philosophy should be taken.
- A simple while intuitive wing airfoil parameter method can give the design in more convenience, and the Hammersley hypercube space sampling approach is suitable to do the multi-dimension sample, which use to set the database to construct the surrogate model.
- Kriging is a non-biases method to construct the surrogate model, it can offer a well objective(s) response at the new training point. And the GA optimum search is a robust approach to search the optimum in the multi-dimension space.
- Currently the CFD simulation can offer the simulation result close to the experiment data; while it is relative cheap and high productive.
- The air flow around the HLC airfoil is complex, a good design needs a detail understand of the flow mechanic.
- Variable camber airfoil not only do favor to the transonic flight, but it also can do contribute to wing HLC performance, currently the newest long range civil transport all equipment with it, for it can control the main wing camber and the gap between the main wing and the flap more accuracy and easily, it both release the actuator system design difficulty and offer a more wide design space.

5.2 Future work

Aerodynamic is an interesting subject, not only refers to its application in engineering, but also owing to its complex mechanics to govern its behavior, such as N-S equations and turbulence model, it need a further demand to master the mathematic tools.

Use the CFD tools to do aerodynamic design, even optimization design; it is a challenge task, for it involves such subjects, as geometry parameter, optimization and using surrogate model, to understand their function and the mathematic modelling is a very tough job.

In this thesis a 2-D airfoil design optimization have a success process, while any flow exists in the world are 3-D, a one dimension increase, the imagination space and the difficulties need to deal with it boost a lot.

REFERENCES

[1] Jameson, A. and Fatica, M. (2006), "Using Computational Fluid Dynamics for Aerodynamics", .

[2] Flaig, A. and Hilbig, R. (1993), "High-lift design for large civil aircraft.", *High-lift system Aerodynamics, AGARD CP 515,* pp. 31-1-31-12.

[3] Neittaanmäki, P., Rossi, T., Korotov, S., Oñate, E., Périaux, J. and Knörzer, D. "AERODYNAMIC DESIGN OF AIRBUS HIGH-LIFT WINGS IN A MULTIDISCIPLINARY ENVIRONMENT", .

[4] Wild, J. and Brezillon, J. (2005), "APPLICATION OF MULTI OBJECTIVE CONSTRAINED OPTIMIZATION IN AERODYNAMIC HIGH LIFT DESING", in Schilling, R., Haase, W., Periaux, J., et al (eds.), *Evolutionary and Deterministic Methods for Design, Optimization and Control with Applications to Industrial and Societal Problems,* FLM, Munich, .

[5] Lian, Y. and Liou (2005), "Multi-objective optimization of transonic compressor blade using evolutionary algorithm", *Journal of Propulsion and Power,* vol. 21, no. 6, pp. 979-987.

[6] Song, W. and Keane, A. J. (2007), "Surrogate-based aerodynamic shape optimization of a civil aircraft engine nacelle", *AIAA Journal,* vol. 45, no. 10, pp. 2565-2574.

[7] Arabnia, M. and Ghaly, W. (2008), "A strategy for multi-objective shape optimization of turbine stages in three-dimensional flow", *12th AIAA/ISSMO Multidisciplinary Analysis and Optimization Conference,* 10 –12 September 2008, Victoria, British Columbia Canada, .

[8] Wallcoo.net (23 December 2011), *Beautiful Japanese Cranes in Wi... Wallpaper*, available at: http://www.walltor.com/wallpaper/beautiful-japanese-cranes-in-winter-photo-of-a-beautiful-japanese-crane-in-snow-59320 (accessed 20 November 2013).

[9] Daily Mail Reporter (21 April 2009), *Follow the leader... Flock of cranes learn to migrate by following a microlight aircraft*, available at: http://www.dailymail.co.uk/sciencetech/article-1172312/Follow-leader--Flock-cranes-learn-migrate-following-microlight-aircraft.html (accessed 21 November 2013).

[10] Herzog, J. (13 September 2012), *A320 Enhanced (A320E) prototype (F-WWIQ) with sharklets at ILA Berlin Air Show 2012*, available at: http://commons.wikimedia.org/wiki/File:F-WWIQ_Airbus_A320_sharklet_ILA_2012_07.jpg (accessed 20 November 2013).

[11] 新华网(xinhuanet). (25 May 2007), *空客落户天津 中国大飞机借力(New Airbus Factory settled in TianJin, Push the China Civil airplane industrial forward)*, available at: http://news.xinhuanet.com/world/2007-05/25/content_6150547.htm (accessed November/21/2013).

[12] Air Transport Action Group (November 2010), *Beginner's Guide to Aviation Efficiency*, available at: http://www.enviro.aero/Content/Upload/File/ATAG_BeginnersGuidetoAviationEfficiency_MIDRESO(1).pdf (accessed 21 November 2013).

[13] Lee, J. J., Waitz, I. A., Kim, B. Y., Fleming, G. G., Maurice, L. and Holsclaw, C. A. (2007), "System for assessing Aviation's Global Emissions (SAGE), Part 2: Uncertainty assessment", *Transportation Research Part D: Transport and Environment,* vol. 12, no. 6, pp. 381-395.

[14] Straathof, M. H. (2012), *Shape Parameterization in Aircraft Design: A Novel Method, Based on B-Splines.*Universiteit Delft, .

[15] Schrauf, G., Wood, N. and Gölling, B. (2006), "Key Aerodynamic Technologies for Aircraft Performance Improvement", *5th Community Aeronautics Days,* .

[16] Peeters, P., Middel, J. and Hoolhorst, A. (2005), *Fuel efficiency of commercial aircraft,* NLR-CR-2005-669, Air Transport of National Aerospace Laboratory NLR.

[17] Secretariat, I. (2010), "ICAO Environmental Report 2010: AIRCRAFT TECHNOLOGY IMPROVEMENTS", *ICAO Environmental Report,* vol. Chapter 2, pp. 68-68.

[18] Babikian, R., Lukachko, S. P. and Waitz, I. A. (2002), "The historical fuel efficiency characteristics of regional aircraft from technological, operational, and cost perspectives", *Journal of Air Transport Management,* vol. 8, no. 6, pp. 389-400.

[19] Kesseler, E. (2006), "Advancing the state-of-the-art in the civil aircraft design: A knowledge-based multidisciplinary engineering approach", Citeseer, .

[20] Hawk, J. L. (12 April 2005), *The Boeing 787 Dreamliner: More Than an Airplane (PowerPoint Presentation)*, available at: http://depts.washington.edu/amtas/events/amtas_05spring/Miller.pdf (accessed 20 November 2013).

[21] Rogers, M. M. (2012), *Technical Challenges to Reducing Subsonic Transport Drag (PowerPoint Presentation)*, available at: http://www.aiaa.org/uploadedFiles/About-AIAA/Press-

Room/Key_Speeches-Reports-and-Presentations/2012/Rogers-EA-SFW-GEPC1-3-AIAAjan2012.pdf (accessed 23 November 2013).

[22] Jahanmiri, M. (2011), *Aircraft Drag Reduction: An Overview,* Research report 2011:02, Chalmers University of Technology, SE-412 96 Göteborg.

[23] Tennekes, H. (2009), *The simple science of flight: from insects to jumbo jets.* The MIT Press.

[24] Henne, P. A. *Applied computational aerodynamics (Vol. 125. AIAA),* .

[25] Ellegren, H. and Fransson, T. (1992), "Fat loads and estimated flight‐ranges in four Sylvia species analysed during autumn migration at Gotland, South‐East Sweden", *Ringing & Migration,* vol. 13, no. 1, pp. 1-12.

[26] *U2 Utility Flight Handbook. Page.135,* (1959), , Department of Defense.

[27] *, An Aerodynamic Example: The Boeing 747*, available at: http://public.fh-wolfenbuettel.de/~haeuser/sommer/aerodyn/Airbus380&Boeing747.pdf (accessed 25 November 2013).

[28] Sadraey, M. (2009)*, Aircraft Performance Analysis: chapter 3: Drag Force and Drag Coefficient*, available at: http://faculty.dwc.edu/sadraey/Chapter%203.%20Drag%20Force%20and%20its%20Coefficient.pdf (accessed 20 November 2013).

[29] Strang, W. J. and Mckinlay, R. M. (1978), "Concorde in service", *Aircraft Engineering and Aerospace Technology,* vol. 50, no. 12, pp. 2-10.

[30] Bechert, D. W., Bruse, M., Hage, W. and Meyer, R. (2000), "Fluid mechanics of biological surfaces and their technological application", *Naturwissenschaften,* vol. 87, no. 4, pp. 157-171.

[31] Fitzgerald, S. (2010)*, Picture of the Boeing 707-436 aircraft*, available at: http://www.airliners.net/photo/British-Airtours/Boeing-707-436/1823541/L/ (accessed 24 November 2013).

[32] JCMusser *, Boeing 747-8JK Intercontinental*, available at: http://www.jcmusser.com/photo/747.htm (accessed 24 November 2013).

[33] Abbott, I. H. and Doenhoff, A. E. (1959), *Theory of wing sections: including a summary of airfoil data,* Dover Publications, INC., New York.

[34] Obert, E., Slingerland, R., Leusink, D. J. W., Berg, T. V. D. and Koning, J. H. (2009), *Aerodynamic Design of Transport Aircraft,* IOS Press under the imprint Delft University Press, NETHERLANDS.

[35] Jenkinson, L. R., Simpkin, P., Rhodes, D., Jenkison, L. R. and Royce, R. (1999), *Civil jet aircraft design (page 106-107),* Lightning Source UK Ltd, United Kingdom.

[36] Samareh, J. A. (1999), "A survey of shape parameterization techniques", *NASA CONFERENCE PUBLICATION,* Citeseer, pp. 333.

[37] Reckzeh, D. (2004), "AERODYNAMIC DESIGN OF AIRBUS HIGH-LIFT WINGS IN A MULTIDISCIPLINARY ENVIRONMENT", in Neittaanmäki, P., Rossi, T., Korotov, S., et al (eds.), *European Congress on Computational Methods in Applied Sciences and Engineering,* Vol. ECCOMAS 2004, 24—28 July 2004, Jyväskylä, .

[38] Nelson, T. (2005)*, 787 Systems and Performance*, available at: http://dibley.eu.com/documents/B787SystemsandPerf-GeorgeBeyle-31mar09.pdf (accessed 10 February 2013).

[39] Carter, D. L., Osborn, R. F., Hetrick, J. A. and Kota, S. (2007), "The quest for efficient transonic cruise", *AIAA Paper,* vol. 7812, pp. 2007.

[40] Raymer, D. P. (1992), *Aircraft design: a conceptual approach,* 2nd ed, American Institute of Aeronautics and Astronautics, United States of America.

[41] Bertin, J. J. and Smith, M. L. (1989), *Aerodynamics for engineers,* Prentice Hall Englewood Cliffs.

[42] Hurt, H. H. and JR (1965), *Aerodynamics for naval aviators,* NAVAIR 00-80T-80 ed, DIRECTION OF COMMANDER, NAVAL AIR SYSTEMS COMMAND.

[43] Atassi, H. M. *, Compressibility Effects on Airfoil Lift*, available at: http://www3.nd.edu/~atassi/Teaching/ame%2060639/Notes/compressible.pdf (accessed 25 November 2013).

[44] From Wikipedia *, Flap (aircraft) .*, available at: http://en.wikipedia.org/wiki/Flap_(aircraft) (accessed 4 December 2013).

[45] Harris, C. D. (1990), *NASA Supercritical Airfoil,* NASA Technical Paper 2969, Langley research center Hampton, virginia.

[46] Talay, T. A. (1975), *Introduction to the Aerodynamics of Flight,* Scientific and Technical Information Office, National Aeronautics and Space Administration.

[47] Roedts, R., Somero, R. and Waskiewicz, C. *, Airbus A380 Analysis (PowerPoint Presentation)*, available at:

http://www.dept.aoe.vt.edu/~mason/Mason_f/A380Roedts.pdf (accessed 24 February 2013).

[48] XPMorten (3 March 2010), *Supercritical wing and Mcrit*, available at: http://www.pprune.org/tech-log/407474-supercritical-wing-mcrit.html (accessed 15 January 2013).

[49] McCormick, B. W. (1995), *Aerodynamics, aeronautics, and flight mechanics,* 2nd ed, Wiley New York, United States of America.

[50] RUDOLPH, P. K. C. (1996), *High-lift systems on commercial subsonic airliners,* NASA Contractor Report 4746, National Aeronautics and Space Administration, Ames Research Center, Moffett Field, California 94035-1000.

[51] Van Dam, C. P. (2002), "The aerodynamic design of multi-element high-lift systems for transport airplanes", *Progress in Aerospace Sciences,* vol. 38, no. 2, pp. 101-144.

[52] Meredith, P. T. (1993), "Viscous phenomena affecting high-lift systems and suggestions for future CFD development", *High-Lift System Aerodynamics,* Vol. AGARD-CP-515 (IV), 5-8 October 1992, Banff, Alberta, Canada, AGARD, 7 RUE ANCELLE 92200 NEUILLY SUR SEINE FRANCE, pp. 19-1.

[53] Ruijgrok, G. J. J. (1996), *Elements of airplane performance,* Delft university press.

[54] Wikipedia (23 July 2013), *Leading-edge slats*, available at: http://en.wikipedia.org/wiki/Leading_edge_slats (accessed 20 August 2013).

[55] Smith, A. M. O. (1975), "High-lift Aerodynamics", *Journal of Aircraft,* vol. 12, no. 6, pp. 501-530.

[56] Goldberg, D. E. (1997), *Genetic Algorithms in Search, Optimization, and Machine Learning.* Addison Wesley Longman, Inc., Canada.

[57] From Wikipedia (15 June 2013), *Kriging*, available at: http://en.wikipedia.org/wiki/Kriging (accessed 20 June 2013).

[58] Recksiek, M. (2009), "Advanced High Lift System Architecture With Distributed Electrical Flap Actuation", *Aviation System Technology Workshop,* 29-30 March 2009, Hamburg, Germany, .

[59] Federal Aviation Administration (2011), *Aircraft Weight and Balance Handbook,* Skyhorse Publishing Inc.

[60] Ahmed, M. Y. M. and Qin, N. (2009), "Surrogate-Based Aerodynamics Design Optimization: Use of Surrogates in Aerodynamics Design Optimization", *13th International Conference on Aerospace Science & Aviation Technology, Cairo, Egypt,* pp. 26.

[61] Bandler, J. W., Koziel, S. and Madsen, K. (2006), "Space Mapping for Engineering Optimization", in Vicente, L. N. (ed.), *SIAG/OPT Views-and-News,* Vol. 17 Number 1, pp. 20-20.

[62] Giunta, A. A., Wojtkiewicz, S. F. and Eldred, M. S. (2003), "Overview of modern design of experiments methods for computational simulations", *Proceedings of the 41st AIAA Aerospace Sciences Meeting and Exhibit, AIAA-2003-0649,* Vol. 0649, .

[63] Barlow, J. B., Rae, W. H. and Pope, A. (1999), *Low-speed wind tunnel testing,* Wiley New York.

[64] Myers, R. H. and Montgomery, D. C. *Response surface methodology: process and product optimization using designed experiments,* 2nd ed, Wiley. com.

[65] Aslan, N. and Cebeci, Y. (2007), "Application of Box–Behnken design and response surface methodology for modeling of some Turkish coals", *Fuel,* vol. 86, no. 1, pp. 90-97.

[66] Bloor, M. I. G. and Wilson, M. J. (1989), "Generating blend surfaces using partial differential equations", *Computer-Aided Design,* vol. 21, no. 3, pp. 165-171.

[67] Eisert, P. and Girod, B. (1998), "Analyzing facial expressions for virtual conferencing", *Computer Graphics and Applications, IEEE,* vol. 18, no. 5, pp. 70-78.

[68] Balu, R. and Selvakumar, U. (2009), "Optimum hierarchical Bezier parameterization of arbitrary curves and surfaces", *Proceedings of the 11th Annual CFD Symposium,* 11-12 August 2009, Bangalore, pp. 46.

[69] Athanasopoulos, M., Ugail, H. and Castro, G. G. (2009), "Parametric design of aircraft geometry using partial differential equations", *Advances in Engineering Software,* vol. 40, no. 7, pp. 479-486.

[70] *, The NACA airfoil series.*, available at: http://www.stanford.edu/~cantwell/AA200_Course_Material/ (accessed 1 September 2013).

[71] Castonguay, P. and Nadarajah, S. K. (2007), "Effect of shape parameterization on aerodynamic shape optimization", *The 45th AIAA Aerospace*

Sciences Meeting and Exhibit AIAA Paper 2007, Vol. 59, 8-11 January 2007, Reno, Nevada, USA, pp. 8.

[72] *, Choice of Design Variables (PowerPoint Presentation)*, available at: http://www.ims.nus.edu.sg/Programs/wbfst/files/siva3.pdf (accessed 25 November 2013).

[73] *, An examination of the Joukowski airfoil in potential flow, without using complex numbers.*, available at: http://www.jimhawley.ca/downloads/Joukowski_airfoil_in_potential_flow_without_complex_numbers.pdf (accessed 9 August 2013).

[74] Kapania, N. R., Terracciano, K. and Taylor, S. (2008), "Modeling the Fluid Flow around Airfoils Using Conformal Mapping", , pp. 70-99.

[75] Sobieczky, H. (1999), "Parametric airfoils and wings", in *Recent Development of Aerodynamic Design Methodologies,* Springer, , pp. 71-87.

[76] Kumano, T., Jeong, S., Obayashi, S., Ito, Y., Hatanaka, K. and Morino, H. (2006), "Multidisciplinary design optimization of wing shape for a small jet aircraft using kriging model", *AIAA paper,* vol. 932, pp. 9-12.

[77] Sripawadkul, V., Padulo, M. and Guenov, M. (2010), "A comparison of airfoil shape parameterization techniques for early design optimization", *AIAA paper,* vol. 9050.

[78] Jameson, A. (2010)*, Airplane Design with Aerodynamic Shape Optimization. (PowerPoint Presentation)*, available at: http://aero-comlab.stanford.edu/Papers/AirplaneDesignShanghai.pdf (accessed 4 December 2012).

[79] Ball, D. N. (2008)*, Contributions of CFD to the 787-and Future Needs (PowerPoint Presentation)*, available at: http://www.hpcuserforum.com/presentations/Tucson/Boeing%20Ball%20IDC%20pdf.pdf (accessed 10 May 2013).

[80] Bradley, R. G. and Bhateley, I. C. (1983), "Computational aerodynamic design of fighter aircraft Progress and pitfalls", *American Institute of Aeronautics and Astronautics, Atmospheric Flight Mechanics Conference;* Gatlinburg, TN, USA, .

[81] ESDU *, About Us*, available at: http://www.esdu.com/cgi-bin/ps.pl?sess=cranfield5_1131128180534mqr&t=root&p=aboutusroot (accessed 10 October 2013).

[82] European Transonic Windtunnel GmbH *, Press: Gallery*, available at: http://www.etw.de/cms/index.php?site=gallery#AC (accessed 25 November 2013).

[83] European Transonic Windtunnel GmbH , *ETW - The Leading Quality of Wind-Tunnel Testing*, available at: http://www.etw.de/cms/ (accessed 25 Octerber 2013).

[84] Quest, J., Wright, M. C. N., Hansen, H. and Mesuro, G. G. (2002), "First measurements on an Airbus high lift configuration at ETW up to flight Reynolds number", *40th AIAA Aerospace Sciences Meeting & Exhibit,* Vol. AIAA 2002-0423, 14-17 January 2002, Reno, NV, USA, American Institute of Aeronautics & Astronautics, .

[85] From Wikipedia (30 August 2013), *Supercritical airfoil*, available at: http://en.wikipedia.org/wiki/Supercritical_airfoil (accessed 15 October 2013).

[86] News Center of COMAC (6 November 2013), *ARJ21-700 AC104 flies to Urumchi for natural icing flight test*, available at: http://english.comac.cc/home/photo/201311/13/t20131113_1204396.shtml (accessed 20 November 2013).

[87] From Wikipedia (26 August 2011), *L. M. Milne-Thomson*, available at: L. M. Milne-Thomson (accessed 6 August 2013).

[88] Erwin Moerland, B. S. (2011), *Development of an aeroelastic analysis tool for structural sizing of high-lift devices during preliminary design.*Faculty of Aerospace Engineering, Delft University of Technology, .

[89] Drela, M. , *XFOIL subsonic Airfoil Development System*, available at: http://web.mit.edu/drela/Public/web/xfoil/ (accessed 4 December 2012).

[90] , *Xflr5*(November 2012), available at: http://www.xflr5.com/xflr5.htm (accessed 16 July 2013).

[91] Menter, F. R. (2011), "Turbulence Modeling for Engineering Flows .", *Ansys, Inc,* .

[92] Anderson, J. D. (1995), *Computational fluid dynamics,* McGraw-Hill New York.

[93] Schäfer, M. (2006), *Computational engineering: introduction to numerical methods,* Springer.

[94] Tennekes, H. and Lumley, J. L. (1972), *A first course in turbulence,* The MIT press.

[95] , *Condensation over wing in flight.*, available at: https://www.youtube.com/watch?v=-A0fN7PijgY (accessed 24 December 2013).

[96] Andersson, B., Andersson, R., Håkansson, L., Mortensen, M., Sudiyo, R. and van Wachem, B. (2012), *Computational Fluid Dynamics for Engineers.* Cambridge: Cambridge University Press.

[97] Menter, F. R., Kuntz, M. and Langtry, R. (2003), "Ten years of industrial experience with the SST turbulence model", *Turbulence, heat and mass transfer,* vol. 4, pp. 625-632.

[98] Menter, F. R. (1993), "Zonal two equation K-ω turbulence models for aerodynamic flows.", *c1993,* vol. 2906.

[99] El-Behery, S. M. and Hamed, M. H. (2009), "A comparative study of turbulence models performance for turbulent flow in a planar asymmetric diffuser", *World Academy of Science, Engineering and Technology,* vol. 53, pp. 769-780.

[100] Rumsey, C. L., Long, M., Stuever, R. A. and Wayman, T. R. (2011), "Summary of the First AIAA CFD High-Lift Prediction Workshop", *Journal of Aircraft,* vol. 48, no. 6, pp. 2068-2079.

[101] Versteeg, H. K. and Malalasekera, W. (2007), *An Introduction to Computational Fluid Dynamics The Finite Volume Method.* 2nd ed, 世界图书出版公司(World Publishing Company).

[102] Thornber. (Cranfield University), (2013), *Introduction to Turbulence (Powerpoint Presentation).*

[103] Wilcox, D. C. (2006), *Turbulence modeling for CFD,* 3rd ed, DCW industries La Canada.

[104] *, Y plus wall distance estimation.*(2011), available at: http://www.cfd-online.com/Wiki/Y_plus_wall_distance_estimation (accessed 12 June 2013).

[105] Ihme, M., Marsden, A. L. and Pitsch, H. (2006), *On the optimization of artificial neural networks for application to the approximation of chemical systems,* Annual Research Briefs, Center for Turbulence Research.

[106] Sacks, J., Welch, W. J., Mitchell, T. J. and Wynn, H. P. (1989), "Design and analysis of computer experiments", *Statistical science,* vol. 4, no. 4, pp. 409-423.

[107] Keane, A. J. and Nair, P. B. (2005), *Computational approaches for aerospace design: the pursuit of excellence,* John Wiley & Sons.

[108] Arias-Montano, A., Coello Coello, C. A. and Mezura-Montes, E. (2012), "Multi-objective airfoil shape optimization using a multiple-surrogate approach", *Evolutionary Computation (CEC), 2012 IEEE Congress on,* IEEE, pp. 1.

[109] , *Pareto efficiency*, available at: http://en.wikipedia.org/wiki/Pareto_efficiency (accessed 10 February 2013).

[110] Obayashi, S. (1998), "Multidisciplinary design optimization of aircraft wing planform based on evolutionary algorithms", *Systems, Man, and Cybernetics, 1998. 1998 IEEE International Conference on,* Vol. 4, IEEE, pp. 3148.

[111] Bertsimas, D. and Tsitsiklis, J. (1993), "Simulated annealing", *Statistical Science,* , pp. 10-15.

[112] Henderson, D., Jacobson, S. H. and Johnson, A. W. (2003), "The theory and practice of simulated annealing", in *Handbook of metaheuristics,* Springer, , pp. 287-319.

[113] Busetti, F. (2003), *Simulated annealing overview*, available at: http://163.18.62.64/wisdom/Simulated%20annealing%20overview.pdf (accessed 6 July 2013).

[114] Escalante, H. J., Montes, M. and Sucar, L. E. (2009), "Particle swarm model selection", *The Journal of Machine Learning Research,* vol. 10, pp. 405-440.

[115] Poli, R., Kennedy, J. and Blackwell, T. (2007), "Particle swarm optimization An overview", *Swarm intelligence,* vol. 1, no. 1, pp. 33-57.

[116] Glover, F. (1995), *Tabu search fundamentals and uses.* Citeseer.

[117] Glover, F., Laguna, M. and Marti, R. (2007), "Principles of tabu search", *Approximation Algorithms and Metaheuristics,* vol. 23, pp. 1-12.

[118] Carrese, R. (2012), *Identifying preferred solutions for multi-objective aerodynamic design optimization.* School of Aerospace Mechanical and Manufacturing Engineering, RMIT University, Melbourne, Australia.

[119] Likeng, H. and Zhenghong, G. (2012), "WING-BODY OPTIMIZATION BASED ON MULTI-FIDELITY SURROGATE MODEL", *28TH INTERNATIONAL CONGRESS OF THE AERONAUTICAL SCIENCES,* .

[120] NASA , *Test/Validation Cases RAE 2822 Airfoil.*, available at: http://cfl3d.larc.nasa.gov/Cfl3dv6/cfl3dv6_testcases.html#raederiv (accessed 4 December 2012).

[121] Drela, M. (1998), "Pros and cons of airfoil optimization", *Frontiers of computational fluid dynamics,* vol. 1998.

[122] , *Airfoil Design*, available at: http://mail.tku.edu.tw/095980/airfoil%20design.pdf (accessed 5 May 2013).

[123] Burgess, N. K. and Mavriplis, D. J. (2012), "Robust computation of turbulent flows using a discontinuous Galerkin method .", *AIAA paper,* vol. 457.

[124] Bodart, J. and Larsson, J. (2011), "Wall-modeled large eddy simulation in complex geometries with application to high-lift devices", *Annual Research Brief,* , pp. 37-48.

[125] Fluid Dynamics TC, AFOSR and DLR , *1st International Workshop on High-Order CFD Methods*, available at: http://dept.ku.edu/~cfdku/hiocfd.html (accessed 6 May 2013).

APPENDICES

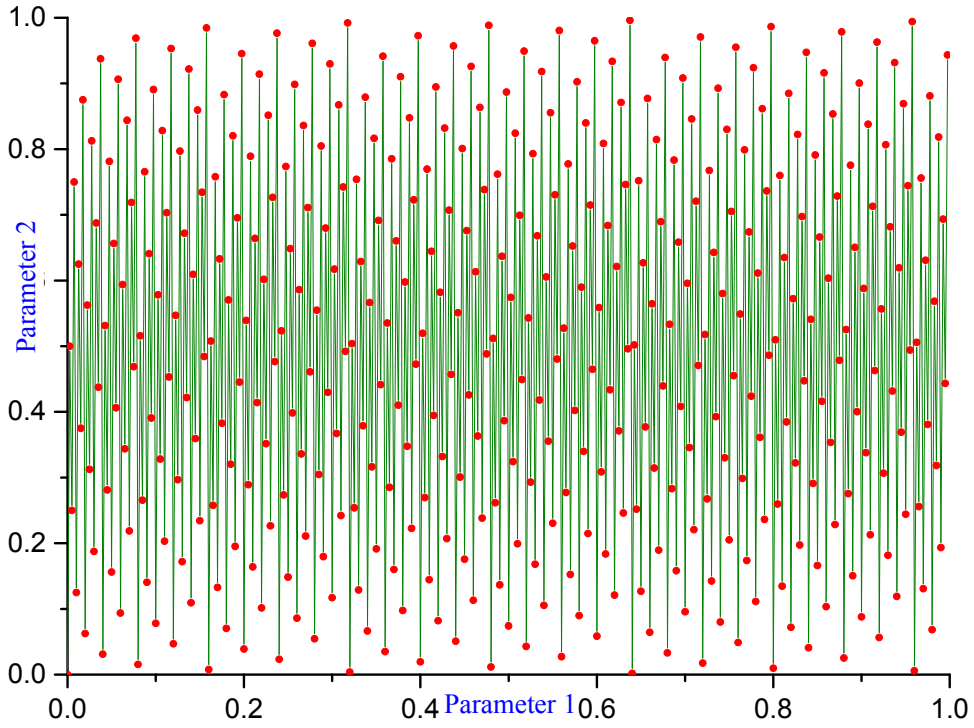

Figure 5-1: Parameter 1 ~ Parameter 2 of 400 samples

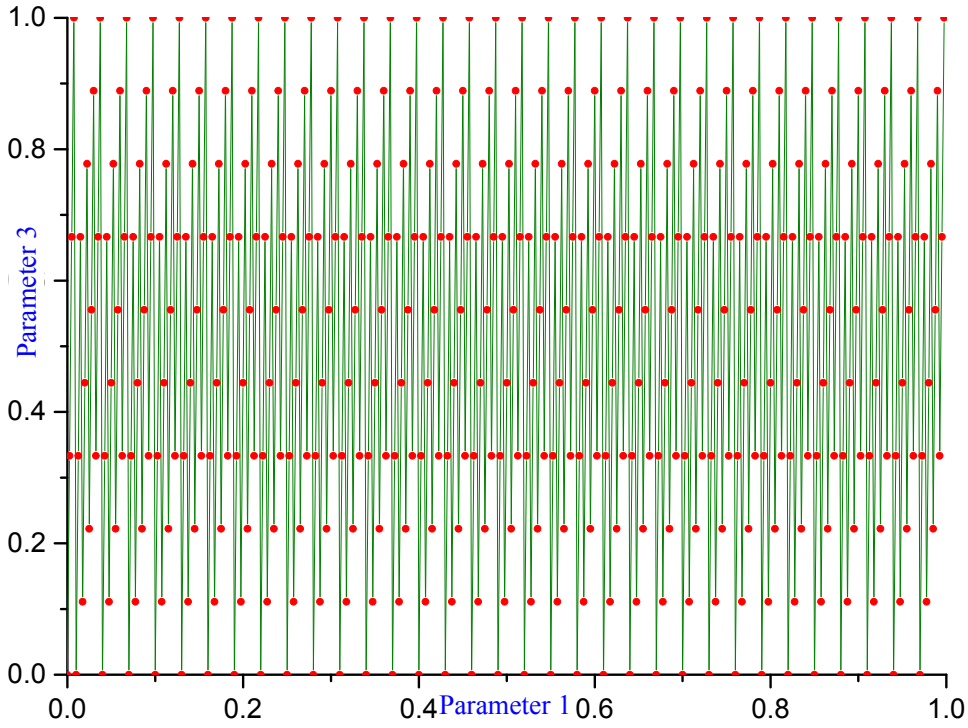

Figure 5-2: Parameter 1 ~ Parameter 3 of 400 samples

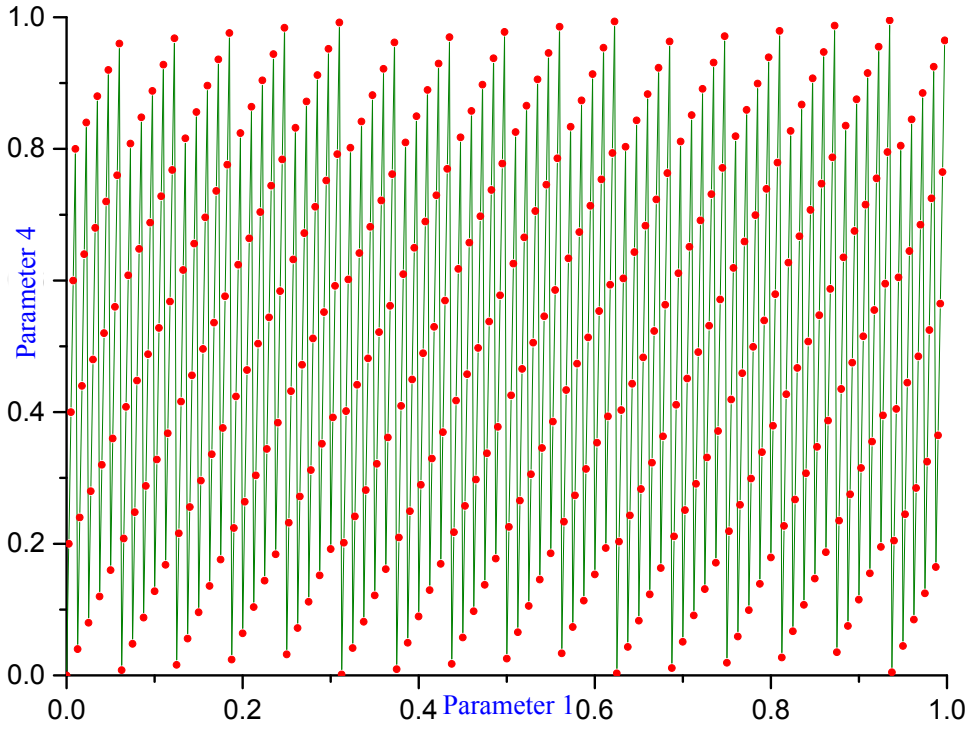

Figure 5-3: Parameter 1 ~ Parameter 4 of 400 samples

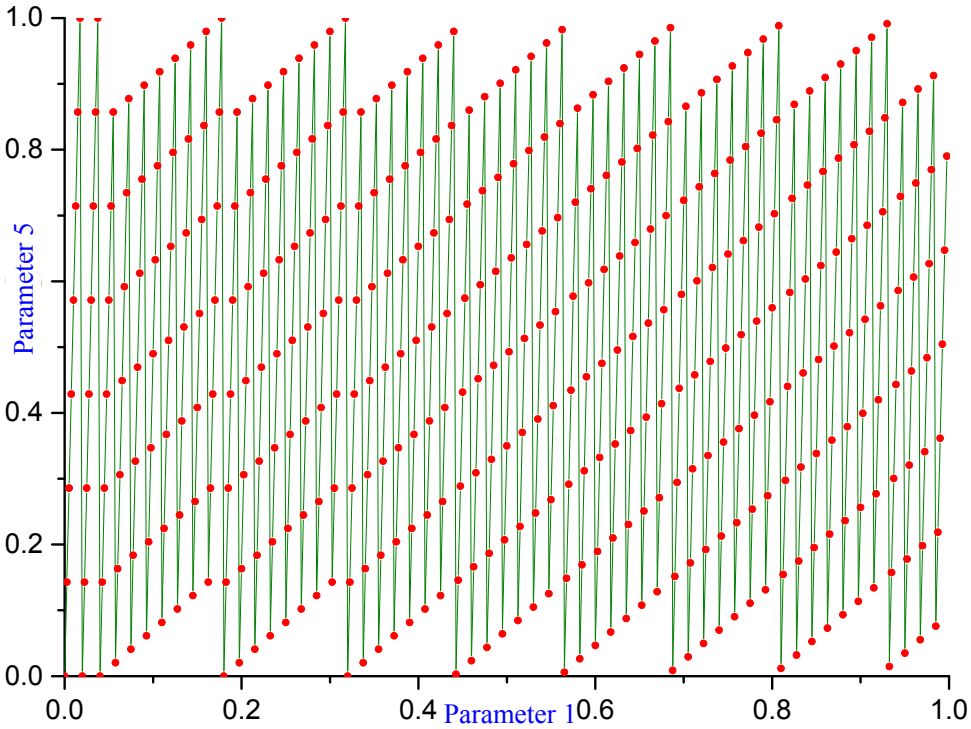

Figure 5-4: Parameter 1 ~ Parameter 5 of 400 samples

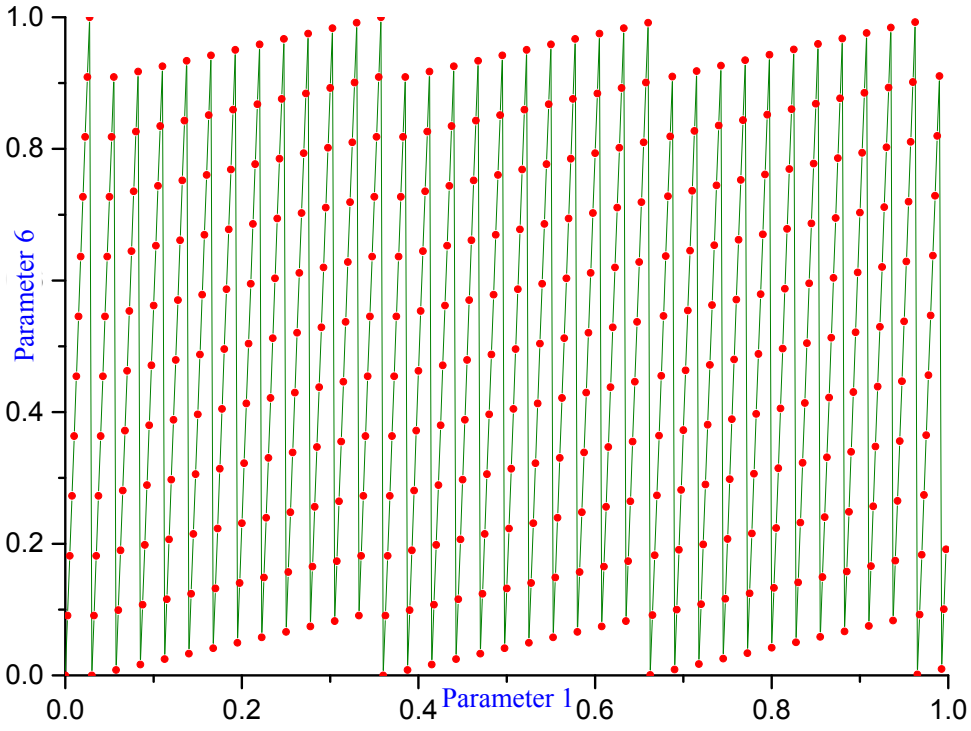

Figure 5-5: Parameter 1 ~ Parameter 6 of 400 samples

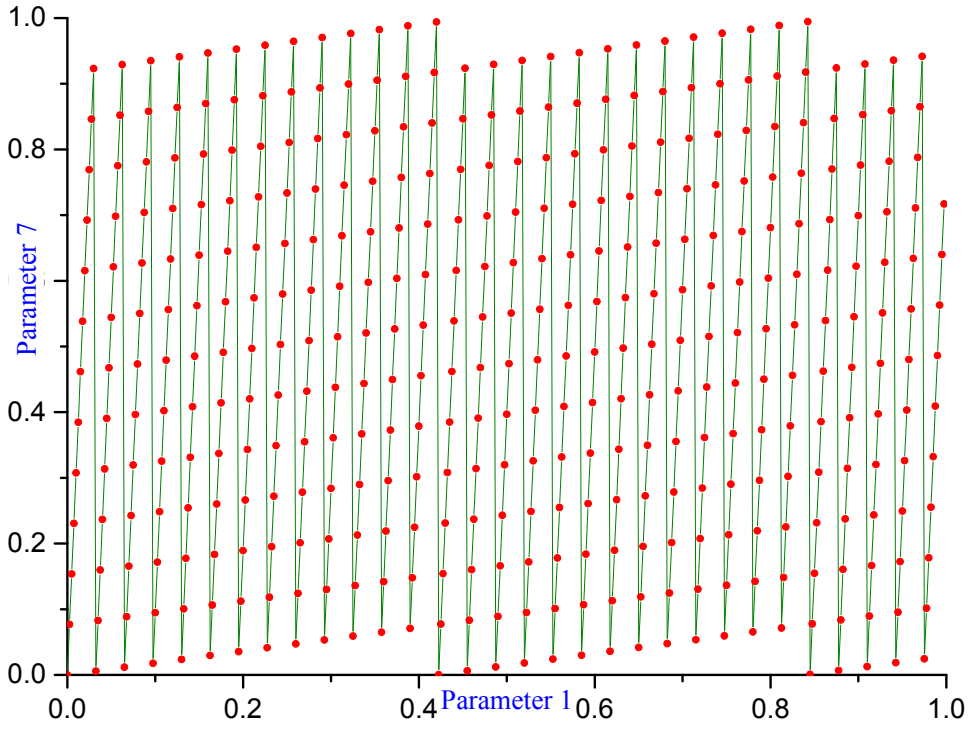

Figure 5-6: Parameter 1 ~ Parameter 7 of 400 samples

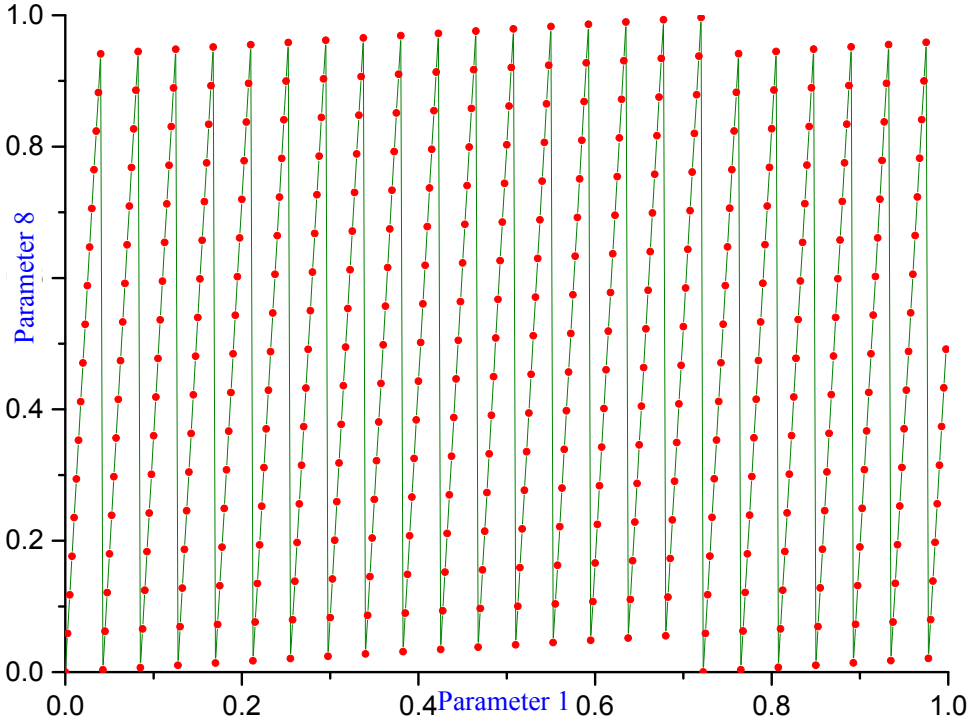

Figure 5-7: Parameter 1 ~ Parameter 8 of 400 samples

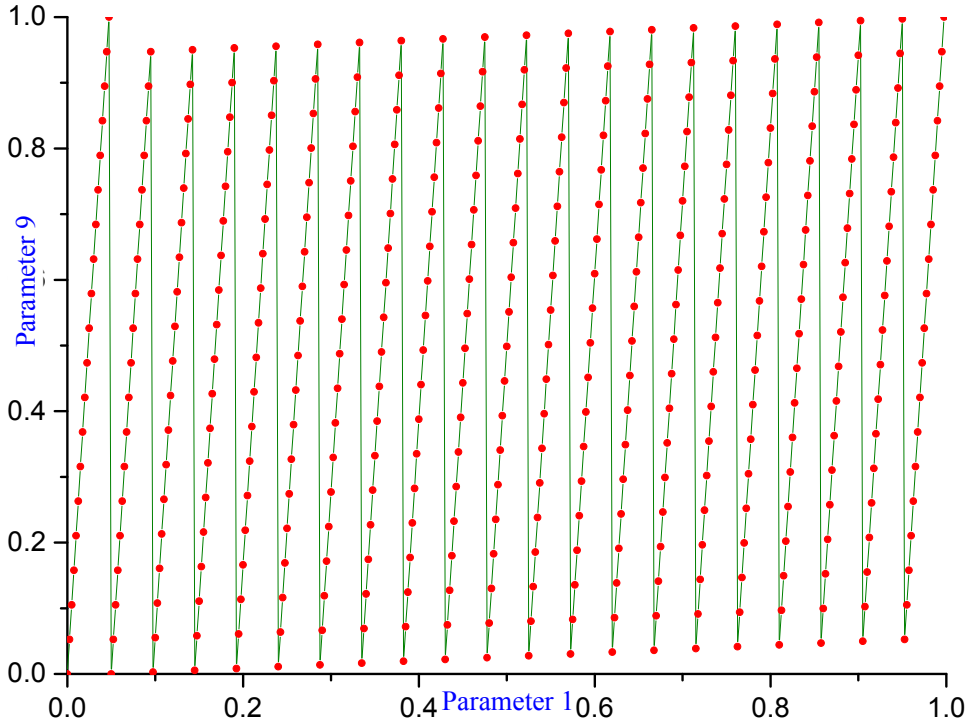

Figure 5-8: Parameter 1 ~ Parameter 9 of 400 samples

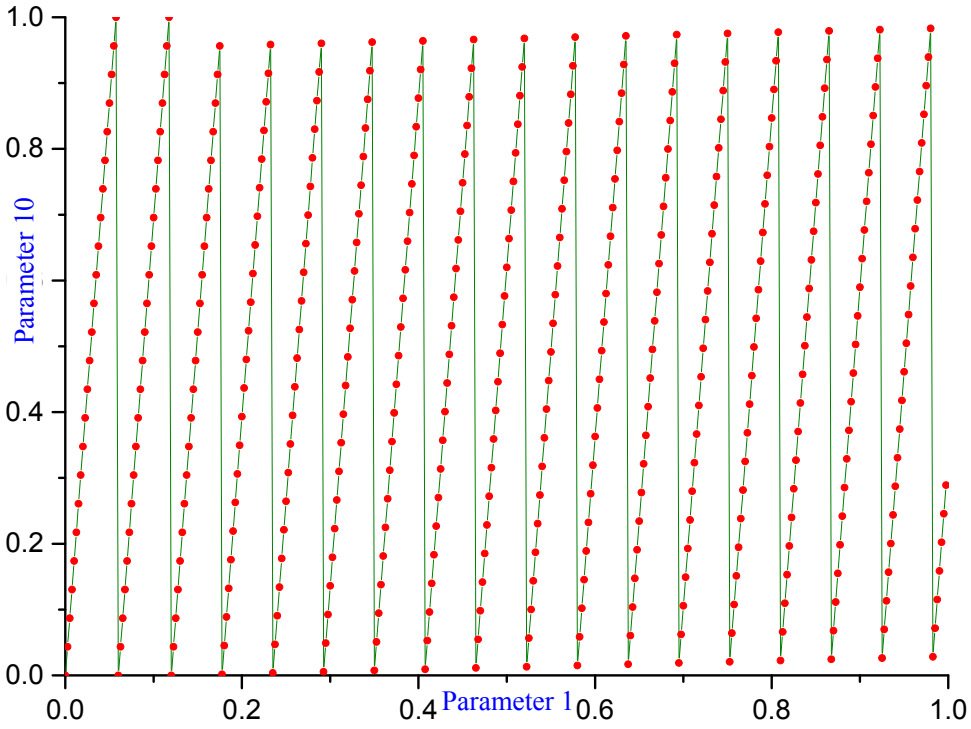

Figure 5-9: Parameter 1 ~ Parameter 10 of 400 samples

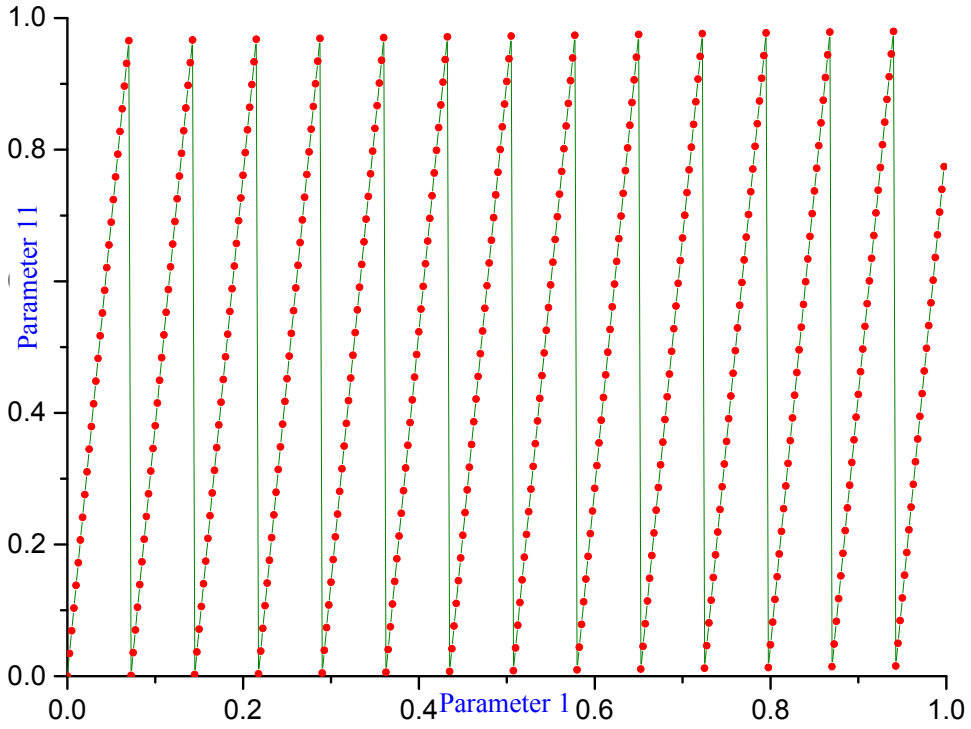

Figure 5-10: Parameter 1 ~ Parameter 11 of 400 samples

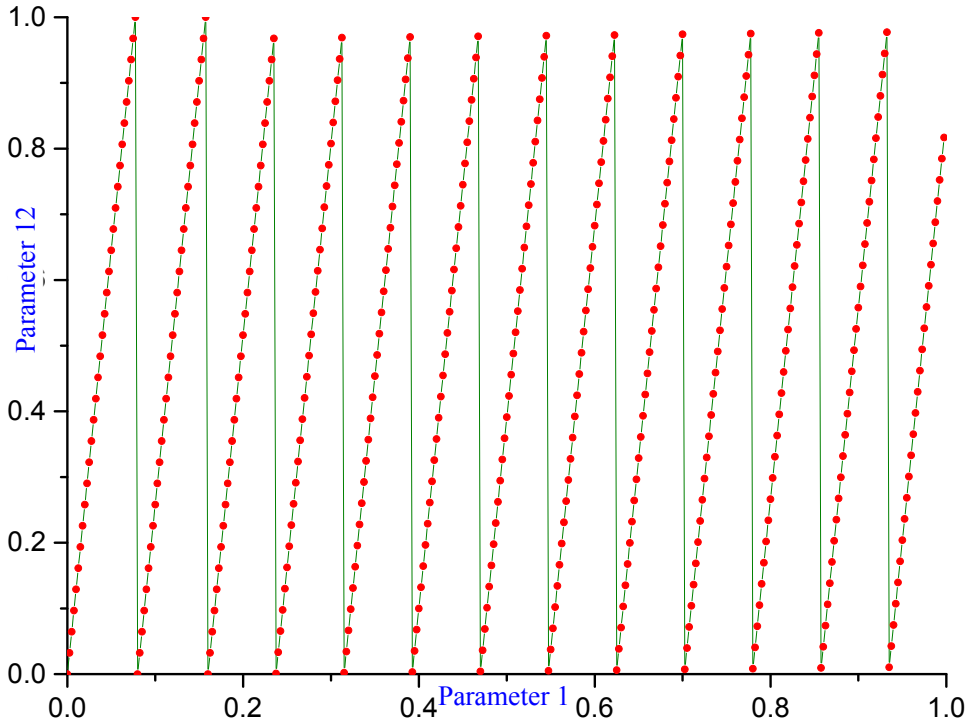

Figure 5-11: Parameter 1 ~ Parameter 12 of 400 samples

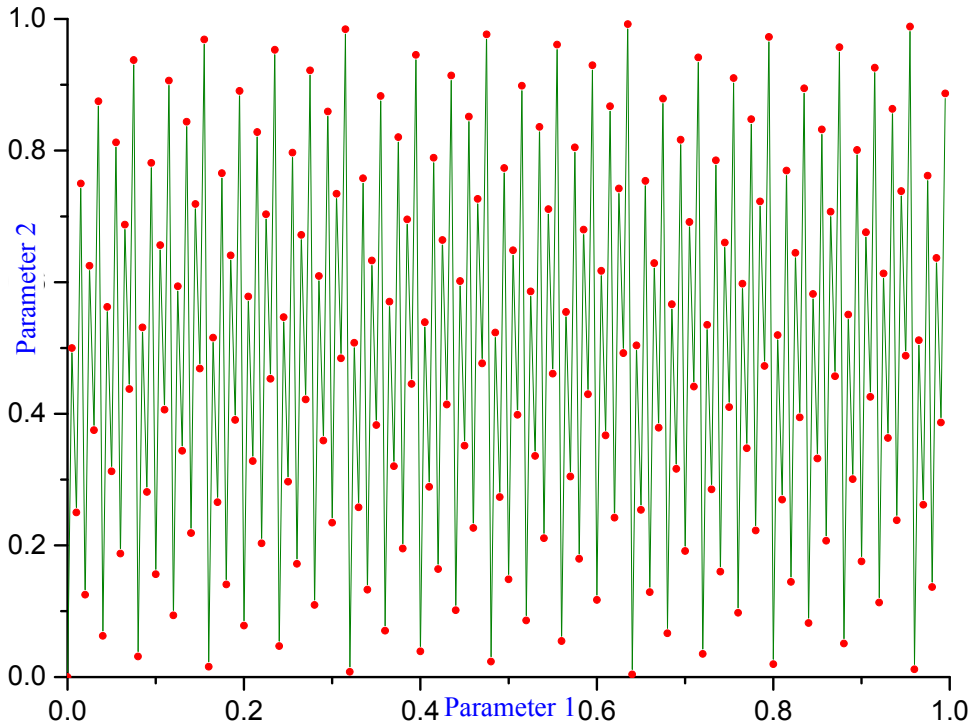

Figure 5-12: Parameter 1 ~ Parameter 2 of 200 samples

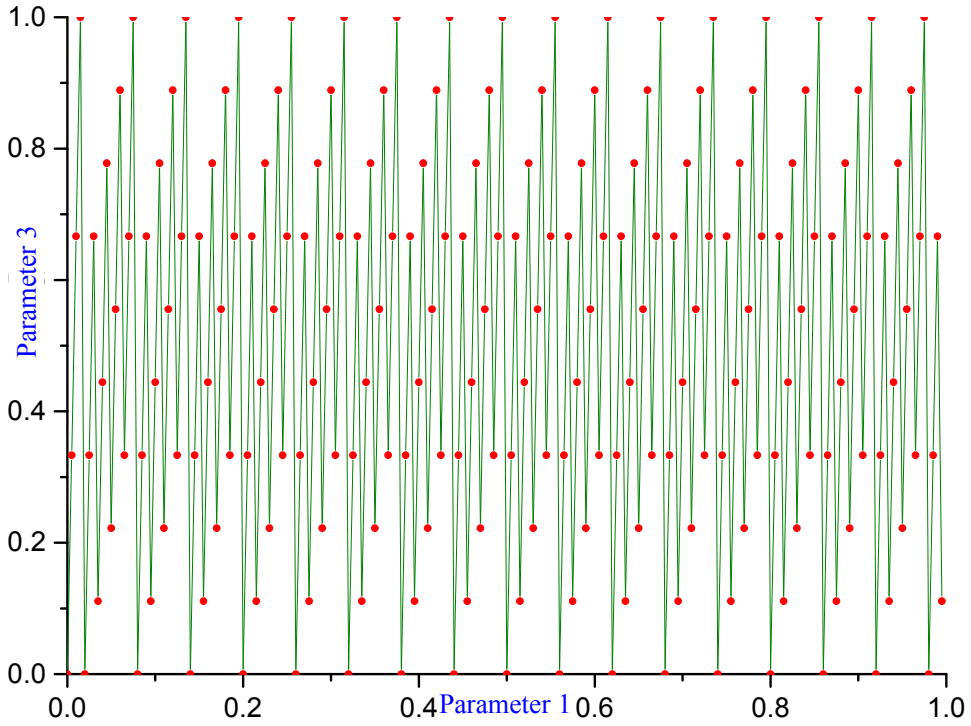

Figure 5-13: Parameter 1 ~ Parameter 3 of 200 samples

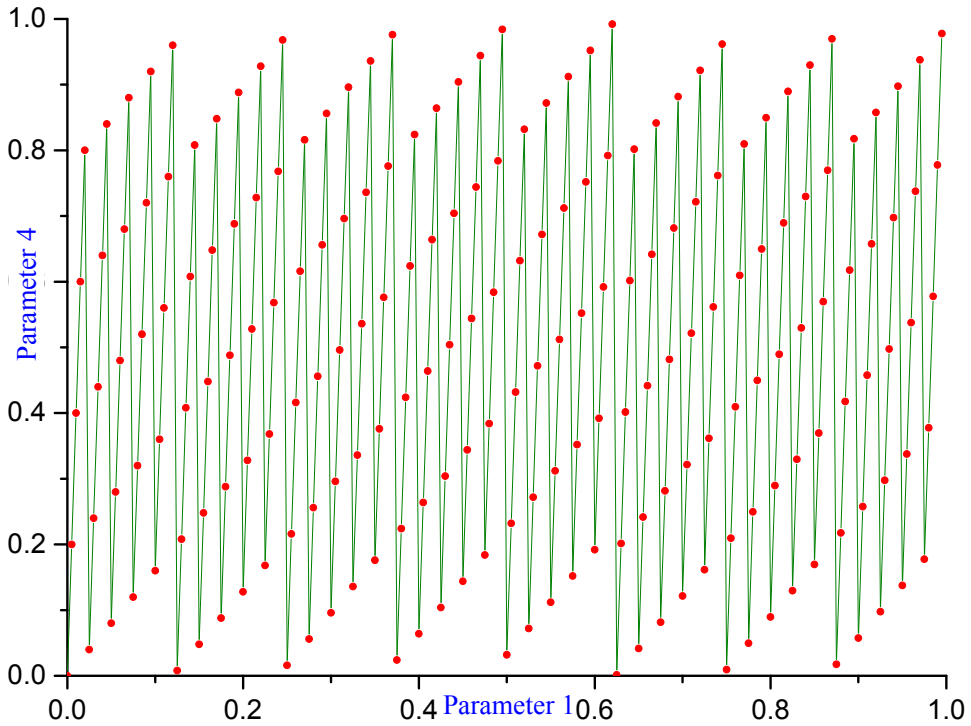

Figure 5-14: Parameter 1 ~ Parameter 4 of 200 samples

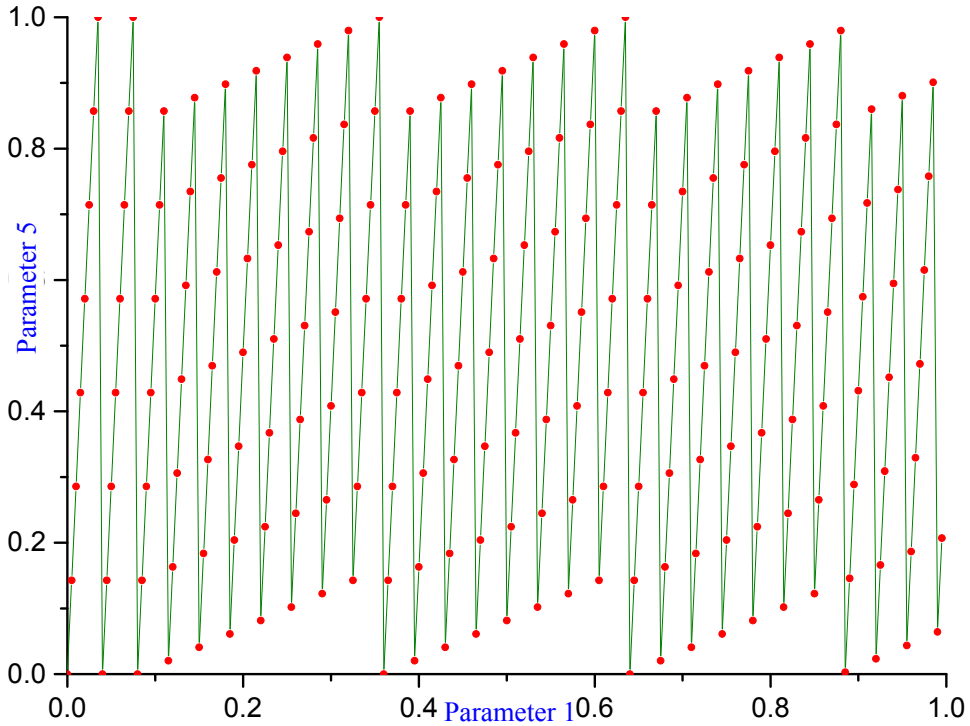

Figure 5-15: Parameter 1 ~ Parameter 5 of 200 samples

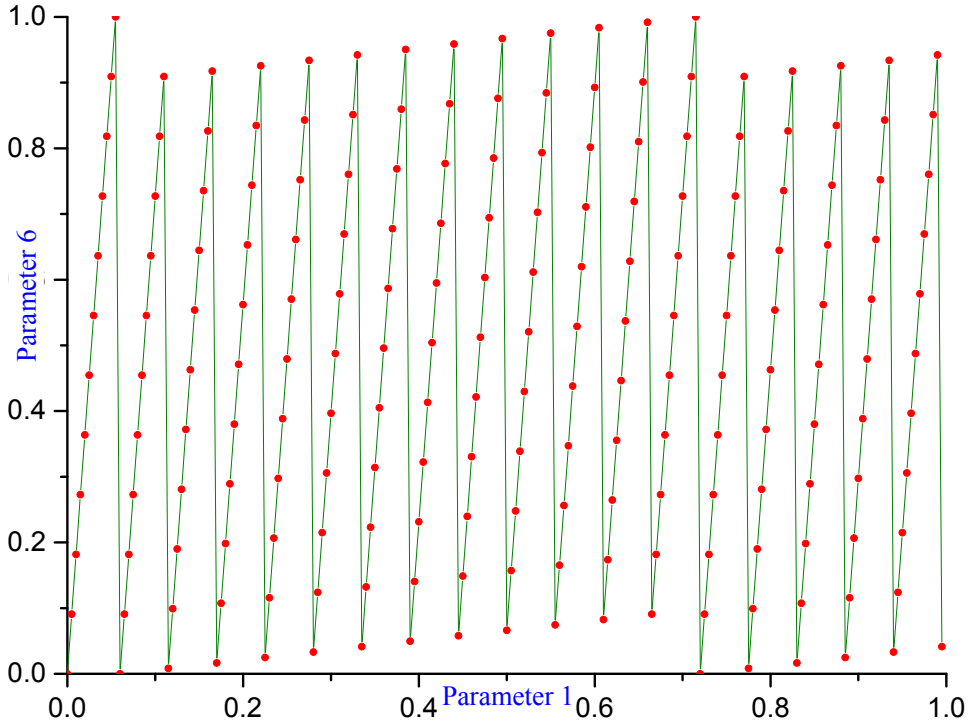

Figure 5-16: Parameter 1 ~ Parameter 6 of 200 samples

Table 5-1: 400 airfoil Transonic simulation result (9 cases)

No.	Case1	Case2	Case3	Case4	Case5	Case6	Case7	Case8	Case9	Average
1	53.52	46.93	39.63	50.59	41.95	34.30	40.62	33.37	27.61	40.95
2	64.13	61.18	54.93	66.21	70.58	62.11	64.57	54.39	43.47	60.17
3	48.56	41.14	34.47	41.08	34.50	28.93	34.00	29.23	24.57	35.16
4	67.08	59.36	46.27	61.13	50.01	38.35	50.54	40.01	32.19	49.44
5	59.66	52.50	45.90	50.64	43.66	37.18	39.47	33.95	29.63	43.62
6	62.73	59.13	53.78	60.65	64.81	69.23	63.83	58.40	46.84	59.93
7	57.98	48.30	39.59	49.93	41.27	33.93	43.93	35.90	29.69	42.28
8	53.75	52.80	27.90	48.04	49.38	53.58	44.37	46.88	45.64	46.93
9	46.80	40.59	27.90	39.52	34.49	30.50	33.35	29.39	26.18	34.30
10	64.55	57.93	49.98	57.98	49.19	41.50	48.73	40.84	33.46	49.35
11	65.31	62.76	55.26	68.77	68.28	56.36	65.69	53.70	42.25	59.82
12	66.34	65.79	61.76	65.61	65.08	63.07	65.44	70.29	64.39	65.31
13	43.30	37.40	32.37	36.70	31.82	27.55	31.31	27.19	23.65	32.37
14	58.00	56.58	59.97	62.70	62.47	63.15	61.42	60.32	56.20	60.09
15	57.08	52.89	47.58	56.03	48.11	41.87	48.16	41.12	35.03	47.54
16	62.48	59.08	52.94	64.61	60.64	51.24	64.32	57.62	52.32	58.36
17	45.11	45.03	44.32	53.42	50.28	42.81	51.62	43.83	36.70	45.90
18	29.72	29.92	28.71	39.36	36.59	39.46	47.95	46.22	47.98	38.43
19	37.30	37.36	35.03	44.23	41.24	36.61	44.03	38.68	33.27	38.64
20	30.56	30.68	31.98	39.97	40.43	40.71	45.16	44.46	43.92	38.65
21	31.25	31.60	31.13	40.57	39.13	35.31	44.59	39.60	33.79	36.33
22	39.34	40.18	40.48	48.58	49.26	49.82	56.54	56.97	54.00	48.35
23	27.55	27.27	28.89	38.08	38.63	40.06	47.28	48.25	48.27	38.25
24	29.75	29.87	30.82	40.25	40.08	40.69	49.48	49.37	48.39	39.85
25	39.62	35.52	31.84	34.65	30.87	29.11	30.06	27.87	26.63	31.80
26	55.67	54.97	52.46	53.68	52.51	50.67	51.27	54.78	62.19	54.25
27	50.13	48.07	44.28	53.48	48.84	42.26	51.97	44.62	38.18	46.87
28	54.93	54.45	52.28	59.15	57.04	52.42	60.44	55.39	49.46	55.06
29	43.30	45.85	43.94	51.04	51.84	51.09	53.46	49.53	44.74	48.31
30	66.38	63.24	56.99	56.32	49.75	41.64	43.69	37.26	31.98	49.69
31	53.01	44.30	37.77	54.43	43.38	34.93	44.20	35.74	29.50	41.92
32	41.37	41.64	43.25	38.02	41.52	47.85	37.51	40.52	38.40	41.12
33	41.94	36.32	32.04	35.14	30.74	27.07	29.65	26.01	22.94	31.32
34	64.50	53.84	42.92	53.75	43.73	35.42	44.26	35.87	29.62	44.88
35	60.00	56.71	50.69	56.98	49.99	42.98	47.89	40.84	34.74	48.98
36	61.38	59.84	55.05	59.58	57.56	53.49	57.39	62.23	64.64	59.02
37	41.11	35.11	30.11	34.95	29.91	25.82	29.87	25.78	22.33	30.56
38	59.29	59.35	59.63	62.44	62.78	63.48	60.74	61.30	58.68	60.85
39	61.51	57.12	49.47	57.64	49.93	42.17	49.96	41.82	34.78	49.38
40	52.33	48.43	46.28	49.04	46.00	42.14	44.45	40.28	34.63	44.84
41	42.32	42.68	43.50	51.17	50.39	45.87	51.91	45.30	37.51	45.63
42	50.56	49.72	51.71	56.63	56.83	57.26	57.49	58.70	57.53	55.16

No.	Case1	Case2	Case3	Case4	Case5	Case6	Case7	Case8	Case9	Average
43	53.28	50.56	45.21	53.71	46.83	39.44	47.44	39.80	32.76	45.45
44	48.60	48.63	48.25	51.51	49.74	49.44	47.38	45.70	44.26	48.17
45	48.14	46.17	40.98	48.39	42.99	37.29	42.76	37.17	32.40	41.81
46	49.38	49.79	50.27	57.62	57.73	54.40	63.50	60.70	61.24	56.07
47	40.94	42.70	42.11	50.29	51.10	50.80	55.34	55.28	54.56	49.24
48	51.23	51.24	52.40	57.89	57.93	55.80	59.80	56.95	54.42	55.30
49	35.89	32.76	31.25	31.71	29.63	28.33	28.35	26.66	25.00	29.95
50	70.26	68.00	63.91	67.07	60.46	52.75	54.95	47.41	39.67	58.28
51	56.73	48.88	39.86	51.05	42.73	35.83	45.90	37.62	31.31	43.32
52	57.86	56.02	51.93	61.31	57.69	50.74	60.25	54.60	47.66	55.34
53	30.06	31.66	30.52	40.85	41.01	41.25	47.42	46.59	43.52	39.21
54	39.21	38.65	38.20	46.75	45.05	44.93	47.01	47.06	47.43	43.81
55	43.79	44.22	43.95	51.44	49.08	45.15	54.75	48.35	41.85	46.95
56	25.72	24.71	23.93	25.69	24.88	23.54	23.83	23.10	22.46	24.21
57	38.88	37.71	38.24	46.49	43.72	38.10	46.50	40.41	34.02	40.45
58	44.74	45.82	47.25	53.19	53.10	51.86	58.81	56.94	53.45	51.68
59	62.99	57.51	50.53	53.56	45.35	38.27	41.50	34.95	29.41	46.01
60	61.37	58.98	54.95	54.54	50.10	42.28	44.68	39.53	32.23	48.74
61	38.43	31.97	26.61	32.65	27.42	22.76	27.57	23.04	19.88	27.81
62	59.61	59.51	62.53	56.98	60.23	55.20	51.67	46.47	38.02	54.47
63	61.91	53.95	42.97	54.03	43.91	35.17	43.67	35.09	28.87	44.40
64	58.27	56.82	46.05	52.04	45.04	36.77	42.38	35.61	29.91	44.76
65	53.69	47.18	41.27	44.42	38.74	33.95	35.60	31.20	27.56	39.29
66	57.28	58.27	57.99	59.97	60.88	67.06	59.81	60.49	51.35	59.23
67	55.11	49.55	41.37	50.39	42.19	34.33	42.49	34.64	28.31	42.04
68	53.47	51.83	52.18	50.54	49.25	48.88	45.62	44.92	44.53	49.02
69	38.75	36.79	33.69	41.67	36.90	32.55	38.35	33.46	29.19	35.71
70	45.19	44.44	43.28	49.40	46.95	43.87	48.86	44.03	39.07	45.01
71	35.18	36.03	34.25	44.54	44.32	44.87	49.30	49.80	50.49	43.20
72	56.90	55.67	54.02	52.85	53.21	54.88	50.67	56.28	57.80	54.70
73	39.72	34.62	30.69	34.14	30.22	27.34	29.62	26.63	24.27	30.80
74	61.15	61.74	62.32	64.38	64.65	62.64	60.34	56.04	49.11	60.26
75	56.90	51.21	44.92	50.57	44.25	38.58	42.71	36.83	32.26	44.25
76	62.10	56.55	48.77	59.79	52.85	45.14	55.62	50.20	44.86	52.88
77	55.53	55.33	52.78	60.32	59.95	56.26	54.65	49.03	41.65	53.95
78	60.66	60.27	60.31	58.57	59.60	62.88	55.55	56.91	53.08	58.65
79	59.28	58.11	52.82	62.33	56.07	47.62	57.11	48.51	39.59	53.50
80	45.33	43.28	42.50	43.98	42.99	41.93	40.03	39.08	38.96	42.01
81	47.20	43.44	38.08	46.43	40.23	33.56	40.97	34.22	28.73	39.21
82	54.33	56.12	51.09	61.91	59.75	52.70	65.19	61.63	51.05	57.09
83	50.48	49.20	49.13	56.00	58.07	53.42	57.10	52.84	46.73	52.55
84	54.04	52.73	54.30	58.43	58.64	58.34	59.85	60.17	60.40	57.43
85	45.31	39.73	34.55	39.82	34.95	30.73	34.29	30.14	27.00	35.17

No.	Case1	Case2	Case3	Case4	Case5	Case6	Case7	Case8	Case9	Average
86	27.64	28.15	27.90	36.58	35.92	35.81	39.68	38.13	37.56	34.15
87	27.61	27.89	27.90	38.15	38.21	39.09	46.50	46.96	45.45	37.53
88	61.78	60.76	27.90	58.93	55.26	45.51	52.04	43.91	35.65	49.08
89	53.98	50.03	27.90	48.24	42.35	36.59	38.58	33.50	28.83	40.00
90	60.95	59.23	27.90	57.76	53.35	48.58	47.95	42.71	36.94	48.37
91	59.43	52.29	27.90	56.46	45.92	36.66	47.20	37.37	29.96	43.69
92	41.42	39.66	27.90	38.34	37.91	37.57	35.16	35.23	36.55	36.64
93	49.64	47.62	27.90	49.78	43.66	37.20	43.04	36.53	30.50	40.65
94	52.23	51.46	27.90	56.25	54.52	51.08	54.32	49.08	43.56	48.93
95	59.21	58.53	27.90	54.10	49.19	42.54	42.27	37.12	32.41	44.81
96	50.99	49.54	27.90	45.70	45.49	46.96	42.90	49.26	53.61	45.82
97	34.17	30.55	27.90	29.41	26.23	23.27	25.17	22.41	19.64	26.53
98	71.22	71.43	27.90	64.80	58.02	48.94	49.84	42.44	35.31	52.21
99	52.57	44.97	27.90	43.69	37.03	31.46	35.48	30.58	26.36	36.67
100	63.39	56.65	47.95	54.45	46.75	38.40	44.27	37.81	31.00	46.74
101	64.87	66.65	61.07	61.45	54.21	44.53	46.22	38.21	31.74	52.11
102	62.76	62.64	62.58	60.04	64.23	64.42	56.97	53.20	44.68	59.06
103	62.27	61.04	54.46	64.73	58.31	48.10	58.85	48.59	39.50	55.09
104	49.47	47.78	46.11	45.18	43.76	43.29	39.88	39.73	40.73	43.99
105	44.36	41.38	36.36	42.62	37.33	32.58	37.54	32.47	28.28	36.99
106	49.31	49.46	48.07	56.54	55.02	50.15	59.28	57.53	59.68	53.90
107	43.06	42.26	42.65	49.76	48.92	50.17	52.38	52.40	49.29	47.88
108	44.28	44.10	44.05	50.20	49.86	49.34	50.59	50.41	51.17	48.22
109	45.43	41.08	36.31	43.74	37.88	32.42	37.92	32.83	28.39	37.33
110	42.31	42.13	42.25	50.59	49.98	49.52	51.90	50.64	49.07	47.60
111	41.99	42.78	43.22	51.21	51.95	49.76	57.39	56.06	56.94	50.14
112	50.80	50.06	50.05	57.26	57.88	57.61	60.58	60.17	59.05	55.94
113	33.70	35.93	35.79	45.03	44.45	43.47	47.14	43.51	38.67	40.85
114	40.16	42.43	42.47	49.92	50.01	49.18	53.45	52.97	52.23	48.09
115	41.99	40.32	41.16	49.02	45.59	43.35	48.58	43.54	37.91	43.49
116	29.36	29.02	28.84	33.81	33.22	31.96	33.98	33.14	31.56	31.65
117	54.11	45.87	37.33	45.02	36.83	29.71	35.34	28.66	23.39	37.36
118	63.98	51.87	41.51	50.75	43.53	34.48	38.99	33.02	28.33	42.94
119	55.76	49.17	41.72	42.59	36.74	31.70	32.94	29.26	25.78	38.41
120	58.74	56.65	54.88	52.42	49.31	44.85	43.08	39.20	34.83	48.22
121	35.09	30.30	26.57	30.32	26.33	22.93	26.22	22.66	19.73	26.68
122	57.07	58.03	61.61	56.12	56.73	51.89	49.35	44.43	37.62	52.54
123	58.11	50.82	43.32	51.00	43.20	35.58	41.64	35.26	29.38	43.15
124	64.43	60.76	55.16	59.28	54.04	45.97	51.84	43.66	35.42	52.28
125	53.68	49.68	44.12	44.37	40.13	35.88	35.73	32.15	28.75	40.50
126	46.86	46.03	45.08	43.39	45.99	54.02	44.19	47.95	43.29	46.31
127	69.70	64.94	59.89	75.84	66.38	51.35	62.14	49.32	38.98	59.84
128	44.68	42.82	41.69	38.71	37.85	38.86	34.04	35.26	37.81	39.08

No.	Case1	Case2	Case3	Case4	Case5	Case6	Case7	Case8	Case9	Average
129	48.54	42.37	36.88	41.35	35.70	31.18	34.17	29.85	26.36	36.27
130	67.47	63.54	54.99	63.38	54.70	45.99	52.33	43.79	36.60	53.64
131	48.61	48.12	45.51	50.27	55.77	55.76	55.47	52.51	44.68	50.74
132	53.52	51.50	50.83	55.29	53.98	52.97	52.37	52.98	56.13	53.29
133	44.91	39.25	32.98	39.02	33.41	29.00	33.61	28.97	25.22	34.04
134	55.45	53.70	52.50	55.10	54.17	56.25	52.31	51.36	49.96	53.42
135	58.91	55.28	48.85	54.92	48.83	41.36	47.00	39.90	33.48	47.61
136	59.49	57.02	54.82	63.05	61.68	57.21	64.20	63.16	67.79	60.93
137	16.02	13.76	13.74	27.07	27.60	27.93	36.09	35.48	34.05	25.75
138	27.62	28.47	28.26	38.03	38.59	38.13	44.00	43.35	42.73	36.58
139	34.46	35.00	35.17	44.37	43.35	40.55	47.94	43.00	37.73	40.17
140	27.63	28.21	28.96	36.79	36.60	35.07	39.18	37.36	35.59	33.93
141	59.49	57.61	52.98	63.62	56.43	46.47	53.95	44.28	36.15	52.33
142	61.58	61.52	59.10	62.84	61.47	58.64	64.15	68.96	61.96	62.25
143	52.45	54.64	53.26	55.76	56.01	56.89	54.17	53.83	50.20	54.13
144	44.82	45.19	41.50	46.83	46.31	45.57	45.02	44.25	44.62	44.90
145	38.13	32.32	29.53	34.20	29.88	26.48	30.19	26.93	24.26	30.21
146	60.13	64.66	60.89	57.89	51.50	42.50	44.20	37.30	31.48	50.06
147	50.62	42.32	35.18	41.56	34.67	28.88	33.25	28.13	24.09	35.41
148	69.37	60.47	49.09	59.96	49.04	38.31	48.32	37.72	31.42	49.30
149	51.48	45.93	40.20	40.94	35.90	31.31	31.86	28.32	24.91	36.76
150	59.95	57.77	55.04	52.60	48.07	42.62	41.82	37.72	33.52	47.68
151	61.72	58.47	47.36	61.50	48.53	38.49	47.02	37.67	30.67	47.94
152	38.73	38.05	38.28	34.62	35.99	40.55	32.68	36.20	36.62	36.86
153	49.84	42.66	36.18	41.40	35.27	29.96	33.56	28.74	25.21	35.87
154	62.74	61.09	55.39	61.39	53.90	44.45	50.09	42.13	33.89	51.67
155	53.56	51.89	49.15	50.43	46.73	41.30	42.57	37.41	32.63	45.07
156	52.40	51.13	49.21	48.79	49.26	53.99	47.23	51.46	49.61	50.34
157	40.58	37.19	33.02	41.70	35.62	29.47	37.18	31.28	25.87	34.66
158	41.46	39.86	40.26	45.25	43.16	42.41	42.76	41.59	41.68	42.05
159	48.41	48.80	48.33	55.16	52.58	48.77	53.66	48.22	41.12	49.45
160	47.11	44.00	41.07	44.70	41.21	39.19	40.04	37.17	34.54	41.00
161	33.35	33.85	34.94	41.97	42.11	40.95	43.90	40.39	34.88	38.48
162	42.89	43.82	42.62	48.79	47.64	47.78	48.34	48.36	49.01	46.58
163	47.97	47.81	45.25	53.48	48.92	42.60	49.36	42.20	34.97	45.84
164	48.08	46.55	46.31	43.26	42.99	44.52	39.05	40.15	40.42	43.48
165	55.57	48.90	43.89	48.20	41.17	35.81	38.28	33.25	29.46	41.62
166	65.27	61.39	54.84	63.47	61.28	67.19	69.00	67.67	54.03	62.68
167	60.21	60.90	61.66	59.25	60.37	56.08	52.45	47.50	40.40	55.42
168	57.35	56.69	55.89	52.80	53.92	57.80	50.29	53.61	52.37	54.52
169	42.83	36.82	32.88	35.73	31.90	28.97	30.61	27.65	25.42	32.53
170	53.36	55.00	53.40	53.68	53.04	52.16	50.98	47.73	43.55	51.44
171	23.16	24.14	22.54	33.98	35.82	37.23	45.01	46.24	44.43	34.73

No.	Case1	Case2	Case3	Case4	Case5	Case6	Case7	Case8	Case9	Average
172	34.50	35.05	34.94	44.09	43.77	42.78	49.41	48.46	48.45	42.38
173	26.71	27.01	26.80	35.88	35.71	34.98	38.85	37.43	35.42	33.20
174	34.98	34.75	35.32	42.43	41.92	41.30	43.26	42.53	41.81	39.81
175	53.91	47.31	40.10	43.86	38.31	31.30	35.53	29.96	25.09	38.37
176	36.16	35.23	35.54	31.96	33.10	37.59	30.14	33.40	33.78	34.10
177	46.16	38.85	32.43	37.82	31.56	26.73	30.40	25.56	21.88	32.38
178	66.85	65.85	55.60	64.26	55.18	43.01	51.40	40.83	32.30	52.81
179	57.54	55.39	51.05	51.37	46.59	40.06	41.01	35.56	30.43	45.45
180	60.32	56.98	54.76	53.24	50.02	45.84	44.31	39.99	34.63	48.90
181	44.61	36.47	30.04	37.17	30.70	25.26	30.62	25.45	21.36	31.30
182	53.33	52.79	54.11	50.29	51.90	53.90	47.10	46.23	40.63	50.03
183	56.42	57.46	52.10	58.48	53.64	44.74	50.30	41.99	33.81	49.88
184	55.65	54.03	52.54	52.82	50.62	47.38	48.21	43.60	36.46	49.04
185	42.22	39.66	38.21	41.30	38.21	35.08	36.34	32.79	29.26	37.01
186	43.12	42.59	41.98	44.33	43.64	44.04	41.89	42.99	45.09	43.30
187	64.09	55.50	45.11	54.52	44.22	36.32	41.01	34.35	29.38	44.94
188	34.62	33.49	32.63	31.14	30.90	31.48	28.70	29.86	32.54	31.71
189	55.83	54.19	49.39	54.46	48.13	41.42	44.97	38.49	32.87	46.64
190	60.03	59.61	59.71	63.47	61.91	57.53	57.99	52.28	45.51	57.56
191	49.52	48.05	47.75	47.47	47.82	50.91	45.48	47.30	45.17	47.72
192	54.34	52.62	50.98	49.27	47.97	48.50	43.98	45.28	48.34	49.03
193	39.67	34.52	30.57	33.83	29.80	26.65	28.86	25.69	23.08	30.30
194	60.26	59.61	59.53	58.52	56.62	53.25	50.71	47.03	41.58	54.12
195	56.71	50.42	44.39	49.61	43.09	37.19	40.92	35.25	30.67	43.14
196	54.19	55.20	52.69	59.43	58.67	54.25	61.05	63.01	64.33	58.09
197	40.62	39.38	38.23	44.87	42.90	41.02	41.61	38.66	35.35	40.29
198	46.39	45.55	42.56	46.90	47.85	46.53	45.13	44.26	44.25	45.49
199	49.55	48.18	46.61	54.87	53.26	47.00	53.66	47.06	40.48	48.96
200	38.58	38.85	38.25	40.28	38.30	37.73	36.85	35.09	34.23	37.57
201	41.82	41.14	39.96	50.52	46.29	41.83	49.72	42.01	35.48	43.20
202	48.72	49.65	49.44	55.42	57.26	56.09	60.00	62.56	61.74	55.65
203	40.65	38.63	38.15	47.74	57.26	46.60	48.40	46.27	44.95	45.40
204	58.55	57.70	55.70	51.42	48.10	41.04	41.97	36.29	30.56	46.81
205	42.98	37.04	31.93	36.07	31.27	26.62	30.21	26.07	22.22	31.60
206	47.11	45.52	44.58	43.56	43.77	46.26	40.64	43.44	43.89	44.31
207	59.59	60.12	58.79	63.24	59.34	48.89	55.15	45.53	35.99	54.07
208	55.65	53.93	53.13	53.47	52.44	50.80	49.27	46.14	39.28	50.46
209	36.39	35.15	33.43	37.62	35.14	31.74	33.77	30.54	27.11	33.43
210	54.51	53.44	51.27	49.15	45.83	40.83	39.67	35.78	31.59	44.67
211	58.59	48.46	38.73	46.07	37.37	30.86	35.42	29.87	25.28	38.96
212	37.10	37.87	41.59	35.18	38.30	39.59	33.61	33.84	31.05	36.46
213	53.00	46.76	39.50	43.32	37.17	31.19	33.95	29.26	25.70	37.76
214	65.23	63.08	56.32	58.12	50.88	42.71	46.20	39.07	32.60	50.47

No.	Case1	Case2	Case3	Case4	Case5	Case6	Case7	Case8	Case9	Average
215	53.60	51.21	47.14	45.69	42.07	37.54	36.66	32.95	29.07	41.77
216	46.57	45.87	46.84	43.51	47.19	53.90	43.78	45.98	41.45	46.12
217	39.91	33.74	29.49	33.19	28.80	25.11	28.11	24.71	21.63	29.41
218	53.01	54.03	54.96	50.60	50.25	46.68	43.45	40.08	34.79	47.54
219	57.55	50.59	44.55	49.09	41.58	35.53	38.82	33.65	28.77	42.23
220	65.64	60.61	57.71	58.63	53.89	47.72	49.39	43.91	37.04	52.72
221	52.18	52.96	53.54	50.58	50.58	48.18	44.79	41.45	36.18	47.83
222	26.77	26.24	25.38	31.97	30.58	30.03	32.60	31.13	30.86	29.51
223	36.84	36.26	37.08	45.55	45.93	45.72	49.62	48.22	44.55	43.31
224	30.09	29.14	27.59	31.67	30.12	28.56	29.57	28.13	27.12	29.11
225	38.34	36.49	33.16	39.35	34.92	30.51	34.72	30.35	26.70	33.84
226	40.39	39.97	41.46	47.35	48.56	47.62	52.40	53.51	57.21	47.61
227	23.17	24.66	24.24	33.33	33.26	32.88	39.00	38.61	38.57	31.97
228	32.91	34.84	33.00	41.52	39.90	40.59	42.74	41.29	40.65	38.61
229	38.88	36.30	34.38	42.01	36.67	31.62	38.40	33.11	28.73	35.57
230	32.59	33.27	34.60	42.28	39.77	38.80	42.91	40.86	39.89	38.33
231	31.62	31.81	31.96	42.30	40.78	43.46	49.37	50.36	52.38	41.56
232	40.48	42.39	41.05	51.19	46.22	49.40	54.28	52.79	51.61	47.71
233	39.28	33.88	29.16	30.32	26.68	23.79	24.84	22.62	20.41	27.89
234	55.47	50.43	43.00	43.13	36.79	33.64	33.57	30.49	26.21	39.19
235	47.88	41.54	35.71	38.68	33.65	29.32	31.08	27.18	23.87	34.32
236	34.66	36.04	41.33	33.37	37.77	38.25	32.69	32.39	29.26	35.08
237	53.22	44.26	36.39	40.46	33.75	28.54	31.27	26.93	23.52	35.37
238	68.07	63.45	51.19	55.13	46.96	38.64	41.79	36.72	30.14	48.01
239	51.17	50.72	49.33	45.95	43.61	39.49	37.91	34.29	30.69	42.57
240	53.50	50.17	49.10	46.75	44.67	43.09	39.52	37.60	34.45	44.32
241	39.90	33.80	28.77	33.60	28.82	24.56	28.30	24.36	21.16	29.25
242	50.36	50.88	51.80	48.94	50.18	49.95	44.93	43.19	38.31	47.62
243	59.45	54.95	46.92	52.59	44.80	37.62	42.29	35.65	29.83	44.90
244	62.18	61.32	60.05	60.64	56.29	49.98	51.87	45.81	38.37	54.06
245	47.49	45.02	42.02	41.22	38.07	34.73	34.19	31.06	27.90	37.97
246	45.74	45.01	44.99	42.40	43.60	46.85	40.43	42.82	42.04	43.76
247	61.75	63.05	59.79	62.49	57.06	47.60	51.70	43.31	35.74	53.61
248	31.63	29.67	29.44	30.08	29.02	27.90	27.53	26.74	26.70	28.75
249	43.34	39.24	36.63	41.78	37.38	33.10	36.19	31.71	27.53	36.32
250	49.74	49.31	47.41	50.00	46.91	42.93	44.27	40.34	35.19	45.12
251	37.78	39.38	36.73	43.07	41.03	43.68	41.69	42.18	43.18	40.97
252	48.21	46.20	43.75	44.93	44.61	44.56	42.16	41.63	42.72	44.31
253	50.66	45.69	41.72	51.36	43.88	36.91	44.36	36.85	30.46	42.43
254	42.38	44.55	41.18	44.78	43.50	41.67	40.97	38.93	38.65	41.85
255	47.17	47.12	47.21	52.00	53.18	48.50	52.20	48.20	42.39	48.66
256	50.65	49.12	47.12	48.36	46.58	43.74	43.48	42.59	42.37	46.00
257	44.28	42.63	42.32	45.61	42.81	39.39	39.77	35.65	31.05	40.39

No.	Case1	Case2	Case3	Case4	Case5	Case6	Case7	Case8	Case9	Average
258	50.02	48.89	48.19	49.41	49.24	49.94	46.57	46.66	45.23	48.24
259	58.28	56.05	50.83	57.66	51.00	43.81	48.20	41.23	34.53	49.07
260	42.69	41.34	39.92	39.76	38.19	37.42	35.32	34.78	35.02	38.27
261	37.99	36.36	34.53	46.39	46.78	43.93	49.43	43.90	36.80	41.79
262	64.60	69.19	60.73	63.09	55.32	44.24	48.71	40.38	32.68	53.21
263	53.83	52.85	48.74	46.37	42.19	36.73	36.49	32.15	27.91	41.92
264	53.70	52.83	53.22	48.04	47.28	44.70	40.95	38.44	33.80	45.89
265	36.04	32.50	29.28	30.90	27.93	24.85	26.59	23.83	21.23	28.13
266	50.08	52.68	57.49	49.10	50.40	45.36	42.83	38.41	32.77	46.57
267	62.91	53.42	42.93	49.95	40.94	33.45	37.79	31.66	26.47	42.17
268	65.09	60.58	46.99	54.81	44.59	35.35	41.00	34.01	28.04	45.61
269	46.52	44.05	41.09	39.74	36.37	32.37	32.16	28.78	25.44	36.28
270	51.06	48.84	47.34	43.83	41.76	38.57	36.71	33.89	30.13	41.35
271	65.60	65.90	54.27	61.16	50.80	39.70	45.65	36.65	29.64	49.93
272	37.95	36.34	36.14	33.14	33.11	34.95	30.04	31.17	32.04	33.87
273	45.80	41.78	36.72	41.31	35.95	30.83	34.23	29.39	25.42	35.71
274	46.20	46.49	44.98	50.18	47.41	42.95	45.25	40.79	35.33	44.40
275	36.20	35.95	34.38	38.53	36.11	33.35	34.80	32.14	29.08	34.51
276	33.91	33.64	33.40	37.44	35.68	35.29	35.41	35.21	36.14	35.12
277	32.79	32.35	29.35	38.28	34.83	29.90	38.08	32.23	26.88	32.74
278	29.07	28.84	28.33	34.16	33.32	32.35	34.26	33.19	32.95	31.83
279	60.13	58.82	53.27	54.30	49.09	41.81	43.08	37.91	32.29	47.86
280	60.96	61.52	62.29	59.49	58.68	54.67	53.36	48.22	41.99	55.69
281	44.99	44.53	44.39	42.19	39.88	36.12	35.46	31.62	27.55	38.52
282	48.96	47.83	47.58	45.30	45.98	49.37	42.65	44.11	42.11	45.99
283	62.83	62.63	60.19	64.49	58.40	50.00	53.74	45.49	37.57	55.04
284	40.00	38.47	36.48	35.44	34.19	33.70	31.47	31.47	32.41	34.85
285	58.14	54.49	50.32	53.81	47.82	41.74	43.55	37.87	32.76	46.72
286	58.35	56.84	53.69	55.12	54.72	54.96	52.81	56.71	61.32	56.06
287	41.92	40.36	39.62	41.04	40.77	40.34	39.27	39.12	38.70	40.13
288	47.82	48.02	42.35	43.11	42.78	42.18	39.51	39.53	40.73	42.89
289	40.73	35.53	31.21	34.86	30.81	27.29	30.09	26.54	23.83	31.21
290	16.81	16.43	16.23	27.30	26.53	25.88	33.03	31.41	30.23	24.87
291	61.26	53.34	42.92	51.52	41.40	32.75	38.60	31.03	25.49	42.03
292	60.93	60.20	60.79	59.17	56.41	45.62	49.93	41.80	33.46	52.04
293	44.02	42.57	40.08	39.05	36.06	32.06	31.96	28.56	25.00	35.49
294	49.27	47.75	46.97	43.67	42.21	39.91	37.06	34.83	31.26	41.44
295	53.96	49.01	42.88	45.06	39.47	34.03	36.47	31.42	26.62	39.88
296	34.51	33.06	32.39	30.59	30.21	31.58	27.74	28.93	30.92	31.10
297	52.43	47.01	40.42	45.22	38.35	32.09	35.58	30.04	25.45	38.51
298	60.93	60.70	58.15	58.56	54.77	46.37	49.15	42.19	34.20	51.67
299	49.61	48.01	45.75	44.93	42.22	38.84	37.84	34.44	30.49	41.35
300	45.60	42.67	39.11	41.82	38.44	36.16	35.80	33.60	31.56	38.31

No.	Case1	Case2	Case3	Case4	Case5	Case6	Case7	Case8	Case9	Average
301	47.48	44.39	36.15	47.47	39.39	31.46	40.00	32.41	26.17	38.32
302	40.08	41.56	45.81	39.22	43.00	43.79	37.92	37.02	32.95	40.15
303	65.19	61.46	52.17	54.94	47.01	38.76	40.79	34.55	29.94	47.20
304	59.91	58.09	61.25	57.77	59.41	56.75	52.60	49.36	42.21	55.26
305	44.16	41.22	37.62	37.62	33.48	29.70	29.97	26.99	24.29	33.89
306	46.53	48.64	52.77	46.00	47.93	43.81	40.96	37.09	31.78	43.95
307	56.89	56.05	50.74	55.84	48.57	40.34	44.85	37.36	31.19	46.87
308	34.27	32.66	31.83	30.93	30.38	30.81	28.27	28.94	30.30	30.93
309	51.23	47.51	42.62	45.19	40.31	34.91	37.08	32.56	28.14	39.95
310	57.01	56.87	54.53	54.50	51.53	46.60	46.37	41.38	36.37	49.47
311	39.56	38.89	38.78	39.09	38.96	40.31	37.88	38.48	38.36	38.92
312	43.45	41.91	40.65	39.52	38.39	38.94	35.98	36.65	39.99	39.50
313	41.45	38.02	33.37	40.53	35.19	30.16	35.52	30.34	25.95	34.50
314	37.61	36.67	34.98	39.19	38.17	37.47	37.48	36.34	35.53	37.05
315	45.06	44.57	45.19	49.37	45.84	42.03	45.30	40.53	35.18	43.67
316	46.57	47.14	45.25	50.52	49.32	49.66	48.89	49.25	51.29	48.65
317	29.48	26.90	27.01	32.66	31.99	30.79	32.24	31.90	30.77	30.41
318	32.22	31.81	29.61	37.19	35.77	33.43	34.95	33.67	32.84	33.50
319	39.75	38.24	36.91	48.92	48.05	45.08	49.48	47.12	44.16	44.19
320	36.78	34.21	32.76	31.31	29.84	29.31	27.01	26.19	25.48	30.32
321	47.80	39.86	32.85	37.28	30.92	25.75	29.14	24.53	20.82	32.10
322	66.24	62.02	51.03	56.21	46.56	36.63	42.01	34.33	27.73	46.97
323	51.54	48.91	45.07	43.63	39.33	33.96	34.57	30.14	26.07	39.25
324	48.58	45.40	43.50	43.31	41.24	39.88	37.70	35.97	33.63	41.02
325	37.98	34.10	30.16	31.79	28.29	25.92	27.35	24.06	21.35	29.00
326	40.30	41.00	44.85	39.03	42.87	43.62	37.93	36.89	32.74	39.91
327	63.61	60.50	49.96	53.77	45.28	36.63	40.17	33.46	28.38	45.75
328	59.80	61.18	63.81	56.70	57.33	50.20	49.12	44.68	36.54	53.26
329	42.65	39.64	36.43	35.68	32.27	28.71	28.73	25.75	22.93	32.53
330	47.91	47.17	46.54	42.69	40.75	37.82	35.73	32.89	29.41	40.10
331	64.40	60.77	49.21	55.39	46.02	36.97	40.87	33.82	28.19	46.18
332	32.63	31.47	30.89	29.26	28.98	30.25	26.84	28.16	30.28	29.86
333	55.92	51.96	45.78	47.62	41.55	35.37	37.34	32.11	27.49	41.68
334	59.31	59.13	59.41	56.02	53.72	48.08	47.59	41.90	36.18	51.26
335	47.81	46.57	44.26	42.54	40.29	37.62	35.77	33.11	29.89	39.76
336	41.48	40.51	39.93	37.18	37.54	40.76	34.76	38.23	41.00	39.04
337	41.94	35.62	30.42	34.76	30.08	26.17	29.21	25.39	22.25	30.65
338	48.13	47.04	47.53	45.02	45.01	44.25	40.16	38.72	35.36	43.47
339	50.49	46.69	45.78	49.12	45.04	38.97	42.39	36.97	32.20	43.07
340	51.66	50.14	50.92	54.02	51.43	48.32	48.59	44.13	40.44	48.85
341	13.22	12.91	12.69	20.93	20.39	20.06	24.40	23.91	23.85	19.15
342	22.77	22.71	21.80	27.45	26.43	25.91	28.05	27.18	27.04	25.48
343	25.92	25.71	26.67	34.66	34.95	34.97	40.08	39.33	37.90	33.36

No.	Case1	Case2	Case3	Case4	Case5	Case6	Case7	Case8	Case9	Average
344	22.68	21.89	20.44	26.32	24.74	23.11	25.64	24.02	22.75	23.51
345	28.83	29.24	27.29	35.81	33.45	30.45	35.14	31.46	27.94	31.07
346	24.46	23.92	22.64	34.40	30.32	32.58	40.32	39.29	39.56	31.94
347	14.08	13.74	14.40	24.37	24.03	24.06	29.62	28.77	28.16	22.36
348	47.05	45.66	44.39	43.57	42.62	42.83	39.69	40.59	42.33	43.19
349	38.41	32.88	28.51	31.09	27.22	23.50	26.05	22.56	19.58	27.75
350	44.61	43.37	39.80	37.25	34.47	30.94	30.17	27.67	24.87	34.79
351	64.14	51.45	41.05	45.40	37.55	31.95	34.05	29.66	25.31	40.06
352	54.42	55.70	61.89	53.60	54.16	46.21	46.57	40.12	33.68	49.60
353	42.36	38.75	34.33	34.22	30.43	26.40	27.04	23.93	21.22	30.96
354	48.40	47.91	46.13	42.61	40.35	36.01	34.68	31.49	27.77	39.48
355	48.70	43.06	37.12	39.43	34.11	29.50	31.48	27.56	24.19	35.01
356	31.77	31.83	33.83	29.35	31.80	35.12	28.78	30.57	29.26	31.37
357	54.21	46.31	38.11	41.54	34.89	29.42	31.71	27.20	23.64	36.34
358	54.93	54.69	56.34	54.17	54.07	50.43	48.19	44.15	37.67	50.52
359	43.50	42.55	42.04	40.03	38.62	36.88	34.73	32.61	29.72	37.85
360	47.47	45.66	43.57	43.34	41.23	39.86	37.78	36.04	34.52	41.05
361	46.98	40.25	33.59	40.75	33.67	28.04	33.23	27.79	23.49	34.20
362	42.34	40.93	40.08	39.50	39.38	40.84	36.72	37.47	37.01	39.36
363	54.59	53.48	50.30	51.34	46.73	39.93	42.83	36.72	30.89	45.20
364	55.54	53.35	51.72	51.64	48.80	45.36	44.55	40.97	35.19	47.46
365	28.69	27.37	26.58	29.17	27.46	26.50	27.24	25.72	24.23	27.00
366	31.62	30.67	28.93	31.20	29.97	29.38	28.97	28.97	30.24	29.99
367	36.83	35.54	36.95	42.71	42.13	42.35	43.65	42.31	39.96	40.27
368	26.89	24.64	24.08	26.34	24.41	23.73	24.12	22.87	22.21	24.36
369	34.04	33.10	31.52	37.28	33.86	30.18	33.74	29.92	26.46	32.23
370	41.84	42.11	41.52	45.73	43.59	40.47	41.86	38.23	35.10	41.16
371	44.33	44.39	45.78	42.79	42.22	38.64	36.83	33.21	29.12	39.70
372	42.35	41.81	42.73	39.25	41.14	44.82	38.22	40.27	38.20	40.98
373	48.26	42.41	36.47	40.31	34.44	30.04	32.94	28.70	25.35	35.44
374	44.12	42.86	43.84	40.21	40.35	40.85	36.81	36.26	34.97	40.03
375	47.33	46.31	45.33	50.51	48.19	44.43	46.21	42.03	37.38	45.30
376	43.73	42.51	41.04	43.09	41.71	40.29	39.42	38.98	38.91	41.08
377	32.06	31.43	30.23	34.50	33.76	33.09	33.55	32.49	31.17	32.48
378	40.75	41.29	43.20	38.15	39.13	37.86	34.12	32.66	29.48	37.40
379	55.35	50.39	43.37	45.61	39.26	33.16	35.31	30.17	25.36	39.78
380	34.07	32.78	32.45	29.95	29.65	29.94	26.69	26.63	26.20	29.82
381	54.43	55.63	50.47	50.15	44.03	36.59	38.85	32.62	27.37	43.35
382	54.65	55.85	58.93	51.92	51.54	44.35	44.19	38.73	32.02	48.02
383	42.63	42.68	43.57	38.99	38.68	36.23	33.77	31.41	27.82	37.31
384	42.90	40.33	39.96	36.82	36.22	35.84	32.23	31.50	29.16	36.11
385	35.65	31.99	28.51	30.30	26.96	23.84	25.78	22.78	20.00	27.31
386	44.09	44.37	46.89	42.08	44.07	42.50	38.64	36.33	31.33	41.14

No.	Case1	Case2	Case3	Case4	Case5	Case6	Case7	Case8	Case9	Average
387	59.12	51.87	42.44	47.69	39.48	31.66	35.85	29.70	24.53	40.26
388	60.84	59.06	58.91	56.01	53.98	46.07	47.69	41.44	33.56	50.84
389	40.22	38.54	37.71	36.12	34.22	31.73	30.87	28.31	25.40	33.68
390	46.47	44.09	42.49	40.03	38.61	37.19	34.50	32.84	30.35	38.51
391	46.82	47.00	50.58	51.01	51.46	47.46	46.73	41.54	34.68	46.36
392	19.07	17.76	16.76	20.41	19.35	18.37	19.90	19.11	18.59	18.81
393	26.79	26.56	25.72	32.35	30.50	28.42	32.30	29.03	25.66	28.59
394	54.33	54.01	52.53	51.80	48.83	43.46	43.21	38.50	33.53	46.69
395	42.12	40.68	38.53	38.72	36.49	34.17	33.40	30.74	28.00	35.87
396	37.78	36.65	35.63	34.64	34.28	35.60	32.12	34.55	38.61	35.54
397	53.70	47.26	40.83	46.62	39.62	33.07	37.24	31.36	26.77	39.61
398	38.57	37.29	36.50	35.77	35.42	36.10	32.94	33.68	33.99	35.58
399	53.80	52.81	51.30	50.89	47.49	42.92	42.86	38.34	33.56	46.00
400	58.29	54.73	54.55	53.75	52.49	50.48	47.16	44.50	40.55	50.72

Table 5-2: Transonic airfoil optimization sample points of Case 1

No	Par.1	Par.2	Par.3	Par.4	Par.5	Par.6	Par.7	Par.8	Par.9	Par.10	Par.11	Par.12	CFD CD/CL	Surrogate CD/CD	Deviation
1	0.055	0.709	0.483	0.491	0.469	0.476	0.572	0.428	0.421	0.428	0.403	0.406	0.0153	0.0105	-31.31%
2	0.333	0.653	0.641	0.616	0.525	0.663	0.870	0.241	0.547	0.284	0.601	0.368	0.0158	0.0132	-16.97%
3	0.286	0.694	0.630	0.300	0.212	0.513	0.522	0.668	0.390	0.509	0.411	0.163	0.0154	0.0132	-14.46%
4	0.072	0.646	0.345	0.337	0.400	0.226	0.663	0.267	0.225	0.218	0.368	0.095	0.0156	0.0138	-11.80%
5	0.391	0.720	0.761	0.581	0.759	0.440	0.262	0.556	0.539	0.256	0.651	0.402	0.0162	0.0139	-14.14%
6	0.230	0.619	0.558	0.269	0.566	0.867	0.936	0.644	0.517	0.444	0.554	0.265	0.0152	0.0140	-7.97%
7	0.279	0.731	0.741	0.283	0.302	0.866	0.679	0.759	0.639	0.656	0.483	0.396	0.0154	0.0144	-6.54%
8	0.388	0.769	0.809	0.588	0.901	0.150	0.662	0.527	0.816	0.397	0.592	0.661	0.0160	0.0151	-5.85%
9	0.145	0.647	0.437	0.434	0.302	0.819	0.693	0.327	0.485	0.384	0.350	0.338	0.0157	0.0146	-6.93%
10	0.036	0.659	0.458	0.616	0.673	0.335	0.304	0.706	0.382	0.644	0.532	0.350	0.0159	0.0146	-8.06%
11	0.245	0.728	0.677	0.366	0.664	0.202	0.561	0.679	0.471	0.588	0.531	0.421	0.0154	0.0148	-4.00%
12	0.161	0.741	0.571	0.491	0.178	0.566	0.553	0.495	0.242	0.395	0.426	0.438	0.0154	0.0151	-1.76%

Table 5-3: Transonic airfoil optimization sample points of Case 2

No.	Par.1	Par.2	Par.3	Par.4	Par.5	Par.6	Par.7	Par.8	Par.9	Par.10	Par.11	Par.12	CFD CD/CL	Surrogate CD/CD	Deviation
1	0.828	0.717	0.929	0.440	0.832	0.531	0.345	0.494	0.613	0.348	0.594	0.461	0.0175	0.0155	-11.51%
2	0.806	0.688	0.947	0.254	0.833	0.775	0.392	0.429	0.457	0.328	0.560	0.319	0.0170	0.0167	-1.71%
3	0.828	0.709	0.908	0.122	0.833	0.637	0.398	0.796	0.547	0.529	0.496	0.320	0.0174	0.0174	0.00%
4	0.828	0.674	0.910	0.286	0.833	0.544	0.398	0.577	0.586	0.482	0.523	0.319	0.0175	0.0172	-1.98%
5	0.814	0.789	0.994	0.131	0.824	0.797	0.266	0.807	0.506	0.460	0.488	0.349	0.0172	0.0174	1.05%
6	0.828	0.772	0.990	0.076	0.817	0.788	0.282	0.801	0.524	0.511	0.457	0.405	0.0175	0.0173	-1.46%
7	0.828	0.750	0.976	0.331	0.832	0.634	0.388	0.656	0.649	0.316	0.610	0.461	0.0172	0.0175	2.01%
8	0.828	0.733	0.961	0.254	0.801	0.841	0.400	0.673	0.567	0.338	0.594	0.383	0.0172	0.0168	-1.99%
9	0.813	0.795	0.992	0.190	0.825	0.711	0.280	0.775	0.618	0.337	0.506	0.326	0.0170	0.0170	-0.02%
10	0.805	0.803	0.994	0.190	0.833	0.716	0.264	0.775	0.602	0.341	0.507	0.326	0.0175	0.0170	-2.80%

Table 5-4： Takeoff Samples

No.	CL	CL/CD	No.	CL	CL/CD	No.	CL	CL/CD	No.	CL	CL/CD
1	2.14	63.88	101	2.19	61.92	201	2.41	61.99	301	2.53	55.06
2	2.15	55.78	102	2.16	52.51	202	2.39	51.17	302	2.24	56.46
3	2.18	55.94	103	2.14	51.57	203	2.44	61.17	303	2.48	52.94
4	2.16	44.14	104	2.14	49.65	204	2.39	47.27	304	2.49	40.21
5	2.27	63.44	105	2.35	60.46	205	2.37	53.14	305	2.57	51.34
6	2.26	54.94	106	2.36	51.15	206	2.36	51.68	306	2.12	55.66
7	2.27	54.52	107	2.43	60.55	207	2.33	49.48	307	2.11	55.18
8	2.29	53.53	108	2.41	50.74	208	2.24	37.21	308	2.12	52.57
9	2.30	59.58	109	2.44	55.41	209	2.55	63.38	309	2.14	57.47
10	2.27	49.25	110	2.46	53.31	210	2.40	44.02	310	2.10	44.40
11	2.30	57.49	111	2.43	50.08	211	2.14	56.44	311	2.14	55.30
12	2.26	47.73	112	2.42	43.84	212	2.17	54.98	312	2.09	42.25
13	2.24	49.99	113	2.49	62.07	213	2.18	57.08	313	2.33	55.80
14	2.46	54.05	114	2.44	52.88	214	2.18	47.81	314	2.37	54.39
15	2.50	54.14	115	2.40	50.34	215	2.24	58.25	315	2.39	54.17
16	2.49	44.32	116	2.01	51.28	216	2.22	47.09	316	2.37	41.18
17	2.56	52.96	117	2.01	51.28	217	2.25	56.09	317	2.44	56.05
18	2.56	57.06	118	2.15	48.30	218	2.25	54.00	318	2.27	36.70
19	2.56	55.62	119	2.24	58.99	219	2.24	53.06	319	2.45	52.20
20	2.32	48.95	120	2.20	46.93	220	2.18	38.48	320	2.40	45.25
21	2.11	58.40	121	2.27	56.77	221	2.25	58.10	321	2.46	58.42
22	2.08	47.27	122	2.29	55.82	222	2.40	53.76	322	2.40	47.15
23	2.12	56.75	123	2.30	55.12	223	2.43	52.99	323	2.40	54.08
24	2.08	45.08	124	2.29	41.90	224	2.22	28.74	324	1.78	21.16
25	2.10	52.57	125	2.34	61.15	225	2.52	61.23	325	1.96	49.32
26	2.11	51.89	126	2.33	52.77	226	2.51	53.20	326	2.16	54.04
27	2.27	55.37	127	2.32	51.43	227	2.52	52.71	327	2.19	54.72
28	2.26	43.29	128	2.30	49.38	228	2.35	30.57	328	2.16	39.23

29	2.39	62.98	129	2.30	55.96	229	2.54	54.23	329	2.28	63.03
30	2.38	54.47	130	2.24	45.88	230	2.08	52.27	330	2.27	54.20
31	2.40	54.49	131	2.54	59.59	231	2.09	53.14	331	2.30	56.90
32	2.42	53.64	132	2.54	51.27	232	2.05	38.92	332	2.31	58.18
33	2.46	61.30	133	2.60	56.80	233	2.12	61.00	333	2.32	58.05
34	2.42	50.98	134	2.61	54.77	234	2.09	50.88	334	2.28	46.12
35	2.43	58.39	135	2.13	54.43	235	2.27	54.57	335	2.30	54.32
36	2.38	47.81	136	2.11	41.61	236	2.31	54.28	336	2.26	43.44
37	2.38	51.68	137	2.20	63.91	237	2.36	60.08	337	2.27	52.85
38	2.35	48.72	138	2.18	54.94	238	2.34	48.11	338	2.25	49.60
39	1.91	27.21	139	2.18	54.53	239	2.38	61.53	339	2.49	51.51
40	2.06	40.67	140	2.18	52.35	240	2.35	46.20	340	2.47	40.12
41	2.20	64.07	141	2.18	56.98	241	2.40	57.46	341	2.53	52.44
42	2.21	55.92	142	2.15	46.09	242	2.41	56.22	342	2.34	38.31
43	2.23	55.70	143	2.16	53.79	243	2.40	54.10	343	2.52	44.35
44	2.26	54.97	144	2.34	46.94	244	2.34	40.35	344	2.13	49.93
45	2.29	59.32	145	2.40	57.35	245	2.37	60.77	345	2.17	58.66
46	2.26	48.35	146	2.44	57.06	246	2.35	49.50	346	2.15	48.04
47	2.32	58.17	147	2.47	57.32	247	2.14	37.29	347	2.20	58.15
48	2.27	46.87	148	2.43	44.71	248	2.51	43.47	348	2.15	44.49
49	2.28	55.28	149	2.51	63.72	249	2.16	60.08	349	2.16	51.30
50	2.28	53.82	150	2.48	52.93	250	2.14	47.38	350	2.16	47.83
51	2.26	52.47	151	2.49	53.97	251	2.24	60.43	351	2.16	50.35
52	2.20	40.73	152	2.48	48.03	252	2.22	48.17	352	2.28	38.00
53	2.47	62.77	153	2.47	55.86	253	2.26	55.42	353	2.42	61.94
54	2.47	54.42	154	2.00	46.92	254	2.27	52.97	354	2.36	46.53
55	2.50	54.31	155	2.04	55.94	255	2.27	51.77	355	2.45	54.98
56	2.56	22.96	156	2.01	44.75	256	2.19	37.47	356	2.43	47.38
57	2.57	59.64	157	2.21	54.84	257	2.28	62.17	357	2.47	54.10
58	2.55	51.35	158	2.25	53.53	258	2.26	53.81	358	2.43	56.34
59	2.12	58.29	159	2.28	53.52	259	2.24	53.22	359	2.44	50.82
60	2.09	47.00	160	2.24	40.79	260	2.23	50.01	360	2.45	36.77
61	2.12	52.70	161	2.37	64.74	261	2.45	60.12	361	2.45	53.36
62	2.13	51.64	162	2.37	57.32	262	2.45	50.25	362	2.42	48.21
63	2.13	50.96	163	2.36	56.96	263	2.48	50.88	363	2.02	51.57
64	2.07	37.96	164	2.35	53.32	264	2.49	40.93	364	1.98	36.49
65	2.16	60.13	165	2.36	58.02	265	2.56	55.96	365	2.21	59.95
66	2.35	57.29	166	2.31	47.21	266	2.47	61.97	366	2.24	53.29
67	2.38	57.31	167	2.34	55.56	267	2.58	54.44	367	2.26	52.54
68	2.41	60.50	168	2.27	44.75	268	2.05	40.60	368	2.29	32.93
69	2.42	60.25	169	2.25	48.81	269	2.14	61.16	369	2.34	59.38
70	2.40	50.34	170	2.53	54.58	270	2.11	49.97	370	2.32	47.44
71	2.46	59.63	171	2.53	55.07	271	2.12	51.99	371	2.36	60.98
72	2.41	52.42	172	2.52	45.09	272	2.12	49.46	372	2.34	43.90
73	2.43	55.61	173	2.16	62.97	273	2.12	57.48	373	2.36	61.68
74	2.43	54.52	174	2.16	53.21	274	2.28	50.37	374	2.33	49.14
75	2.41	52.75	175	2.18	53.09	275	2.35	59.48	375	2.30	48.33
76	2.35	42.80	176	2.20	52.50	276	2.36	50.16	376	2.24	36.12
77	2.38	54.34	177	2.24	61.38	277	2.40	56.41	377	2.30	55.06
78	1.97	49.90	178	2.20	49.87	278	2.40	63.14	378	2.41	37.64
79	2.15	53.18	179	2.25	58.72	279	2.40	53.82	379	2.46	44.31
80	2.18	51.76	180	2.10	36.44	280	2.35	39.50	380	2.48	51.24
81	2.25	61.93	181	2.21	53.03	281	2.44	61.43	381	2.55	49.23
82	2.23	51.52	182	2.22	51.25	282	2.41	56.46	382	2.11	44.55

83	2.30	61.10	183	2.40	54.66	283	2.39	52.02	383	2.17	56.21
84	2.28	50.29	184	2.38	42.22	284	2.25	54.60	384	2.14	41.32
85	2.30	55.78	185	2.47	54.55	285	2.36	51.02	385	2.19	55.35
86	2.31	54.36	186	2.52	56.23	286	1.86	24.05	386	2.21	55.49
87	2.29	53.31	187	2.52	56.37	287	2.16	58.53	387	2.21	55.09
88	2.25	41.16	188	2.52	32.89	288	2.14	44.05	388	2.21	55.09
89	2.32	59.85	189	2.51	57.66	289	2.22	57.90	389	2.22	57.27
90	2.28	51.04	190	2.46	47.92	290	2.22	54.10	390	2.18	47.28
91	2.25	49.96	191	2.50	51.57	291	2.25	57.09	391	2.39	54.91
92	2.49	52.01	192	2.03	43.59	292	2.22	42.78	392	2.35	45.15
93	2.53	58.82	193	2.06	55.23	293	2.31	62.66	393	2.46	57.87
94	2.52	48.28	194	2.07	53.36	294	2.28	52.98	394	2.42	48.90
95	2.57	58.52	195	2.07	52.57	295	2.28	52.20	395	2.41	45.93
96	2.54	46.94	196	2.20	44.01	296	2.29	51.16	396	2.42	45.26
97	2.12	56.98	197	2.32	63.65	297	2.28	57.33	397	2.49	53.13
98	2.14	55.77	198	2.32	55.26	298	2.24	45.87	398	2.44	44.97
99	2.15	55.21	199	2.34	55.02	299	2.25	52.32	399	2.46	53.33
100	2.11	42.75	200	2.37	51.49	300	2.45	45.94	400	2.40	35.11

Table 5-5: Takeoff optimization process

No.	Par.1	Par.2	Par.3	Par.4	Par.5	Par.6	Par.7	Par.8	Par.9	Par.10	Par.11	Par.12	CFD 1/K'	Surrogate 1/k'	Devia-tion
1	0.331	0.386	0.016	0.314	0.484	0.160	0.638	0.222	0.655	0.770	0.528	0.649	0.0168	0.0112	-33.3%
2	0.716	0.187	0.108	0.700	0.669	0.826	0.591	0.650	0.732	0.670	0.426	0.508	0.0176	0.0134	-23.8%
3	0.437	0.097	0.699	0.742	0.076	0.951	0.712	0.951	0.731	0.626	0.628	0.185	0.0178	0.0123	-33.8%
4	0.593	0.093	0.680	0.981	0.517	0.361	0.431	0.695	0.821	0.816	0.981	0.596	0.0162	0.0123	-24.0%
5	0.934	0.317	0.365	0.244	0.737	0.654	0.464	0.123	0.575	0.401	0.562	0.424	0.0171	0.0126	-26.5%
6	0.383	0.315	0.503	0.524	0.839	0.218	0.372	0.611	0.605	0.455	0.899	0.258	0.0168	0.0136	-19.4%
7	0.781	0.474	0.589	0.144	0.506	0.482	0.394	0.182	0.734	0.802	0.195	0.783	0.0194	0.0132	-32.0%
8	0.278	0.469	0.225	0.503	0.718	0.133	0.521	0.947	0.767	0.872	0.663	0.810	0.0165	0.0126	-23.7%
9	0.134	0.149	0.383	0.866	0.465	0.569	0.279	0.027	0.824	0.992	0.546	0.830	0.0169	0.0106	-37.5%
10	0.573	0.470	0.003	0.259	0.918	0.264	0.779	0.694	0.813	0.267	0.364	0.626	0.0171	0.0146	-14.5%
11	0.185	0.249	0.338	0.983	0.924	0.251	0.354	0.258	0.631	0.590	0.082	0.715	0.0165	0.0122	-25.7%
12	0.219	0.037	0.761	0.540	0.853	0.747	0.221	0.023	0.910	0.903	0.517	0.416	0.0161	0.0129	-20.2%
13	0.250	0.326	0.298	0.412	0.014	0.503	0.114	0.273	0.603	0.378	0.750	0.568	0.0165	0.0132	-20.1%
14	0.338	0.351	0.125	0.480	0.789	0.085	0.405	0.885	0.862	0.819	0.118	0.416	0.0150	0.0134	-10.7%
15	0.521	0.051	0.966	0.527	0.999	0.263	0.534	0.276	0.636	0.412	0.095	0.353	0.0176	0.0127	-27.7%
16	0.389	0.412	0.214	0.199	0.298	0.126	0.292	0.654	0.919	0.755	0.247	0.890	0.0134	0.0140	4.3%

Table 5-6: Landing samples

No.	CL	CD	No.	CL	CD	No.	CL	CD	No.	CL	CD
1	2.75	0.0539	51	2.88	0.0745	101	2.78	0.0561	151	2.80	0.0793
2	2.79	0.0662	52	1.84	0.2241	102	2.79	0.0704	152	2.84	0.0936
3	2.79	0.0690	53	2.94	0.0669	103	2.80	0.0738	153	2.96	0.0720
4	2.69	0.0907	54	2.78	0.0784	104	2.76	0.0704	154	2.81	0.0994
5	2.07	0.0978	55	1.96	0.1403	105	2.00	0.1083	155	2.02	0.1313
6	2.87	0.0724	56	2.92	0.0787	106	2.86	0.0891	156	2.67	0.0893
7	2.94	0.0757	57	2.83	0.0599	107	3.00	0.0695	157	2.74	0.0786
8	2.94	0.0690	58	2.69	0.0879	108	2.82	0.0958	158	2.74	0.0763
9	2.76	0.0819	59	2.71	0.0632	109	2.08	0.1290	159	2.70	0.0783
10	1.91	0.1492	60	2.55	0.0840	110	1.94	0.1442	160	1.49	0.2124
11	2.92	0.0768	61	2.83	0.0770	111	2.91	0.0922	161	2.87	0.0719
12	2.92	0.0994	62	2.92	0.0750	112	1.67	0.2073	162	2.92	0.0805
13	2.71	0.0718	63	2.86	0.0791	113	2.86	0.0549	163	2.92	0.0795
14	2.67	0.0703	64	1.86	0.2284	114	2.70	0.0689	164	2.09	0.1240
15	2.53	0.0743	65	1.99	0.1226	115	1.89	0.1209	165	1.96	0.1313
16	1.86	0.1899	66	2.86	0.0771	116	2.87	0.0730	166	2.88	0.1014
17	2.88	0.0596	67	2.89	0.0800	117	2.95	0.0668	167	2.78	0.0642
18	2.79	0.0712	68	2.71	0.0646	118	2.81	0.0940	168	2.68	0.0925
19	2.67	0.0761	69	2.67	0.0627	119	2.07	0.1187	169	2.67	0.0750
20	1.94	0.1248	70	1.84	0.1258	120	1.84	0.1577	170	1.89	0.1191
21	2.94	0.0707	71	2.92	0.0649	121	3.00	0.0824	171	2.82	0.0801
22	2.90	0.1003	72	2.86	0.0860	122	2.90	0.0946	172	1.62	0.2473
23	2.91	0.0833	73	2.77	0.0710	123	2.69	0.0703	173	2.84	0.0695
24	2.55	0.0806	74	2.06	0.1112	124	1.73	0.2087	174	2.01	0.1298
25	1.86	0.1125	75	1.87	0.1363	125	1.93	0.1002	175	1.83	0.1494
26	2.77	0.0690	76	1.74	0.2364	126	2.81	0.0749	176	2.84	0.0979
27	2.84	0.0729	77	3.00	0.0680	127	2.88	0.0811	177	3.04	0.0794
28	1.86	0.1928	78	2.98	0.0794	128	2.91	0.0786	178	2.64	0.0870
29	2.83	0.0627	79	2.69	0.0712	129	2.78	0.0692	179	2.71	0.0644
30	1.99	0.1229	80	2.57	0.0680	130	1.96	0.1404	180	2.55	0.0887
31	2.80	0.0819	81	2.81	0.0616	131	2.88	0.0753	181	2.77	0.0820
32	2.92	0.0768	82	2.76	0.0883	132	2.94	0.0925	182	2.84	0.0803
33	2.93	0.0735	83	2.89	0.0639	133	2.95	0.0858	183	2.87	0.0822
34	2.14	0.1264	84	2.74	0.0852	134	2.70	0.0680	184	1.77	0.2303
35	2.58	0.0601	85	1.92	0.1320	135	2.59	0.0725	185	1.97	0.1200
36	2.74	0.0769	86	2.94	0.0790	136	1.67	0.2209	186	2.86	0.0822
37	2.83	0.0718	87	2.90	0.0811	137	2.89	0.0622	187	2.92	0.0890
38	2.79	0.0686	88	1.92	0.2304	138	2.86	0.0690	188	2.89	0.0936
39	2.70	0.0753	89	2.14	0.1196	139	2.74	0.0801	189	2.65	0.0664
40	1.50	0.2129	90	2.51	0.0640	140	1.95	0.1288	190	2.49	0.0963
41	2.95	0.0635	91	2.81	0.0721	141	2.95	0.0760	191	2.81	0.0746
42	2.95	0.0741	92	2.85	0.0691	142	2.94	0.1001	192	2.64	0.1163
43	2.89	0.0764	93	2.85	0.0662	143	2.87	0.0773	193	2.78	0.0789
44	2.07	0.1252	94	2.63	0.0958	144	2.01	0.1545	194	2.69	0.0774
45	1.94	0.1350	95	1.90	0.1237	145	2.48	0.0703	195	1.89	0.1285
46	2.69	0.0837	96	2.85	0.0973	146	2.78	0.0687	196	1.57	0.2596
47	2.82	0.0618	97	2.93	0.0758	147	2.82	0.0701	197	2.93	0.0839
48	2.70	0.0826	98	2.86	0.0768	148	1.58	0.2298	198	2.87	0.0945
49	2.65	0.0711	99	2.01	0.1356	149	2.71	0.0668	199	1.97	0.1471
50	1.87	0.1218	100	1.41	0.2327	150	1.85	0.1308	200	1.85	0.1142

Table 5-7: Landing optimization process

No.	X_{Slat}	Y_{slat}	α_{slat}	X_{flap}	Y_{flap}	α_{flap}	CFD CL	Surrogate CL
1	0.540	0.180	0.088	0.253	0.006	0.999	2.908	4.064
2	0.969	0.543	0.023	0.427	0.803	0.998	2.965	4.645
3	0.001	0.661	0.997	0.529	0.016	0.144	2.667	4.429
4	0.993	0.000	0.727	0.287	0.000	0.141	2.760	4.037
5	0.385	1.000	0.494	0.470	0.571	0.800	2.902	3.544
6	0.867	0.322	0.602	0.455	0.788	0.998	2.969	3.756
7	0.604	0.000	0.995	0.001	0.717	1.000	2.864	4.109
8	0.435	0.999	0.013	0.388	0.576	0.785	2.962	3.721
9	0.583	0.455	0.597	0.428	0.529	0.857	2.934	3.524
10	0.002	0.022	0.804	0.104	0.001	0.999	2.851	4.944
11	0.001	1.000	0.000	0.000	1.000	0.546	2.909	5.444
12	0.000	0.195	0.899	0.285	1.000	0.999	3.039	4.972
13	0.949	0.004	0.982	0.413	0.725	0.999	2.995	3.811
14	0.455	0.540	0.025	0.436	0.438	0.999	2.973	3.766
15	0.800	1.000	0.559	0.009	0.054	1.000	2.791	4.651
16	0.206	0.003	0.159	0.418	0.998	0.999	3.050	5.230
17	0.523	0.001	0.898	0.357	0.017	0.209	2.797	3.713
18	0.008	0.636	0.753	0.478	0.217	0.434	2.816	3.523
19	0.720	0.391	0.901	0.007	0.265	1.000	2.827	3.675
20	0.008	0.997	0.258	0.003	0.439	0.979	2.861	3.650
21	0.004	0.456	0.008	0.467	0.998	0.168	2.866	5.239
22	0.002	0.419	0.725	0.006	0.999	0.011	2.706	4.272
23	0.971	0.009	0.346	0.315	0.999	0.991	3.071	3.405
24	0.980	0.133	0.343	0.120	1.000	0.843	3.004	3.207
25	0.980	0.067	0.001	0.318	1.000	0.830	3.004	3.322
26	0.789	0.001	0.300	0.317	0.999	0.999	3.086	3.115